Encoding and Decoding Nuclear Calcium Signalling in Plant Root Development and Endosymbiosis

Emily Caroline Tipper

Thesis submitted for the degree of
Doctor of Philosophy
University of East Anglia
John Innes Centre
October 2023

This copy of the thesis has been supplied on condition that anyone who consults it is understood to recognise that its copyright rests with the author and that use of any information derived therefrom must be in accordance with current UK Copyright Law. In addition, any quotation or extract must include full attribution.

Abstract

Calcium ions (Ca^{2+}) are used as secondary messengers across eukaryotes. The encoding and decoding of each calcium signal is vital to maintain its fidelity and specificity. In *Medicago truncatula*, nuclear calcium oscillations are required for root endosymbioses with arbuscular mycorrhizal (AM) fungi and rhizobia bacteria. In *Arabidopsis thaliana,* nuclear calcium releases in the root apical meristem are required for normal primary root development. In both cases, these nuclear calcium releases are generated by the calcium ion channel CNGC15 and the counter cation channel DMI1. In this thesis, their regulation is studied in both species separately.

Heterotrimeric G protein signalling has been implicated in root legume symbioses with Gβ acting as a positive regulator of nodulation in soybean. Here, I identify an interactor of Medicago Gβ, APSR1, that is required for proper AM colonisation and is regulated by phosphate at the transcript level, suggesting that it is involved in the regulation of AM endosymbiosis by phosphate.

In *Arabidopsis thaliana*, using a combination of homology modelling, and electrophysiology, I show that the mutation of a highly conserved aspartic acid in the C-linker domain is sufficient to impair the gating of AtCNCG15. This is the first time the C-linker region of a plant CNGC has been implicated in channel gating. In addition, I show that in the presence of nitrate AtCNGC15 relocalises to the plasma membrane specifically in the columella cells. I hypothesise that the induction of primary nitrate response genes, such as *LBD37*, *LBD38*, and *LBD39*, is modulated by different inputs of cytoplasmic or nuclear calcium release. Finally, I identify the EF-hand containing protein RSA1 as a potential decoder of the nuclear calcium release in Arabidopsis root apical meristems.

Keywords: nuclear calcium signalling, root development, channel gating, nitrate, endosymbiosis

Access Condition and Agreement

Each deposit in UEA Digital Repository is protected by copyright and other intellectual property rights, and duplication or sale of all or part of any of the Data Collections is not permitted, except that material may be duplicated by you for your research use or for educational purposes in electronic or print form. You must obtain permission from the copyright holder, usually the author, for any other use. Exceptions only apply where a deposit may be explicitly provided under a stated licence, such as a Creative Commons licence or Open Government licence.

Electronic or print copies may not be offered, whether for sale or otherwise to anyone, unless explicitly stated under a Creative Commons or Open Government license. Unauthorised reproduction, editing or reformatting for resale purposes is explicitly prohibited (except where approved by the copyright holder themselves) and UEA reserves the right to take immediate ‘take down’ action on behalf of the copyright and/or rights holder if this Access condition of the UEA Digital Repository is breached. Any material in this database has been supplied on the understanding that it is copyright material and that no quotation from the material may be published without proper acknowledgement.

Contents

Abstract 2
List of Figures 6
List of Tables 7
Acknowledgements 7
Chapter I: General Introduction 9
1.1 Calcium signalling in plants 9
1.1.1 Plant calcium ion channels and decoders 10
1.1.2 The role of calcium in nitrate signalling 17
1.1.3 Calcium signalling in the nucleus 19
1.2 The establishment of endosymbiosis in land plants 21
1.2.1 Overview of arbuscular mycorrhization development 23
1.2.2 Symbionts release elicitors to initiate endosymbiotic signalling 23
1.2.2 Perception of elicitors by plants 25
1.2.3 Signal transduction from the plasma membrane to the nucleus 27
1.2.4 Generation of nuclear calcium oscillations 30
1.2.5 The regulation of nodulation in legumes by nutrient status. 31
1.2.6 The regulation of mycorrhization by phosphate 32
1.3 *Arabidopsis thaliana* root development and the role of calcium 38
1.3.1 Overview of *Arabidopsis thaliana* root development 38
1.3.2 The role of calcium ions in Arabidopsis primary root development 40
1.5 Thesis Aims 43
Chapter II: Material and Methods 45
2.1 *Medicago truncatula* (Medicago) plant materials and growth conditions 45
2.2 Medicago nutrient treatments 45
2.3 Medicago nodulation and mycorrhization treatments 46
2.4 *Arabidopsis thaliana* (Arabidopsis) plant materials and growth conditions 47
2.5 Genotyping 48
2.6 Generation of the *Arabidopsis* double mutants by crossing 49
2.7 Quantification of gene expression 49
2.8 Yeast Two-Hybrid Assay 51
2.9 Modelling the AtCNGC15 structure 52
2.10 Expression in *Xenopus laevis* oocytes 52
2.11 Electrophysiology 54
2.12 Confocal laser scanning microscopy of *Xenopus* oocytes 55
2.13 Whole genome sequencing 55

2.14 Primary root length measurements and lateral root length analysis 56
2.15 Root apical meristem visualisation and measurement 56
2.16 Confocal laser scanning microscopy of Arabidopsis roots 57
2.17 Nitrate treatment of Arabidopsis roots 57
2.18 Calcium imaging of NR-GECO1.2 CYCB1.1-GFP seedlings 57
2.19 Molecular Biology Methods 58
2.19.1 Polymerase Chain Reaction (PCR) 58
2.19.2 Gel electrophoresis 58
2.19.3 Gel DNA extraction 59
2.19.4 Sequencing of PCR products and plasmids 59
2.19.5 Gateway Cloning 59
2.19.6 Transformation of *Escherichia coli* 60
2.19.7 Plasmid purification 60
2.19.8 Plasmid linearization by restriction digest 61
2.20 Computational Methods 61
2.20.1 Design of *in silico* sequences 61
2.20.2 Database searches for domains and protein families 62
2.20.3 Phylogenetic tree construction 62
2.20.4 Searching for APSR1 *tnt* insertion lines 63
2.20.5 Transcriptome analyses 63
2.20.6 Sequence analysis 63
2.20.7 Primer design 64
2.20.8 Statistical analyses 64
Chapter III: An investigation of the role of *MtAPSR1* in *Medicago truncatula* root endosymbiosis 69
3.1 Introduction 69
3.2 Results 72
3.2.1 MtAPSR1 interacts with the G protein β subunit via a yeast two-hybrid assay. 72
3.2.2 MtAPSR1 is part of the NRG2 family, with orthologs in Arabidopsis. 73
3.2.3 *MtAPSR1* is induced by phosphate treatment. 76
3.2.4 Identification and characterisation of two *Mtapsr1 tnt* insertion lines 79
3.3 Discussion 83
Chapter IV – Investigation of a novel allele of CNGC15, and its dual function in Arabidopsis root apical meristems 86
4.1 Introduction 86

4.2 Results 88
4.2.1 The D408N point mutation is in the C-linker region of CNGC15 88
4.2.2 The D408N mutation affects the gating properties of CNGC15 in *Xenopus laevis* oocytes 90
4.2.3 Cyclic adenosine monophosphate (cAMP) may assist the gating of *AtCNGC15*^{D408N}. 93
4.2.4 The dual function of AtCNGC15 is promoted by high nitrate. 94
4.2.5 Does the nuclear calcium signal generated by AtCNGC15 and AtDMI1 affect the regulation of the cell cycle in the primary root meristem? 97
4.3 Discussion 99
Chapter V – An investigation of nuclear calcium regulators and decoders in Arabidopsis roots 103
5.1 Introduction 103
5.2 Results 106
5.2.1 Whole genome sequencing and analysis of *cngc15*^{D408N} EMS-mutagenized lines 106
5.2.2 Genotyping of the *rsa1-3* mutant line 110
5.2.3 *rsa1-3* and *dmi1-2 rsa1-3* have shorter primary root lengths and increased lateral root densities. 111
5.2.4 *rsa1-3* and *dmi1-2 rsa1-3* have reduced primary root meristem sizes. 114
5.2.5 *dmi1-1 rsa1-3* also displays a short primary root phenotype and increased lateral root density. 116
5.3 Discussion 116
Chapter VI – General Discussion 120
6.1 The common symbiosis pathway and the regulation of endosymbiosis 120
6.2 A dual role of CNGC15 in root apical meristem development and nitrate signalling 123
6.3 RSA1 as a putative nuclear calcium signalling in Arabidopsis primary root development 127
6.4 Final Thoughts 130
List of Abbreviations 133
List of References 135

List of Figures

Figure 1.1 Localisation and Function of Arabidopsis and rice Ca^{2+} channels and transporters in response to abiotic (A) and biotic (B) stresses	15
Figure 1.2 The common symbiosis pathway	25
Figure 1.3 The role of G protein subunits in early endosymbiosis signalling upon Nod factor perception in *Lotus japonicus*.	30
Figure 1.4 Summary model of the SPX/PHR mediated regulation of AM colonisation under different phosphate conditions in Medicago.	37
Figure 1.5 The balance between auxin and cytokinin levels in the Arabidopsis primary root tip maintains meristem size and root growth.	39
Figure 3. 1 APSR1 interacts with the G protein β subunit via a Yeast two-hybrid assay in one configuration.	73
Figure 3.2 Phylogenetic analysis of the NRG2 family.	74
Figure 3.3 A closer look at the clade containing MtAPSR1.	75
Figure 3.4 Mean relative expression of *APSR1* in Medicago truncatula R108 roots under nitrate and phosphate treatments, with and without inoculation with *S. meliloti* 2011 or *R. irregularis*.	77
Figure 3.5. Expression of APSR1 is not altered by treatment with Nod factor or infection with *Rhizophagus irregularis*.	78
Figure 3.6 Characterisation of 2 *Mtapsr1 tnt* insertion lines.	80
Figure 3.7 NF4464 and NF12622 lines have reduced arbuscular mycorrhizal colonisation.	81
Figure 3.8 Nodulation assay of wild type R108 and tnt insertion line NF12622 plants.	82
Figure 3.9 Nodulation assay of wild type R108 and tnt insertion line NF4464 plants.	83
Figure 4.1 The D408N mutation is predicted to disrupt salt bridges between adjacent AtCNGC15 subunits. Figure produced in collaboration with Professor David Lawson (JIC).	89
Figure 4.2 The D408N mutation impairs the gating of CNGC15.	92
Figure 4.3 cAMP may assist the gating of $AtCNGC15^{D408N}$.	94
Figure 4.4 AtCNCG15 is required for nitrate induced gene expression.	95
Figure 4.5 AtCNCG15 relocalises to the plasma membrane of columella cells upon high nitrate treatment, and not in the absence of nitrate.	97
Figure 4.6 Summary model for the dual role of AtCNGC15 in root apical meristem (RAM) development and nitrate signalling in the columella cell layer of 6 day old Arabidopsis seedlings.	101
Figure 5.1 Identification of EMS lines that recover wild type primary root length.	106
Figure 5.2 Visualisation and manual inspection of single nucleotide polymorphisms (SNPs).	108
Figure 5.3 Characterisation of *rsa1-3*.	111
Figure 5.4 *rsa1-3* and *dmi1-2 rsa1-3* have significantly shorter primary root lengths, and an increased lateral root density.	113
Figure 5.5 *rsa1-3* and *dmi1-2 rsa1-3* have significantly shorter root apical meristems.	114
Figure 5.6 *dmi1-1 rsa1-3* has a significantly shorter primary root length, and an increased lateral root density.	115

List of Tables

Table 2.1: Primers used in this thesis. 65
Table 2.2: List of media compositions for culture of bacteria, yeast, and plants..... 68

Table 5.1: Contigs and SNPs screened using a 3kb window and how they were classified. 109

Acknowledgements

This work would not have been possible without the continuous support and guidance of Myriam Charpentier. Thank you for being a great supervisor, for caring about my progress, and for encouraging rigorous, critical, and imaginative scientific thinking. Thank you for being on hand to calm my nerves where necessary, and for reminding me that there is always a solution to any problem.

Many thanks to my secondary supervisor, David Seung, for our interesting discussions, for your support and advice, and for your friendly presence in the Bateson first floor corridor.

Thank you to UK Research and Innovation for funding the Norwich Research Park Doctoral Training Programme, which enabled me to carry out this research.

Throughout my PhD, I have had the pleasure of learning many different skills from people who have gone out of their way to help me. Thanks must go to Burkhard Steuernagel, for teaching me Bash scripting and how to analyse my Whole Genome Sequencing data, to Yi Chen, for teaching me electrophysiology skills, and to Eva Wegel and Sergio Lopez for microscopy training and support. Thank you all for your time, patience, and expertise.

Thank you to the current and former members of the Charpentier lab: Anson, Cat, Clem, Ed, Giulia, Janni, Lauren, Nic :), Nico, Nuno, Pablo, Pierre and Sunny. Thank you for your camaraderie, knowledge, assistance, and time. I have learnt much from each of you, both scientifically and personally. Particular mentions must go to Anson for helping me with phylogenetics, to Nuno for your advice and experience at Synthace, to Nic :) for being the backbone of the lab and

keeping us organised, and to Lauren for your friendship and listening ear on our car journeys to and from Hill Farm.

This work could not have been done without the laboratory support staff, media kitchen staff and horticultural services. Thank you to Eleanor Rickaby for keeping Bateson first floor running, and to Tim Wells for looking after my plants.

Thanks to Rue Jones-Green and the Gurdon Institute, Cambridge, for supplying me with your spare oocytes for my experiments.

Thank you to East Alga (Calum, Sam, Yang and Andy) for such an incredible time during the BiotechYES competition. The stressful late nights were worth it in the end!

To Sam, Josh, Ed, and Hannah: thank you for the meals, pints, and beach trips we have shared, and more importantly for your friendship.

Thanks to Joe Sallmen for hosting the best quizzes at the Rec Centre, even if the Charpentier team is forever doomed to second place!

Thank you to Violet at Hill Farm Riding Centre, and to Pema, for keeping me happy and healthy.

A big thank you to Kayleigh Poacher and BBC Radio Norfolk. You brightened my working day with your continuous chatter and questionable music choices, and kept me sane during the more tedious experiments. Credit must also go to Greg James and Radio 1 Breakfast for getting me out of bed in the morning!

Many thanks to all my past teachers, lecturers, and advisors for shaping me into the scientist, and the person, that I am today.

To my friends, Lucy, Izzy, Alice, Hannah, and Emma, thank you for teaching me to be the best version of myself, and encouraging me to follow my dreams.

Finally, a huge thank you to my parents, to Claudia, to Monty, and to Alistair for your unwavering support and belief in me throughout the highs and the lows. I couldn't have done it without you.

Chapter I: General Introduction

1.1 Calcium signalling in plants

Calcium ions (Ca^{2+}) are universal secondary messengers that coordinate a variety of plant and animal cellular functions. They are involved in many biotic and abiotic stress responses, as well as growth and development. In plants, calcium signalling is used as one of the earliest signalling events in response to pests and pathogens, such as mechanical damage by insect herbivory, and in PAMP (pathogen associated molecular pattern) triggered immunity (PTI), but also in response to beneficial organisms such as endosymbionts (Kim et al., 2022; Tian et al., 2020). Calcium signalling is involved in the response to abiotic stresses such salinity stress, stomatal closure during drought stress, and the uptake and homeostasis of various ions including nitrate (Dong et al., 2022). It is also involved in the development of pollen tubes (Frietsch et al., 2007, Tunc-Ozdemir et al., 2013, Pan et al., 2019), root hairs (Zhang et al., 2017, Brost et al., 2019, Tan et al., 2020) and roots (Leitão et al., 2019), and trap closure in the Venus flytrap (Suda et al., 2020). As calcium ions are such ubiquitous and versatile signalling molecules, specificity is achieved by the location of their release at the organ, cellular, and subcellular level, and the time, duration, and frequency of calcium release. These spatiotemporal patterns of calcium release are known as the calcium signature (Aldon et al., 2018). Unique properties of calcium signatures, such as their frequency and duration, have been shown to encode specific information, as their variation is sufficient to modulate physiological and developmental processes (Allen et al., 2001, Leitão et al., 2019).

Why has the calcium ion (Ca^{2+}) become such a ubiquitous signalling molecule, and not a similar ion such as the magnesium ion (Mg^{2+})? Chemical properties of Ca^{2+}, such as its size and valency, allow it to be bound quickly, and in several flexible configurations within biological molecules (Carafoli and Krebs, 2016). Ca^{2+} is a larger ion than Mg^{2+}, which means it has a higher coordination number, so it can be bound to more sites within a compound, and

it can form bonds of variable lengths. It also has a higher polarizability (its electron cloud can be distorted more readily), meaning it binds to other ions more strongly than Mg^{2+}. This may seem counterintuitive, as Mg^{2+} has a greater charge density than Ca^{2+}, due to it being a smaller ion with the same valency. However, when many-body effects are taken into account, which are the collective effects of many interacting bodies forming bonds in close proximity, the binding of Ca^{2+} is associated with a lower cost than binding of Mg^{2+} (Jing et al., 2018). This combination of properties means Ca^{2+} can be bound in a range of different configurations, which is useful for binding to diverse and inflexible protein structures (Carafoli and Krebs, 2016). This is in contrast to Mg^{2+}, which must have a fixed octahedral geometry (Carafoli and Krebs, 2016).

Calcium ions were present in the oceans where early life evolved, but are predicted to have been at low concentrations (Kazmierczak et al., 2013). An essential factor contributing to the success of Ca^{2+} as a signalling molecule is the fact that early life developed with a phosphate-based energy currency. Calcium phosphate salts are insoluble, providing a requirement to keep Ca^{2+} concentrations low in early cells (Carafoli and Krebs, 2016). A low initial Ca^{2+} concentration is, of course, a prerequisite for signalling, which requires a transient, detectable increase in Ca^{2+} concentration. Magnesium ions are at high concentrations in seawater, and magnesium phosphate salts are soluble, abolishing the selective pressure to keep Mg^{2+} concentrations low (Carafoli and Krebs, 2016). As a result, Mg^{2+} is used to bind to and activate adenosine triphosphate (ATP) and its cellular concentrations are in the millimolar ranges (Kleczkowski and Igamberdiev, 2021), whilst Ca^{2+} is kept at the 100nM in the cytoplasm at resting state (Costa et al., 2018).

1.1.1 Plant calcium ion channels and decoders

Calcium signalling requires the detection of a stimulus, encoding of that stimulus into a calcium signal that can be propagated, reception by calcium binding proteins, and decoding of the signal to give a response. The encoding of the signal is carried out by calcium ion channels that can selectively move calcium from one compartment to another upon perception of a particular

stimulus. Plants have a plethora of calcium ion influx channels responsible for encoding a complex range of biotic and abiotic signals. These include Glutamate Receptor-Like Channels (GLRs), Two-Pore Channels (TPCs), Hyperosmolality-Gated Calcium Permeable Channels (OSCAs), Nucleotide-binding Leucine-Rich Repeat Receptors (NLRs), Annexins, and Cyclic Nucleotide-Gated Channels (CNGCs). They also have calcium efflux channels, such as Ca^{2+}-ATPases, Ca^{2+}/cation antiporters and Ca^{2+}/H^{+} Exchangers. Figure 1.1 summarises the localisation and function of these known calcium channels in Arabidopsis and rice.

1.1.1.1 GLRs

Plant GLRs are non-selective cation permeable channels that reside in various cellular membranes, including the plasma membrane, vacuole, endoplasmic reticulum, plastids and mitochondrial membranes (Simon et al., 2023). Plant GLRs are similar in channel structure and amino acid sequence to the mammalian ionotropic glutamate receptors (iGluRs), that produce glutamate-induced excitatory currents in neurons (Park & Shin, 2022). However, whilst iGluRs are only regulated by glutamine, GLRs can be regulated by other amino acids; up to 6 for some Arabidopsis GLRs (Stephens et al., 2008), and up to 11 for some rice GLRs (Yu et al., 2022). Plant GLRs have varying selectivity to cations when heterologously expressed in *Xenopus laevis* oocytes. For example, AtGLR1.4 is a nonselective cation channel, permeable to Ca^{2+} (Tapen et al., 2013), whereas AtGLR3.4 was found to be highly selective for Ca^{2+} (Vincill et al., 2012). GLRs have diverse roles, and in Arabidopsis are known to be involved in the regulation of seed germination under salt stress (Cheng et al., 2016), pollen tube growth, response to mechanical wounding and herbivory, and in drought and cold responses (reviewed in Yu et al., 2022 (2)). GLR3.6 in Arabidopsis plays a role in root development, with the loss of function mutant *Atglr3.6-1* displaying a smaller meristem size, reduced primary root growth and reduced lateral root number (Singh et al., 2016). This was associated with increased transcript abundance of the cell cycle inhibitor KIP-RELATED PROTEIN 4 (AtKRP4), reduced expression of the cell cycle marker

proCYCB1;1::GUS, and reduced cytoplasmic calcium in an aequorin bioluminescence assay. Auxin levels, and *PIN1* mRNA was also reduced in the mutant, suggesting that AtGLR3.6 mediated calcium influx regulates PIN mediated polar auxin transport, and therefore root development (Singh et al., 2016). In addition, AtGLR3.2 and 3.4 have been shown to form a heteromer involved in lateral root development, with both the single and double knockout mutants having an increased number of lateral root primordia, and irregular placement of these primordia along the length of the primary root (Vincill et al., 2013).

1.1.1.2 TPCs

Plant two pore channels are non-selective cation channels co-regulated by both voltage and calcium ions, and generate slow vacuolar currents (Park & Shin, 2022). They are generally believed to be localised to the vacuole, with some studies also demonstrating plasma membrane localisation (Singh et al., 2014 (2)). Arabidopsis TWO-PORE CHANNEL 1 (AtTPC1) is particularly well studied, and is known to form a homodimer, with 2 EF hand domains per homodimer (Schulze et al., 2011; Dadacz-Narloch et al., 2011). It is activated by both membrane depolarisation and by Ca^{2+}_{cyt}, and is inhibited by vacuolar Ca^{2+} (Beyhl et al., 2009). AtTCP1 has roles in plant immunity signalling, with the AtTCP1 gain-of-function mutant *fou2,* which is not inhibited by vacuolar Ca^{2+} (Beyhl et al., 2009), having increased resistance to the fungus *Botrytis cinerea* (Bonaventure et al., 2007). In rice, OsTCP1 is also involved in the induction of defence related genes, oxidative bursts, MAP kinase activation and cell death upon the perception of pathogenic elicitors (Kurusu et al., 2005).

1.1.1.2 NLRs

As well as their known roles as intracellular immune receptors (Zhang et al., 2022), NLR oligomerizations have more recently been shown to act as calcium channels. NLRs are classified by specific domains in their N-termini, such as a coiled-coil (CC) domain or a Resistance to Powdery Mildew 8 (RPW8)-like CC domain, and these domains can confer pore formation and cation

conductance (Maruta et al., 2022). In Arabidopsis, the NLR HOPZ-ACTIVATED RESISTANCE 1 (ZAR1) forms a complex with other proteins, termed the ZAR1 resistome, which can be activated by ATP (Wang et al., 2019). This resistome formation was found to be triggered *in vivo* by bacterial effectors, and is involved in disease resistance (Hu et al., 2020). The resistome was also found to have calcium channel activity, with this calcium influx activity essential for the triggering of cell death (Bi et al 2021). Similarly, the complex formed by the Arabidopsis NLR N REQUIREMENT GENE 1.1 (NRG1.1) also appears to act as a non-selective cation channel, permeable to calcium ions (Jacob et al., 2021).

1.1.1.3 OSCAs

The first osmosensing calcium ion channel to be identified in plants was OSCA1, which was identified using a forward genetic screen of Arabidopsis mutants that displayed reduced intracellular Ca^{2+} increases under water stress conditions (hyperosmolality). The *osca1* mutant line displayed impaired osmotic calcium signalling in the guard and root cells (Yuan et al., 2014). Since then, 15 OSCA genes have been identified in Arabidopsis (Liu et al., 2018), whilst rice is predicted to have 11 (Li et al., 2015). They are likely nonselective cation channels, as they have been shown to be permeable to calcium, potassium and sodium ions when expressed in *X. laevis* oocytes (Hou et al., 2014). As well as sensing osmolality, OSCAs have been shown to be involved in plant defence. AtOSCA1.3 controls stomatal closure during immune signalling, via its phosphorylation by BOTRYTIS-INDUCED KINASE1 (BIK1) upon the perception of PAMPs (Thor et al., 2020).

1.1.1.4 Annexins

Annexins are phospholipid binding proteins with diverse functions in both plants and animals. In plants, they are expressed in a variety of cell types and subcellular locations, and their expression can vary under different biotic and abiotic conditions (Davies, 2014). Their binding to lipid membranes is dependent on various factors, including the presence of calcium ions (Laohavisit & Davies, 2010). In plants, it has been shown that the expression of

annexins can be regulated by Ca^{2+}, and that they are involved in passive Ca^{2+} transport. It is unclear whether annexins are acting as calcium channels themselves, or simply facilitating calcium ion transport through other channels (Laohavisit et al 2012; Richards et al 2014). In the case of *ANNEXIN 1* in Arabidopsis (At*ANN1*), this involvement in Ca^{2+} elevation has been implicated in root development (Laohavisit et al 2012), response to hydrogen peroxide (Richards et al 2014) and response to wounding and herbivory (Malabarba et al, 2021).

1.1.1.5 Efflux channels

As well as these calcium influx channels, plants also have an array of calcium efflux channels. These include Ca^{2+}-ATPases, Ca^{2+}/cation antiporters and Ca^{2+}/H^{+} Exchangers (CAXs). These are predominantly involved in the termination of calcium signalling and maintenance of ion homeostasis (Park & Shin, 2022). For example, in Arabidopsis, AtCAX1 and AtCAX3 have been implicated in the maintenance of calcium ion homeostasis following elevated Ca^{2+} levels, for example those produced during immunity signalling (Wang et al., 2024).

1.1.1.6 CNGCs

Whilst plant CNGCs were first identified in barley in 1998 (Schuurink et al., 1998), the equivalent animal Cyclic Nucleotide Gated (CNG) channels, and the related, but differently regulated Hyperpolarization-activated Cyclic Nucleotide–gated (HCN) channels have been studied for far longer. CNG channels and CNGCs function in homo- or heterotetramers, and subunits have a highly conserved protein structure, with six transmembrane segments (S1-S6), a pore region that determines pore selectivity and diameter between S5 and S6, a cyclic nucleotide binding domain (CNBD), a calmodulin (CaM) binding domain, and a C-linker region (Matulef and Zagotta, 2003).

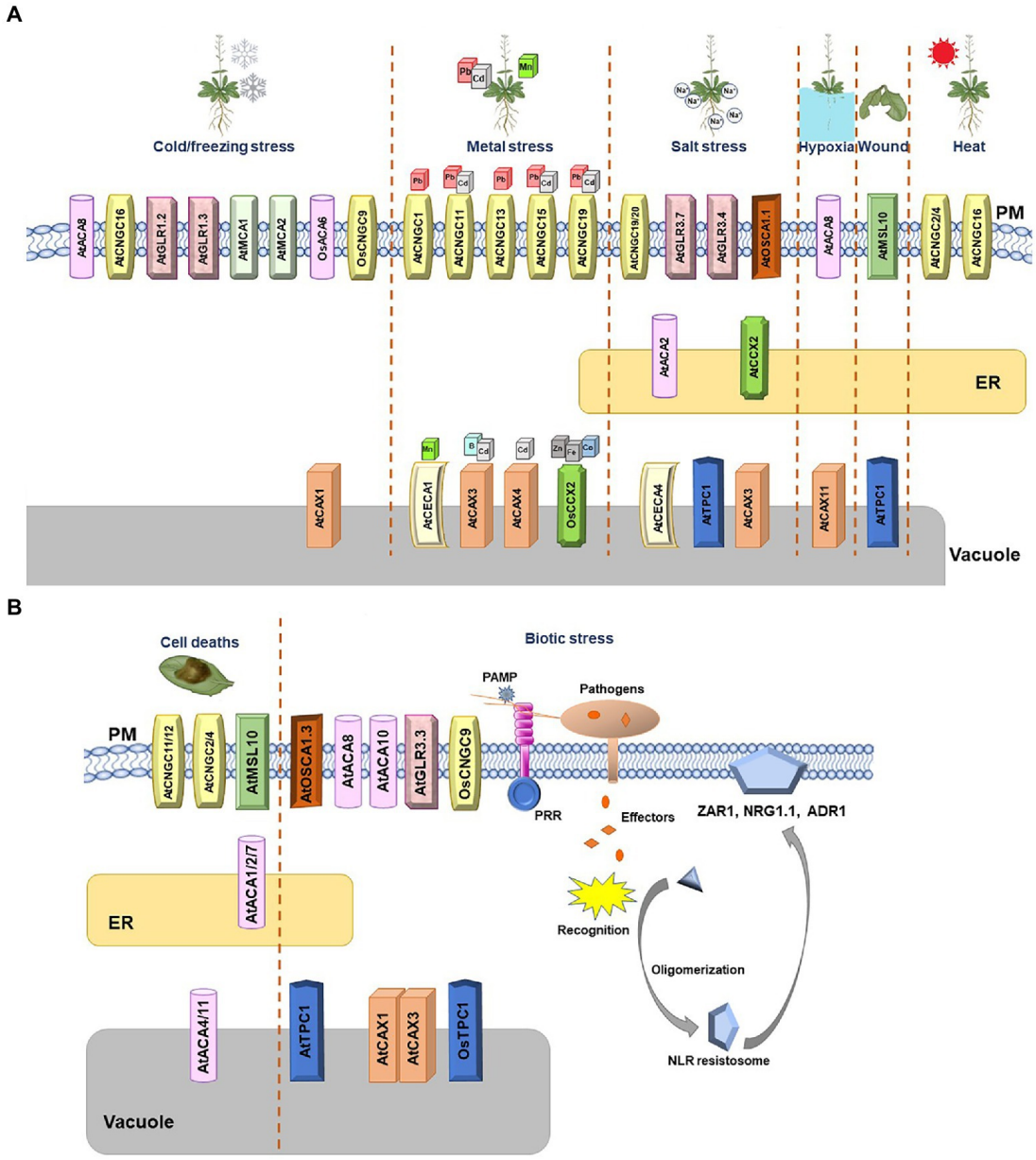


Figure 1.1 Localisation and Function of Arabidopsis and rice Ca^{2+} channels and transporters in response to abiotic (A) and biotic (B) stresses.

Calcium ion channels and transporters are localised in a range of different cell types, including the plasma membrane (PM), the endoplasmic reticulum (ER) and the vacuole. They are involved in calcium transport in response to both abiotic and biotic stresses, such as temperature, osmolality, presence of heavy metals, wounding, cell death, and the perception of pathogens. Figure from Park & Shin (2022).

In plants, CNGCs have many described roles, including in pollen tube development in Arabidopsis, with pollen tubes having a strong apical Ca^{2+} gradient required for their growth. CNGC7, 8 and 18 are required for normal pollen germination, with CNGC7 and 8 showing redundant function (Tunc-Ozdemir et al., 2013)). CNGC18 was found to interact with both CNGC7 and CNGC8, and these channels form a heterotetramer that was found to inhibit calcium influx in *Xenopus laevis* oocytes (Pan et al., 2019). This highlights an important feature of CNGCs: that the specific components of the tetrameric complex are important for their function. Other roles of CNGCs include CNGC14 in tip growth in root hair cells and in root gravitropism in Arabidopsis (Zhang et al., 2017, Shih et al., 2015), CNGCs 2, 4, 11 and 12 in generating cytoplasmic calcium influx in early immunity signalling in Arabidopsis (Clough et al., 2000, Jurkowski et al., 2004, Yoshioka et al., 2006), and CNGC15 in the establishment of endosymbioses in legumes (Charpentier et al., 2016) and root development in Arabidopsis (Tipper et al., 2023).

1.1.1.7 Calcium ion decoders

Calcium decoders must be able to directly bind calcium or interact with other proteins that bind calcium. Many known calcium decoders have an EF-hand calcium binding domain. For example, CaMs have a pair of EF-hand domains at both the N-terminus and the C-terminus of the protein, allowing the binding of four calcium ions (Kretsinger, 1997). Other families of proteins containing EF-hands include calcineurin B-like proteins (CBLs), Ca^{2+}-dependent protein kinases (CDPKs or CPKs) and the Calmodulin-like protein (CML) family (Dodd et al., 2010; Kudla et al., 2018; Tang et al., 2020; Dong et al., 2021). These proteins bind calcium and facilitate downstream signalling by directly binding to or phosphorylating proteins such as transcription factors and CBL-interacting protein kinases (CIPKs).

CBLs and their interacting CIPKs have well known roles in nutrient uptake and homeostasis (Dong et al., 2021), acting as a regulatory hub in these processes. CBLs are thought to have diverged from CaMs, as they share little sequence identity, although they do still have 4 EF hand domains (Kudla et al.,

2018). CDPKs, as calcium binding kinases, combine both the calcium sensing and signalling capabilities in one protein. This has been implicated in a range of biotic and abiotic stress responses (Dekomah et al., 2022). However, they have also been shown to act independently of calcium, and further research is needed to assess how these kinases are regulated in vivo (Kudla et al., 2018).

1.1.2 The role of calcium in nitrate signalling

One example of how calcium channels and decoders can be integrated to transmit and receive a signal is in the nitrate signalling pathway. Nitrogen is an essential plant macronutrient required for the biosynthesis of nitrogen-containing molecules, such as amino acids and nucleic acids, and as such is integral for maintaining plant productivity (Wang et al., 2018). As a result, nitrogen homeostasis and signalling is vital, with nitrate being the primary way in which nitrogen is assimilated (Wang et al., 2018).

In natural soils, the availability of nitrogen is often low and highly variable, so plants have evolved numerous mechanisms to enhance both its acquisition and its utilization (Kiba & Krapp, 2016). One of the ways that plants can maximise nitrogen uptake is by altering the root architecture in response to availability. Plants have the ability to sense their overall nitrogen status by integrating multiple signals from both the root and the shoot, and when nitrogen availability appears to be sufficient this inhibits root growth. In contrast, uniformly low nitrogen conditions promote growth of primary and lateral roots up to a certain point (Oldroyd & Leyser, 2020), but severe nitrogen limitation results in inhibition of growth of the entire root system (Kiba & Krapp, 2016). When plants are grown in patchy nitrogen conditions, root growth is promoted in nitrogen rich patches and inhibited in nitrogen deprived patches (Oldroyd & Leyser, 2020).

Nitrate is taken up at the plasma membrane by the nitrate and peptide (NPF) and nitrate transporter 2 (NRT2) gene families in Arabidopsis. NRT2 genes encode high affinity nitrate transporters whilst NFP genes largely encode low affinity transporters. The exception to this is NITRATE TRANSPORTER 1.1 (NRT1.1, also known as NITRATE TRANSPORTER 1/PEPTIDE TRANSPORTER

FAMILY 6.3 and CHLORATE-RESISTANT 1), which has dual affinity (Kiba & Krapp, 2016). NRT1.1 was later termed a 'transceptor' due to its dual nitrate receptor and transporter roles (Remans et al., 2006, Ho et al., 2009, Wang et al., 2009). NRT1.1 can transport nitrate at both low and high affinities, depending on the phosphorylation status of the threonine (Thr) 101 residue. Phosphorylation of Thr 101 confers NRT1.1 as a high affinity transporter, able to transport nitrate across the plasma membrane at lower concentrations (Liu and Tsay, 2003).

Calcineurin B-like Interacting Protein Kinase 23 (CIPK23) is responsible for the phosphorylation of the Thr-101 residue (Liu and Tsay, 2003), and Calcineurin B-like Interacting Protein Kinase 8 (CIPK8) is a positive regulator of the low affinity phase of NRT1.1 (Hu et al., 2009). Calcineurin B-like 1 and 9 (CBL1 and 9) are interactors of CIPK23 that inhibit nitrate transport through NRT1.1 (Cheong et al., 2007, Ho et al., 2009, Léran et al., 2015). The dual affinity of NRT1.1 is used not only for transport, but also for nitrate sensing and signalling, with NRT1.1 being able to sense nitrate a wide range of concentrations and trigger the correct response (Ho et al., 2009).

In addition to its role in the regulation of NRT1.1, calcium has been implicated in the transcriptional response to nitrate in leaves in Arabidopsis for many years (Sakakibara et al., 1997, Sueyoshi et al., 1999), and nitrate causes an elevation in cytoplasmic Ca^{2+} levels in Arabidopsis roots (Riveras et al., 2015). Both the nitrate sensing and transporting functions of NRT1.1 are required for this nitrate-induced cytoplasmic calcium influx in roots, as well as the activation of nitrate responsive genes such as *TGACG SEQUENCE-SPECIFIC BINDING PROTEIN 1* (*TGA1)* and *AUXIN SIGNALING F-BOX 3* (*AFB3)* (Riveras et al., 2015). To identify the calcium decoders that are responding to the calcium influx, an in-gel kinase assay was used, which identified high levels of CPK activity in response to nitrate within 10 minutes (Liu et al., 2017). To identify which of the 34 Arabidopsis *CPK* genes was responsible, the activity of CPK promoters upon nitrate treatment was assessed using a *pCPK-NIR-LUC* system (CPK promoter driving *NITRITE REDUCTASE* and *LUCIFERASE*). This revealed activity within subgroup III of the CPKs, and although there was a high degree

of redundancy, the double knockout mutant lines *cpk10,32*, *cpk30,32,* and the *icpk* inducible triple mutant line did display defects in nitrate-responsive gene expression (Liu et al., 2017). CPKs 10, 30 and 32 were found to control the induction of a wide range of genes upon nitrate treatment, through their phosphorylation of the transcription factor NLP7 (Liu et al., 2017). This indicates the existence of a Ca^{2+}-CPK-NLP signalling cascade in Arabidopsis in which calcium perception triggers the translocation of CPKs to the nucleus, where they phosphorylate NPL7, facilitating its nuclear retention and activation of nitrate responsive genes. In addition to CPKs, CBLs have been implicated in nitrate signalling in rice (Yang et al., 2019) and wheat (Adavi et al., 2023). Whilst the role of calcium in nitrate signalling has been predominantly studied in roots, nitrate has been shown to trigger unique cytoplasmic Ca^{2+} signatures in Arabidopsis leaf mesophyll protoplasts (Liu et al., 2017), indicating a crucial role of nitrate-induced calcium signalling in a range of cell types.

As for the generation of the nitrate-induced calcium influx in Arabidopsis, the ion channel(s) responsible had not been identified until the discovery that a loss of function of *CNGC15* blocks nitrate-induced calcium influx (Wang et al., 2021c). *CNGC15* was found to be partially required for the induction of several primary nitrate response genes, and to interact with NRT1.1 via Bimolecular Fluorescence Complementation (BiFC) in *N. benthamiana*, and co-immunoprecipitation (Co-IP) in Arabidopsis mesophyll cells (Wang et al., 2021c). This interaction between NRT1.1 and CNGC15 was found to inhibit calcium influx in *Xenopus laevis* oocytes, leading to the suggestion that nitrate perception by NRT1.1 leads to its dissociation with CNGC15 at the plasma membrane, lifting this repression (Wang et al., 2021c). However, it must be noted that these experiments were carried out in heterologous systems, or in mesophyll protoplasts, and so they do not represent the Arabidopsis root system.

1.1.3 Calcium signalling in the nucleus

The specificity of a calcium signature is not only conferred by the nature of the stimulus, such as the presence or absence of nitrate, but also by the

subcellular compartment into which Ca^{2+} is released. Given the ability of calcium signalling to transmit information precisely, and the importance of coordinating gene transcription with external stimuli, it is unsurprising that it is used in the nucleus to regulate gene expression.

Calcium can be released into the nucleus in several ways. In early endosymbiosis signalling in legumes such as *Medicago truncatula*, chemical elicitors from arbuscular mycorrhizal (AM) fungi or rhizobia bacteria trigger nuclear calcium oscillations in root epidermal cells, where the calcium is released from the nuclear envelope into the nucleoplasm through calcium ion channels (Charpentier et al., 2016). These calcium oscillations originate from the nucleus, with some diffusion into the cytoplasm, indicating that they are produced by a nuclear calcium store independent of the cytoplasmic calcium (Kelner et al., 2018). This store is the nuclear lumen between the inner and outer nuclear membranes, which is continuous with the endoplasmic reticulum. In a similar way, calcium was found to be released into both the nucleus and the cytoplasm independently in response to osmotic, salt, and cold stress in Arabidopsis (Huang et al., 2017, Kelner et al., 2018). In the case of salt and cold stress, the nuclear calcium release was observed after the cytoplasmic calcium release However, the differences in the timings and amplitudes of the signals in the two compartments suggests that whilst the nuclear calcium release may have been triggered by the cytoplasmic calcium release, it is not simply a result of passive diffusion (Kelner et al., 2018). This reinforces the idea that the nuclear lumen can act as its own independent store of calcium which can be used for signalling. Nuclear calcium release has also been observed in response to L-glutamate (Costa et al., 2013), extracellular adenosine triphosphate (ATP) (Costa et al., 2013), both in Arabidopsis root cells, and pathogenic elicitors such as cryptogein and flagellin 22 in *Nicotiana tabacum* leaf cell suspensions (Lecourieux et al., 2005). However, without the use of both cytoplasmic and nuclear calcium reporters simultaneously, it is impossible to identify whether this nuclear calcium release is occurring independently, or if it is a result of diffusion from the cytoplasm.

Even if the exact mechanism of nuclear calcium release is not known, the presence of nuclear localised calcium binding proteins indicates the importance of calcium signalling in the nucleus. SHORT ROOT IN SALT MEDIUM 1 (RSA1) is one such calcium binding protein, that contains an EF hand calcium binding domain (Guan et al., 2013b). RSA1 was found to have roles in gene regulation in a wide range of contexts, including in salt stress tolerance, embryo development, and regulation of flowering time in Arabidopsis (Guan et al., 2013b, Zhang et al., 2020).

In addition to calcium release directly into the nucleus, calcium release into the cytoplasm can trigger shuttling of regulatory components to the nucleus, transducing the signal and influencing gene transcription. For example, nuclear retention of NLP7 is not only important in nitrate signalling (Liu et al., 2017), but also in response to cold stress in Arabidopsis. Phosphorylation by calcium activated CALCIUM DEPENDENT PROTEIN KINASE 28 (CPK28) maintains NLP7 in the nucleus, where it is involved in transcriptional reprogramming upon cold treatment (Ding et al., 2022). CALCIUM DEPENDENT PROTEIN KINASE 12 (CPK12) is translocated from the cytoplasm to the nucleus upon hypoxia stress conditions, where it interacts with and phosphorylated group VII ethylene responsive (ERF-VII) transcription factors (Fan et al., 2023). In addition, evidence for calcium responsive *cis*-elements in plant promoters highlights the importance of calcium in the regulation of gene transcription (Kaplan et al., 2006).

1.2 The establishment of endosymbiosis in land plants

Over 80% of land plant species, from all major lineages except mosses, form endosymbioses with arbuscular mycorrhizal (AM) fungi of the Glomeromycota and Mucoromycotina phyla (Wang and Qiu (2006), Bidartondo et al. (2011)). This endosymbiosis is one of the most globally and phylogenetically widespread and is of extreme ecological importance. It is hypothesised to have been crucial for the colonisation of land by formerly aquatic algae in the middle Cambrian–Early Ordovician interval, 400-450

million years ago (Morris et al. (2018), Pirozynski and Malloch (1975), Strullu-Derrien et al. (2014), Humphreys et al. (2010)). This is due to the fungi's branching hyphae that take up nutrients (including nitrates and inorganic phosphates) and water from the soil, and exchange it with the plant cells at tree-like structures called arbuscules (Pearson and Jakobsen (1993), Rich et al. (2021), Cliquet et al. (1997), Khalvati et al. (2005)). This increases the surface area of soil available to the plant, and in return, the plant provides the fungi with carbohydrates and lipids in a nutrient exchange (Solaimanand and Saito, 1997, Bago et al., 2003, Rich et al., 2021).

In addition to this, four related orders in the Eurosid clade of angiosperms (the Fagales, Fabales, Cucurbitales and Rosales) are able to form root endosymbioses with nitrogen fixing bacteria. Members of the Fagales, Rosales and Cucurbitales form associations with actinorhizal bacteria of the genus *Frankia*, while the *Fabaceae* (legume) plant family, which constitutes the majority of the Fabales order, form associations with rhizobia bacteria (Markmann and Parniske, 2009). The exception to this is the genus *Parasponia*, which is part of the Rosales clade but forms associations with rhizobia bacteria (Trinick, 1973). The interaction between legumes and rhizobia allows the plant to obtain fixed nitrogen from atmospheric nitrogen (N_2). The rhizobia enter the plant at the root hairs or through cracks in the epidermis, and are housed in oxygen-deprived root nodules, where they use the nitrogenase enzyme to fix N_2 to ammonia (Oldroyd and Downie, 2008).

The complex and intricate relationship between legumes and both rhizobia and AM fungi helps the plant to gain sufficient nutrients with a reduced need for external fertilisation, making them species of ecological, agricultural and economic importance (Vasconcelos et al., 2020). Nitrogen is an essential nutrient for plant growth, and its availability is often the primary factor that limits crop yields (Rosenblueth et al., 2018). However, only 30-50% total nitrogen in crop fields is derived from biological nitrogen fixation (BNF), with the rest being supplied in the form of expensive, inefficient and environmentally damaging nitrogen (N) fertilisers (Rosenblueth et al., 2018). Many species of

legume, such as the common bean *(Phaseolus vulgaris*), soybean (*Glycine max*), and pea (*Pisum sativum*), are used as food crops due to their protein-rich seeds and non-reliance on N fertilisers.

1.2.1 Overview of arbuscular mycorrhization development

AM fungi are obligate biotrophs, meaning that they require another living organism, in this case a plant, to complete their life cycle. Perception of the plant by the fungi (Section 1.2.2) helps to promote spore germination and hyphal branching (Akiyama et al., 2005), and perception of the fungi by the plant triggers nuclear calcium oscillations in the epidermal cell layer, priming the cells for fungal entry (Genre et al., 2013). Upon contact between the fungal hyphae and the root epidermal layer, a hyphopodium is formed that adheres to the surface of an atrichoblast cell (Parniske, 2008). This triggers the assembly of the pre-penetration apparatus, a specific complex of cytoplasm, in the underlying plant epidermal cell (Genre et al., 2005). This pre-penetration apparatus allows for the invasion of the epidermal cell layer by the fungi, and controls the direction of the fungal hyphae, ensuring the hyphae move inside the root towards the cortical cell layer (Genre et al., 2008). Here, the intraradical hyphae infect inner cortical cells and form highly branched hyphal structures called arbuscules. These arbuscules are key sites of bi-directional exchange of nutrients between the plant and the fungi, and they occupy the majority of the cell volume (Bonfante and Genre, 2010). They are enclosed by a plant-derived periarbuscular membrane (PAM), containing transporters to regulate the flux of nutrients (Javot et al. (2007), Harrison et al. (2002)). At later time points, the fungi develop storage organs called vesicles within the cortical cell layer, that are rich in lipids (Bach et al., 2018).

1.2.2 Symbionts release elicitors to initiate endosymbiotic signalling

The establishment of root endosymbioses with both AM fungi and rhizobia requires a complex series of physical and chemical interactions between the plant and the endosymbiont. Both species must undergo morphological transitions and significantly alter their gene expression profiles

to form a successful endosymbiosis. Some of the components involved in these early signalling events are used for the establishment of endosymbiosis with both AM fungi and rhizobia, in what is termed the 'common symbiosis pathway' (Figure 1.1). The chemical communication starts with the secretion of strigolactones and flavonoids by the plant as signalling molecules to kickstart the molecular 'conversation' with AM fungi and rhizobia respectively. In order to be perceived by the plant, AM fungi secrete Myc factors: a diverse group of lipochitooligosaccharides (LCOs) and chitooligosaccharides (COs) that induce a downstream signalling cascade in the plant (Maillet et al., 2011). In the case of rhizobia, the secreted plant flavonoids are detected and trigger the bacterial NodD transcription factor, which activates a cassette of common *nod* genes, resulting in the production of Nodulation (Nod) factors (Lerouge et al., 1990) (with one reported exception; Giraud *et al*., 2007). Nod factors are diffusible LCOs that activate diverse developmental responses in the plant. Both Nod and Myc factors have a conserved core structure of a chitin backbone, with an addition of an N-linked fatty acid group in LCOs (Oldroyd and Downie, 2008). The backbones are decorated with a variety of species-specific side groups that assist with partner selection. For example, the length and degree of saturation of the fatty acid group varies between rhizobia species, and this also contributes to the specificity of the interactions between the plant and the bacteria (Oldroyd and Downie, 2008).

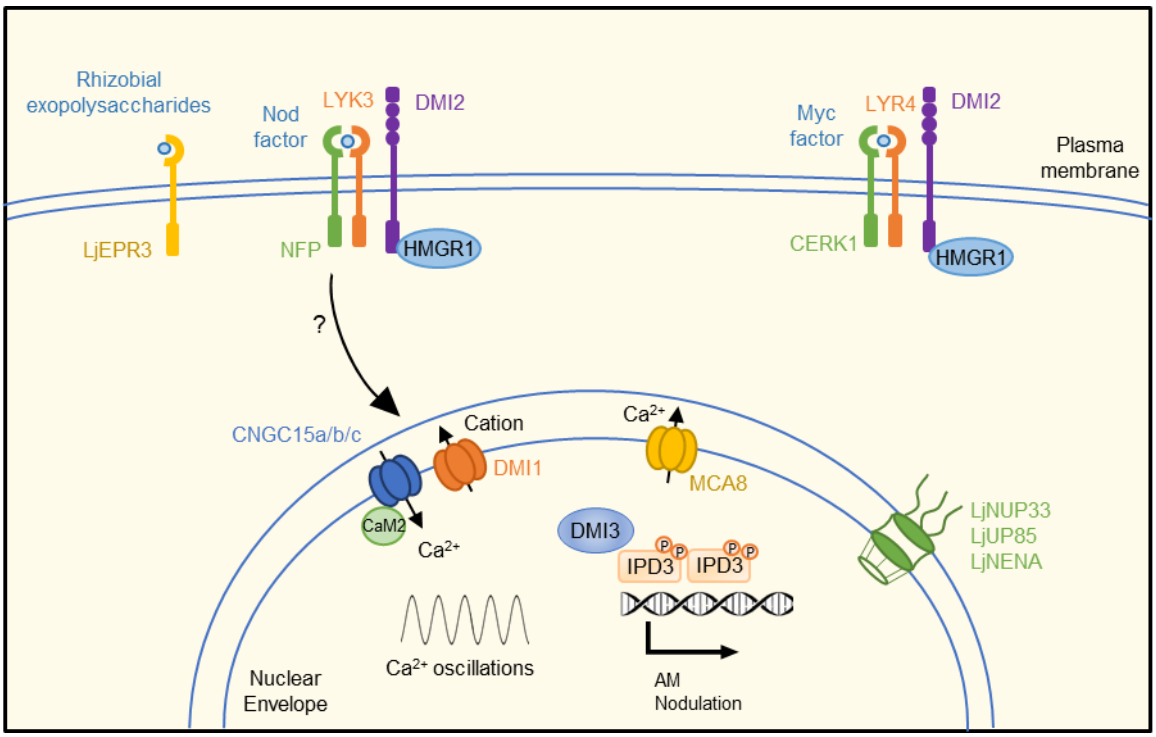


Figure 1.2 The common symbiosis pathway

Nod factor and Myc factor perception by the LysM receptors at the plasma membrane trigger nuclear calcium oscillations mediated by CNGC15s, DMI1 and MCA8. The exact mechanism for transduction of the signal from the plasma membrane to the nucleus is yet to be defined. Calcium oscillations are perceived by DMI3. DMI3 phosphorylates IPD3, which acts as a homodimer to activate the expression of genes required for AM symbiosis and nodulation. See text for full gene names. Gene names are for *Medicago truncatula* unless otherwise stated.

1.2.2 Perception of elicitors by plants

Nod factors are perceived at the plant plasma membrane by receptor-like kinases (RLKs) that have a *N*-acetyl-glucosamine–binding lysin motif (LysM) in their extracellular domain (Mulder et al., 2006). In Medicago, the Nod factor receptors are LysM RECEPTOR KINASE 3 (LYK3) and NOD FACTOR PERCEPTION (NFP) (Limpens et al. (2003), Madsen et al. (2003) Arrighi et al. (2006), Haney et al. (2011), Smit et al. (2007), Moling et al. (2014)), whose orthologs in *L. japonicus* have been shown to directly bind to LCOs produced by rhizobia bacteria (Broghammer et al., 2012). These receptors help to determine the specificity of the interaction, as Medicago transformed with the *L. japonicus* Nod Factor Receptors 1 and 5 (*LjNFR1/5*) are able to perceive the natural symbiont of *L. japonicus* (*Mesorhizobium loti*) as well as its own

symbiont (*Sinorhizobium meliloti*) (Radutoiu et al., 2007). In addition to LYK3 and NFP, the receptor-like kinase DOES NOT MAKE INFECTIONS (DMI2) in Medicago (SYMBIOTIC RECEPTOR LIKE KINASE (SYMRK) in *L. japonicus*) is indispensable for endosymbiosis with AM and rhizobia (Stracke et al., 2002, Endre et al., 2002, Ané et al., 2002), although its precise role remains to be elucidated. In *L. japonicus*, knocking out SYMRK results in no development of infection pockets or threads (Stracke et al., 2002), whilst overexpression results in spontaneous nodulation in the absence of rhizobia (Ried et al., 2014). SYMRK contains three leucine rich repeat (LRR) domains and one malectin-like domain (MLD) in its extracellular domain, and a kinase domain in its intracellular domain (Stracke et al., 2002, Hok et al., 2011). It can associate with NFR1 and NFR5 *in planta*, and its association appears to be partly dependent on the cleavage of the extracellular domain (Antolín-Llovera et al., 2014, Ried et al., 2014). Consistent with this, transformation of Medicago *dmi2* mutants with only the intracellular domain of DMI2 was able to induce spontaneous nodulation in the absence of rhizobia (Saha et al., 2014). Another LysM-RLK EXOPOLYSACCHARIDE RECEPTOR 3 (EPR3) identified in *Lotus* recognises rhizobia exopolysaccharides, rather than Nod factors, indicating the presence of an additional symbiotic signal that can be recognised to facilitate infection (Kawaharada et al., 2015, Kawaharada et al., 2017).

Recognition of Myc factors by Medicago requires several LysM-RLKs, including the CHITIN ELICITOR RECEPTOR KINASE 1 (MtCERK1) and the LYSM RECEPTOR 4 (MtLYR4) which are receptors of the chitooligosaccharide CO8, and NFP, which may perceive LCOs from fungi as well as rhizobia bacteria (Feng et al., 2019). MtCERK1 and MtLYR4 have dual functionality in both symbiosis and immunity signalling, and the specificity of its role is determined by the presence or absence of MtDMI2, respectively, in the complex (Feng et al., 2019). This is similar to the situation identified in rice, where the CO receptors MYC FACTOR RECEPTOR 1 (OsMYR1) and CHITIN ELICITOR BINDING PROTEIN (OsCEBiP) compete for OsCERK1, conferring symbiosis or immunity signalling respectively (He et al. (2019); Zhang et al. (2021)).

1.2.3 Signal transduction from the plasma membrane to the nucleus

Perception of Nod or Myc factors ultimately results in the production of regular Ca^{2+} spikes in the nucleus, known as nuclear calcium oscillations. These oscillations drive changes in gene expression which are required for AM or rhizobial colonisation. The generation of nuclear calcium oscillations requires three nuclear pore complex proteins, LjNUCLEOPORIN85 (LjNUP85), LjNUP133 and LjNENA, that were identified through genetic screens of symbiosis defective mutants of *L. japonicus*. *nup133* mutants have reduced nodulation at 22°C and no nodulation at 26°C, no AM colonisation, and no nuclear calcium spiking upon addition of Nod factor (Kanamori et al., 2006). *nup85* mutants form few nodules and arbuscules, and the AM phenotype is temperature sensitive, with lower arbuscule formation at 22°C compared to 18°C. *nup85* mutants also fail to produce nuclear calcium oscillations (Saito et al., 2007). NENA was shown to interact with NUP85, and *nena* mutants do not produce calcium oscillations. They display reduced nodulation and premature abortion of hyphal progression, failing in most cases to reach the cortical cell layer (Groth et al., 2010). The nodulation and AM phenotypes were also temperature sensitive, with reduced colonisation observed at higher temperatures, similar to *nup133* and *nup85* (Groth et al., 2010). This suggests that the nuclear pore complex is required for the generation of nuclear calcium oscillations and subsequent endosymbiosis, potentially by transporting a secondary messenger from the cytoplasm to the nucleoplasm.

One candidate secondary messenger is mevalonate (MVA). 3-hydroxy 3-methylglutaryl CoA reductase 1 (HMGR1) is an enzyme in the MVA pathway that catalyses the conversion of HMG-CoA to MVA. RNA interference (RNAi) based silencing of *HMGR1* in Medicago reduces nodule development, prevents nuclear calcium oscillations and results in decreased expression of *EARLY NODULIN 11* (*ENOD11)*, an early nodulation gene frequently used in as a marker of early symbiosis signalling. In addition, the product of HMGR1 activity, MVA, appears to restore calcium oscillations in HMGR1-silenced roots

(Venkateshwaran et al., 2015). Therefore, MVA could be involved in the signal transduction from the plasma membrane to the nuclear envelope.

Another described signal transduction mechanism involves G protein signalling. Heterotrimeric G proteins are formed of Gα, Gβ, and Gγ subunits and are used widely in signalling across eukaryotes. Their widespread and complex roles in animals have been well described (Wettschureck and Offermanns, 2005; Syrovatkina et al., 2016), and they have several described roles in plants, including in immunity and development (Wu et al. (2020); Ninh et al. (2021)). In legumes, nodulation gene expression can be induced by the G protein agonist mastoparan independently of DMI1 and DMI2 (Charron et al., 2004). In addition, nuclear calcium oscillations can be induced by the synthetic analogue of mastoparan Mas7, and this activation does not require DMI1, DMI2 or NFP, implicating a role of G protein signalling in activating the nuclear calcium oscillations without DMI1 or Nod/Myc factor perception (Sun et al., 2007).

Gα proteins cycle between resting and activated states depending on whether they are bound to guanosine diphosphate (GDP) or guanosine triphosphate (GTP), respectively. Activated GTP-bound Gα dissociates from the Gβγ heterodimer, freeing both entities to interact with downstream signalling components. Gα has an innate, but slow, GTP hydrolysis activity which is accelerated by GTPase activity accelerating proteins (GAPs) such as the REGULATOR OF G-PROTEIN SIGNALLING (RGS) proteins and Phospholipase C (PLC) enzymes. Hydrolysis of GTP to GDP returns Gα to its inactive state, where it reforms the heterotrimer with Gβγ (Mohanasundaram and Pandey, 2022).

An investigation of the roles of G protein signalling in legumes revealed differential expression of certain G protein subunits in soybean (*Glycine max*) upon infection with the native symbiont *Bradyrhizobium japonicum.* In addition, downregulation or upregulation of G protein subunits was found in nonnodulating or supernodulating soybean mutants respectively, suggesting that expression level of G proteins is important for nodule development (Choudhury and Pandey, 2013). Overexpression of particular Gβ and Gγ subunits led to increased nodule numbers (Choudhury and Pandey, 2013),

indicating they are positive regulators of nodulation, whilst Gα was identified as a negative regulator of nodulation via RNAi and overexpression analyses (Choudhury and Pandey, 2015). In addition, RNAi and overexpression analyses showed that the soybean RGS1 and 2 proteins are positive regulators of nodulation, and that this regulation is dependent on its GAP activity (Choudhury and Pandey, 2015).

Interestingly, Gα1, RGS1, and RGS2 were found to interact with NFR1α *in planta* (Choudhury and Pandey, 2013, Choudhury and Pandey, 2015). NFR1α was shown to phosphorylate RGS1 and 2, but not Gα1 *in vitro*, and expression of phosphomimetic RGS2 increased its GAP activity on Gα1 and restored some nodulation in a non-nodulating mutant background (Choudhury and Pandey, 2015).

Whilst RGS 1 and 2 are phosphorylated by NFR1α, Gα1 is phosphorylated by the soybean *GmSYMRKα in vitro* (Roy Choudhury and Pandey, 2022). This phosphorylation was found to inhibit the ability of Gα1 to bind to both GTP and Gβγ, thus making it biochemically inactive and freeing the Gβγ heterodimer to transduce a downstream signal. Expression of phosphomimetic Gα1 increases the number of soybean nodules, presumably by freeing Gβγ to promote nodulation (Roy Choudhury and Pandey, 2022). These findings suggest that G-protein signalling is being controlled by a pair of RLKs, NFR1 and SYMRK, in a two-step signalling mechanism that can fine tune the activation of G protein subunits (Figure 1.3). The action of NFR1 phosphorylating RGS1/2 maintains Gα1 in its inactive GDP-bound state. This would normally sequester the positive regulator of nodulation, Gβγ, in a heterotrimer. However, the action of SYMRKs phosphorylating Gα abolishes this binding, leaving the Gβγ component free to induce nodulation (Figure 1.3).

The role of G protein signalling in Medicago has also been investigated. Medicago Gβ1 was found to be a positive regulator of nodulation, like its soybean counterpart, as reducing its expression via RNAi resulted in fewer nodules, and a decreased expression of early symbiotic marker genes (Bovin et al., 2021).

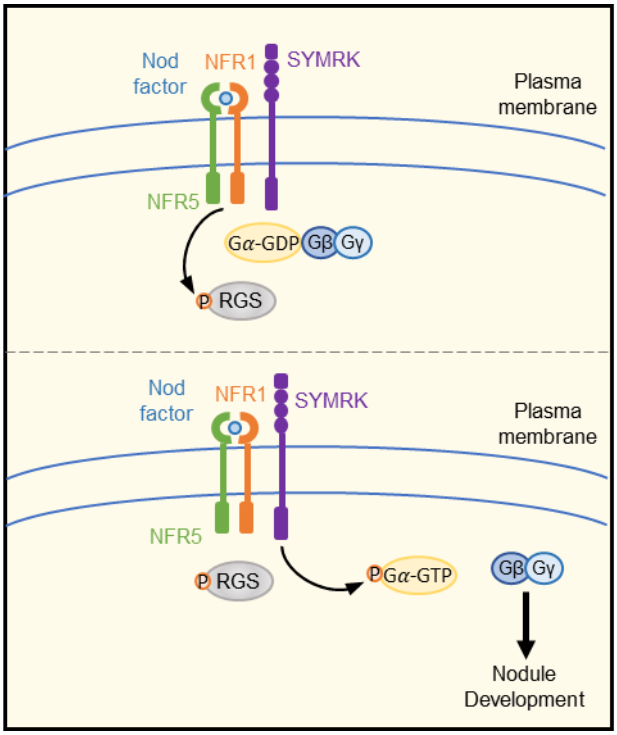


Figure 1.3 The role of G protein subunits in early endosymbiosis signalling upon Nod factor perception in *Lotus japonicus*.

Nod factor perception by the LysM receptors NFR1 and NFR5 results in the phosphorylation of RGS by NFR1. This activates the GTPase accelerating properties of RGS, converting GDP-bound G*α* to GTP-bound G*α*, which sequesters the Gβγ subunits in a heterotrimer. Nod factor perception also results in the phosphorylation of G*α*-GTP by SYMRK, causing a release of the Gβγ subunits, which subsequently promote nodule development. See text for full gene names. Gene names are for *Lotus japonicus*.

1.2.4 Generation of nuclear calcium oscillations

In both rhizobial and AM symbiosis, perception of Nod and Myc factors at the plasma membrane results in the generation of nuclear calcium oscillations. In Medicago, the channels required to generate such oscillations are the non-selective cation channel DOES NOT MAKE INFECTIONS 1 (DMI1) (Ané et al., 2004), the calcium-dependent adenosine triphosphatase *M. truncatula* CALCIUM ATPASE (MCA8) (Capoen et al., 2011), and the CYCLIC NUCLEOTIDE GATED CHANNEL (CNGC) 15a, b and c (Charpentier et al. (2016)). Although Medicago only requires *DMI1* to encode the non-selective cation channel, many land plants require two *DMI1* paralogues, such as *POLLUX* and *CASTOR* in *L. japonicus* (Imaizumi-Anraku et al. (2005); Charpentier et al. (2008)). The CNGC15 calcium channel is encoded by three

homologous genes, all of which are required for full activation of nuclear calcium oscillations and reside on the nuclear envelope, where they are hypothesised to be arranged in a complex (Charpentier et al., 2016). The current model suggests that DMI1 and CNGC15 are simultaneously activated by an undefined secondary messenger which allows Ca^{2+} release into the nucleoplasm from the nuclear membrane lumen, and a counter-flow of cations by DMI1 in the opposite direction. This is supported by mathematical modelling and evidence that DMI1 interacts with all three CNGC15s in the nucleus (Charpentier et al., 2016). CNGC15s were found to interact with holo-CaM2 in Medicago root hairs, and was found to regulate the calcium oscillations by facilitating the closure of the CNGC15 tetramer once the calcium had been released (Del Cerro et al., 2022).

Generation of nuclear calcium oscillations activates the nuclear Calcium-Calmodulin Kinase (CCaMK) MtDMI3/LjCCaMK, causing it to phosphorylate the transcription factor INTERACTING PROTEIN OF DMI3 (MtIPD3/LjCYCLOPS), providing a link between calcium spiking and regulation of transcription (Lévy et al. (2004); Mitra et al. (2004); Yano et al. (2008); Singh et al. (2014); Jin et al. (2018)). A range of other transcription factors such as NODULATION SIGNALLING PATHWAY 1 and 2 (NSP1/2) (Hirsch et al., 2009) and REDUCED ARBUSCULAR MYCORRHIZATION 1 (RAM1) (Pimprikar et al., 2016) are consequently activated, with RAM1 involved in AM symbiosis (Gobbato et al., 2012), and NSP1/2 involved in both AM and rhizobial symbioses (Maillet et al. (2011); Delaux et al. (2013); Lauressergues et al. (2012)).

1.2.5 The regulation of nodulation in legumes by nutrient status.

The establishment of endosymbiosis is energetically expensive, as it requires a restructuring of the root tissue to accommodate the endosymbiont, as well as supplying the endosymbiont with fixed carbon and lipids. As a result, plants need to regulate the degree to which they are colonized by arbuscular mycorrhizal (AM) fungi or rhizobia bacteria depending on the nutrient status of the plant. For example, nodulation, which provides the plant with nitrogen (N) in the form of ammonia by biological nitrogen fixation, is negatively

regulated by nitrate and ammonia (Streeter and Wong, 1988).When nitrate is abundant, legumes exhibit decreased nodulation, indicating a method of systemic nitrogen signalling (Roy et al., 2020). In addition, very few infection events result in the formation of a nodule, so the plants must have a mechanism of sensing the degree of root colonization and aborting nodules where necessary (Oldroyd & Leyser, 2020).

The regulation of nodulation in response to nitrate availability is carried out by several signalling pathways. Legumes have evolved the autoregulation of nodulation (AON) pathway, a complex and interconnected signalling network that allows the plant to control the degree to which it is nodulated in response to different environmental conditions. In Medicago, the CLE (Clavata3/ESR) peptides CLE12 and CLE13 (CLE-RS1/2/3 in L. japonicus) are produced in the root in response to rhizobial infection and travel to the shoot where they are perceived by MtSUNN (HAR1 in L. japonicus), a receptor-like kinase (RLK). This results in downregulation of the production of miR2111, a shoot-derived miRNA, which acts as a shoot-to-root signal. miR2111 targets and silences the negative regulators of nodulation TOO MUCH LOVE 1 (TML1) and TML2 in the roots. Therefore, a decrease in miR2111 expression in response to rhizobia results in increased activity of TML1 and TML2, which causes nodulation to be inhibited. In the absence of rhizobia, miR2111 is not downregulated, so can silence TML1 and TML2 and maintain the root competency for nodulation. In addition, cytokinin signalling has also been implicated as a shoot-to-root signal regulating TML1/2 (Roy et al., 2020).

1.2.6 The regulation of mycorrhization by phosphate

The establishment of AM symbiosis is negatively regulated by both inorganic phosphate (Pi) and N (Azcón et al., 1982, Hepper, 1983, Thomson et al., 1986, Trinick, 1977).Knockdown lines of AM-specific phosphate transporters (PTs) display early termination of AM symbiosis (Javot et al., 2007, Maeda et al., 2006), suggesting a mechanism to sense the amount of phosphate being transported from the fungus, and sustain the symbiosis accordingly. For example, knockdown of *Lotus japonicus PHOSPHATE TRANSPORTER 3 (PT3)*

caused a reduction in the number of arbuscules (Maeda et al., 2006), and knocking down (via RNA interference, RNAi) or removing the phosphate transport function of *Medicago truncatula PHOSPHATE TRANSPORTER 4 (PT4)* leads to infrequent, degenerating arbuscules, and low levels of colonisation (Javot et al., 2007). In addition, the arbuscules showed premature collapse and degeneration in *MtPT4* knockdown and knockout lines, indicating premature abortion of symbiosis, presumably related to the reduced Pi uptake by the plant (Javot et al., 2007). This suggests that the repression of these phosphate transporters by Pi is a cause, rather than a consequence, of arbuscule degeneration. To determine the sequence of events, Breuillin et al. (2010) treated AM colonised *Petunia hybrida* (Petunia) with 5mM KH_2PO_4 (high Pi) and monitored the effect on AM colonisation and *PHOSPHATE TRANSPORTER 5* (*PhPT5)* expression. They found that downregulation of *PhPT5* occurred 4 days post treatment, whereas a decline in AM colonisation was not observed until 14 days post treatment (Breuillin et al., 2010). This indicates that Pi is regulating the maintenance of AM symbiosis, potentially mediated via AM specific PTs.

Further evidence that phosphate transporters could be essential to sustain plant-beneficial fungal interaction came from the observation that the *Arabidopsis thaliana PHOSPHATE TRANSPORTER (PHT) 1.2* and *1.3* are required for the maintenance of the symbiosis between Arabidopsis and the root endophyte *Colletrotrichum tofieldiae* (Hiruma et al., 2016). Although *C. tolieldiae* is not an AM fungus, it does supply Arabidopsis with Pi via hyphae specifically under phosphate starvation conditions, promoting plant growth by increasing root length and shoot fresh weight. This colonisation increased expression levels of *AtPHT1.2* and *AtPHT1.3*, and the promotion of plant growth by *C. tolieldiae* was diminished in the *phosphate transporter traffic facilitator 1* (*phf1)* mutant impaired in phosphate uptake (González et al., 2005) and *phosphate starvation response 1* (*phr1)* and *phr1-like (phl1)* double mutant impaired in the phosphate starvation response (Bustos et al. (2010); Hiruma et al. (2016)). Interestingly, *C. tolieldiae* biomass, assessed via qPCR, was increased in both *phf1* and *phr1 phl1* under low Pi conditions, indicating that normal

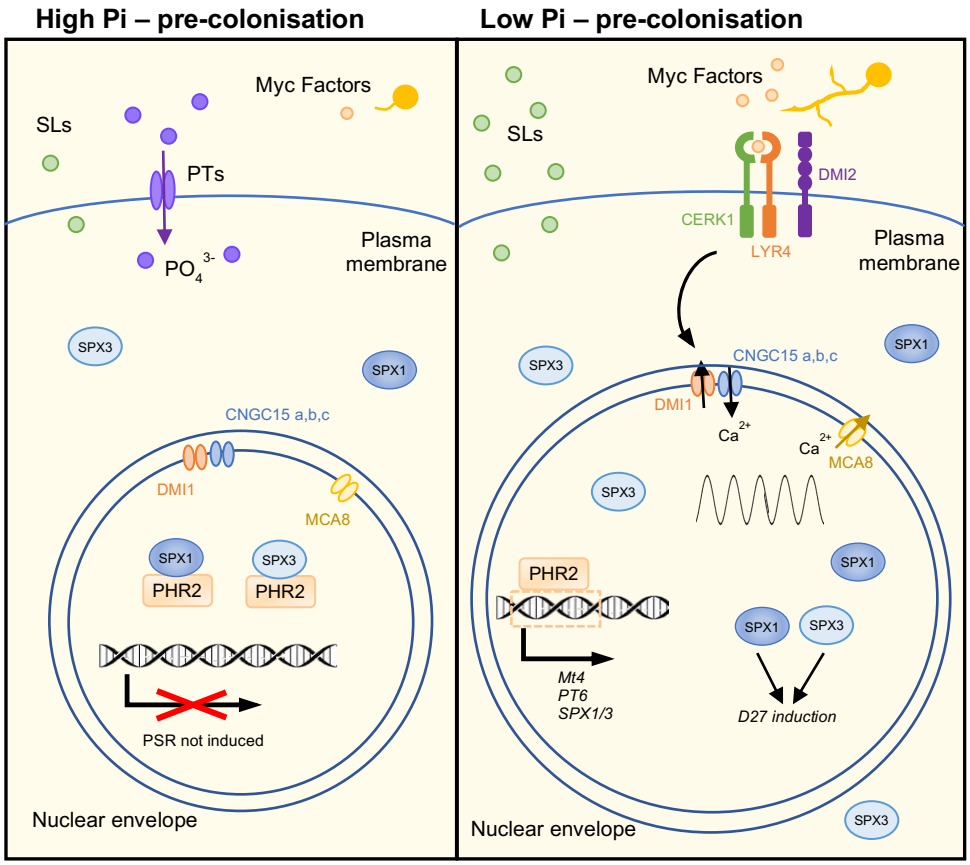
phosphate starvation response (PSR) is required to regulate colonisation under phosphate starvation. This suggests that components of the PSR pathway, such as *PHR* and *SYG1/PHO81/XPR1 DOMAIN (SPX)* genes that have well described roles in Pi signalling and homeostasis (Lv et al., 2014), are implicated in the regulation of Pi uptake from symbionts. In accordance with this, PSR components such as Medicago *PHOSPHATE 1* (*MtPHO1)* gene family members and *LjPHR1* have been shown to regulate Pi homeostasis in Medicago and *L. japonicus* nodules respectively (Lu et al., 2020, Nguyen et al., 2020).

The first evidence for the roles of *PHR*s in the regulation of AM by Pi was carried out in rice, where it was found that *Oryza sativa* PHR1/2/3 bound to the promoters of many known AM related genes at the PHR1 binding sequences (P1BS) (Shi et al., 2021). The P1BS is a motif present in the promoters of many Pi regulated genes, that confers binding, and therefore regulation, by PHRs (Rubio et al., 2001). In addition, SPX proteins, that are implicated in rice phosphate starvation response by binding to and inhibiting PHRs, were also implicated in the phosphate dependent regulation of AM symbiosis. OsSPX1 suppressed OsPHR2 mediated activation of the promoters of *REDUCED ARBUSCULAR MYCORRHIZATION 1 (RAM1), WRINKED 5 (WRI5)* and *PHOSPHATE TRANSPORTER 11 (PT11)*, and overexpression of *OsSPX1* and *OsSPX2* significantly reduced AM colonisation in rice roots (Shi et al., 2021). In agreement, *OsPHR2* stimulates AM by activating expression of AM related genes, and this role is conserved in *Lotus japonicus* (Das et al., 2022). The proposed model in rice is that SPXs perceive Pi by binding to inositol polyphosphates (PP-InsPs) (Jung et al., 2018). This causes SPXs to bind to PHRs and inhibit them, either by inhibiting their direct binding to the P1BS domain (Wang et al., 2014), or by inhibiting their translocation to the nucleus (Hu et al., 2019). In low Pi conditions, SPXs are degraded, lifting this repression which allows for the activation of PHR-regulated genes, such as *CAROTENOID CLEAVAGE DIOXYGENASE 7* (Os*CCD7)*, required for strigolactone biosynthesis that induces spore germination and hyphal branching, and components of the common symbiotic pathway such as Os*CERK1* and Os*SYMRK* (Das et al., 2022).

In Medicago, it was found that *MtSPX1* and *MtSPX3* were induced upon Pi starvation in both uninoculated and inoculated roots (Wang et al., 2021a). This contrasts with the situation in rice, where OsSPX4 has been shown to be degraded in Pi starvation conditions (Lv et al., 2014). MtSPX1 and 3 were found to be localised in the cytoplasm and the nucleus, and in inoculated plants they were preferentially expressed in arbuscule containing cells. They were both found to interact with MtPHR2 specifically in high Pi conditions (Wang et al., 2021a). Analysis of knock out mutant lines reveal that MtSPX 1 and 3 are involved in the regulation of arbuscule degeneration, as *spx1,3* plants had fewer degrading arbuscules (Wang et al., 2021a). Interestingly, their promoters contain P1BS domains, indicating that as well as regulating the activity of PHR2, they themselves are also regulated by PHRs (Wang et al., 2021a). This suggests a potential feed-forward regulation mechanism to fine tune the levels of SPX depending on the Pi and colonisation status of the plant. Finally, *DWARF27* (*D27)*, involved in strigolactone biosynthesis and usually upregulated upon Pi starvation (Liu et al., 2011) was not upregulated in Pi starvation conditions in *spx1/3*. This suggests a positive role of SPX1 and 3 in strigolactone biosynthesis in Medicago. This contrasts with the situation in rice, where it is OsPHR2 that induces the strigolactone biosynthesis gene *CCD7,* and OsPHR2 is negatively regulated by SPXs (Das et al., 2022). A full picture of the roles of SPXs in both rice and Medicago has not been elucidated yet, especially in Medicago, where only SPX1 and 3 have been described. Therefore, further research could assist our understanding of these differences in PHR-SPX pathways between species. Figure 1.4 summarises the known roles of Medicago SPXs in regulating colonisation and arbuscule degradation depending on Pi status.

In addition to the PHR-SPX pathway, gibberellic acid (GA) signalling has also been implicated in the regulation of AM by phosphate. The phytohormone GA regulates the degradation of DELLA proteins, as their binding to GA receptors triggers polyubiquitination and degradation by the 26S proteasome pathway (Davière and Achard, 2013). GA and DELLAs have different effects on different parts of AM colonisation. For example, GA has a negative effect on arbuscule formation, as the induction of *RAM1* requires

DELLAs (Floss et al., 2013, Pimprikar et al., 2016). In contrast, GA has a positive effect on hyphal branching (Takeda et al., 2014). Gene expression analysis of GA and AM related genes in Petunia revealed that Pi treatment reduced the expression of both GA and AM related genes. In contrast, GA treatment transiently induced AM related genes (Nouri et al., 2021). Overexpression of Arabidopsis *GIBBERELLIN METHYLTRANSFERASE 1* and *2* (*AtGAMT1* and *2)* in transgenic Tobacco plants lead to faster AM colonisation under low Pi, and less reduction of AM colonization in high Pi. This is consistent with the role of GA as a negative regulator of AM, which is induced upon phosphate treatment (Nouri et al., 2021).



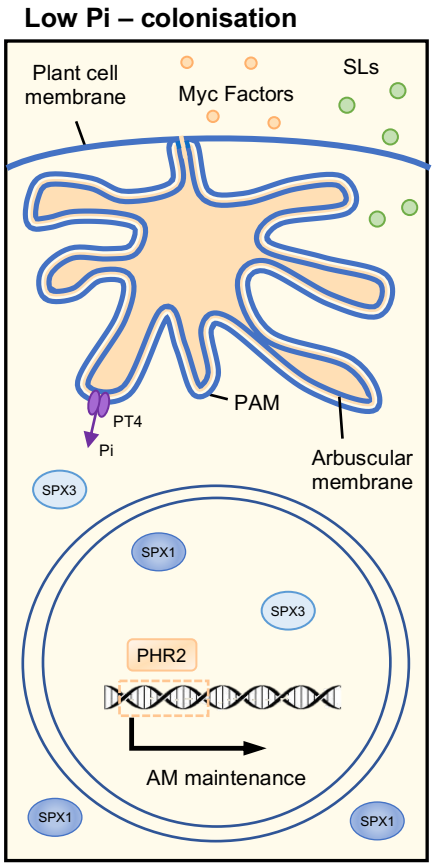


Figure 1.4. Summary model of the SPX/PHR mediated regulation of AM colonisation under different phosphate conditions in Medicago.

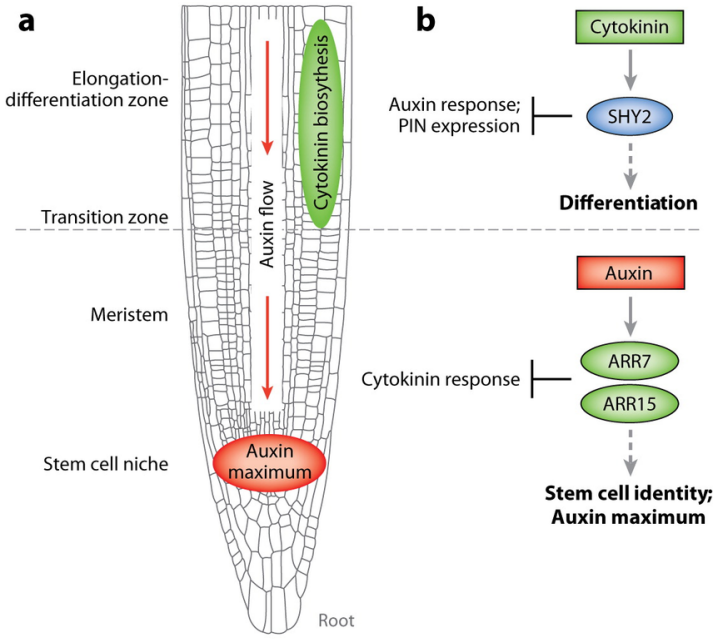
Phosphate is taken up at the plasma membrane by phosphate transporters (PTs). SPX DOMAIN (SPX) 1 and 3, which localise to the cytosoplasm and nucleus, bind to PHOSPHATE STARVATION RESPONSE 2 (PHR2) specifically under high phosphate conditions, preventing it from binding to P1BS domains and initiating the phosphate starvation response (PSR). Under low phosphate conditions, SPX1 and 3 do not bind to PHR2, enabling the induction of PSR genes. In addition, SPX1 and 3 act in an unknown pathway to induce *D27,* thus increasing the production of strigolactones (SLs). These stimulate hyphal branching and Myc factor production in the fungi, leading to early symbiosis signalling and the induction of nuclear calcium oscillations. Once the plant has been colonised, SPX 1 and 3 are involved in the regulation of arbuscule degeneration, by monitoring the phosphate uptake through periarbuscular membrane (PAM) phosphate transporters such as PT4. Wang et al., (2021)c.

1.3 *Arabidopsis thaliana* root development and the role of calcium

1.3.1 Overview of *Arabidopsis thaliana* root development

In plants, all post-embryonic primary root tip growth takes place at the root apical meristem (RAM), where new cells are generated by mitosis. The RAM is divided into multiple zones, each containing different cell types. Stem cells are maintained at the quiescent centre (QC) where they divide and produce daughter cells. These daughter cells divide and differentiate in the stem cell niche (SCN) surrounding the QC, giving rise to the different root cell files. Differentiated cells move upwards and continue to divide in the region known as the proximal meristem (PM). Further up the root in the elongation zone (EZ), cells are elongating rather than dividing. The transition zone (TZ) describes the region between the PM and the EZ where cells are transitioning from division to elongation (Svolacchia et al., 2020).

Preserving a balance between cell division and elongation is essential for RAM maintenance. The phytohormones auxin and cytokinin are key players in the maintenance of this balance (Dello Ioio et al., 2007, Ioio et al., 2008, Müller and Sheen, 2008), although other plant hormones, such as gibberellin (Moubayidin et al., 2016, Ubeda-Tomás et al., 2009), ethylene (Street et al., 2015), and abscisic acid (Sun et al., 2018) also play a role. In canonical auxin signalling, high levels of auxin at the QC promote degradation of Aux/IAA (indole-3-acetic acid) transcription factors by a Skp, Cullin, F-box containing (SCF) complex, $SCF^{TIR1/AFB}$. In this complex, the TRANSPORT INHIBITOR1/AUXIN-SIGNALLING F BOX (TIR1/AFB) family of F-box proteins act as auxin receptors, activated by auxin to facilitate the ubiquitination and subsequent degradation of Aux/IAA transcription factors. This lifts the repression on auxin responsive genes (Kepinski and Leyser, 2005, Maraschin Fdos et al., 2009, Boer et al., 2014).



Chapman EJ, Estelle M. 2009.
Annu. Rev. Genet. 43:265–85

Figure 1.5 The balance between auxin and cytokinin levels in the Arabidopsis primary root tip maintains meristem size and root growth.

Auxin concentration is at a maximum at the stem cell niche, lifting the repression of auxin responsive genes, leading to the maintenance of stem cell identity and cell division. Here, cytokinin biosynthesis is repressed by ARR7 and ARR15. At the elongation zone, cytokinin biosynthesis facilitates cell elongation rather than division, and activates SHY2, leading to downregulation of PINs and reduced auxin expression. Figure taken from Chapman & Estelle, 2009.

Auxin and cytokinin act antagonistically to control cell division and cell differentiation in the root meristem. This interaction involves a regulatory circuit mediated by SHORT HYPOCOTYL 2 (SHY2), which is a member of the Aux/IAA family (Ioio et al., 2008). Auxin is in high concentration at the PM, where it activates auxin response genes via auxin response factors (ARFs). This maintains auxin transport via PIN-FORMED (PIN) proteins, promotes cell division, and leads to degradation of SHY2 by SCF^{TIR1} (Ioio et al., 2008, Dos Santos Maraschin et al., 2009). It also activates AUXIN RESPONSE REGULATOR (ARR) 7 and 15, which are negative regulators of cytokinin signalling. In contrast, cytokinin signalling is controlled by Arabidopsis Histidine Kinases (AHKs) that activate Arabidopsis Response Regulators

(ARRs) to induce target gene expression (Hwang and Sheen, 2001, To et al., 2004). For example, in the TZ, cytokinin activates SHY2 via a two-component system of ARABIDOPSIS HISTIDINE KINASE 3 (AHK3) and ARABIDOPSIS RESPONSE REGULATOR 1 (ARR1). This promotes expression of cytokinin responsive genes and downregulation of PIN proteins, resulting in suppressed cell division and promotion of differentiation and polyploidy (Moubayidin et al., 2009). Figure 1.5 highlights the zones of the Arabidopsis primary root, and the role of auxin and cytokinin in balancing cell division versus differentiation in these different zones.

Lateral root development is also regulated by gradients of auxin and cytokinin. During lateral root development, cell divisions in the pericycle produce the daughter cells that create the lateral root primordium (Malamy and Benfey, 1997). This cell division is initiated by auxin, which activates the IAA14-ARF7-ARF19 signalling module (Fukaki et al., 2002, Okushima et al., 2005). ARF7 and ARF19 then activate transcription factors such as LATERAL ORGAN BOUNDARIES DOMAIN (LBD) 16 and 29, important for maintaining cell polarity and lateral root initiation (Okushima et al., 2007). Following the initial cell divisions in the pericycle, repeated divisions of primordia cells create a larger primordia that is able to push through the overlying primary root tissues (Malamy and Benfey, 1997). As with primary root development, cytokinin antagonises auxin during lateral root development. It acts as a negative regulator and controls the regular spacing between lateral root primordia (Chang et al., 2015).

1.3.2 The role of calcium ions in Arabidopsis primary root development

Calcium signalling plays several roles in primary root development, partially by influencing auxin signalling. The level of cytosolic calcium in root cells, including root hair cells, has been shown to impact their elongation and subsequently the overall root length (Schiefelbein et al., 1992; Bibikova et al., 1997; Wymer et al., 2002; Chen et al., 2006; Bai et al., 2009). Auxin triggers extracellular pH changes, membrane depolarisation and calcium influx, which is dependent on the TIR1/AFB-Aux/IAA nuclear auxin perception (Monshausen

et al., 2011, Fendrych et al., 2016). In roots, root bending redirects auxin to the lower side of the root via PIN proteins, causing increased cytosolic calcium and extracellular alkalization. Auxin inhibits cell expansion, leading to downward root bending and gravitropism. *cngc14* knockout mutants do not display this cytosolic calcium increase on the lower side, and alkalization is delayed, resulting in defects in gravitropism (Shih et al., 2015). *cngc14* has a more acidic root surface, and a loss of the alkaline domain at the TZ that is important for gravitropism. This alkaline domain at the TZ was found to be dependent on AUX1, AFB, and CNGC14, highlighting the importance of calcium influx and signalling in root development (Serre et al., 2023). In root hairs, the calcium response to auxin is also dependent on CNGC14, as well as auxin influx by AUX1, and perception by the $SCF^{TIR1/AFB}$ complex (Dindas et al., 2018).

In addition to CNGC14, CNGC2 and 4 also play a role in modulating auxin homeostasis. This was identified from the observation that the *yucca6* (*yuc6*) knockout mutation in a *cngc2* background can mask *cngc2* phenotypes, including reduced gravitropism, which is a hallmark of perturbed auxin homeostasis (Chakraborty et al., 2021). *YUCCA6* encodes a component of the auxin biosynthesis pathway, and *cngc2* and *cngc4* display a hyperaccumulation of IAA (Chakraborty et al., 2021). Potentially this hyperaccumulation is compensated by *yuc6*, restoring wild type phenotypes. Like CNGC14, CNGC2 was found to be required for auxin induced calcium signalling and TIR1/AFB signalling (Chakraborty et al., 2021). It would be tempting to predict that these components from a heterotetramer at the plasma membrane responsible for the cytosolic calcium influx upon auxin perception, however given the pleiotropic effects of *cngc2* are not observed in *cngc14*, it may be more likely that these components are acting independently. Potentially the calcium influx mediated by CNGC2 and CNGC4 is involved in regulating auxin biosynthesis via YUC6, while CNGC14 mediates calcium influx upon auxin treatment.

Following cytosolic calcium influx, the action of calcium binding proteins enables the signal to be decoded and responded to. In the context of auxin signalling in primary root development, CA^{2+}-DEPENDENT MODULATOR OF ICR1 (CMI1) was identified as an EF-hand containing protein

with functions in root development. *cml1* knockout plants have shorter primary roots and smaller meristems, caused by reduced auxin levels in the QC. CML1 was found to be induced by auxin in a TIR1/AFB dependent mechanism (Hazak et al., 2019).

Downstream of calcium binding proteins, there is a complex network of interacting proteins, often with kinase activity, that are involved in decoding the signals. CBL-INTERACTING PROTEIN KINASE 25 (CIPK25) is positively regulated by auxin, and negatively regulated by cytokinin. *cipk25* knockout plants display shorter root lengths due to reduced RAM size and reduced auxin transport, and are less responsive to auxin mediated root growth retardation, whilst overexpression of *CIPK25* results in longer root lengths and increased expression of auxin related genes (Kumar Meena et al., 2018). CIPK25 was found to act as an active kinase in yeast, and interact with the calcium binding CALCINEURIN B-LIKE 4 and 5 (CBL4 and CBL5) in *N. benthamiana* leaves by BiFC. The short root phenotype of *cipk25* can be complemented by loss of *SHY2*, suggesting that *CIPK25* is genetically epistatic to *SHY2,* and is acting as its negative regulator (Kumar Meena et al., 2018). Given that *CIPK25* is also downregulated by cytokinin, and is partially involved in the downregulation of *PIN1* upon cytokinin treatment, it is plausible that CIPK25 is acting as a mediator of both auxin and cytokinin signalling in root development, through regulating *SHY2* and PIN proteins (Kumar Meena et al., 2018).

In addition to the role of cytoplasmic calcium influx in primary root development, nuclear calcium influx has also been found to play a role. The nuclear membrane-localized ion channels DMI1 and CNGC15 are not only required for nuclear calcium signalling in Medicago roots, but also in Arabidopsis roots that do not form endosymbioses, where they are implicated in primary root development (Leitão et al., 2019, Tipper et al., 2023). The AtDMI1 loss of function mutants *dmi1-1* have longer primary roots, caused by longer elongating cells in the EZ. When the nuclear calcium release was analysed, *dmi1-1* meristematic nuclei had an increase in both the rise and fall times of Ca^{2+} release (Leitão et al., 2019). In contrast, the T-DNA insertion line *dmi1-2,* which has an increased expression of *AtDMI1*, has shorter primary roots

caused by a reduction in the number of RAM cells. This is associated with a decrease in the frequency of nuclear calcium release, both in terms of the number of plants with observable nuclear calcium release, and the number of releases per meristem (Leitão et al., 2019). A point mutation in *CNGC15*, *cngc15*^{D408N}, was also found to cause a reduction in the number of RAM cells, and a shorter primary root length, like *dmi1-2*. This is also associated in a decrease in the frequency of nuclear calcium release (Tipper et al., 2023).

Interestingly, the double mutant *dmi1-1 cngc15*^{D408N} has the both the reduced frequency characteristic of *cngc15*^{D408N}, and the increased rise time and fall time characteristic of *dmi1-1* calcium release. These double mutants have an intermediate root length, highlighting the crucial role of these two ion channels in modulating root development (Tipper et al., 2023). These results suggest that specific nuclear calcium signatures are required for normal root meristem development, but it is not known how these calcium signatures are decoded. In addition, it was found that auxin homeostasis is involved in modulating the calcium signatures: the defects in the calcium signatures of *dmi1-1* and *dmi1-2* was associated with altered auxin distribution in the root meristem and differential expression of auxin related genes (Leitão et al., 2019).

1.5 Thesis Aims

The nuclear calcium signals generated by CNGC15 have been studied in two root systems, where it has been found to have different roles. In *Medicago truncatula,* it has roles in the establishment of symbiosis (Charpentier et al., 2016), and in Arabidopsis it has roles in primary root development (Tipper et al., 2023) and nitrate signalling (Wang et al., 2021c). In this thesis, I investigate the downstream components of the nuclear calcium signals in both systems.

In the context of endosymbiosis, the G protein β subunit is known to be a positive regulator of root nodule symbiosis in soybean, where it has been hypothesised to be involved in the activation nuclear calcium signalling. Here, I investigate a putative interactor of Gβ, APSR1, and its role in the regulation of

AM symbiosis upon phosphate treatment. I aim to investigate this by answering the following questions in Chapter 3:

1. Does APSR1 interact with Gβ?
2. What is the phylogeny of APSR1, and can closely related genes help inform its function?
3. Is *APSR1* regulated by nutrient treatment?
4. What is the phenotypic effect of *apsr1* loss-of-function?

In the context of Arabidopsis root development, a point mutation in CNGC15, *cngc15*^{D408N}, has been shown to alter nuclear calcium signalling and subsequent primary root development (Tipper et al., 2023). My aims are to further explore the effect of this point mutation, by answering the following questions in Chapters 4 and 5:

1. What effect does the novel mutation *cngc15*^{D408N} have on the structure and function of CNGC15 in Arabidopsis?
2. Given CNGC15 also has a role in nitrate signalling (Wang et al., 2021c), how do these 2 roles interplay? Are they occurring in different cell types or at different developmental stages?
3. What is responding to the nuclear calcium release mediated by CNGC15? What are the potential regulators and decoders facilitating normal primary root development?

Chapter II: Material and Methods

2.1 *Medicago truncatula* (Medicago) plant materials and growth conditions

The Medicago R108 ecotype and the *tnt1* insertion lines NF4464 and NF12622 purchased from the Noble Research Institute (https://medicago-mutant.noble.org) were used in this study.

Seeds were scarified with sandpaper, surface-sterilized in 12% (v/v) sodium hypochlorite for 5 minutes, and washed 5 times in sterile water. Seeds were soaked in a solution of 5µg/ml nystatin (Duchefa Biochemie; N0138) and 50µg/ml augmentin (Duchefa Biochemie; A0189) for at least 4 hours, changing the liquid at least once in this time. They were washed once in sterile water, then plated on square plates (Greiner Bio-One; 120/120/17mm; ID:688161) containing Buffered Nodulation Medium (BNM) with 1% agar and left at 4°C in the dark upside down for 5-6 days, and then placed at room temperature overnight to germinate.

Under sterile conditions, the seed coats were removed, and the seeds were plated on square plates containing Modified Fahraeus Plant media (ModFP) pH6 1% (w/v) agar (Sigma-Aldrich; A7921) media lined with Whatman® filter paper (Sigma-Aldrich; WHA10334365) (to prevent the roots penetrating the media) and moved to the growth cabinet for one week (23°C, 16-hour photoperiod, 32% humidity and 300 µmol/m^2/s light intensity). For nutrient and symbiosis assays, plants were placed in terragreen and sand as outlined in sections 2.2 and 2.3, and transferred to a controlled environment room (22°C, 16-hour photoperiod, and 300 µmol/m^2/s light intensity) for 2-5 weeks, depending on the experiment.

2.2 Medicago nutrient treatments

Seedlings were grown in 40 cell trays of Terragreen/Sand (Oil-Dri Company, Wisbech, UK) in a 1:1 ratio. Low and high phosphate conditions were made by watering with 1mM and 5mM KH_2PO_4 respectively. High nitrate conditions were made by watering with 5mM KNO_3. Pots were watered with

their respective nutrient treatments, or water, every three days as needed when the Terragreen/Sand became dry. Roots were harvested after 2 weeks of treatment.

2.3 Medicago nodulation and mycorrhization treatments

For nodulation assays, plants were grown in pots of sterilised Terragreen/Sand in a 1:1 ratio and inoculated with 5ml *Sinorhizobium meliloti* strain 2011 (*Sm*2011) at OD_{600} = 0.01 per plant under sterile conditions. *Sm*2011 was prepared by growing on selective Lysogeny Broth (LB) 1% (w/v) agar plates (Greiner Bio-One; 120/120/17mm; ID:633181) containing 100µM spectinomycin and 4µM tetracyclin for 2-3 days at 28°C. A single colony was inoculated in 10ml selective LB liquid medium and grown for 2-3 days at 28°C with rotation at 300 revolutions per minute (rpm) in a sterile universal. The culture was spun down by centrifugation at 4000rpm for 10 minutes and resuspended in sterile deionised H_2O (dH_2O) so the Optical Density at 600nm (OD_{600}) was 0.01. The OD_{600} was measured with a spectrophotometer. 5ml of this diluted suspension was used to inoculate each plant using a Corning® Stripettor™ and 25ml sterile stripettes (Corning®; 4489). Nodulation was assessed at 2 weeks and 4 weeks post inoculation using a light microscope. Plants were watered with dH_2O or 5mM KNO_3 every three days.

For mycorrhization assays, plants were grown in 1:1 Terragreen/Sand (Oil-Dri Ltd., UK) and inoculated with 10% (v/v) mycorrhizal inoculum (homogenized soil substrate containing *Allium schoenoprasum* roots colonised with *Rhizophagus irregularis* DAOM 197198). Pots were watered with dH_2O, or 1mM or 5mM KH_2PO_4 every three days. Plants were dug up and stained around 7 weeks post inoculation, when the level of arbuscule colonisation in R108 was around 50%. Fungal structures in roots inoculated with *R. irregularis* were stained by first clearing the roots in 10% (v/v) KOH at 98°C for 18 minutes, washing in water, then staining with 5% (v/v) acetic acid and 3% (v/v) permanent blue ink (Parker) for 6 minutes at 98°C and washed in water. Percentage colonisation was counted using a light microscope and the Gridline

Intersect Method (Giovannetti and Mosse, 1980). The stained root sample was spread out on a square plate marked with a 1cm x 1cm grid. The vertical grid lines were scanned under the light microscope, and at the intersection between the gridline and the root, the presence or absence of intraradical hyphae, arbuscules and vesicles was counted. Percentage colonisation was calculated by dividing the number of occurrences of each structure by the total number of intersections counted.

2.4 *Arabidopsis thaliana* (Arabidopsis) plant materials and growth conditions

The SALK and SAIL lines (N814022: *dmi1-2* (Leitão et al., 2019), N653269: *dmi1-1* (Leitão et al., 2019), N93280: *cngc15*^{D408N} (Tipper et al., 2023), N16026: *rsa1-3* (Guan et al., 2013a)) and wild type Col-0 and Col-0 *er105* were bought from the Nottingham Arabidopsis stock centre. The *cngc15*^{D408N} suppressor mutant lines were generated by an EMS screen of *cngc15*^{D408N} plants prior to my arrival in the lab. Plants that recovered the wild-type root length phenotype and flowering time phenotype were identified and the seeds harvested. The CYCB1.1-GFP line was kindly gifted by Alex Costa.

Seeds were sterilised in 1.2% (v/v) sodium hypochlorite for 20 minutes with rotation, then washed 5 times with sterile water. They were plated on half strength Murashige and Skoog (MS), 1% (w/v) sucrose, 0.8% (w/v) agar (Sigma-Aldrich; A7921) pH 5.8 and left to stratify for 3-5 days in dark conditions at 4ºC. Plates were moved to a growth cabinet (23°C, 16-hour photoperiod, 32% humidity and 300 µmol/m^2/s light intensity). 'Nitrate free' ½ MS and 10 mM nitrate ½ MS were made by adding 1mM L-glutamine (Merck; G7513) and 10 mM KNO_3, respectively, to ½ MS media made with no added nitrate.

For seed production and genotyping, seedlings were transferred 10-14 days post germination (dpg) to 40 cell trays containing Levington F2 starter plus grit (Scotts, 90% (v/v) peat, 10% (v/v) grit). After 2 weeks, seedlings were repotted in 8cm pots containing Levington F2 starter plus grit, and inflorescence stems were caned and tied. After 2 weeks, stems were bagged using 330x180mm glassine bags and cable ties. Watering was reduced and seeds

were harvested when all siliques were brown and dried, around 2 weeks. Seeds were dried at 28°C for at least 2 days before being stored in 2ml Eppendorf tubes with 2 silica drying pearls (Sigma-Aldrich; 94098) per tube.

2.5 Genotyping

Single leaf samples were taken from each plant 7-10 days after planting on soil. DNA extraction was carried out using the DNeasy® 96 plant kit (Qiagen) according to the manufacturer's instructions, with some modifications. In brief, two mature leaves were taken from each plant and placed in collection microtubes (Qiagen; 19560). One tungsten carbide bead (Qiagen; 69997) was placed in each tube and tubes were sealed with the provided caps. Tissue was disrupted with a TissueLyser II (Qiagen) for 1.5 minutes at 30Hz prior to the addition of the Lysis Buffer, and then for another 1.5 minutes at 30Hz with the addition of Lysis Buffer. Plates were briefly centrifuged, Buffer P3 was added, and plates were incubated at -20°C for 10 minutes. Plates were spun at 6,000rpm for 5 minutes and the supernatant was transferred to a new microtube. Buffer AW1 was added, and the solution was loaded into the DNeasy® 96 plates placed on top of the provided S-blocks. Plates were centrifuged, washed with Buffer AW2, and centrifuged twice more to dry the membrane. DNA was eluted using 2 x 25µl Buffer AE.

Genotypes were assessed by PCR using GoTaq G2 Green Master Mix (Promega) according to the manufacturer's instructions (Section 2.18.1 Polymerase Chain Reaction (PCR)). For T-DNA insertion lines, gene-specific primers were designed that flank the T-DNA insertion site, to yield amplification in wild type or heterozygous plants, and a combination of a gene-specific and a T-DNA specific primer was used to yield amplification in heterozygous or homozygous mutant plants. A summary of the primers used can be seen in Table 2.1. The PCR products were sequenced to confirm the location of T-DNA insertions, or the location of the D408N point mutation in the case of *cngc15*^{D408N}. Protocol for sequencing is described in section 2.18.3 (Sequencing of PCR products and plasmids).

2.6 Generation of the *Arabidopsis* double mutants by crossing

The double mutant plants generated in this study are: col0 NR-GECO1.2 CYCB1.1-GFP, *cngc15*^{D408N} NR-GECO1.2 CYCB1.1-GFP, *dmi1-2* NR-GECO1.2 CYCB1.1-GFP, *dmi1-2 rsa1-3* and *dmi1-1 rsa1-3*. Double mutants were generated by manual hand pollination, followed by seed propagation and genotyping of the T2 generation by PCR as described in sections 2.5 (Genotyping) and 2.18.1 (Polymerase Chain Reaction (PCR)) to obtain homozygous mutants.

2.7 Quantification of gene expression

Total RNA was extracted using the Qiagen RNeasy® Plant Mini kit or RNeasy® Micro kit (for extraction from Arabidopsis root tips). Plant tissues were placed in 2ml Eppendorf tubes with one Tungsten Carbide bead (Qiagen; 69997) per tube and flash frozen in liquid nitrogen. They were then disrupted with a TissueLyser II (Qiagen) for one minute at 30Hz, flash frozen in liquid nitrogen, and disrupted again for one minute at 30Hz. The TissueLyser II Adapter was pre-cooled in liquid nitrogen to prevent samples thawing during disruption. Then the extraction was carried out as per the protocol, which for the RNeasy® Plant Mini kit is as follows: Buffer RLT (with β-mercaptoethanol) was added to the ground tissue and vortexed thoroughly, before being transferred to a QIAshredder spin column and centrifuged. The supernatant of the flow-through was transferred to a fresh 1.5ml Eppendorf tube, and 0.5 volumes of ethanol was added and mixed by pipetting. The sample was added to a RNeasy spin column and centrifuged. The sample was washed with Buffer RW1 and Buffer RPE, before a final long centrifugation step to dry the spin column membrane. RNA was eluted in 20µl RNAse-free water. For the RNeasy® Micro kit, again the manufacturer's instructions were followed, and the protocol is similar, but a 3 minute centrifugation step is used to clear the lysate (instead of the QIAshredder column), an on-column DNAse treatment is used, as well as RNeasy MinElute spin columns. RNA was eluted in 14µl RNAse-free water.

Concentration and purity were determined by spectrophotometry (A260/280 and A260/230 ratios using a NanoDrop™ One Spectrophotometer)

and integrity was confirmed by gel electrophoresis (1% (w/v) agarose). Contaminant gDNA was removed using Ambion™ TURBO DNA-free kit (Invitrogen), or on-column DNAse treatment provided in the RNeasy Plant Micro kit, and confirmed by PCR using the primers listed in Table 2.1. cDNA was obtained from 500ng of RNA using the Invitrogen SuperScript IV Reverse Transcriptase following manufacturer's instructions.

Quantitative reverse transcription PCR (qRT-PCR) was performed using a CFX96 Touch™ Real-Time PCR Detection system (BIO-RAD) and SYBR® Green JumpStart™ Taq ReadyMix™ (Sigma-Aldrich). First, the specificity of each primer pair was assessed via PCR using GoTaq® G2 Green Master Mix (Promega) and 2µl 10x diluted cDNA (Section 2.18.1 Polymerase Chain Reaction (PCR)). Next, the amplification efficiency (E) of each primer pair was calculated from the slope of a cDNA dilution series standard curve. Three dilutions of cDNA (10x, 100x, and 1000x) and two technical replicates per dilution were used in 10µl reactions.

The cycling conditions are as follows: initial denaturation (2 min at 95°C), then 40 cycles of amplification and quantification (15 seconds at 95°C, 15 seconds at 58°C or 60°C, and 30 seconds at 72°C with a single fluorescence measurement).

The reaction components for a 10µl reaction are as follows: 5µl SYBR® Green JumpStart™ Taq ReadyMix™, 500nM of each primer and 2µl diluted cDNA, made up to 10µl with sterile dH_2O. cDNA from Medicago samples was diluted 10x, and for Arabidopsis samples it was diluted 50x.

For qRT-PCR of Medicago samples, the equation in Pfaffl (2001) was used to calculate expression levels. For qRT-PCR of Arabidopsis samples, calculation of expression levels was performed using a previously described mathematical equation Pfaffl (2001), adapted to account for the use of 2 reference genes as described in Hellemans et al. (2007), Vandesompele et al. (2002):

$$Relative\ Gene\ Expression = \frac{(E_{GOI})^{\Delta Ct\ GOI}}{GeoMean[(E_{REF1})^{\Delta Ct\ REF1},(E_{REF2})^{\Delta Ct\ REF2}]}$$

Primers used for qPCR are listed in Table 2.1.

2.8 Yeast Two-Hybrid Assay

A GAL4-based yeast two-hybrid assay was carried out using the *Saccharomyces cerevisiae* strain AH109. Coding sequences of *APSR1* and *Gβ* had previously been cloned from Medicago truncatula R108 cDNA by Pierre Dangeville (Charpentier lab). Gateway cloning (Invitrogen™, Section 2.18.5) was used to subclone the coding sequences into the *pGADT7(AD)* and *pGBKT7(BD)* vectors (Clontech). The positive control constructs *pGADT7(AD)-T* and *pGBKT7(BD)-53* (the SV40 large T antigen (T) and the murine p53 (53)) were from Clontech. Yeast was transformed using the lithium acetate method (Gietz and Schiestl, 2007). In brief, a 5ml YPAD culture of AH109 was incubated overnight at 30°C and 300rpm and used to inoculate 100ml of YPAD, which was incubated at 30°C and 300rpm. When the OD_{600} reached 0.6-0.8, the culture was centrifuged at 4000rpm for 5 minutes, and the pellet resuspended in 25ml sterile dH_2O. Cells were centrifuged at 1000rpm for 5 minutes, the supernatant was removed, and cells were resuspended in 1.5ml sterile 100mM LiOAc solution. For each transformation, 100µl cells was added to 300µl PEG/LiOAc transformation solution (40% polyethyleneglycol (v/v), 0.12 M lithium acetate, 0.16 mg/ml salmon sperm DNA, and 2-5 µg of plasmids) and vortexed for one minute. The mixtures were incubated without shaking for 30 minutes at 30°C and 30 minutes at 42°C, then centrifuged for 5 minutes at 700g. Supernatant was removed, and the pellet was resuspended gently in 100µl of 0.9% (w/v) NaCl. Cells were plated on Synthetic Dextrose (SD) minimal media lacking leucine and tryptophan (-LW). Positive transformants were grown in 5ml liquid SD -LW media overnight at 28°C and dropped out at different dilutions on SD minimal media lacking leucine, tryptophan, adenine and histidine (-LWAH). Plates were grown at 28°C for 5 days.

2.9 Modelling the AtCNGC15 structure

Homology modelling was done in collaboration with Professor David Lawson (Biochemistry & Metabolism; John Innes Centre (JIC)) and this method is published in Tipper et al. (2023) and appears here with permission. The Protein Data Bank (PDB) was interrogated using the amino acid sequence of AtCNGC15. This yielded several hits with ~80% coverage of the target sequence, with sequence identities in the range of 17-24%. Homology models were generated using the SWISS-MODEL (SM) server (Waterhouse et al., 2018), which has the advantage of retaining the homotetrameric quaternary structure of the template. We focused on models generated from the structures of Eag1 from *Rattus norvegicus* (PDB code 5K7L) (Whicher and MacKinnon, 2016), human hERG (PDB code 5VA1) (Wang and MacKinnon, 2017), and TAX-4 from *Caenorhabditis elegans* (PDB code 5H3O) (Mazzolini et al., 2018). In all cases, D408 was located on the channel-facing side of helix A' and adjacent to R398 at the junction of helices S6 and A' in the neighbouring subunit.

Given the low sequence identities with known structures, we also generated template-free, *ab initio* predictions of the AtCNGC15 structure using AlphaFold2 (AF2) (Jumper et al., 2021) as implemented in ColabFold (Mirdita et al., 2022). The five independent models generated were very similar to one another and showed high quality local structure (pLDDT scores) across most of the sequence and, crucially, predicted a subunit-subunit interface with relatively high confidence (PAE scores) that was consistent with those observed in the SM results. Furthermore, D408 and R398 from neighbouring subunits were adjacent to one another in all five AF2 models and the same salt-bridge linking the two subunits could be modelled. Structural figures were produced using ChimeraX (Pettersen et al., 2021).

2.10 Expression in *Xenopus laevis* oocytes

A version of this method has been published in Tipper et al. (2023) and appears here with permission. *AtCNGC15* cDNA was synthesised according to the codon usage of *X. laevis* by GenScript and subcloned using Gateway cloning

(Section 2.18.5 Gateway Cloning) into the *pOO2-GW* (Chen et al., 2010) for electrophysiology and the *pGCS-C6(eGFP)* (Wang et al., 2016) for localisation. Site directed mutagenesis of the codon optimised *AtCNGC15* was done using overlapping primers (Table 2.1) to generate the *pOO2-GW-AtCNGC15*^{D408N} and *pGCS-C6(eGFP)-AtCNGC15*^{D408N} constructs using the method described in Section 2.18.1 (Polymerase Chain Reaction (PCR)).

Plasmid purification was carried out using the Qiagen Plasmid Midi Kit according to the manufacturer's instructions to yield a high volume of plasmid for transcription. Description of the procedure can be found in section 2.18.7 (Plasmid purification). Plasmids were linearized with PmlI (*pOO2-GW* constructs) or NotI-HF (*pGCS-C6(eGFP)* constructs) (New England Biolabs) and linearization was confirmed by gel electrophoresis (1% (w/v) agarose). Protocol for gel electrophoresis can be found in section 2.18.2 (Gel electrophoresis).

Linearised plasmid was precipitated as follows: one volume of isopropanol and 1/10 volume 3M sodium acetate (pH 5.2) was added, and the mixture was chilled at -20°C for 5 hours. DNA was pelleted using a microcentrifuge at maximum speed for 15 minutes. The supernatant was removed, and the pellet was resuspended in sterile dH_2O to a final concentration of 0.5µg/µl.

In vitro transcription was performed using the mMESSAGE MMACHINE^{TM} SP6 kit (Ambion), to yield capped and polyadenylated RNA. The transcription was carried out as per the manufacturer's instructions using 1µg of linearised plasmid template in a single 20µl reaction per construct, and a 2-hour incubation at 37°C. The optional TURBO DNase was not added. The RNA was purified using phenol/chloroform extraction: 115µl Nuclease-free water and 15µl Ammonium Acetate Stop Solution was added to the reaction mixture and mixed thoroughly. Then, 150µl phenol/chloroform/isoamyl alcohol pH6.7 (Sigma-Aldrich; P2069) was added and mixed thoroughly by shaking. The tube was centrifuged for 2 minutes at maximum speed in a tabletop centrifuge placed in the fume cupboard. The aqueous phase was recovered and transferred to a new tube. RNA was precipitated by adding 1 volume of isopropanol and mixing well by vortexing. The mixture was chilled for 1 hour at -20°C, then centrifuged

at 20,000 x *g* at 4°C for 15 minutes. Supernatant was removed and the RNA was resuspended in sterile dH_2O. RNA was diluted to 1100ng/µl (concentration measured using NanoDrop™ One Spectrophotometer), divided into 2 µl aliquots and stored at -70°C. Gel electrophoresis of 1µl of diluted RNA mixed with 0.2µl DNA Gel Loading Dye (New England Biolabs) was used to check the quality and size of the RNA transcript. The gel electrophoresis protocol can be found in section 2.18.2 (Gel electrophoresis).

Oocytes were injected with 55 ng of cRNA in 50nL of RNase-free water or with 50nL of RNase-free water using a compressed air system. Injected oocytes were incubated at 17°C in Modified Barth's Solution (MBS) pH 7.4 (88 mM NaCl, 1mM KCl, 2.4 mM $NaHCO_3$, 0.3mM $Ca(NO_3)_2$, 0.41mM $CaCl_2$, 0.82 mM $MgSO_4$, 15mM Hepes) supplemented with 10 g/ml sodium penicillin and 10 µg/ml streptomycin sulphate for two days. One day before electrophysiology, oocytes were transferred to a calcium free MBS (same as above except for the absence of $Ca(NO_3)_2$ and $CaCl_2$).

2.11 Electrophysiology

A version of this method has been published in Tipper et al. (2023) and appears here with permission. Whole oocyte currents and membrane potential were recorded using the two-electrode voltage-clamp technique 2 days after cRNA injection with a Axoclamp 900A microelectrode amplifier and the Digidata 1440A digitizer (Axon Instruments). Voltage-pulse protocols, data acquisition and analysis were performed using pClamp10.7 software (Axon Instruments). Electrodes were filled with 3 M KCl. The oocytes were continuously perfused during the voltage-clamp experiment with either calcium-free MBS or calcium-free MBS supplemented with 20 mM $CaCl_2$ or 20 mM $BaCl_2$. Voltage steps were applied from -165 to +40 mV in +15 mV increments, and the currents were recorded to obtain current-voltage curves.

2.12 Confocal laser scanning microscopy of *Xenopus* oocytes

A version of this method has been published in Tipper et al. (2023) and appears here with permission. Two days after injection with cRNA or H_2O, images were taken using Zeiss LSM780 with ZEN 2012 SP5 (Black) acquisition software, a 10x/0.3 dry objective and the tiling function. A 25mW Argon ion laser was used with an excitation wavelength of 488 nm and emitted fluorescence was collected at 520 nm. Confocal pinhole size = 1AU. The 32-channel GaAsP PMT array was used with 200 V gain. Quantification of fluorescence was carried out in ImageJ. The area, integrated intensity, and mean grey values of each oocyte were measured and compared to that of the background to give the total fluorescence of each oocyte normalised to the background.

2.13 Whole genome sequencing

Seeds from the EMS suppressor lines were sterilised, plated, and grown as described above. The EMS suppressor screen was carried out prior to the work presented in this thesis. It was a saturated EMS suppressor screen using *cngc15*^{D408N} seeds, which has a short root length phenotype (Tipper et al., 2023). Seedlings that displayed a wild type primary root length phenotype in the *cngc15*^{D408N} background were recovered. Root length analysis was conducted at 6dpg and plants that recovered a WT root length phenotype were grown for another 1.5 weeks and used for DNA extraction using Qiagen DNeasy plant mini kit. Around 3-5 seedlings per line were bulked for DNA extraction. Seedlings were placed in 2ml Eppendorf tubes with one Tungsten Carbide bead (Qiagen; 69997) per tube and flash frozen in liquid nitrogen. They were then disrupted with a TissueLyser (Qiagen) for one minute at 30Hz, flash frozen in liquid nitrogen, and disrupted again for one minute at 30Hz. Buffers AP1 and P3 were added as per the protocol, the mixture was incubated on ice, then centrifuged for 5 minutes at 20,000 x *g*. The supernatant was added to a QIAshredder spin column with a collection tube and centrifuged for 2 minutes at 20,000 x *g*. Flow-through was placed in a new tube with 1.5 volumes of Buffer AW1, before

being added to a DNeasy Mini spin column and centrifuged for one minute at 6000 x g. The spin column was placed in a new collection tube for the addition of Buffer AW2, which was centrifuged for one minute at 6000 x g. This wash step was repeated, and the spin column was placed in a new collection tube and spun for 2 minutes at 20,000 x g to ensure the column membrane was completely dry. DNA was eluted in 20µl Buffer AE, with a 10 minute incubation at room temperature prior to centrifugation to ensure maximal yields. After one initial elution, the flowthrough was reapplied to the spin column for a second elution to increase yields.

Quality (A_{260}/A_{280} ratio) and quantity of the genomic DNA was assessed using a NanoDrop™ One Spectrophotometer. Samples from five EMS lines and *cngc15*^{D408N} were sent to Novogene for library construction and Illumina sequencing with 50x coverage.

2.14 Primary root length measurements and lateral root length analysis

Seedlings were grown vertically on ½ MS plates and photographed with a digital single-lens reflex (DSLR) camera at day 6 and day 12 after transfer to the growth chamber. Root length was quantified using ImageJ 1.48v (NeuronJ plugin, 1.4.3v) (Meijering et al., 2004). The number of lateral roots was counted, and lateral root density was calculated by dividing the number of lateral roots by the total primary root length.

2.15 Root apical meristem visualisation and measurement

At 6 days post germination, seedlings were harvested and placed in 6-well plates containing 50% (v/v) methanol 10% (v/v) acetic acid. Plates were sealed with parafilm and placed at 4°C for at least 12 hours. Seedlings were then washed with water, washed with 20mM phosphate buffer (pH7), and incubated in α-amylase solution (0.3 mg/mL in 20 mM phosphate buffer, 2 mM NaCl, 0.25 mM $CaCl_2$) at 37°C for at least 16 hours. The 20mM phosphate buffer was made by dissolving 3.10g Sodium Phosphate Dibasic Heptahydrate (Sigma-Aldrich; 431478) and 1.17g Sodium Phosphate Monobasic Monohydrate (Sigma-Aldrich;

S9638) in 1L dH_2O. Seedlings were rinsed in water, then incubated in 1% (v/v) periodic acid at room temperature for 40 minutes, then washed with water, then incubated in Schiff reagent (100 mM sodium metabisulfite, 0.15 N HCl, 20 µL/mL propidium iodide) for 30 minutes, until the roots were visibly pink. Seedlings were rinsed with water, then placed in chloral hydrate (8g chloral hydrate; 3 mL glycerol; 1 mL water) and left at room temperature in the dark overnight. Samples were mounted in chloral hydrate the following day and imaged using a Zeiss LSM 880 confocal microscope (Carl Zeiss). Cell counting and cell length measuring were performed using ImageJ 1.48v (Cell-o-Tape plugin, 0.7.7v) (French et al., 2012).

2.16 Confocal laser scanning microscopy of Arabidopsis roots

Images of *AtCNGC15:GFP* and *AtCNGC15*^{D408N}*:GFP* localization were collected using a Zeiss LSM780 confocal microscope with a 40x/1.2 water objective or a 20x/0.5 dry objective. The GFP excitation wavelength used was 488 nm, and emitted fluorescence was collected at 500-550 nm.

2.17 Nitrate treatment of Arabidopsis roots

Seedlings were grown on nitrate-free ½ MS plates as described above for 6 days. At day 6, seedlings were incubated in nitrate-free ½ MS supplemented with either 10 mM KNO_3 or 10 mM KCl (control treatment) for 30 minutes. The root tip samples were cut and frozen in liquid nitrogen prior to RNA extraction and qRT-PCR described in section 2.7 (Quantification of gene expression).

2.18 Calcium imaging of NR-GECO1.2 CYCB1.1-GFP seedlings

6 day old seedlings were collected and positioned in a small chamber made with a coverslip and high-vacuum grease (Dow Corning GMBH, Wiesbaden, Germany). The chamber was filled with 50–100 µl MS medium and the whole root was covered with a smaller coverslip. The seedling was left at room temperature for around 45 min before imaging. Images of the root tip were collected every 2–3 s for an average of 4 hours using a Nikon ECLIPSE FN1.

2.19 Molecular Biology Methods

2.19.1 Polymerase Chain Reaction (PCR)

PCRs for genotyping and testing the specificity of qRT-PCR primers were carried out using GoTaq® G2 Green Master Mix (Promega) using either 10µl or 25µl reaction volumes (1µM of each primer, 50ng genomic DNA, supplemented with 3% (w/v) DMSO and 4mM $MgCl_2$). Reaction conditions were set on a thermocycler as follows: initial denaturation at 95°C for 2 minutes, followed by 40 cycles of 95°C for 30 seconds, 30 seconds at the annealing temperature of the primers, and extension at 72°C for 1 min/kb, followed by a final extension of 5 minutes at 72°C. Amplification was assessed by gel electrophoresis (Section 2.18.2)

Site directed mutagenesis with overlapping primers (Liu and Naismith, 2008) was used to generate *pOO2-GW-AtCNGC15*^{D408N} and *pGCS-C6(eGFP)-AtCNGC15*^{D408N}. This was carried out using Phusion™ High Fidelity DNA Polymerase in 50µl reaction volumes: 10µl 5X Buffer HF (New England Biolabs®), 1mM MgCl2, 3% (w/v) DMSO, 0.2µM dNTPs, 500nM primers, 0.5µl Phusion™ High Fidelity DNA Polymerase, 10ng plasmid template, mixed in dH_2O. Cycling conditions are as follows: initial denaturation at 98°C for 2 minutes, followed by 40 cycles of 98°C for 30 seconds, 30 seconds at the annealing temperature of the primers, and extension at 72°C for 30s/kb, followed by a final extension of 5 minutes at 72°C. Amplification was assessed by gel electrophoresis of 2.5ul of the reaction volume mixed with 0.5 µl purple gel loading dye using the protocol described in section 2.18.2 (Gel electrophoresis) Following confirmation of correct amplification, contaminant *Escherichia coli* derived plasmid was digested using DpnI and the restriction digest protocol described below. The final product was then used for transformation into *E. coli* as described below.

2.19.2 Gel electrophoresis

1% (w/v) agarose Tris-Acetate-EDTA (TAE) buffer gels were cast and loaded with the samples and a 1kb plus DNA ladder (New England Biolabs®).

TAE buffer was made by diluting 20ml of TAE Buffer 50X (Formedium) with 980ml dH_2O. If necessary, samples were mixed with Gel Loading Dye (Purple, 6X, New England Biolabs®) to a final concentration of 1X prior to loading. 120V was applied to the gel for ~20 minutes (depending on the thickness of the gel) or until the pink loading dye reached three quarters of the way down the gel. Gels were stained in a 10mg/ml ethidium bromide bath for 15-20 minutes prior to visualisation in a UV light gel imager.

2.19.3 Gel DNA extraction

Gel DNA extraction to assess the exact position of T-DNA insertions was carried out using the QIAquick Gel Extraction kit (Qiagen). DNA bands were first excised in a UV light gel imager with a scalpel and placed in 2ml Eppendorf tubes. Extraction was carried out according to the manufacturer's instructions with the following modifications: Buffer EB was heated to 70°C, and 20µl was used for elution.

2.19.4 Sequencing of PCR products and plasmids

Samples were sent to Genewiz (Azenta, UK) for Sanger sequencing, and prepared in 1.5ml Eppendorf tubes with 30-100ng PCR product or plasmid, and 2.5µM sequencing primer, mixed with dH_2O to a final reaction volume of 10µl.

2.19.5 Gateway Cloning

Gateway cloning was used to subclone synthesised *AtCNGC15* optimised for *X. laevis* codon usage into *pOO2-GW* and *pGCS-C6(eGFP)* destination vectors, and to subclone APSR1 and Gβ coding sequences into *pGADT7* and *pGBKT7* destination vectors (Katzen, 2007). 150ng of entry and destination vectors were used in a 5µl reaction with 1µl Gateway™ LR Clonase II Enzyme Mix (Invitrogen™) and mixed with sterile dH_2O by gently flicking the tube. After a brief centrifugation, the reaction was incubated at 25°C for one hour.

2.19.6 Transformation of *Escherichia coli*

Chemically competent *E. coli* (TOP10, ThermoFisher) was transformed via heat shock: 2.5µl of LR reaction product was mixed with 25µl competent cells thawed on ice and mixed by flicking the tube gently. Cells were incubated for 10 minutes on ice, then heat shocked at 42°C for 30 seconds, then incubated for one minute on ice. The tube was taken off ice and 200µl Super Optimal broth with Catabolite repression medium (SOC) was added. Cells were incubated at 37°C with 300rpm rotation for one hour. 100µl cells were plated on selective LB plates with 100µg/ml ampicillin for *pOO2-GW, pGCS-C6(eGFP) pGADT7* and *pGBKT7* constructs. Plates were incubated at 37°C overnight.

2.19.7 Plasmid purification

Plasmids were purified with the QIAprep Spin Miniprep Kit (Qiagen) or the Plasmid Midi kit (Qiagen) according to the manufacturer's instructions, described below. Initial overnight cultures were made by inoculating 5ml LB (with the appropriate antibiotics) with cells from a single colony on plate, and incubating at 37°C for 12-16 hours with shaking at 300rpm.

In brief, for the QIAprep Spin Miniprep Kit, 4ml of bacterial overnight culture was pelleted by centrifugation for 3 minutes at 18,000 x *g*. The pellet was resuspended in 250µl Buffer P1, and mixed with 250µl Buffer P2 by inversion to lyse the cells. 350µl Buffer N3 was added and mixed by inversion to precipitate the proteins out of the solution. The precipitate was pelleted by centrifugation for 10 minutes at 18,000 x *g* and the supernatant was transferred to a QIAprep 2.0 Spin Column. After centrifugation for one minute at 18,000 x *g,* the column was washed with 750µl Buffer PE and centrifuged for another minute at 18,000 x *g.* Flowthrough was discarded and the column was centrifuged for 2 minutes at 18,000 x *g* to ensure the column membrane was completely dry. Plasmids were eluted with 30µl Buffer EB.

For the Plasmid Midi kit, 100µl of an initial 5ml LB overnight culture was used to inoculate 100ml LB with the appropriate antibiotics (100µg/ml ampicillin) which was grown for 12-16 hours. The culture was split into two 50ml Oak Ridge ultracentrifuge tubes (Thermo Scientific™ 3119-0050). Cells

were harvested by centrifugation at 6000 x *g* for 15 minutes at 4°C. 2ml Buffer P1 was used to resuspend each pellet, then 2ml Buffer P2 per tube was mixed by inversion to lyse the cells. 2ml Buffer N3 at 4°C was added to each tube and mixed by vigorous inversion to precipitate proteins. Proteins were pelleted by centrifugation at 20,000 x *g* for 30 min at 4°C. The QIAGEN-tip100 was equilibrated with 4ml Buffer QBT and allowed to empty by gravity flow into a 50ml centrifuge tube (Corning® 430290) placed underneath. The supernatant from both tubes was then added to the QIAGEN-tip100, and allowed to empty by gravity flow. The QIAGEN-tip100 was washed with 2x10ml Buffer QC and allowed to empty by gravity flow. DNA was eluted with 5ml Buffer QF into a clean 50ml Oak Ridge ultracentrifuge tube, and precipitated with 3.5ml isopropanol and mixed. DNA was pelleted at 15,000 x *g* for 30 minutes at 4°C, with the tubes marked to aid identification of the pellet. Pellet was washed with 2ml room-temperature 70% (v/v) ethanol and centrifuge at 15,000 x *g* for 10 minutes. Supernatant was decanted carefully and the pellet was left to air dry for 30 minutes at 37°C. DNA was redissolved in 1ml TE buffer and the concentration was measured using a NanoDrop™ One Spectrophotometer.

2.19.8 Plasmid linearization by restriction digest

60µl restriction digest reactions were set up with 25µl purified plasmid from Plasmid Midiprep, 10x bovine serum albumin, 6µl restriction enzyme (NotI-HF or PmlI), 6µl CutSmart® buffer (New England Biolabs), mixed with sterile dH_2O. Reaction was incubated at 37°C overnight.

2.20 Computational Methods

2.20.1 Design of *in silico* sequences

Gene and amino acid sequences were obtained from Phytozome (Goodstein et al. (2012)) https://phytozome.jgi.doe.gov), and processed and annotated using A plasmid Editor (ApE, https://jorgensen.biology.utah.edu/wayned/ape/ (Davis and Jorgensen, 2022)

or Benchling (https://benchling.com). Visualisation of Sanger sequencing results was done using Benchling.

2.20.2 Database searches for domains and protein families

Information about *APSR1* gene structure (Gene ID: Medtr5g022530), protein domains, gene family, homologs and sequence data was obtained from Phytozome, InterPro (www.ebi.ac.uk/interpro) and XtalPred (http://ffas.godziklab.org/XtalPred-cgi/xtal.pl). *APSR1* promoter region was predicted using GENESCAN (http://hollywood.mit.edu/GENSCAN.html). Nuclear localization signals were predicted using cNLS Mapper (http://nls-mapper.iab.keio.ac.jp/cgi-bin/NLS_Mapper_form.cgi). Localisation was predicted using Wolf PSORT (https://wolfpsort.hgc.jp/ Horton et al. (2007))

Information about *RSA1* (AT2G03150) gene structure and protein domains was obtained from The Arabidopsis Information Resource (TAIR, https://www.arabidopsis.org/index.jsp) and Phytozome.

2.20.3 Phylogenetic tree construction

Members of the NRG2 family were identified through protein and nucleotide Basic Local Alignment Search Tool (BLAST) searches against genomes on Phytozome. Phylogenetic trees were constructed using the amino acid sequences. Incorrectly predicted gene models were manually curated based on conserved exon-intron structures. DNA coding sequences were then aligned with MAFFT (Multiple Alignment using Fast Fourier Transform) L-INS-I with default settings (Katoh and Standley, 2013). IQ-Tree (v1.6.12) was used to construct phylogenetic trees with the maximum likelihood approach (Nguyen et al., 2014). ModelFinder was used to find the best-fit evolutionary model (JTT+F+I+G4), and ultrafast bootstrap (UFBoot2) with 1,000 replications was used to estimate branch support (Kalyaanamoorthy et al., 2017). Phylogenetic trees were visualized in the interactive Tree Of Life (iTOL) v4 (Letunic and Bork, 2019).

2.20.4 Searching for APSR1 *tnt* insertion lines

The *Medicago truncatula* mutant database (medicago-mutant.dasnr.okstate.edu) was used to identify lines with *tnt* insertion sites in APSR1.

2.20.5 Transcriptome analyses

Gene expression data was obtained from the *Medicago truncatula* Gene Expression Atlas Carrere et al. (2021) https://mtgea.noble.org/v2) using the probe ID: Mtr.26989.1.S1_at.

2.20.6 Sequence analysis

Sequences from Novogene were mapped to the reference genome Arabidopsis thaliana Col-0 version TAIR10 (www.arabidopsis.org) using Burrows-Wheeler Aligner Maximal Exact Match (BWA-MEM) v0.7.12 (Li and Durbin, 2009). The resulting Sequence Alignment Map (SAM) files were sorted and converted to Binary Alignment Map (BAM) format using SAMtools v0.1.19 (samtools -view) (Li et al., 2009). SAMtools was also used to convert the BAM files into MPILEUP format (samtools -mpileup). A custom script was used to call single nucleotide polymorphism (SNP) positions from the MPILEUP format, resulting in a table for each line denoting the chromosome, position, reference base, alternative base, reference allele frequency, alternative allele frequency, and coverage. Another custom script was used to load these SNP tables and integrate them, filtering for positions where *cngc15*^{D408N} was different from Col-0 and filtering for positions where at least three of the lines were different from Col-0. The custom scripts were created by Burkhard Steuernagel, based on the pipelines generated in Steuernagel et al. (2017), Sánchez-Martín et al. (2016). They are deposited at https://github.com/steuernb/oat_mutseq and https://github.com/steuernb/SimpleHunter. Then, contigs of 500bp or 3kb were reported where three or more mutants had a SNP. The Col-0 reference sequence and gene annotations were loaded into Integrative Genomics Viewer (IGV) v2.8.13 (Robinson et al., 2011) along with BAM files for *cngc15*^{D408N} and

the suppressor mutant lines. Reported intervals were manually inspected for overlaps with genes or wrongly called SNPs.

2.20.7 Primer design

Primers for sequencing and PCR were designed using ApE and IDT™ OligoAnalyzer™ tool (Owczarzy et al. (2008), https://eu.idtdna.com/calc/analyzer) to check the annealing temperature and susceptibility to forming selfo- or heterodimers and/or hairpins. Primers for qRT-PCR were designed using NCBI Primer BLAST (Ye et al. (2012), https://www.ncbi.nlm.nih.gov/tools/primer-blast/) to ensure specificity.

2.20.8 Statistical analyses

Statistical analyses were performed using GraphPad Prism version 8.00 for Windows (GraphPad Software, www.graphpad.com). Ordinary one-way ANOVAs with Tukey's multiple comparison post-test was used for comparison of three or more variables. A prior F-test was used to check for homoscedasticity of residuals. Unpaired two-tailed Welch's t-tests were used for comparison of two variables. Chi-squared tests were used to compare the difference in population proportions between groups.

Table 2.1: Primers used in this thesis.

Name	Fwd /rev	Sequence (5" to 3")	Gene	Function	E
APSR1-qPCR-F	fwd	TGGCACCTTGCC GTTGAGCA	*MtAPSR1*	qPCR	E = 2.071 (60°C)
APSR1-qPCR-R	rev	ACCAGACCGTTC CGACATGGA	*MtAPSR1*	qPCR	
MT4-qPCR-F	fwd	AATGATTGCTGG GAATGAACCTT	*MtMT4*	qPCR	E = 2.49 (60°C)
MT4-qPCR-R	rev	TTCCAAAGAGA AAATCCCATCAA	*MtMT4*	qPCR	
PT4-qPCR-F	fwd	TTCGCAATGCAA GGCGTGGG	*MtPT4*	qPCR	E = 1.92 (60°C)
PT4-qPCR-R	rev	CGCAGCTGGAA CAGCACCGA	*MtPT4*	qPCR	
NiR1-qPCR-F	fwd	TCCACTTGATGC TTGGGTCT	*MtNiR1*	qPCR	E = 2.14 (60°C)
NiR1-qPCR-R	rev	TTCCACCTCTGA TCTGAATACTTC	*MtNiR1*	qPCR	
Enodl1-qPCR-F	fwd	CCATTGCCTAAA CCACCTGTTA	*MtEnodl1*	qPCR	E = 2.078 (60°C)
Enodl1-qPCR-R	rev	CTTGTTGCTTGC AAATACGCTT	*MtEnodl1*	qPCR	
UBC9-qPCR-F	fwd	GGTTGATTGCTC TTCTCTCCCC	*MtUBC9*	qPCR	E = 1.99 (60°C)
UBC9-qPCR-R	rev	AAGTGATTGCTC GTCCAACCC	*MtUBC9*	qPCR	
NF4464-F	fwd	TGTACATCCGTT CTCTTCGTTCA	*MtAPSR1*	genotyping	
NF4464-R	rev	TCTTGAAACCAC CATTGCAAGT	*MtAPSR1*	genotyping	
NF12622-F	fwd	GAGTGCAAGTA TGGTCCGTACT	*MtAPSR1*	genotyping	
NF12622-R	rev	GTCCACCGCATG CATTTAGA	*MtAPSR1*	genotyping	
tnt1-R	rev	CAGTGAACGAG CAGAACCTGTG	*tnt1* insertion	genotyping	
AtCNGC15-SDM-D408N-F	fwd	GAAGGACTAAT ACAGAACAGTG GATGC	codon optimised AtCNGC15	site directed mutagenesis	
AtCNGC15-SDM-D408N-R	rev	GTTCTGTATTAG TCCTTCTAATCC TCCAC	codon optimised	site directed mutagenesis	

			AtCNGC15		
LBD37-qPCR-F	fwd	TTGGACCGGCGAATTAACAAC	*AtLBD37*	qPCR	E = 1.99 (60°C)
LBD37-qPCR-R	rev	AACCGAGAGAACAAAACGACG	*AtLBD37*	qPCR	
LBD38-qPCR-F	fwd	AGGAGGAGCAACGACAAAGTT	*AtLBD38*	qPCR	E = 2.14 (60°C)
LBD38-qPCR-R	rev	GCCGTTCAAGCGAAGAGATTG	*AtLBD38*	qPCR	
LBD39-qPCR-F	fwd	TGGTTAAGGGTGATCGTCCG	*AtLBD39*	qPCR	E = 2.07 (60°C)
LBD39-qPCR-R	rev	GATTCCTCCGATGGACTTCCC	*AtLBD39*	qPCR	
NRT1.1-qPCR-F	fwd	TAAGGGATCAGGAAGCGGGA	*AtNRT1.1*	qPCR	E = 2.03 (60°C)
NRT1.1-qPCR-R	rev	TGGAACGGTCCAATGTCTCG	*AtNRT1.1*	qPCR	
Ubi10-qPCR-F	fwd	GGCTTGTATAATCCCTGATGAATAAG	*AtUBIQUITIN10*	qPCR	E = 1.93 (60°C)
Ubi10-qPCR-R	rev	AAAGAGATAACAGGAACGAAACATAGT	*AtUBIQUITIN10*	qPCR	
Ubox-qPCR-F	fwd	TGCGCTGCCAGATAATACACTATT	*AtUBOX*	qPCR	E = 2.01 (60°C)
Ubox-qPCR-R	rev	TGCTGCCCAACATCAGGTT	*AtUBOX*	qPCR	
CS16026-LP	fwd	TCATGTCTCTTCTTCAGCCGC	*AtRSA1*	genotyping	
CS16026-RP	rev	TTCATGTTGTTTCCTTTTCTCACAA	*AtRSA1*	genotyping	
CS16026-insertion	rev	AAGCTGGAGCTCGCTTGA	*AtRSA1*	genotyping	
RSA1-exon17-F	fwd	GTTGAAGATATGAGAGTAACCATTCACAGC	*AtRSA1*	sequencing insertion site in *rsa1-3*	
dmi1-2-LP	fwd	TCATATGCAATCTCGAGCATC	*AtDMI1*	genotyping	
dmi1-2-RP	rev	GAGTTATCCTCTGACTCGGGG	*AtDMI1*	genotyping	
cngc15(D408N)-F	fwd	TTAACCGGGTCGCCTTCTCTTACAA	*AtCNGC15*	genotyping	

cngc15(D408N)-R	rev	TTAACCGGGTCGCCTTCTCTTACAA	*AtCNGC15*	genotyping
LbB1.3	rev	ATTTTGCCGATTTCGGAAC	T-DNA (SALK)	genotyping
LB3	rev	TAGCATCTGAATTTCATAACCAATCTCGATACAC	T-DNA (SAIL)	genotyping

Table 2.2: List of media compositions for culture of bacteria, yeast, and plants

Medium	**Recipe for 1 litre**
ModFP (Modified Fahraeus Plant media) pH6 0.8% (w/v) agar	40mg NH_4NO_3, 40mg $CaCl_2{\cdot}2H_2O$, 40mg $MgSO_4{\cdot}7H_2O$, 30mg KH_2PO_4, 45mg $Na_2HPO_4{\cdot}12H_2O$, 2.5mg $C_6H_5FeO_7$, 2.8mg H_3BO_3, 2mg $MnSO_4{\cdot}4H_2O$, 0.22mg $ZnSO_4{\cdot}7H_2O$, 0.08mg $CuSO_4{\cdot}5H_2O$, 0.08mg H_2MoO_4, pH 6 with KOH.
½ strength MS 1% (w/v) sucrose 0.8% (w/v) agar	2.5g Murashige & Skoog Medium including Vitamins (0.0125mg/L $CoCl_2.6H_2O$, 0.0125mg/L $CuSO_4.5H_2O$, 18.35mg/L NaFe-EDTA, 3.1mg/L H_3BO_3, 0.415mg/L KI, 8.45mg/L $MnSO_4.H_2O$, 0.125mg/L $Na_2.MoO_4.2H_2O$, 4.3mg/L $ZnSO_4.7H_2O$, 166.01mg/L $CaCl_2.2H_2O$, 85mg/L KH_2PO_4, 950mg/L KNO_3, 90.25 mg/L $MgSO_4.7H_2O$, 825mg/L NH_4NO_3, 1mg/L glycine, 50mg/L myo-inositol, 0.25mg/L nicotinic acid, 0.25mg/L pyridoxine HCl, 0.05 mg/L thiamine HCl), 1% (w/v) sucrose. pH adjusted to 5.8 with 1 M NaOH. For solid medium, 0.8% (w/v) bacto agar.
BNM (Buffered Nodulation Medium)	390mg MES hydrate, 340mg $CaSO_4{\cdot}2H_2O$, 61mg $MgSO_4{\cdot}7H_2O$, 34mg KH_2PO_4, 2.3mg $ZnSO_4{\cdot}7H_2O$, 1.6mg H_3BO_3, 5.8mg $MnSO_4{\cdot}4H_2O$, 0.25mg $Na_2MoO_4{\cdot}2H_2O$, 0.025mg $CuSO_4{\cdot}5H_2O$, 0.025mg $CoCl_2{\cdot}6H_2O$, 9.35mg Na_2EDTA, 6.95mg $FeSO_4{\cdot}7H_2O$, pH 6 with KOH
LB (Lysogeny Broth)	10g Tryptone, 5g Yeast Extract, 5g NaCl, pH 7 with NaOH

TY (Tryptone Yeast extract)	5g Tryptone, 3g Yeast Extract, 1.32g $CaCl_2.6H_2O$
SOC (Super Optimal broth with Catabolite repression medium)	2 g Tryptone, 5g Yeast Extract, 0.58g NaCl, 0.19g KCl, 2.03g $MgCl_2$, 2.46 g $MgSO_4 \cdot 7H_2O$, 3.6 g glucose
SD (Synthetic Dextrose minimal media)	6.9g Yeast Nitrogen Base without Amino Acids (Formedium), 20g glucose, 30mg L-isoleucine, 150mg L-valine, 20mg L-adenine hemisulphate, 20mg L-arginine, 30mg L-lysine, 20mg L-methionine, 50mg L-phenylalanine, 200mg L-threonine, 30mg L-tyrosine, 3mg L-tyrosine, 20 mg L-histidine, 100 mg L-leucine, 20mg L-tryptophan, 20mg uracil. pH 5.8 with NaOH. For solid medium, 2% (w/v) agar.
YPAD (Yeast Peptone Adenine Dextrose medium)	10g Yeast Extract, 20g peptone, 20g glucose, 20mg L-adenine hemisulfate. For solid medium, 2% (w/v) agar.

Chapter III: An investigation of the role of *MtAPSR1* in *Medicago truncatula* root endosymbiosis

3.1 Introduction

Current knowledge on the regulation of AM by Pi is centred around the mechanisms by which Pi sensing leads to a termination in AM colonisation (Section 1.2.6), but whether the Pi status can affect the presymbiotic signalling pathways to reduce the initiation of colonisation remains to be established. Previous studies have observed direct effects of Pi on AM spore germination and hyphal growth. Strigolactones, that increase fungal spore germination and hyphal branching, are induced upon phosphate and nitrate starvation in pea (Balzergue et al., 2010). Strigolactones are a diverse group of signalling molecules, but are all derived from carotenoids (reviewed in Wang and Bouwmeester (2018)). Enzymes involved in carotenoid biosynthesis and processing, such as *CAROTENOID CLEAVAGE DIOXYGENASE8* (*CCD8)*, are repressed by high phosphate in AM inoculated *Petunia hybrida* or Medicago, suggesting that reduced strigolactone biosynthesis could be contributing to decreased colonisation (Breuillin et al. (2010); Balzergue et al. (2013)). However, application of synthetic strigolactone was not sufficient to restore AM colonisation in Petunia, indicating that strigolactones are not the primary mechanism for AM regulation upon Pi (Breuillin et al., 2010).

Balzergue et al. (2013) observed that under high Pi (3.75mM) colonisation of Medicago by *Gigaspora gigantea* was frequently terminated prior to the formation of hyphopodia. To try to elucidate whether high Pi affected early signalling between the fungus and the plant, analysis of nuclear calcium signatures in Medicago epidermal root cells in response to *G. gigantea* spores was undertaken (Balzergue et al., 2013). Under both low Pi and high Pi conditions, the spores germinated equally well, but an increased frequency of higher order hyphal branching was observed only in low Pi. Although fewer hyphopodia occurred under high Pi, when they did form, the frequency of calcium oscillations in the underlying epidermal cells was unchanged. This

indicates that there is a mechanism preventing hyphopodia from forming, but when they do form, nuclear calcium spiking seems unperturbed by high Pi (Balzergue et al., 2013). In addition, roots grown under both low and high Pi exhibited the same nuclear calcium response to germinated spore exudates (GSE) and the Myc factor CO4 (Balzergue et al., 2013). However, the parameters used to assess nuclear calcium spiking were the proportion of nuclei responding within a 30-minute imaging period, and the number of spikes recorded within small numbers of plants. Information about the frequency or duration of the calcium oscillations were not measured, and could have been implicated in AM colonization.

In another study, when Medicago roots were grown under low phosphate (Pi) conditions and nuclear calcium oscillations were measured, it was found that there were more active cells in the epidermal cell layer, i.e. more cells in which nuclear calcium oscillations were observed, and an increased frequency of calcium oscillations, compared to plants that were grown under high Pi (Russo et al., 2013). It has recently been established that accelerating the frequency of nuclear calcium oscillation increases nodulation and early AM colonisation in Medicago (Del Cerro et al., 2022). Therefore, it is possible that this increased frequency of nuclear calcium oscillations under Pi starvation conditions could accelerate the fungal colonisation. However, the discrepancy between the results from Balzergue et al. (2013) and Russo et al. (2013) is surprising, as both studies used the same nuclear calcium reporter (*p35S:NupYC2.1*) and the same concentrations of KH_2PO_4 for phosphate treatments. They did, however, use spores and hyphae of different fungal species, which may explain the differences.

Under phosphate starvation conditions, and not in nutrient replete conditions, barley and rice have been shown to display nuclear calcium responses to lipochitooligosaccharides (LCOs) (Li et al., 2022a). In barley, the frequency of calcium oscillations upon LCO or CO perception was increased by N and Pi depletion, and by combined N+Pi depletion (Li et al., 2022a). In Medicago, nuclear calcium oscillations in response to LCOs were enhanced under nutrient starvation conditions, particularly N starvation, whilst the

response to COs was unaffected (Li et al., 2022a). This regulation of calcium oscillations under different nutrient regimes was found to be controlled by *NODULATION SIGNALLING PATHWAY (NSP) 1* and *2*, by regulation of strigolactone and karrikin signalling (Li et al., 2022a). Taken together, these results suggest it is possible that the early stages of fungal colonisation are impacted by low and high phosphate regimes, by a yet uncharacterised mechanism, potentially involving the regulation of nuclear calcium oscillations.

The G protein β subunit is a known positive regulator of nodulation in soybean and Medicago (Choudhury and Pandey, 2013, Bovin et al., 2021). As described in section 1.2.3, G protein signalling has also been implicated in the signal transduction from the plasma membrane to the nucleus, which is required to initiate nuclear calcium oscillations. Nodulation gene expression can be induced by the G protein agonist mastoparan and its synthetic analogue Mas7 independently of DMI1 and DMI2 (Charron et al., 2004; Sun et al., 2007). This suggests that G protein signalling can activate the nuclear calcium oscillations without DMI1 or Nod/Myc factor perception.

A yeast two-hybrid screen to find interactors of MtGβ identified ALTERED PHOSPHATE STARVATION RESPONSE 1 (MtAPSR1) as an interactor in uninoculated root infection zones. The use of uninoculated root samples is particularly important, as it allows for the identification of interactors present before the developmental programme for endosymbiosis is initiated. In this chapter, I investigate the role of MtAPSR1 in the regulation of endosymbiosis, and discuss its potential role in regulating AM in response to phosphate. The aims of this chapter are to answer the following questions:

1. Does APSR1 interact with Gβ?
2. What is the phylogeny of APSR1, and can closely related genes help inform its function?
3. Is *APSR1* regulated by nutrient treatment?
4. What is the phenotypic effect of *apsr1* loss-of-function?

3.2 Results

3.2.1 MtAPSR1 interacts with the G protein β subunit via a yeast two-hybrid assay.

To confirm the interaction between MtAPSR1 and G protein β, a validatory pairwise yeast two-hybrid assay was carried out. Yeast two-hybrid assays were developed by taking advantage of the properties of the GAL4 transcription factor in the yeast *Saccharomyces cerevisiae*: as a transcriptional activator, it is required for the growth of yeast on galactose containing media, and is made up of two distinct domains, a DNA-binding domain (BD), and a transcriptional activator domain (AD). Generation of fusion constructs between genes of interest and either the DNA-binding domain or the transcriptional activation domain of *GAL4* allows an assessment of whether these two proteins interact in the heterologous yeast expression system. If the two proteins interact, they will reconstitute the two domains of GAL4, allowing for the activation of genes required for the growth of yeast on galactose containing media (Fields and Song, 1989).

The coding sequences (CDS) of *APSR1* and *Gβ* were previously cloned by Pierre Dangeville, and Gateway cloning was used to generate the *pGADT7(AD)-Gβ, pGBKT7(BD)-Gβ, pGADT7(AD)-APSR1, pGBKT7(BD)-APSR1, pGADT7(AD)-T* and *pGBKT7(BD)-54* constructs. Pairs of constructs were co-transformed into the yeast strain AH109, which lacks the ability to synthesise histidine or adenine, as the *HIS3* and *ADE2* genes are under the control of the *GAL4* promoter. Upon reconstitution of the AD and BD domains of GAL4, however, the yeast is able to grow on selective media lacking histidine and alanine. Yeast growth was detected on Synthetic Dropout medium lacking histidine and alanine (SD -LWAH) when yeast was co-transformed with both *pGBKT7(BD)-Gβ* and *pGADT7(AD)-APSR1,* confirming the interaction identified in the yeast two-hybrid screen (Figure 3.1). However, yeast growth was not observed on selective media when yeast was co-transformed with both *pGADT7(AD)-Gβ* and *pGBKT7(BD)-APSR1,* indicating that the interaction is specific to one configuration. In addition, yeast growth was observed on selective media when

yeast was co-transformed with *pGBKT7(BD)-APSR1* and *pGADT7(AD)-T,* indicating unspecific interaction of APSR1 with the positive control (Figure 3.1). Therefore, from this yeast to hybrid assay, the interaction between APSR1 and G*β* cannot be conclusively confirmed.

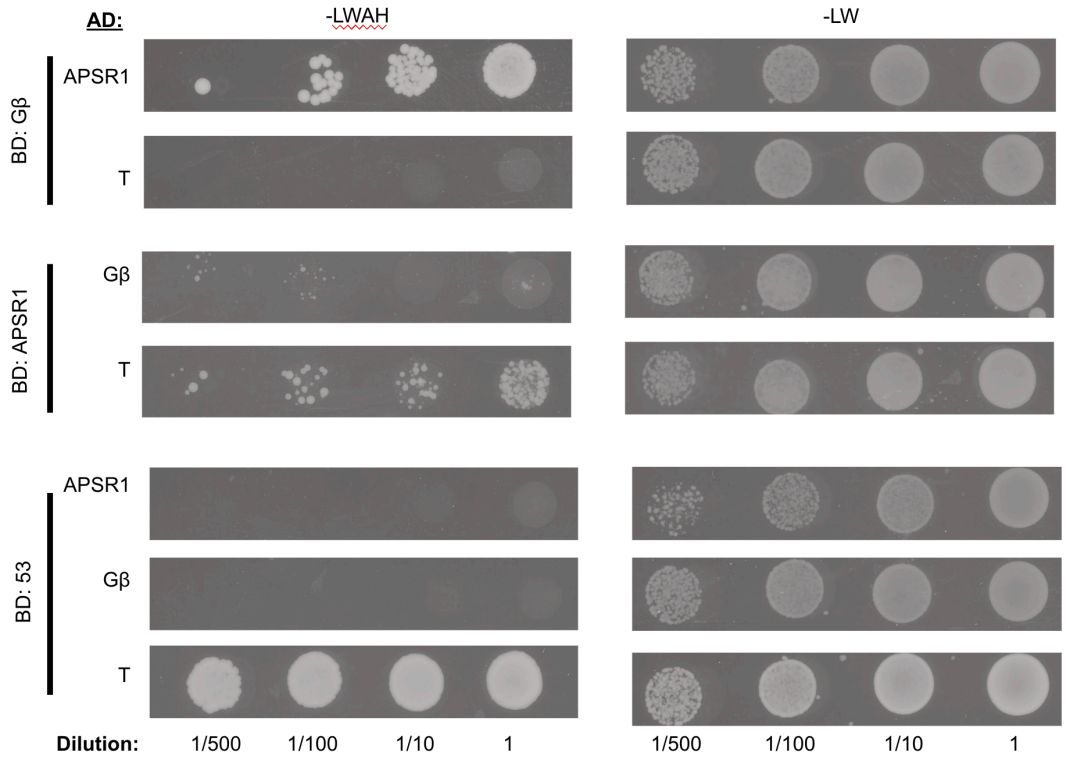


Figure 3.1 APSR1 interacts with the G protein β subunit via a Yeast two-hybrid assay in one configuration.
Yeast strain AH109 was co-transformed with constructs *pGADT7(AD)-Gβ, pGBKT7(BD)-Gβ, pGADT7(AD)-APSR1, pGBKT7(BD)-APSR1, pGADT7(AD)-T* and *pGBKT7(BD)-53* as labelled. Transformants were diluted as labelled and plated on selective synthetic dextrose minimal (SD) medium lacking Leucine, Tryptophan, Alanine and Histidine (-LWAH) and unselective synthetic dextrose minimal (SD) medium lacking Leucine and Tryptophan (-LW) and incubated for 5 days at 30°C. *pGADT7(AD)-T* and *pGBKT7(BD)-54* are positive controls.

3.2.2 MtAPSR1 is part of the NRG2 family, with orthologs in Arabidopsis.

Database searches revealed that *MtAPSR1* is part of the *NITRATE REGULATORY GENE 2 (NRG2)* gene family. To gain more information on the potential function of MtAPSR1, I constructed a phylogenetic tree of the NRG2 gene family (Figure 3.2). I chose sequences from a subset of plant species to reflect the phylogenetic diversity of the plant kingdom, including *Marchantia*

polymorpha as an ancestral land plant to root the tree, *Arabidopsis thaliana* as one of the most studied plant species, *Oryza sativa* as a monocotyledon, and *Glycine max* and *Medicago truncatula* as model legume species. The tree was constructed using aligned amino acid sequences and the maximum likelihood approach. Ultrafast bootstrapping was used to estimate the significance of the branches on the tree.

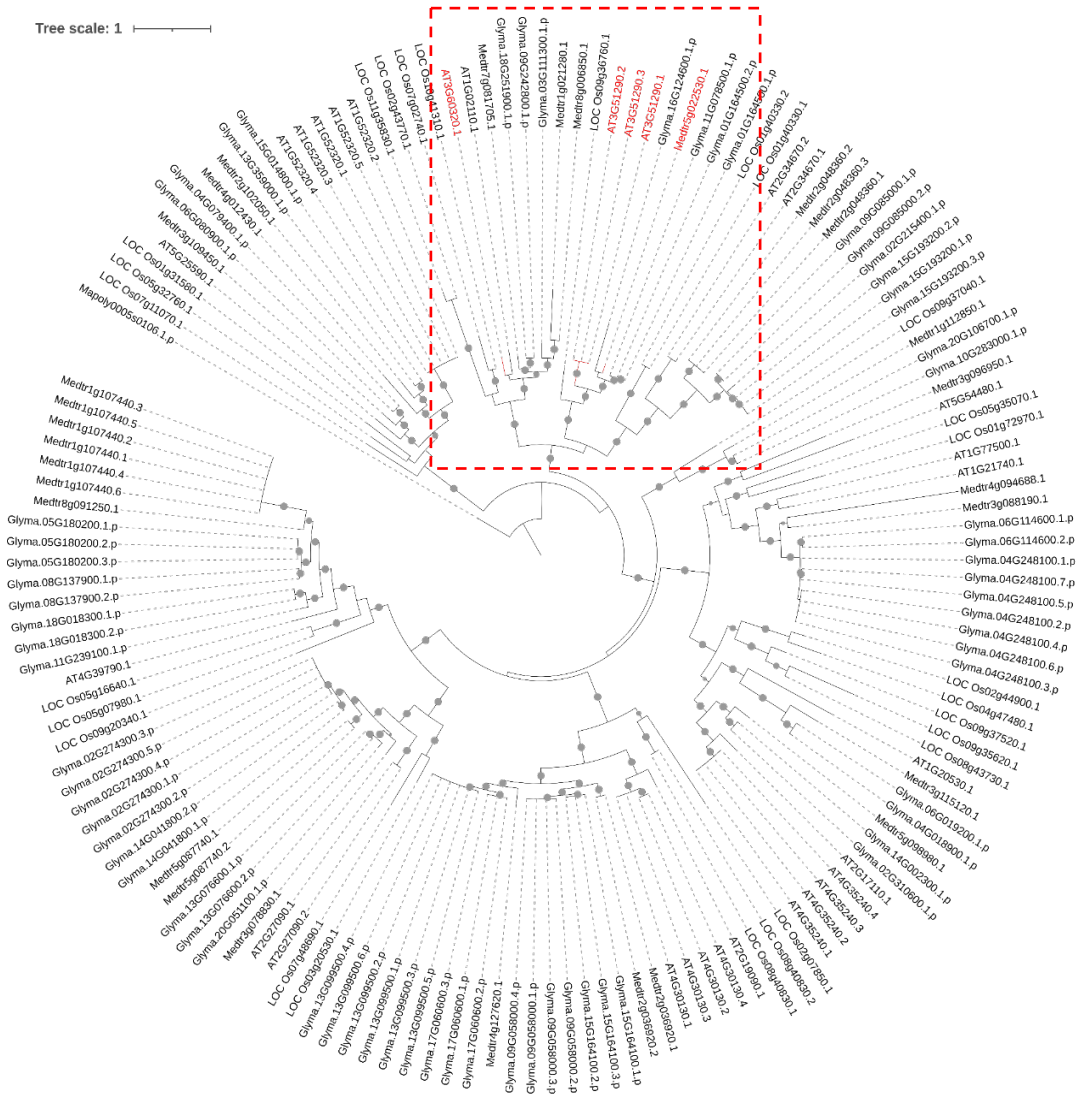


Figure 3.2 Phylogenetic analysis of the NRG2 family.

Rooted maximum likelihood tree using amino acid sequences from *Marchantia polymorpha*, *Arabidopsis thaliana*, *Oryza sativa*, *Glycine max* and *Medicago truncatula*. Genes are labelled according to their gene ID, with splice variants included. Ultrafast bootstrap support values over 95 are displayed by grey circles on the branches. Branch lengths are scaled by the number of substitutions per site, indicated by the scale bar. The red box indicates the clade containing MtAPSR1, which can be seen in more detail in Figure 3.3.

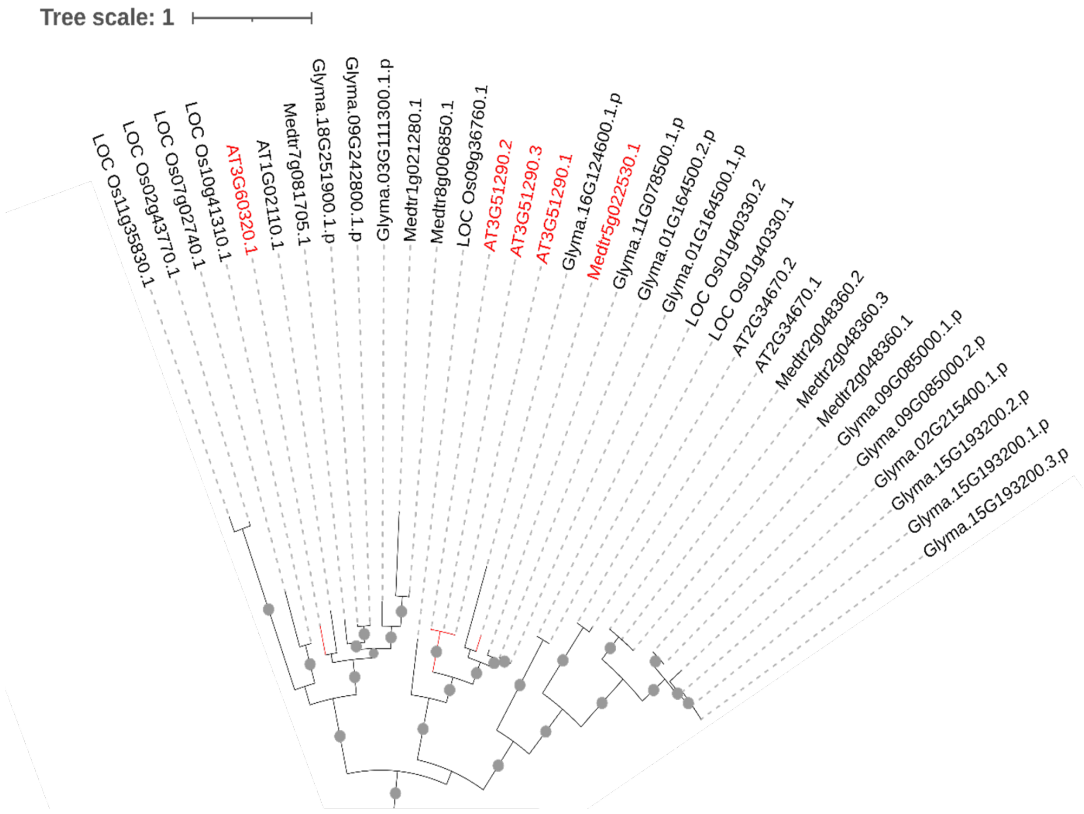


Figure 3.3 A closer look at the clade containing MtAPSR1.

Highlighted in red are *Mt*APSR1 (Medtr5g022530.1), three splice variants of *At*APSR1 (AT3G51290.1, AT3G51290.2, AT3G51290.3) and *At*NRG2 (AT3G60320.1). Genes are labelled according to their gene ID, with splice variants included. Branch lengths are scaled by the number of substitutions per site, indicated by the scale bar. Ultrafast bootstrap support values over 95 are displayed by grey circles on the branches.

This revealed that the closest ortholog to MtAPSR1 in Arabidopsis is AtAPSR1, with AtNRG2 being more distantly related (Figures 3.2 and 3.3). A literature search of *AtAPSR1* revealed one study investigating its role in the phosphate starvation response pathway (González-Mendoza et al., 2013). *AtAPSR1* was found to be upregulated upon phosphate treatment, and removing the gene functionality by either a frame shift EMS mutation or T-DNA insertion led to plants that showed phosphate starvation root phenotypes even in the presence of high phosphate. This raises the possibility that MtAPSR1 is also involved in response to nutrient availability.

3.2.3 *MtAPSR1* is induced by phosphate treatment.

To assess whether *MtAPSR1* is regulated by nutrient availability, its expression was validated in Medicago roots under treatment with different nutrient conditions, in the presence or absence of endosymbionts (Figure 3.4). *MtAPSR1* was induced upon treatment with both 1mM and 5mM KH_2PO_4, but not in the presence of the AM fungi *Rhizophagus irregularis* (Figure 3.4A). The marker genes *MEDICAGO TRUNCATULA 4* (*MT4)*, that is downregulated upon phosphate treatment, (Burleigh and Harrison, 1998)) and *PHOSPHATE TRANSPORTER 4 (PT4),* that is specifically expressed in arbuscule containing cells, (Harrison et al., 2002) were used to confirm the efficacy of the treatments provided (Figure 3.4A). Nitrate treatment, and treatment with *S. meliloti* 2011, did not alter *MtAPSR1* expression (Figure 3.4B). Efficacy of the nitrate treatment was assessed using the marker gene *NITRITE REDUCTASE 1 (NiR1)* and rhizobia inoculation using the marker gene *EARLY NODULIN 11 (Enod11)* (Charron et al., 2004). In addition, nodule number was significantly reduced in plants treated with 5mM KNO_3, indicating normal nitrate-dependent regulation of nodulation (Figure 3.4C) (Streeter and Wong, 1988). The treatment times used were 2 weeks for the nutrient conditions and rhizobia inoculation, and 4 weeks for the AM inoculation, as AM colonisation takes longer to become established. Taken together, these results indicate that, like *AtAPSR1*, *MtAPSR1* is positively regulated by phosphate treatment, but not differentially regulated by the presence of endosymbionts. This is in accordance with data from the *Medicago truncatula* gene expression atlas (Figure 3.5), where expression of *MtAPSR1* was not altered by either Nod factor treatment, or inoculation with AM fungi.

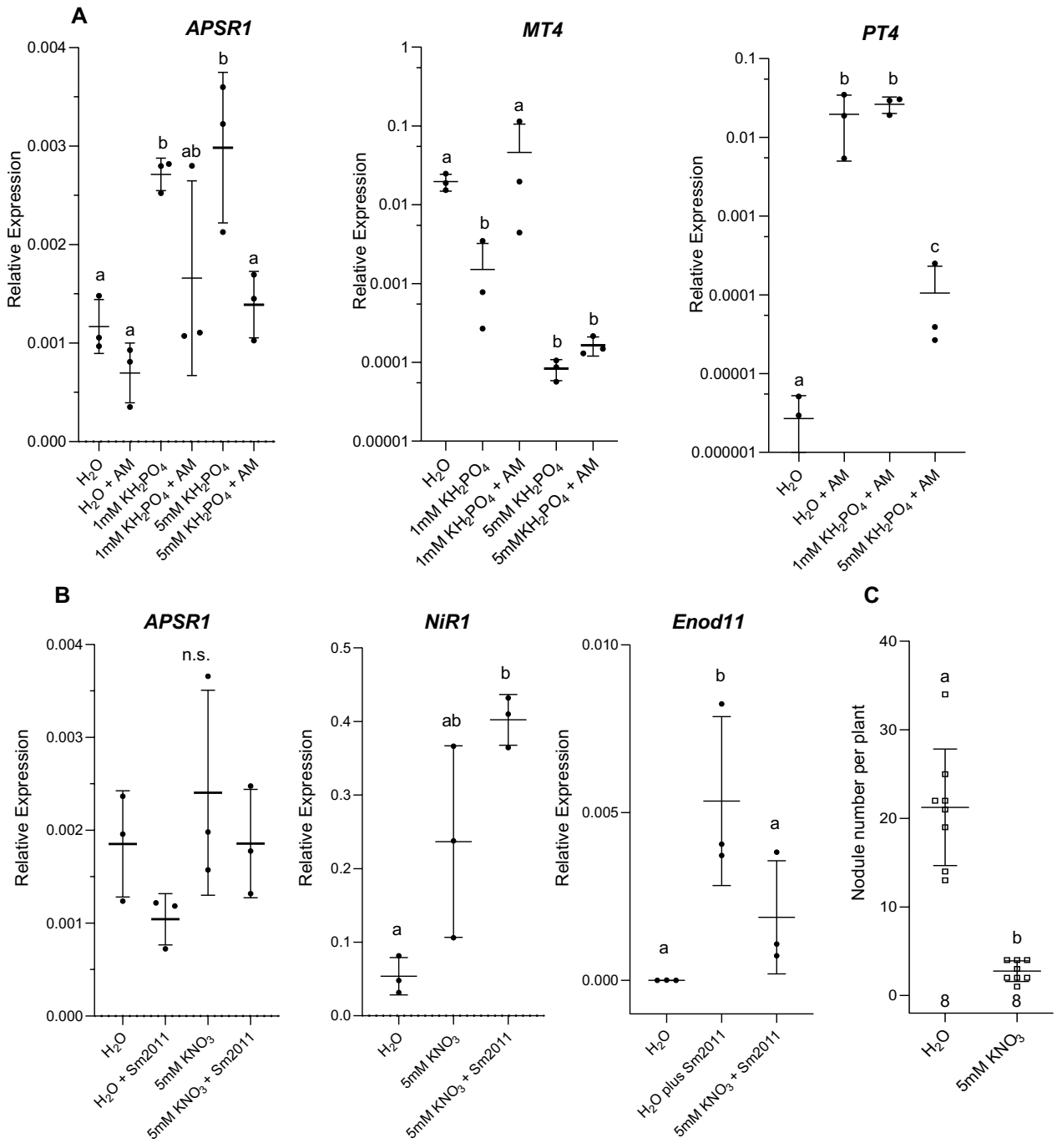


Figure 3.4 Mean relative expression of *APSR1* in Medicago truncatula R108 roots under nitrate and phosphate treatments, with and without inoculation with *S. meliloti* 2011 or *R. irregularis*.

(A) *ALTERED PHOSPHATE STARVATION RESPONSE 1 (APSR1), MEDICAGO TRUNCATULA 4 (MT4)* and *PHOSPHATE TRANSPORTER 4 (PT4)* expression in roots after 2 weeks treatment with H_2O, 1mM KH_2PO_4 or 5mM KH_2PO_4, or 4 weeks treatment with H_2O plus AM, 1mM KH_2PO_4 plus AM or 5mM KH_2PO_4 plus AM. **(B)** *APSR1, NiR1* and *Enod11* expression in roots after 2 weeks treatment with H_2O, H_2O plus *S. meliloti* 2011, 5mM KNO_3, and 5mM KNO_3 plus *S. meliloti*

2011. **(C)** Nodule number per wild type R108 plant used in **(B)**, 2 weeks post inoculation with *S. meliloti* 2011, treated with H_2O or 5mM KNO_3. n numbers are denoted beneath the bars. Error bars represent mean ± SD. **(A,B)** Statistical significance was calculated using one-way ANOVA with prior F-test for homoscedasticity and Tukey's multiple comparison post-test, with letters denoting statistical significance, n.s. = not significant. Data represents three biological replicates, with roots from three plants pooled per replicate. Expression was normalized to the housekeeping gene *MtUBC9* (*Medtr7g116940*). **(C)** Statistical significance was calculated using Welch's t-test.

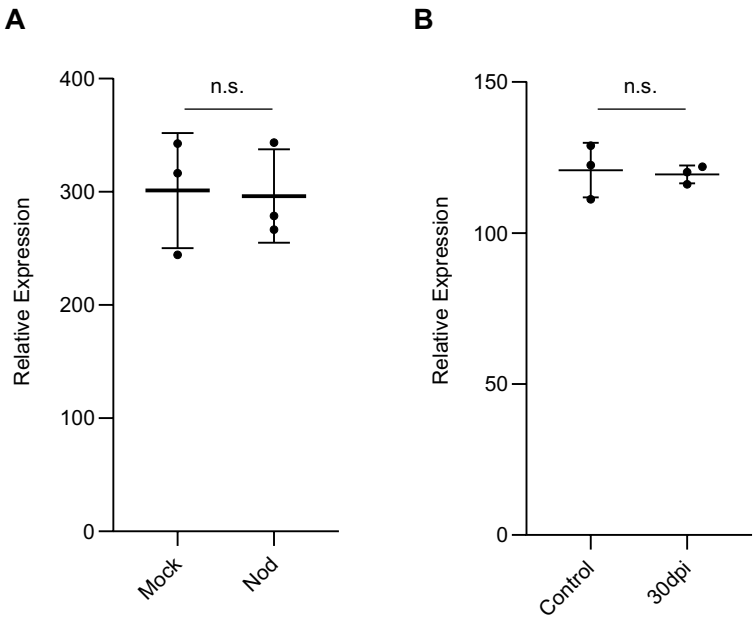


Figure 3.5. Expression of APSR1 is not altered by treatment with Nod factor or infection with *Rhizophagus irregularis*.

(A) Expression of *APSR1* in roots of 5 day old seedlings 24 hours after treatment with a control (mock), 10^{-8}M Nod factor (Nod), (Niebel *et al.*, unpublished). **(B)** Expression of *APSR1* in *Medicago truncatula* roots inoculated with *Rhizophagus irregularis* for 30 days (30dpi) or uninoculated for 30 days (control). (Gomez *et al.* 2009). Error bars represent standard deviation above and below the mean. Mean and SD values were calculated from three replicates for each treatment. Statistical significance was calculated using Welch's t-tests. n.s. = non-significant. Data was retrieved from the *Medicago truncatula* gene expression atlas: https://mtgea.noble.org/v3/ (*APSR1* probe ID: Mtr.26989.1.S1_at).

3.2.4 Identification and characterisation of two *Mtapsr1 tnt* insertion lines

To assess the role of MtAPSR1 in endosymbioses, I searched the *Medicago truncatula* mutant database for lines with *tnt* insertions in *MtAPSR1*. The lines were genotyped, and positions of the *tnt* insertions confirmed via sequencing (Figure 3.6 B and C). Line NF12622 has an insertion in the 3' UTR (Figure 3.6A), so it is not predicted to affect the coding region of the gene. However, the insertion caused a significant reduction in the expression of *MtAPSR1* by qRT-PCR (Figure 3.6E). In contrast, the *tnt* insertion in NF4464 is in exon 1 (Figure 3.6A), so produces a truncated protein of 124 amino acids (Figure 3.6D).

To determine whether MtAPSR1 is required for endosymbioses, I first performed an arbuscular mycorrhization assay. After 7 weeks of inoculation with AM inoculum, the assessment of AM colonization revealed reduced percentage colonisation of intraradical hyphae, arbuscules, and vesicles in both NF12622 and NF4464 compared to wild type R108 (Figure 3.7A). As well as using two independent *tnt* insertion lines, a NF4464 segregating population was used to ensure that this phenotype is due to the *tnt* insertion in *MtAPSR1*, and not an alternative insertion. The reduced AM colonisation was specific to plants homozygous for the *tnt* insertion, indicating that the mutation is recessive, and that *MtAPSR1* is required for normal AM colonisation (Figure 3.7B).

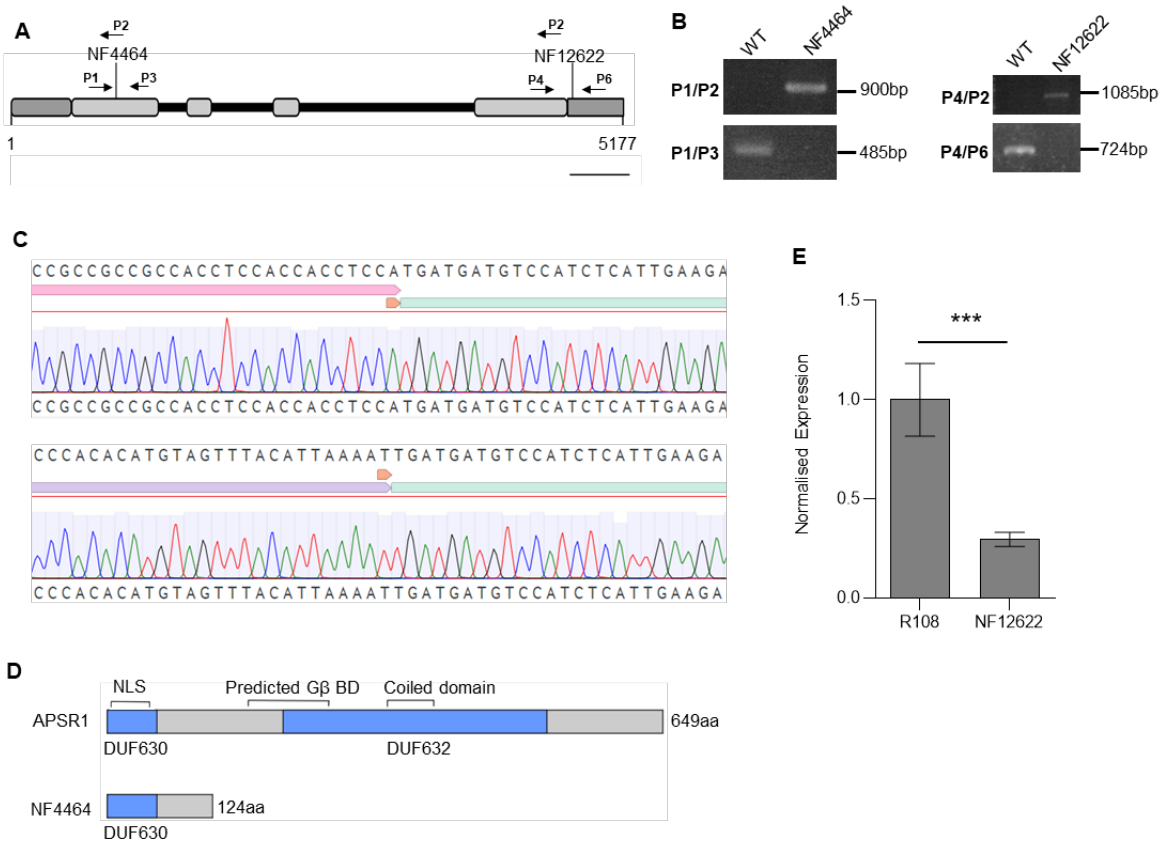


Figure 3.6 Characterisation of 2 *Mtapsr1 tnt* insertion lines.

(A) Schematic showing the structure of the *MtAPSR1* gene and the location of the *tnt* insertion sites in the NF4464 and NF12622 lines. Dark grey boxes represent the 5' UTR and 3' UTR, light grey boxes represent exons, and black lines represent introns. Scale bar represents 500bp. **(B)** Genotyping of the NF4464 and NF12622 lines via PCR, using the primers labelled in **(A)**. Primer sequences can be found in Table 2.1. **(C)** The exact location of the *tnt* insertion sites was determined via sequencing of the bands in **(B)**. Top, NF4464 insertion site. Bottom, NF12622 insertion site. Exon 1 is labelled in pink, 3' UTR in purple, the T-DNA insertion sequences are in blue, and the insertion sites are labelled in orange. The NF4464 insertion site is at 883bp, and the NF12622 insertion site is at 4838bp. **(D)** Schematic of the amino acid sequence of APSR1 (top), and the predicted consequence of the *tnt* insertion on APSR1 in the NF4464 line (bottom). Domain of unknown function (DUF) domains are labelled in blue, and the locations of the nuclear localisation signal (NLS), predicted Gβ binding domain (BD), and coiled domain are labelled. **(E)** Quantitative real-time PCR (qRT-PCR) analysis of the transcript level of *APSR1* in 7-day old roots of wild type R108 and mutant line NF12622. n=3, bars represent mean ±SD. Expression was normalized to the housekeeping gene *MtUBC9* (*Medtr7g116940*) and displayed as fold-change relative to the wild type R108. Statistical significance was calculated using Welch's t-test (***$p < 0.001$).

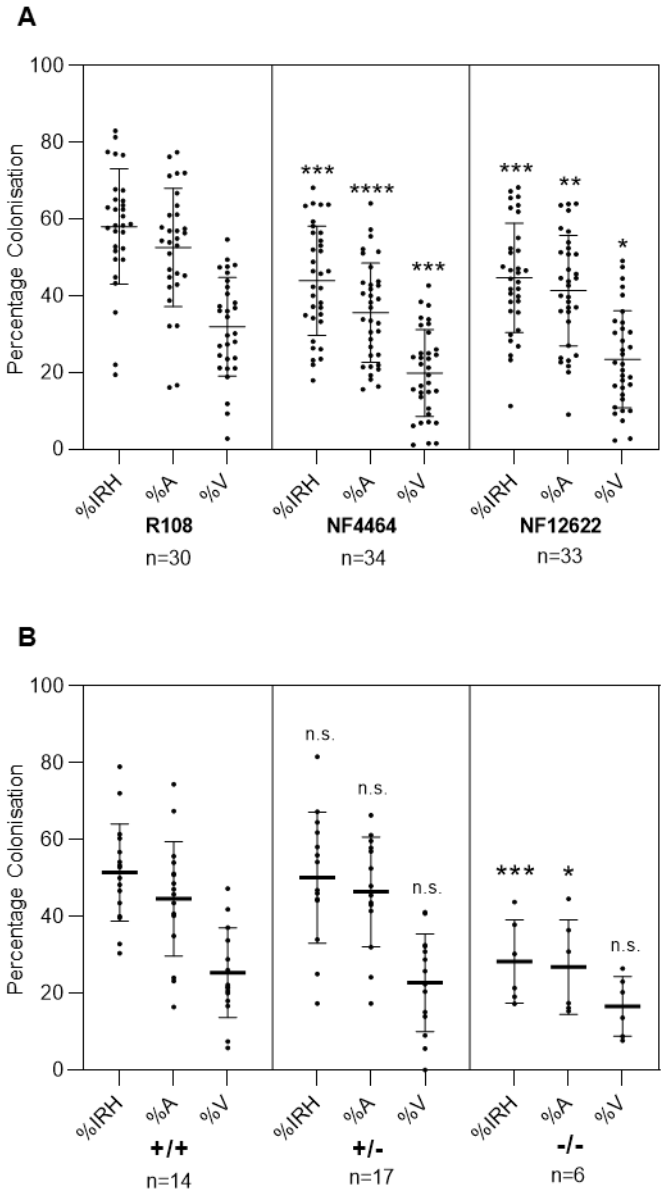


Figure 3.7 NF4464 and NF12622 lines have reduced arbuscular mycorrhizal colonisation.

(A) Arbuscular mycorrhization assay of wild type R108 plants and *tnt* insertion lines NF4464 and NF12622. Data represents 3 independent biological replicates. **(B)** Arbuscular mycorrhization assay of a segregating population of NF4464, containing plants that are wild type (+/+), heterozygous (+/-) and homozygous (-/-) for the *tnt* insertion. Data represents one biological replicate. Percentage colonisation of intraradical hyphae (%IRH), arbuscules (%A) and vesicles (%V), approximately 7 weeks post inoculation with *R. irregularis*. Bars represent mean ± SD. Statistical significance was calculated using Welch's t-tests, comparing the percentage of each structure to the control (R108 in **A**, +/+ in **B**) (*$p < 0.05$, **$p < 0.01$, ***$p < 0.001$, ****$p < 0.0001$, n.s. = not significant).

In contrast, neither NF12622 or NF4464 lines showed a different nodulation phenotype to wild type when inoculated with *S. meliloti* strain 2011 (Sm2011), with or without treatment with 5mM KNO_3 (Figures 3.8 and 3.9). Both lines showed a reduction in nodule number upon treatment with nitrate. Taken together, the endosymbiosis phenotypes suggest that *MtAPSR1* is specifically required for AM colonisation, but not nodulation.

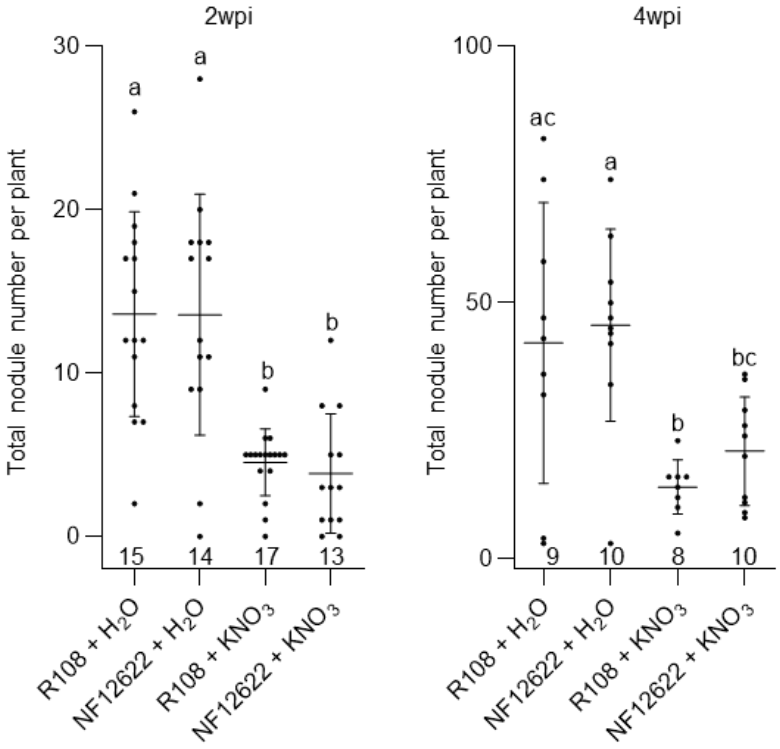


Figure 3.8 Nodulation assay of wild type R108 and tnt insertion line NF12622 plants.

Total nodule number per plant at 2 weeks post inoculation (wpi) **(A)** and 4 wpi **(B)** with *S. meliloti* 2011. Plants were treated with water, or 5mM KNO_3. Number of plants (n) is denoted underneath the bars. Bars represent mean ± SD. Letters indicate statistical significance (one-way ANOVA with prior F-test for homoscedasticity and Tukey's multiple comparison post-test). Data represents 2 independent biological replicates.

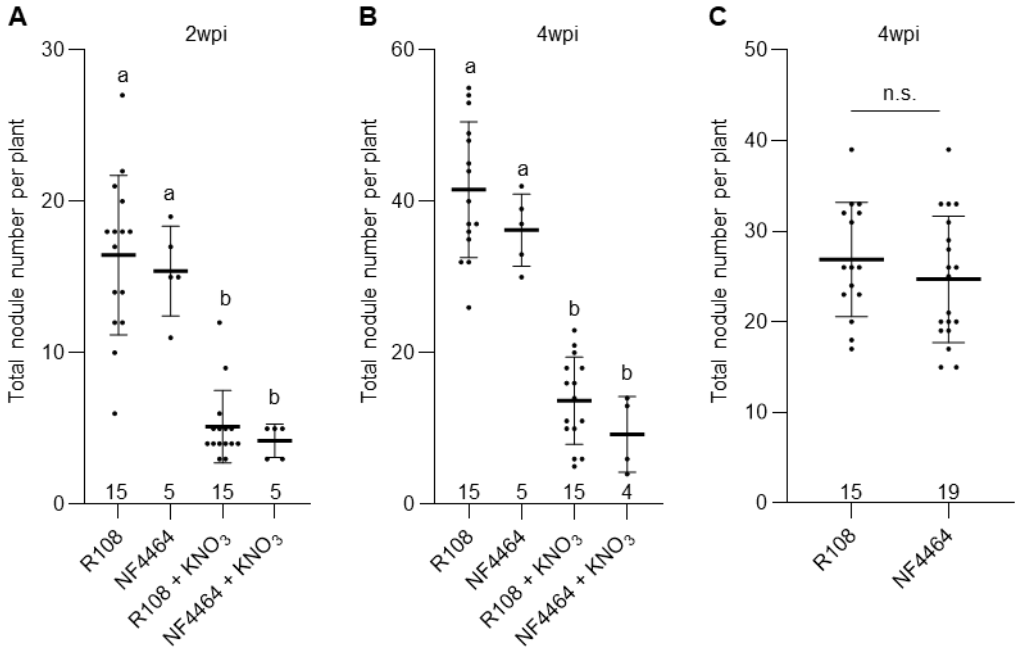


Figure 3.9 Nodulation assay of wild type R108 and tnt insertion line NF4464 plants.

Total nodule number per plant at 2 weeks post inoculation (wpi) **(A)** and 4 wpi (**B** and **C**) with *S. meliloti* 2011. Plants were treated with water, or 5mM KNO_3. Number of plants (n) is denoted underneath the bars. Bars represent mean ± SD. Letters indicate statistical significance (**A,B** one-way ANOVA with prior F-test for homoscedasticity and Tukey's multiple comparison post-test, **C** Welch's t-test, n.s. = not significant). **(A)** and **(B)** represent one biological replicate, and **(C)** represents a second biological replicate at the 4wpi timepoint.

3.3 Discussion

In this chapter, I have demonstrated that an interactor of *MtGβ*, *MtAPSR1*, is induced at the transcript level by phosphate treatment (Figure 3.4A), like its ortholog *AtAPSR1*, and specifically impacts AM colonisation and not nodulation (Figures 3.7-3.9). The *AtAPSR1* knockout mutant line *apsr1-1* displays a phosphate starvation phenotype of reduced primary root length and longer root hairs when grown in high phosphate conditions (1mM Pi), suggesting a reduced sensitivity to phosphate (González-Mendoza et al., 2013). Own-promoter localisation experiments suggest that AtAPSR1 localises to the nucleus, however the functionality of the predicted promoter was not validated by complementation experiments. MtAPSR1 is also predicted to localise to the nucleus by Wolf PSORT. Both *MtAPSR1* and *AtAPSR1,* as well as the members

of the NRG2 family in Figure 3.2, contain the Domains of Unknown Function (DUF) 630 and 632 (Figure 3.6D). These domains are as yet uncharacterised, and although DUF630 can be found in putative plant bZIP proteins, the function of these regions is not known.

I observed reduced AM colonisation in both the NF12622 and NF4464 *tnt* insertion lines under phosphate starvation, indicating that MtAPSR1 is acting as a positive regulator of AM colonisation in this case. MtAPSR1 is also induced upon phosphate treatment at the transcript level, and phosphate treatment results in reduced AM colonization (Hepper, 1983). This upregulation may increase the interaction between MtAPSR1 and MtGβ, impeding the ability of MtGβ to regulate endosymbiosis. The fact that MtAPSR1 affects AM colonization, but not nodulation (Figures 3.7-3.9), is surprising as MtGβ has been shown to play a role in nodulation (Bovin et al., 2021) but not yet in AM. The data suggests that MtGβ might also play a role in AM.

Nodulation is regulated by phosphate to some extent, with phosphate starvation causing a reduction in nodule number (Jakobsen, 1985, Hernández et al., 2009), potentially through activation of the autoregulation of nodulation (AON) pathway (Isidra-Arellano et al., 2020). However, inhibition of endosymbiosis in sufficient phosphate conditions is specific to AM colonisation, and requires pathways such as the PHR-SPX regulatory network to trigger the abortion of arbuscules. In addition, the early stages of AM colonization have been shown to be inhibited by high phosphate (Balzergue et al., 2013) implying the presence of an alternative mechanism to inhibit the initiation of infection. Given that MtAPSR1 is predicted to bind to MtGβ, and that the putative promoter region 3kb region upstream of *MtAPSR1* does not contain any P1BS domains known to be recognised by PHRs (Wang et al., 2021a), it seems unlikely to be involved in the early termination of AM symbiosis mediated by PHR-SPX. In Medicago, it has been shown that N+Pi starvation conditions enhance nuclear calcium oscillations upon treatment with S-LCOs and NS-LCOs (Li et al., 2022a). In addition, it has been suggested that low phosphate conditions may enhance the nuclear calcium oscillations in response to AM fungi (Russo et al., 2013), although as I have described, the literature is inconclusive.

Therefore, it is possible that MtAPSR1 is regulating nuclear calcium oscillations in response to phosphate via its interaction with MtGβ.

To elucidate the role of *MtAPSR1* in the regulation of AM upon phosphate treatment, an AM assay of NF4464 and NF12622 should be carried out under high phosphate conditions. If *MtAPSR1* is involved in the downregulation of AM upon Pi, I would expect NF4464 and NF12622 plants to be insensitive to phosphate treatment, and therefore the reduction in AM colonisation will be less, or abolished entirely. In addition, the localisation of MtAPSR1 needs to be established, under low and high Pi conditions, and the interaction between MtAPSR1 and MtGβ needs to be validated *in planta,* for example by bimolecular fluorescence complementation in Medicago transformed hairy roots, FRET-FLIM (Förster resonance energy transfer by fluorescence lifetime imaging) experiments and co-immunoprecipitation.

Chapter IV – Investigation of a novel allele of CNGC15, and its dual function in Arabidopsis root apical meristems

Parts of this chapter are published in Tipper et al. (2023) and appear here with permission. Homology modelling was done in collaboration with Professor David Lawson (JIC).

4.1 Introduction

Plant cyclic nucleotide-gated channels (CNGCs) are central to calcium signalling in a wide range of processes, including in development, and biotic and abiotic stress responses (Jarratt-Barnham et al. (2021)). In recent years, advances in their characterisation have revealed that the modular architecture of the CNGCs, which assemble as homo- and/or hetero-tetramers, contributes to their plurality of function and mechanisms of regulation (Pan et al., 2019, Yu et al., 2019). In plants, each CNGC subunit consists of six membrane-spanning segments designated S1 to S6, along with a cyclic nucleotide-binding domain (CNBD), a C-linker region, and a calmodulin-binding domain (Matulef and Zagotta, 2003).

Whilst the direct binding of cyclic nucleotides is essential for the function of mammalian cyclic nucleotide-gated (CNG) channels (Fesenko et al., 1985, Kaupp et al., 1989, Dhallan et al., 1990), in plants some CNGCs are regulated by cyclic nucleotides in heterologous systems (Leng et al. (2002a); Hua et al. (2003)), and others are not (Zhang et al., 2019). However, these studies used different heterologous systems, such as Human Embryonic Kidney 293 (HEK293) cells (Hua et al. (2003)), *X. laevis* oocytes (Zhang et al. (2019)) or both (Leng et al. (2002a)). The use of heterologous systems, and different ones at that, makes it difficult to assess the cyclic nucleotide (cNMP) requirement *in planta*.

CNGCs mediate calcium release in various plant cell types and cellular compartments (Dietrich et al., 2020, Jarratt-Barnham et al., 2021). In Medicago, three nuclear-localized CNGC15 paralogues, CNGC15a, CNGC15b, and CNGC15c, in complex with the ion channel Does not Make Infections 1 (DMI1),

are required for the generation of nuclear calcium oscillations that are essential for the establishment of nitrogen-fixing bacterial and arbuscular mycorrhizal symbioses (Charpentier et al., 2016). The C-termini of the three MtCNGC15s associate with holo-Calmodulin 2, which modulates their activities by providing the negative feedback to close the CNGC15 channel (Del Cerro et al., 2022). Interestingly, the three CNGC15s have different affinities for holo-Calmodulin 2, suggesting that they could form a heterocomplex to regulate nuclear calcium oscillation (Del Cerro et al., 2022). In Arabidopsis, that cannot perform symbioses with arbuscular mycorrhizal or nitrogen-fixing bacteria, the functional orthologue of *MtDMI1* is encoded by *AtDMI1* and modulates the nuclear calcium release associated with primary root apical meristem development and auxin homeostasis (Leitão et al., 2019). In contrast to Medicago, only one *AtCNGC15* is present in the Arabidopsis genome (Mäser et al., 2001). Expression of *AtCNGC15* complements the symbiosis defect of the double mutant *MtCNGC15c,b* (Leitão et al., 2019), and AtCNGC15 localizes at the nuclear envelope in close proximity to AtDMI1 at the early stages of root development (6 days post germination, dpg) (Leitão et al., 2019, Wang et al., 2021c). In addition, along with AtDMI1, AtCNGC15 has been found to contribute to the generation of nuclear calcium release in Arabidopsis root apical meristem (RAM) development (Tipper et al., 2023). The novel mutant allele *Atcngc15*^{D408N} causes a reduction in primary root length, due to a reduced meristem size and number of meristematic cells (Tipper et al., 2023). This is similar to the phenotype of *dmi1-2*, and, like *dmi1-2,* is also associated with a reduced frequency of nuclear calcium release in the RAM (Leitão et al., 2019, Tipper et al., 2023). Therefore, modulation of the nuclear calcium release mediated by AtDMI1 and AtCNGC15 impacts RAM development and subsequent primary root growth.

In addition, in Arabidopsis it was recently shown that at a later stage of root growth (12dpg), AtCNGC15 can form a complex with the plasma membrane nitrate transceptor NRT1.1 to regulate nitrate signalling (Wang et al., 2021c). As AtCNCG15 localizes to the nuclear envelope in young roots, this observation

suggests that nitrate signalling would occur independently of AtCNGC15 at this early stage.

In this chapter, I continue the characterisation of this novel *Atcngc15*^{D408N} mutant allele, using homology modelling and electrophysiology, and use gene expression analyses and localisation experiments to assess the role of CNGC15 in nitrate signalling. I aim to answer the following questions:

1. What effect does the D408N point mutation have on the structure of the ion channel?
2. What effect does the D408N point mutation have on the permeability of CNGC15^{D408N} to calcium, and its gating?
3. Does cAMP assist in the gating of CNGC15^{D408N}?
4. Is CNGC15 required for nitrate induced gene expression?
5. Does the nuclear calcium release generated by CNGC15 and DMI1 affect the cell cycle?

4.2 Results

4.2.1 The D408N point mutation is in the C-linker region of CNGC15.

It has been shown that the D408N mutation in CNGC15^{D408N} is semi-dominant (Tipper et al., 2023), as the heterozygous plants display an intermediate primary root phenotype in comparison to the wild-type and homozygous mutants. This suggests that irrespective of whether AtCNGC15 functions as a homo- or heterocomplex, D408N is sufficient to impair calcium release. To further investigate the effect of the D408N mutation on AtCNGC15 function at the molecular level, AlphaFold2 and homology modelling was used to predict its structure, which revealed that D408 is positioned in the C-linker region (Figure 4.1 A,B), known to modulate the opening and closing, also known as gating, of animal CNG channels (Mazzolini et al., 2018). The D408N mutation is predicted to disrupt a salt bridge that forms at each interface, between D408 from one subunit and R398 of its neighbour, and thereby impact the gating properties of the channel (Figure 4.1 B–F).

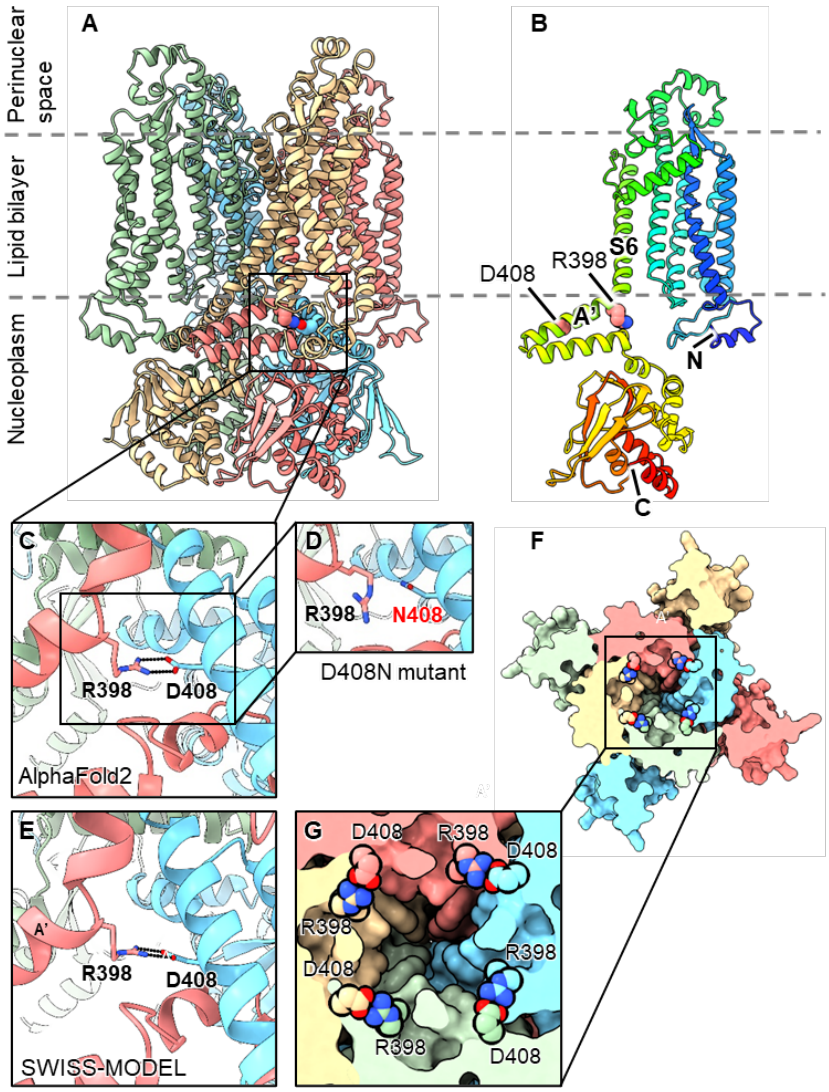


Figure 4.1 The D408N mutation is predicted to disrupt salt bridges between adjacent AtCNGC15 subunits. Figure produced in collaboration with Professor David Lawson (JIC).

(A) Cartoon representation of the AtCNGC15 model generated by AlphaFold2 (AF2), with the subunits illustrated in different colours. Poorly predicted regions at the N- and C-termini were deleted (residues 1-53 and 604-678, respectively). In the highlighted region, the residues contributing to one of the salt-bridges are shown as van der Waals spheres. **(B)** Single protomer corresponding to the salmon-coloured subunit in **(A)** illustrated with rainbow colouration from blue at the N-terminus through to red at the C-terminus. The positions of the residues D408 and R398 in the C-linker region referred to as the A' helix are indicated. **(C)** Close-up of the region highlighted in **(A)** showing one of the four symmetry-related salt-bridges (for clarity the yellow subunit in the foreground of **(A)** is omitted). The inset **(D)** shows the loss of this potential salt-bridge in the D408N mutant. **(E)** Structurally equivalent region to that shown in **(C)** for the SWISS-MODEL homology model based on the Eag1 structure, illustrating the similarity to the AF2 model. **(F)** View of the AF2 model from the nucleoplasm (i.e. from below with respect to the view shown in **(A)**) with the structure depicted as a solid molecular surface which is cutaway at the level of the salt-bridges. The latter are shown as van der Waals spheres. Note the location of the salt-bridges adjacent to the lumen of the channel. The inset **(G)** shows a close-up of this central region.

4.2.2 The D408N mutation affects the gating properties of CNGC15 in *Xenopus laevis* oocytes.

To test the hypothesis that the D408N mutation is affecting the gating of CNGC15^{D408N}, I expressed *AtCNGC15* and *AtCNGC15^{D408N}* in oocytes of *Xenopus laevis* and recorded the channel activity using a two-electrode voltage clamp (TEVC) system in the presence of 20 mM $CaCl_2$ or 20 mM $BaCl_2$ (Figure 4.2 A–C). TEVC is a method to study ion channels expressed in heterologous systems, such as *X. laevis* oocytes, that was developed in the 1940s (Cole (1950); Marmont (1949)). Given that passage through ion channels, whether voltage gated or not, will be affected by the membrane potential of the cell, the membrane potential needs to be kept constant in order to effectively study the activity of the ion channel. TEVC allows for this by using two electrodes, one to measure the membrane potential of the cell, and the other to inject a current so that the membrane potential is at the desired voltage (Guan et al., 2013a). TEVC is used for large cells, such as *X. laevis* oocytes, which are useful systems for studying ion channels due to their ability to translate injected RNA and produce heterologous proteins, and their low expression of endogenous receptors and ion channels (Guan et al., 2013a).

Oocytes injected with *AtCNGC15* cRNA or *AtCNGC15^{D408N}* cRNA displayed a significant inward current in the presence of 20 mM $CaCl_2$ (Figure 4.2A, B). The results confirm that CNGC15 is a calcium channel, in line with previous studies (Wang et al., 2021c), and further demonstrate that the AtCNGC15^{D408N} channel is permeable to calcium. For I/V curves, the x-intercept represents the voltage at which there is no net current across the membrane. From Figure 4.2A and B, this value is -26.204mV for AtCNGC15, and -26.169mV for AtCNGC15^{D408N} and represents the equilibrium potential for the Ca^{2+} ion in this system (PhysiologyWeb, 2014). This is similar to the values obtained for MtCNGC15a (Charpentier et al., 2016). Whilst *X. laevis* oocytes do contain native ion channels, including calcium permeable channels, they do not contain CNGCs or related CNGs (Weber et al., 1999). The water-injected oocytes were used as a control in order to account for the native ion channels present in the oocytes.

Although the calcium current recorded in oocytes expressing *AtCNGC15*^{D408N} is comparable to that recorded in oocytes expressing *AtCNCG15*, the percentage of oocytes displaying inward calcium current was significantly reduced (Figure 4.2D). Only 30% of oocytes injected with *AtCNCG15*^{D408N} presented open ion channels. This heterogeneity was observed even within the same clutch of *X. laevis* oocytes injected with the same preparation of cDNA.

To assess whether this reduced frequency was due to a perturbation in the translation and/or localisation of AtCNGC15^{D408N}, I expressed either *AtCNGC15* or *AtCNGC15*^{D408N} fused to GFP in oocytes (Figure 4.2E, F). The localisation and the fluorescence intensity of AtCNGC15:GFP and AtCNGC15^{D408N}:GFP are both identical (Figure 4.2E, F), demonstrating that the absence of a calcium current in 70% of the oocytes recorded is not due to altered translation and/or mislocalisation, but to the impaired opening of AtCNGC15^{D408N}. However, once the mutant channel opens, a wild-type calcium current is produced. This observation is consistent with the *in planta* phenotype of *Atcngc15*^{D408N}, which shows a reduced frequency of nuclear calcium release but without altering the rise and fall time of the calcium signal (Tipper et al., 2023). Together, these results demonstrate that the opening properties of AtCNGC15 are perturbed by the D408N mutation, which is predicted to weaken the interaction between the C-linker neighbouring units in the tetrameric CNGC15 complex. The gating mechanism of plant CNGCs is unknown, and these results support a role of the C-linker region in this gating, as is the case for animal CNG channels.

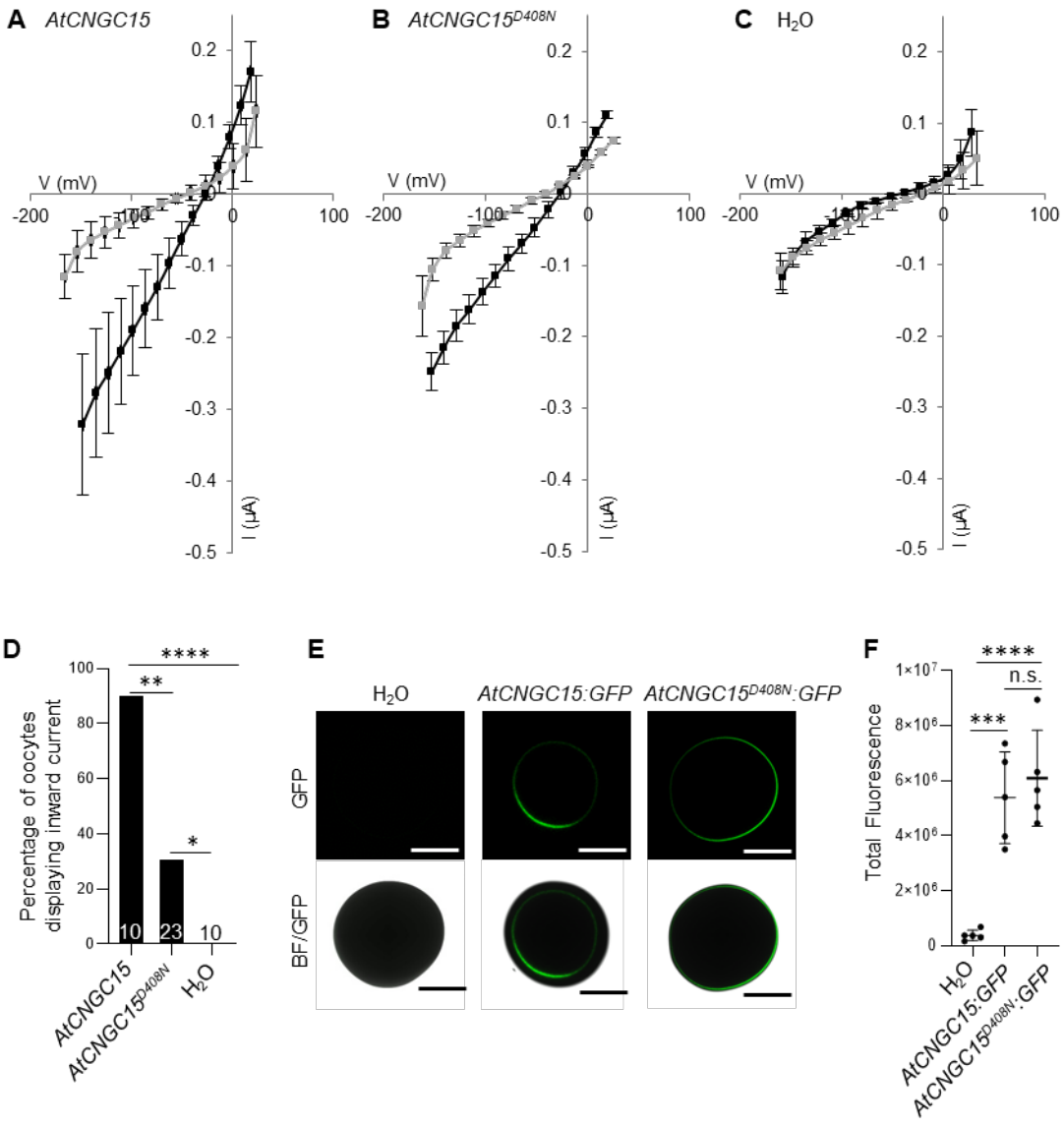


Figure 4.2 The D408N mutation impairs the gating of CNGCl5.

(**A**)-(**C**), Average current/voltage (I/V) curves in *Xenopus laevis* oocytes expressing *AtCNGCl5, AtCNGCl5*^{D408N}, or injected with water in the presence of 20mM $BaCl_2$ (grey) or 20mM $CaCl_2$ (black). Values represent means ± SD. (**D**) Percentage of oocytes displaying inward current upon calcium treatment when injected with At*CNGCl5* or *AtCNGCl5*^{D408N} cRNA, or water control. Statistical significance was calculated using Chi-squared tests (* p<0.05, *** p<0.001, **** p<0.0001). Numbers in bars denote sample size. **(E)** Green Fluorescence Protein (GFP) fluorescence (upper panel), and merged GFP and bright field images (bottom panel) of oocytes injected with either H_2O, *AtCNGCl5:GFP* cRNA or *AtCNGCl5*^{D408N}*:GFP* cRNA, taken with laser scanning confocal microscopy. Scale bars represent 500µm. **(F)** Quantified fluorescence intensity of oocytes injected with either H_2O, *AtCNGCl5:GFP* cRNA or *AtCNGCl5*^{D408N}*:GFP* cRNA. Fluorescence of each oocyte was measured relative to the background. Error bars represent mean ± SD. Statistical significance calculated using one-way ANOVA with Tukey's multiple comparison post-test, (n=5, *** p<0.001, **** p<0.0001, n.s.= not significant).

4.2.3 Cyclic adenosine monophosphate (cAMP) may assist the gating of *AtCNGC15*^{D408N}.

Animal CNG channels are directly activated by cyclic nucleotides, and several plant CNGCs have also been shown to be activated by either cAMP or cyclic guanosine monophosphate (cGMP) or both (Leng et al. (2002a); Hua et al. (2003)) , whilst other plant CNGCs do not appear to be activated by cyclic nucleotides (Zhang et al., 2019). The opening of AtCNGC15, and subsequent calcium conductance, does not require the external application of cyclic nucleotides (Figure 4.2 and Wang et al. (2021c)). However, the AtCNGC15^{D408N} mutant channel is perturbed in gating (Figure 4.2) potentially due to the mutation affecting the flexibility of the C-linker region. This raises the question as to whether application of cyclic nucleotides would assist in the opening of the AtCNGC15^{D408N} mutant channel, by causing a conformational change that would increase the gating flexibility. Therefore, I applied 10µM cAMP to the perfusion bath of *X. laevis* oocytes expressing *AtCNGC15*^{D408N} that had shown no response to calcium perfusion. In two separate instances, application of cAMP lead to channel opening and conductance of calcium, suggesting that cAMP can assist the opening of the channel (Figure 4.3). It is worth noting that applying a voltage step of -165 mV may have activated endogenous chloride channels within the oocyte (Kowdley et al., 1994), so future experiments should avoid using such hyperpolarising voltages.

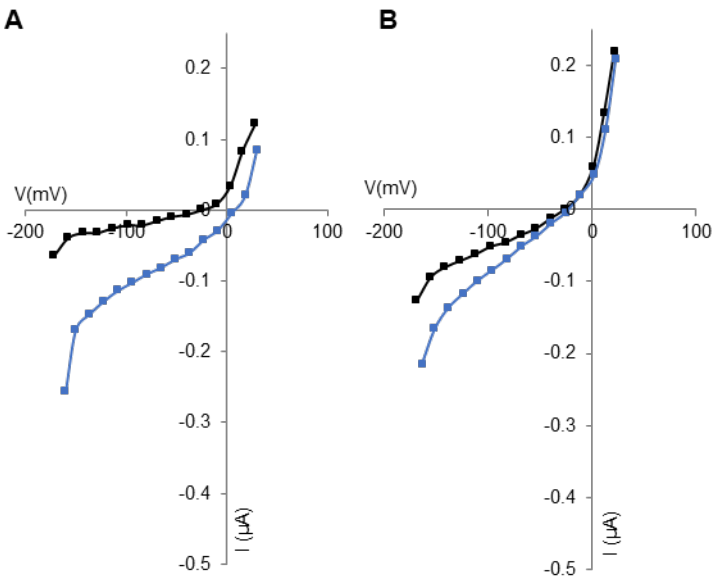


Figure 4.3 cAMP may assist the gating of *AtCNGC15*^{D408N}.

(**A**), (**B**) Current/voltage (I/V) curves in *X. laevis* oocytes expressing *AtCNGC15*^{D408N}, in the presence of 20mM $CaCl_2$, with (blue) and without (black) the application of 10µl cAMP at 10µM concentration. Each graph represents an I/V curve from an individual oocyte.

4.2.4 The dual function of AtCNGC15 is promoted by high nitrate.

Primary nitrate sensing is modulated by the nitrate transceptor NRT1.1 (Ho et al., 2009). NRT1.1 localises at the plasma membrane of the outer cell layer of the root tip and root columella (Krouk et al., 2010), where it is required for the nitrate-induced cytoplasmic calcium release that contributes to the expression of primary nitrate-responsive genes (Riveras et al. (2015); Liu et al. (2017)). Notably, high nitrate causes nuclear translocation of the calcium-dependent protein kinase (CPK) 10, CPK30, and CPK36, which control the rapid induction of primary nitrate responsive genes, including the *LATERAL ORGAN BOUNDARIES DOMAIN* (*LBD*)*37*, *LBD38*, and *LBD9* (Liu et al., 2017). Recent work demonstrated that AtCNGC15, which localises at the nuclear envelope during root apical meristem establishment (Leitão et al. (2019); Wang et al. (2021c)) relocalises to the plasma membrane at later stage (12 dpg) of root growth, and associates with NRT1.1 to regulate the high nitrate-induced cytoplasmic calcium release and primary nitrate responsive gene expression

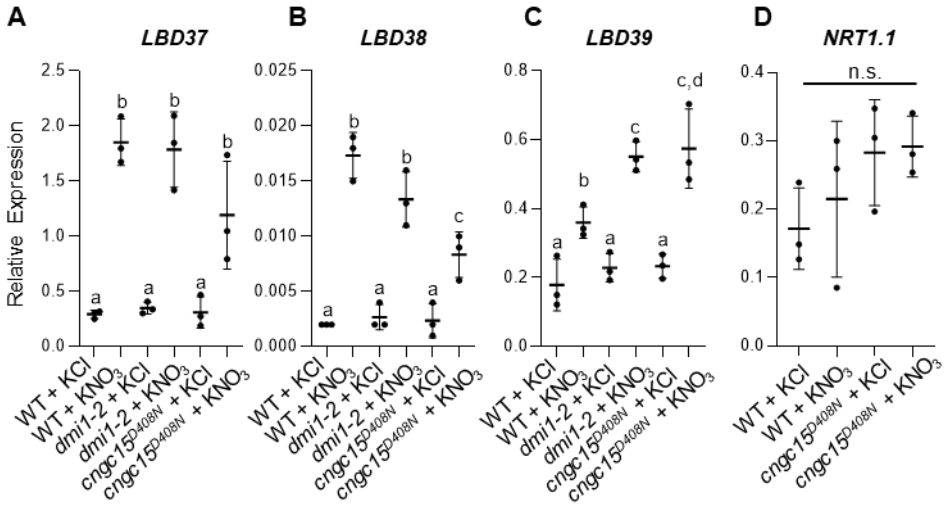


Figure 4.4 AtCNCG15 is required for nitrate induced gene expression.

(**A**) Quantitative expression analyses of the transcript level of nitrate-regulated genes by qPCR in 6 day old root tips of WT, *dmi1-2* and *cngc15*^{D408N} seedlings (n=3, each sample is a pool of approximately 100 plants) on treatment with either 10mM KCl or 10mM KNO_3 for 30 minutes. Expression was normalised to *UBIQUITIN 10 (At4g05320)* and *UBOX* (*At5g15400*). Expression is displayed relative to these reference genes. Error bars represent mean ± SD. Letters denote statistical significance calculated using one-way ANOVA with Tukey's multiple comparison post-test. n.s. = not significant.

(Wang et al., 2021c). This observation suggests that during early stages of root development (6 dpg) the function of AtCNCG15 is distinct from nitrate signalling.

To test this hypothesis, the expression of the nitrate-induced *LBD37*, *LBD38*, and *LBD39* (Liu et al. (2017); Alvarez et al. (2020)) was quantified in 6-day-old root tips of wild type, *Atdmi1-2* and *Atcncg15*^{D408N} mutant lines, after a 30 minute treatment with either 10 mM KNO_3 or 10mM KCl as a control (Figure 4.4). Both *Atdmi1-2* and *Atcncg15*^{D408N} are impaired in nuclear calcium release, displaying a reduced frequency of nuclear calcium spiking (Leitão et al. (2019), Tipper et al. (2023)). The expression of *LBD37*, *LBD38*, and *LBD39* was significantly induced by nitrate in the wild type, demonstrating that primary nitrate signalling is unaffected at this developmental stage (Figure 4.4). Induction of *LBD37* was not affected in *Atdmi1-2* or *Atcngc15*^{D408N}, indicating that *LBD37* expression is not

impaired by alterations in nuclear calcium release (Figure 4.4A). In contrast, the expression of the nitrate-induced *LBD39* was significantly enhanced in comparison with the wild type in both *Atdmi1-2* and *Atcngc15*^{D408N}, suggesting that *LBD39* expression is negatively regulated by nuclear calcium release (Figure 4.4C). Unexpectedly, induction of *LBD38* was significantly reduced in *Atcngc15*^{D408N} but not in *Atdmi1-2* root tips, suggesting, on one hand, that an impaired nuclear calcium release does not interfere with *LBD38* expression, and on the other hand, that AtCNGC15 might play a dual role at 6 dpg in the presence of high nitrate (Figure 4.4B). The expression of *NRT1.1* was unaffected in both *Atdmi1-2* and *Atcngc15*^{D408N} (Figure 4.4D), so the differential regulation of *LBD38* and *LBD39* is not due to altered expression of NRT1.1, and the expression of NRT1.1 is not affected by the reduced frequency of nuclear calcium release.

The impaired induction of *LBD38* in *Atcngc15*^{D408N} and not *Atdmi1-2* suggests that AtCNGC15 is acting independently to AtDMI1 at this developmental stage. One hypothesis is that there is a relocalisation of AtCNGC15 to the plasma membrane induced by nitrate. To test this, seedlings expressing *AtCNGC15:GFP* under its own promoter were grown on nitrate-free medium supplemented with either 10 mM KNO_3 or 1 mM L-glutamine. Under both conditions, AtCNGC15 localised to the nuclear envelope in the root apical meristem at 6dpg (Figure 4.5). However, in the columella cells under high nitrate, AtCNGC15 localised to the plasma membrane as well as the nuclear envelope (Figure 4.5E, F). This relocalisation was not observed in the absence of nitrate (Figure 4.5G-L), indicating that plasma membrane localisation of AtCNGC15 at the columella cells is induced by nitrate treatment. This observation correlates with the expression of *NRT1.1*, which is highly expressed in, and localises to, columella cells (Remans et al. (2006); Krouk et al. (2010)). Together, the results indicate that in young seedlings, AtCNGC15 functions at the nuclear envelope to regulate nuclear calcium release that modulates both root development and nitrate-induced *LBD39* expression. However, upon high nitrate, AtCNGC15 relocalises specifically to the plasma membrane of the columella cells where it contributes to the regulation of nitrate-

induced *LBD38* expression. These results further suggest that differential inputs of calcium are required to modulate *LBD38* and *LBD39* expression in response to nitrate.

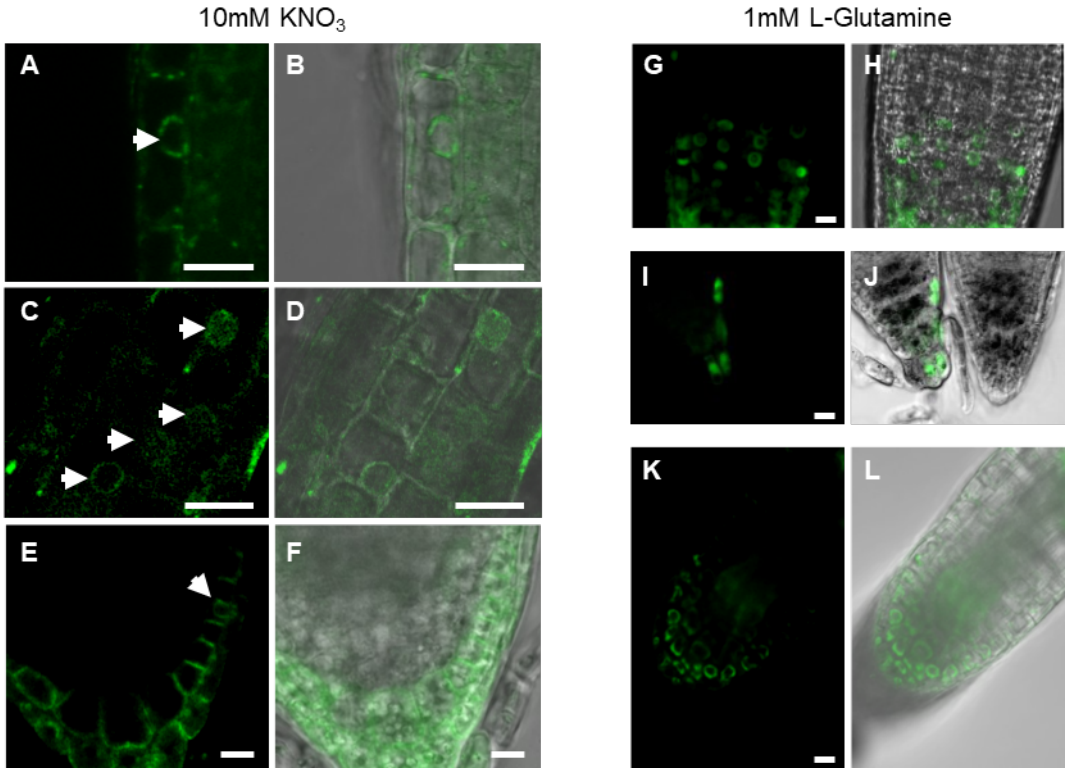


Figure 4.5 AtCNCG15 relocalises to the plasma membrane of columella cells upon high nitrate treatment, and not in the absence of nitrate.

Laser scanning confocal microscopy pictures of 6 day old *A. thaliana* root meristems expressing *pAtCNGC15::AtCNGC15:GFP* grown in the presence of 10mM nitrate **(A-F)** or in the presence of 1 mM L-Glutamine as the nitrogen source **(G-L)**. Green fluorescent protein (GFP) detection **(A, C, E, G, I, K)** and overlay picture of the green channel and bright field **(B, D, F).** In **(I)** and **(J)**, the left seedling expresses *pAtCNGC15::AtCNGC15:GFP* and the right seedling is a non-transformed seedling as a control. Scale bars represent 20µm. Arrowheads indicate nuclear envelope localisation of AtCNGC15:GFP.

4.2.5 Does the nuclear calcium signal generated by AtCNGC15 and AtDMI1 affect the regulation of the cell cycle in the primary root meristem?

The short root phenotype of *cngc15*^{D408N} was found to be caused by a reduction in the size of the primary root meristem. It was identified that *cngc15*^{D408N} and *dmi1-2* seedlings had fewer meristematic cells compared to WT, and these cells were on average larger (Leitão et al., 2019; Tipper et al., 2023).

In contrast, *dmi1-1* seedlings, which have an increased duration of calcium release, have an increased primary root length but a wild type meristem size. The increased root length is caused by longer elongating and mature cells in the transition zone (Leitão et al., 2019). This suggests that the cell cycle is being perturbed in these mutants, and potentially the reduced frequency of nuclear calcium release in *dmi1-2* and *cngc15*^{D408N} is resulting in fewer cell divisions. To test this hypothesis, *cngc15*^{D408N}, *dmi1-2* and wild type seedlings expressing NR-GECO1.2 (nuclear-localised red-GECO1.2, a nuclear localised fluorescent calcium sensor; Kelner et al., 2018) were crossed with a CYCB1.1-GFP line, a commonly used cell division marker for the late G2 phase of cell division (Echevarría et al., 2021). Seedlings resulting from the cross were screened for dual fluorescence, and the T2 population was genotyped for the D408N mutation and for the *dmi1-2* T-DNA insertion by PCR.

The aim in generating these crosses was to assess whether the reduced nuclear calcium release in *cngc*^{D408N} and *dmi1-2* is correlated with fewer cell divisions, using the fluorescence of CYCB1.1-GFP as a proxy. In addition, I wanted to assess whether there was a correlation between the nuclear calcium release and the onset of a cell division. For example, could the nuclear calcium release be acting as a signal to trigger cell division?

To assess this, I imaged *cngc15*^{D408N} and col0 seedlings containing the NR-GECO1.2 and CYCB1.1-GFP fluorescent markers at 6 days old using a Nikon ECLIPSE FN1. The average time for a cell to complete the G2 phase of cell division in the root apical meristem is 3-4 hours, depending on the cell type (Desvoyes et al., 2021). Given CYCB1.1-GFP marks the late G2 phase of cell division, the seedlings had to be imaged for several hours to observe the full cycle of CYCB1.1-GFP fluorescence in a cell. Preliminary imaging identified that the available experimental set up was not suitable for this long-term imaging, as the seedlings were prone to movement, growth, stress and desiccation. This meant it was difficult to keep the meristem within focus, and analysis would be challenging given calcium signalling is also triggered by abiotic stress (Dong et al., 2022). I tried using medical adhesive to reduce movement, which was unsuccessful, and researched techniques for long term imaging (Rahni &

Birnbaum, 2019; Kirchelle et al., 2017). Whilst this would be an interesting and novel avenue of research, the investment required to undertake these experiments rigorously would be high. Therefore, this was deprioritised in favour of other hypotheses, and remains a future area of exploration.

4.3 Discussion

Whilst the D408N mutation in *AtCNGC15* has been shown to be sufficient to reduce the frequency of nuclear calcium release in the Arabidopsis RAM, and subsequently reduce meristem size (Tipper et al., 2023), it was not known what effect this mutation was having on the structure of the channel, and its permeability. In this chapter, I identify that the D408N mutation is positioned in the C-linker region of the ion channel (Figure 4.1). In line with a role of the C-linker in gating animal CNG channels, the D408N mutation is sufficient to impair the gating of AtCNGC15 in *X. laevis* oocytes (Figure 4.1), demonstrating that the C-linker is associated with the gating of CNGCs in plants. As the residue D408 is highly conserved among AtCNGCs (Tipper et al., 2023), it might represent a valuable target to develop new AtCNGC alleles and assess the effect of modulating the level of calcium release in CNGC-associated biological processes. Remarkably, although the D408N mutation is sufficient to impair the mechanism involved in opening AtCNGC15, the channel can still be opened, less readily, both *in planta* and in oocytes (Figure 4.2). This observation suggests that various mechanisms of activation might coexist, potentially including various ligands and/or cofactors whose effects can be influenced by the D408N mutation. In accordance with this, application of cAMP was found to assist the opening of CNGC15^{D408N} channels in oocytes that had previously shown no inward current upon calcium treatment (Figure 4.3). This indicates that, in the heterologous *X. laevis* oocyte system, cyclic nucleotides may increase the gating flexibility of the inflexible CNGC15^{D408N} channels. The homology modelling (Figure 4.1) revealed that the D408N mutation disrupts a salt bridge between the aspartic acid 408 of one subunit and the arginine 398 of the neighbouring subunit. Future work could assess if disrupting the salt

bridge by mutating the arginine 398 residue would also affect the gating of the channel.

Trafficking of mammalian CNG channels to subcellular domains is critical for their multiple physiological roles, with cell type and specific heterotetrametric assembly influencing this relocalisation (Wojtyniak et al., 2013). Recently, it was shown that at later stages of Arabidopsis root growth, overexpressed AtCNGC15 relocalises to the plasma membrane of root cells where, in complex with NRT1.1, it contributes to the nitrate-induced cytoplasmic calcium release and gene expression changes (Wang et al., 2021c). The dual localization of AtCNGC15 was hypothesized to be developmental stage specific. As AtCNCG15 localizes to the nuclear envelope at 6 dpg, this suggests that nitrate-induced gene expression in Arabidopsis root tips at 6 dpg would be independent of *AtCNGC15*. Here, it is demonstrated that the induction of the primary nitrate responsive genes, *LBD37, LBD38* and *LBD39*, occurs in 6-day-old Arabidopsis root tips. Interestingly, *LBD37, LBD38*, and *LBD39* are differentially regulated in the Arabidopsis mutants impaired for nuclear calcium release (*Atdmi1-2* and *Atcngc15*^{D408N}) (Figure 4.4). The level of expression of *LBD39* is enhanced in comparison with the wild type in both mutants, while the expression of *LBD37* is similar, suggesting that nuclear calcium release negatively regulates expression of *LBD39* (Figure 4.4 A,C). In contrast, the nitrate induction of *LBD38* is only impaired in *Atcngc15*^{D408N} (Figure 4.4B). In addition, AtCNGC15 expressed under its own promoter localizes to the nuclear envelope of the root meristem cells and relocalises specifically in the columella cells to the plasma membrane in the presence of high nitrate (Figure 4.5). Taken together, this demonstrates that nuclear calcium mediated by *AtCNGC15* can modulate nitrate-induced *LBD39* expression and root development. However, in addition to regulating nuclear calcium signal in young seedlings, relocalisation of AtCNGC15 at the plasma membrane specifically in columella cells can be induced by nitrate treatment where it contributes to regulating nitrate-induced *LBD3*8 expression. The differential regulation of the nitrate-induced *LBD37/38/39* in *Atdmi1-2* and *Atcngc15*^{D408N} highlights that the

regulation of *LBD37, LBD38*, and *LBD39* expression requires different inputs of cytoplasmic and/or nuclear calcium.

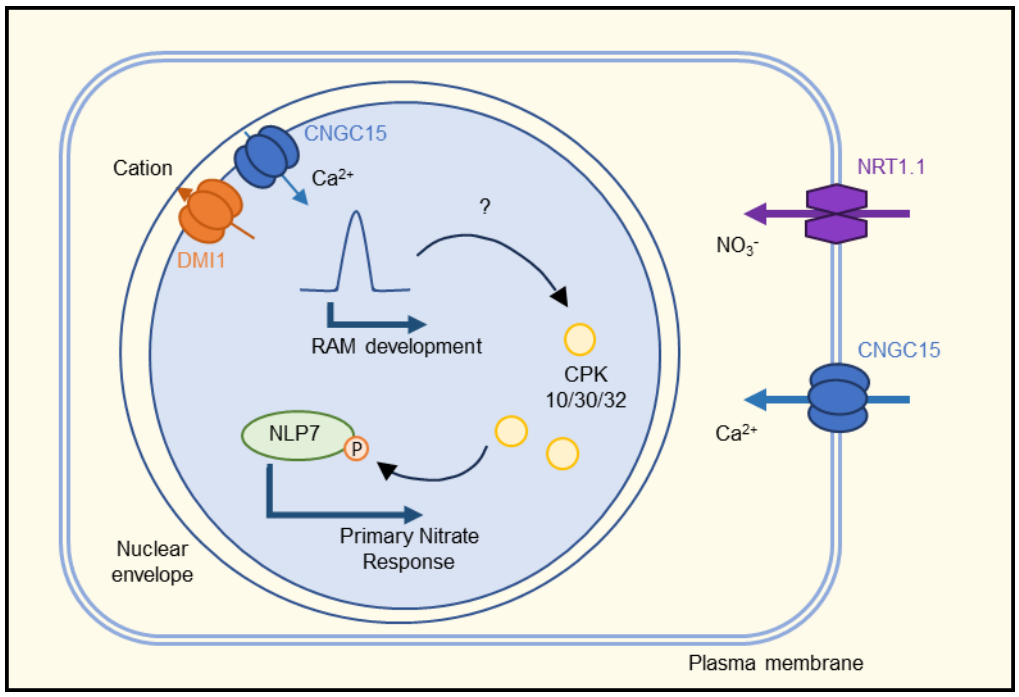


Figure 4.6 Summary model for the dual role of AtCNGC15 in root apical meristem (RAM) development and nitrate signalling in the columella cell layer of 6 day old Arabidopsis seedlings.

Nitrate perception by NRT1.1 triggers a conformational change which inhibits the interaction between CNGC15 and NRT1.1 at the plasma membrane (Wang et al., 2021). In high nitrate conditions, CNGC15 is trafficked to the plasma membrane by an unknown mechanism (Tipper et al., 2023), where it is predicted to be involved in the generation of cytoplasmic calcium influx upon nitrate treatment (Wang et al., 2021). The cytoplasmic calcium activates CPK10/30/32 and facilitates their translocation to the nucleus (Liu et al., 2017). Here, they phosphorylate NLP7, causing its nuclear retention and activation of Primary Nitrate Response genes (liu et al., 2017). NLP7 is itself a nitrate sensor, activated by the direct binding of nitrate (Liu et al., 2022). In addition, CNGC15 and DMI1 at the nuclear envelope generate nuclear calcium releases required for RAM development (Leitão et al., 2019, Tipper et al., 2023). These nuclear calcium releases are implicated in the induction of *LBD39*, so potentially nuclear calcium is required for the fine tuning of the Primary Nitrate Response by a currently unknown mechanism, potentially involving calcium binding proteins such as CPK10/30/32.

The expression of *LBD37/38/39* is dependent on the activity of the calcium-regulated CPK10, CPK30, and CPK36, which were shown to relocalise to the nucleus upon nitrate treatment (Liu et al., 2017). Here, they

phosphorylate NLP7, triggering its nuclear retention. NLP7 is itself a nitrate sensor, with the ability to bind directly to nitrate (Liu et al., 2022). These data and our findings raise the question of whether the activities of CPK10, CPK30, and CPK36 require different amounts of cytoplasmic and/or nuclear calcium in a cell-specific manner to modulate nitrate-induced gene expression. Figure 4.6 provides a summary and model of the dual roles of CNGC15, and the link between CNGC15 and nitrate signalling. The identification of *Atcngc15* mutant alleles impaired in gating, such as *Atcncg15*^{D408N}, represents a valuable tool to assess *in planta* the connection between calcium input and specific activation of calcium decoders for future work.

Chapter V – An investigation of nuclear calcium regulators and decoders in Arabidopsis roots

5.1 Introduction

Calcium signalling is comprised of three key steps, an initial encoding of information into an internal signal that can be transmitted, decoding of the received signal, and a response. The encoding is carried out by calcium influx channels and calcium efflux transporters in response to a stimulus, generating specific calcium signatures that can vary in their frequency, amplitude and subcellular location (Demidchik et al. (2018)). Decoding the calcium signature in plants requires calcium binding proteins such as calmodulins (CaMs), CaM-like proteins (CMLs) (Yang and Poovaiah (2003)), calcium-dependent protein kinases (CDPKs) (Blowers and Trewavas, 1989), calcineurin B-like (CBL) proteins (Kudla et al., 1999) and CBL-interacting protein kinases (CIPKs) (Shi et al., 1999). The EF-hand domains in these proteins are responsible for binding calcium, with one EF-hand domain of 30 amino acid residues being capable of binding one calcium ion (Nakayama et al., 2000). The proteome diversity between different organelles, cell types, and organs means there are different calcium binding proteins present in different cellular and subcellular spaces, causing different responses to calcium signals.

The roles of DMI1 and CNGC15 in generating nuclear calcium influx in Arabidopsis has been described in Leitão et al. (2019) and Tipper et al. (2023). Nuclear calcium influx mediated by these components is essential for normal root apical meristem (RAM) development and primary root growth. Auxin distribution in the root meristem is correlated with the nuclear calcium phenotypes of *dmi1-1* and *dmi1-2* lines; the increased calcium input in *dmi1-1* is associated with increased auxin levels, whilst the decreased calcium input of *dmi1-2* is associated with decreased auxin levels (Leitão et al., 2019). However, the decoding mechanism responsible for regulating these changes is not known. In addition, calcium channels often interact with regulatory components that modulate the calcium release. For example, in Medicago, the CNGC15 complex interacts with calcium-bound holo-CaM2, which modulates the closure of

CNGC15s (Del Cerro et al., 2022). Therefore, there are likely to be regulators involved in the generation of nuclear calcium spiking in Arabidopsis.

To try to identify such regulators, an ethyl methanesulfonate (EMS) screen of an Arabidopsis *cngc15*^{D408N} population was carried out which identified five lines that restored the wild-type root length phenotype. In this chapter, I describe how whole genome sequencing and analysis was used to try to identify point mutations in candidate genes that caused the restoration of primary root length.

As well as searching for putative modulators, I also investigated potential decoders of the nuclear calcium in Arabidopsis. This was done by conducting a literature search for published nuclear localised calcium binding proteins that are involved in root growth in Arabidopsis. This revealed a publication characterising the role of *EMBRYO DEFECTIVE 1579* (*EMB1579)* in nuclear condensate formation and regulation of gene expression (Zhang et al., 2020). *EMB179* had previously been characterised as *SHORT ROOT IN SALT MEDIUM 1* (*RSA1*) in a forward genetic screen for players involved in salt tolerance (Guan et al., 2013b). *RSA1* is expressed in the RAM (Zhang et al., 2020), localises to the nucleus, and contains an EF hand domain that was shown to bind calcium (Guan et al., 2013b). What is particularly striking is the published phenotype of *rsa1* knockout lines, which is very similar to that of *cngc15*^{D408N}, with a shorter primary root length and root apical meristem (RAM) (Zhang et al., 2020). This led to my hypothesis that RSA1 may be acting as a calcium decoder in the nuclei of Arabidopsis RAMs, responsible for sensing and responding to the nuclear calcium influx generated by CNGC15 and DMI1.

Interestingly, RSA1 was found to form dynamic liquid-like condensates in the nucleus by liquid-liquid phase separation (Zhang et al., 2020). Liquid-liquid phase separation is the process by which macromolecules, such as proteins, form dense condensates, meaning a previously homogenous solution separates into distinct phases (Alberti et al., 2019). The formation of these condensates was found to be crucial for its function in controlling the expression of many genes, including *FLC* (Zhang et al., 2020). This ability to form condensates is an important for the normal functioning of RSA1, so may

affect its potential function as a decoder. In addition, RSA1 was found to bind to the basic helix-loop-helix (bHLH) transcription factor RSA1 INTERACTING TRANSCRIPTION FACTOR 1 (RITF1) via yeast two-hybrid, Bimolecular Fluorescence Complementation analysis in Arabidopsis protoplasts and *Nicotiana benthamiana* (tobacco) leaves, Split Luciferase complementation in tobacco leaves and Co-immunoprecipitation analysis in tobacco plants (Guan et al., 2013b). Although none of these interaction analyses were conducted using Arabidopsis roots, it does indicate that RSA1 can bind to transcription factors. In addition, RITF1 was found to bind to the promoters of genes misregulated in *rsa1-1* knockout mutants, suggesting they share a common pathway for gene expression (Guan et al., 2013b). Therefore, RSA1 is a promising candidate decoder of the nuclear calcium influx involved in Arabidopsis primary root development.

To summarise, the aim of this chapter is to investigate the following questions:

1. What is responding to the nuclear calcium release mediated by CNGC15?
2. What are the potential regulators and decoders facilitating normal primary root development?
3. Is RSA1 a decoder of the nuclear calcium release mediated by CNGC15 and DMI1?

5.2 Results

5.2.1 Whole genome sequencing and analysis of *cngc15*^{D408N} EMS-mutagenized lines

To try to identify regulators of the nuclear calcium signal mediated by CNGC15 and DMI1, an EMS suppressor screen was carried out on *cngc15*^{D408N}. Since *cngc15*^{D408N} plants have a reduced primary root length (Tipper et al., 2023), the aim was to identify seedlings that recovered wild type root length in the *cngc15*^{D408N} background. This suppressor mutant screen approach has been successfully used to identify components acting in shoot apical meristem development, for example in the identification of *CORYNE (CRN*), where an EMS screen on a *CLAVATA3 (CLV3)* overexpressing line, that has a weak meristem arrest phenotype, identified lines where this meristem arrest was abolished (Müller et al., 2008). In addition, EMS mutagenesis and subsequent selection of particular root length phenotypes has been used to identify new players in Arabidopsis root development, for example *RETARDED ROOT GROWTH (RRG)* (Zhou et al., 2011) and *DET2* (Lv et al., 2018). The *cngc15*^{D408N} background for the EMS screen has a reduced frequency of nuclear calcium release (Tipper et al., 2023). Therefore, in lines where primary root length is restored, I might expect to identify mutations in regulators of the nuclear calcium release that may recover this nuclear calcium frequency. Alternatively, restoration of the primary root length could be due to mutations in components acting in different pathways affecting Arabidopsis root development.

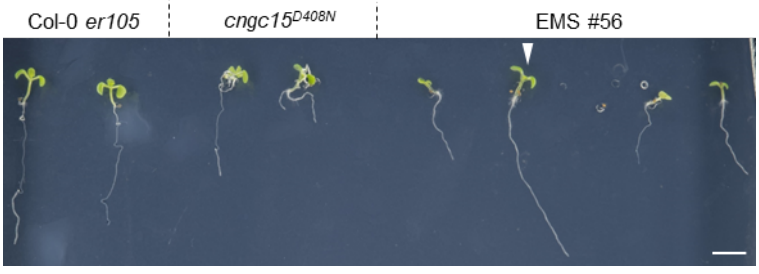


Figure 5.1 Identification of EMS lines that recover wild type primary root length.

Representative image of 6-day old seedlings of wild type Col-0 *er105*, *cngc15*^{D408N} and ethyl methanesulfonate (EMS) line #56 showing segregation of the primary root length phenotype. The seedling selected for whole genome sequencing is marked with an arrowhead. Scale bar represents 5mm.

5 lines were identified, but all had segregating root length phenotypes (Figure 5.1), indicating that the parent plant was heterozygous for the EMS point mutation. I selected five seedlings from each line for bulk DNA extraction and whole genome sequencing, as well as the *cngc15*^{D408N} for sequence comparison. I mapped the sequence data from the *cngc15*^{D408N} and the 5 EMS suppressor lines individually to the reference genome Col-0 (TAIR10). Then, the single nucleotide polymorphisms (SNPs) were called using custom scripts. Positions where the EMS suppressor lines and *cngc15*^{D408N} had the same allele were filtered out. In addition, I filtered out SNPs that were present in the exact same location in three or more lines, as these represent differences between the Col-0 *er105* genome (the ecotype of *cngc15*^{D408N}) and the Col-0 genome that was used as the reference, rather than polymorphisms that differ between *cngc15*^{D408N} and the EMS suppressor lines. To be conservative, I allowed for SNPs that were present in the exact same position in two EMS suppressor lines.

After this initial screening, a sliding window approach with a custom script was used to screen the genome for a region where at least three EMS suppressor lines had a SNP. Initially I used a 500bp window, but this was then expanded to a 3kb window. This was chosen as the average gene size of Arabidopsis thaliana is 2.4kb (Yu et al., 2002), and I wanted a window size that was big enough to capture entire genes, whilst decreasing the probability of there being more than one gene within a window. Given the initial EMS suppressor lines had segregating root length phenotypes, I needed to allow for SNPs that were heterozygous. Therefore, I set the threshold for SNP calling at 30% for alternative alleles, to be conservative. This means that any alternative alleles (different from the reference allele) that had allele frequencies over 30% would be called. The output from the script was a list of contigs, the positions of the SNPs, and the line in which each SNP was present. In addition, whether each SNP was present in a gene coding region was also labelled.

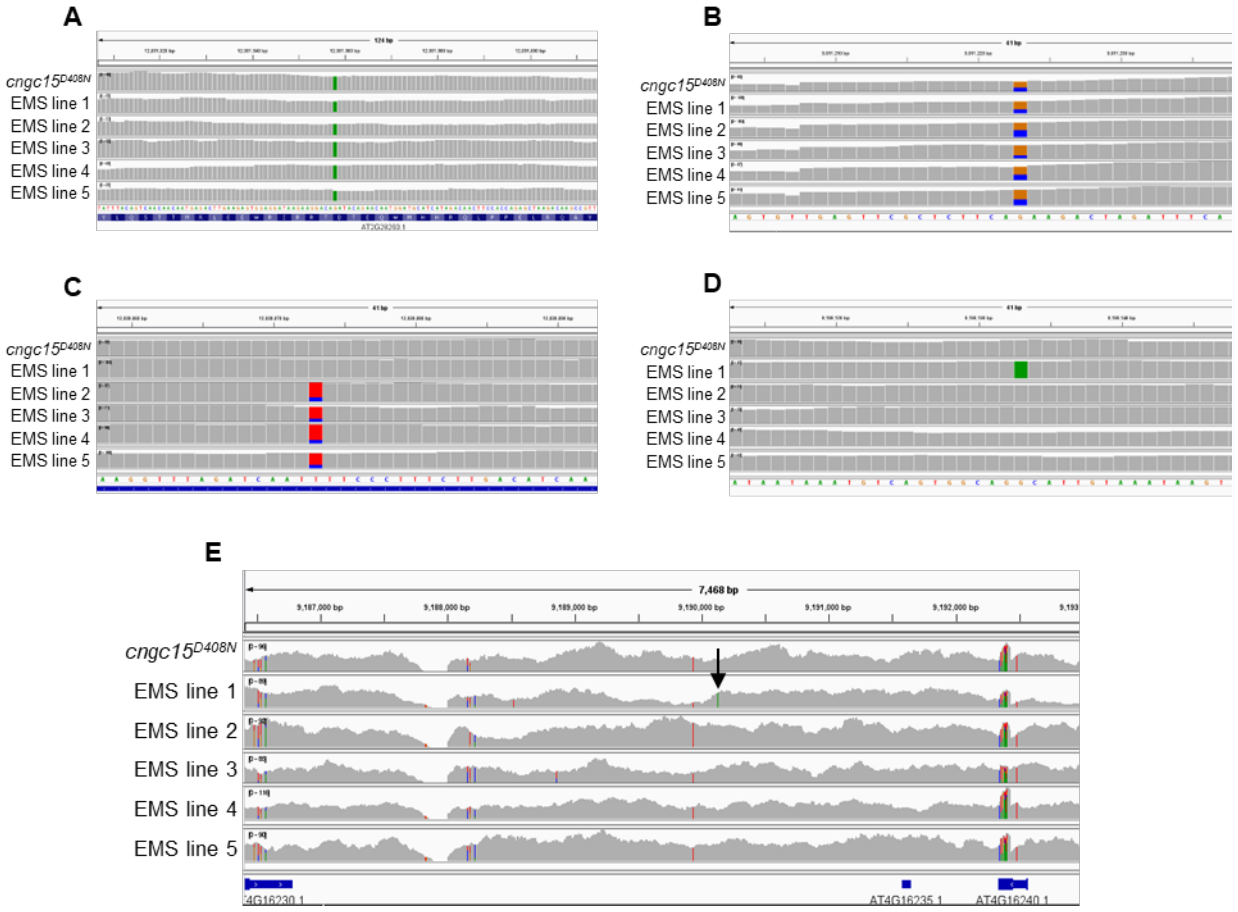


Figure 5.2 Visualisation and manual inspection of single nucleotide polymorphisms (SNPs).

Screenshots from Integrative Genomics Viewer (IGV) of SNPs identified in the ethyl methanesulfonate (EMS) suppressor screen. Sequencing data from *cngc15*^{D408N} is in the top row, followed by each of the EMS suppressor lines as labelled. Sequence from the reference genome *A. thaliana* Col-0 (TAIR10) is in the bottom row, with coding regions highlighted in blue. (**A**) Confirmation that each of the five EMS lines, as well as *cngc15*^{D408N}, contain the guanine to adenine substitution responsible for the aspartic acid to asparagine amino acid change in *cngc15*^{D408N}. (**B**) Example of a discarded polymorphism present in all five EMS lines as well as *cngc15*^{D408N}. (**C**) Example of a discarded polymorphism present in more than two EMS suppressor lines. (**D**) Example of a true candidate SNP (guanine to adenine) present in one of the EMS suppressor lines and not present in any other line. (**E**) Visualisation of the 7.5kb window surrounding the SNP shown in (**D**), with the position of the SNP marked with an arrow.

These SNPs were manually inspected using the genome browser Integrative Genomics Browser (IGV). This confirmed that all five lines contained the guanine to adenine substitution in *CNGC15* responsible for the aspartic acid to asparagine amino acid change in *cngc15*^{D408N} (Figure 5.2A). Then I manually inspected the SNPs to search for candidate contigs, regions of

the genome, containing SNPs in at least three EMS suppressor lines. These SNPs do not have to be at the exact same position, but do have to be within the same 3kb contig. Since I was screening for SNPs that were potentially heterozygous, I used a high allele frequency threshold (0.7) which meant that I had a high proportion of false positives upon manual inspection. For example, I found that some SNPs that were also present in *cngc15*^{D408N} were not filtered out, as they met the threshold in the EMS suppressor lines but not in *cngc15*^{D408N} (Figure 5.2B). In the same way, some SNPs that were present in three or more EMS suppressor lines were also not filtered out (Figure 5.2C). Several true polymorphisms were identified (Figure 5.2D), but they were only present in one of the EMS suppressor lines within a 3kb contig (Figure 5.2E). In addition, the SNP in Figure 5.2D was in an intergenic region, 1.5kb from the nearest start codon (Figure 5.2E). Details of the number of SNPs screened using a 3kb sliding window, and how they were classified, can be seen in Table 5.1. Due to the number of SNPs that were screened by manual inspection, I chose to classify only those that were present within a 3kb window of a coding region.

Total Number of Contigs screened	301
Number of contigs with at least one SNP in a coding region	16
Total number of SNPs screened	549
Total number of SNPs in/around a coding region	57
- Number of SNPs that were also present in *cngc15*^{D408N}	29
- Number of SNPs that were present in more than 2 EMS suppressor lines	24
- 'True' SNPs	4

Table 5.1: Contigs and SNPs screened using a 3kb window and how they were classified.

The presence of a point mutation in the same gene in at least three of the five lines could indicate that gene is responsible for modulating the nuclear calcium signalling. Given the *cngc15*^{D408N} line has a reduced frequency of calcium signalling (Tipper et al., 2023), in order for wild type primary root length to be restored, the frequency of calcium influx must be increased, or an alternative mechanism might be at play to restore root development in spite of

the reduced calcium frequency. Unfortunately, I did not find any candidate genes in my sequence analysis, even when checking for point mutations in introns, and in intergenic regions which may have affected gene regulation or splicing. This likely indicates that the restoration of wild type root length in each line is due to independent EMS mutations in different genes in each line, or that the method for screening for EMS point mutations was not robust enough.

5.2.2 Genotyping of the *rsa1-3* mutant line

To investigate whether RSA1 is decoding the nuclear calcium signal mediated by DMI1 and CNGC15, *rsa1-3* seeds were ordered from the Nottingham Arabidopsis Seed Centre and genotyped for the T-DNA insertion in intron 17 (Figures 5.3A and 5.3B). The amplified DNA was sequenced by Sanger sequencing to confirm the exact location of the T-DNA insertion site (Figure 5.2C). Interpro was used to search the amino acid sequence for domains, which identified an EF hand domain at the C-terminus of the protein (Figure 5.3D). This was also predicted in Guan et al. (2013b), where the calcium binding activity of the EF hand was confirmed via calcium overlay assays of purified recombinant protein. The T-DNA insertion in *rsa1-3* lies very close to the predicted EF hand domain, and whilst the 12 amino acids responsible for binding calcium are not impacted by the T-DNA insertion, it may cause structural changes that impede the normal function of the calcium binding. In any case, the insertion was found to abolish the expression of *RSA*1 via qRT-PCR, rendering this line a null mutant (Guan et al., 2013b).

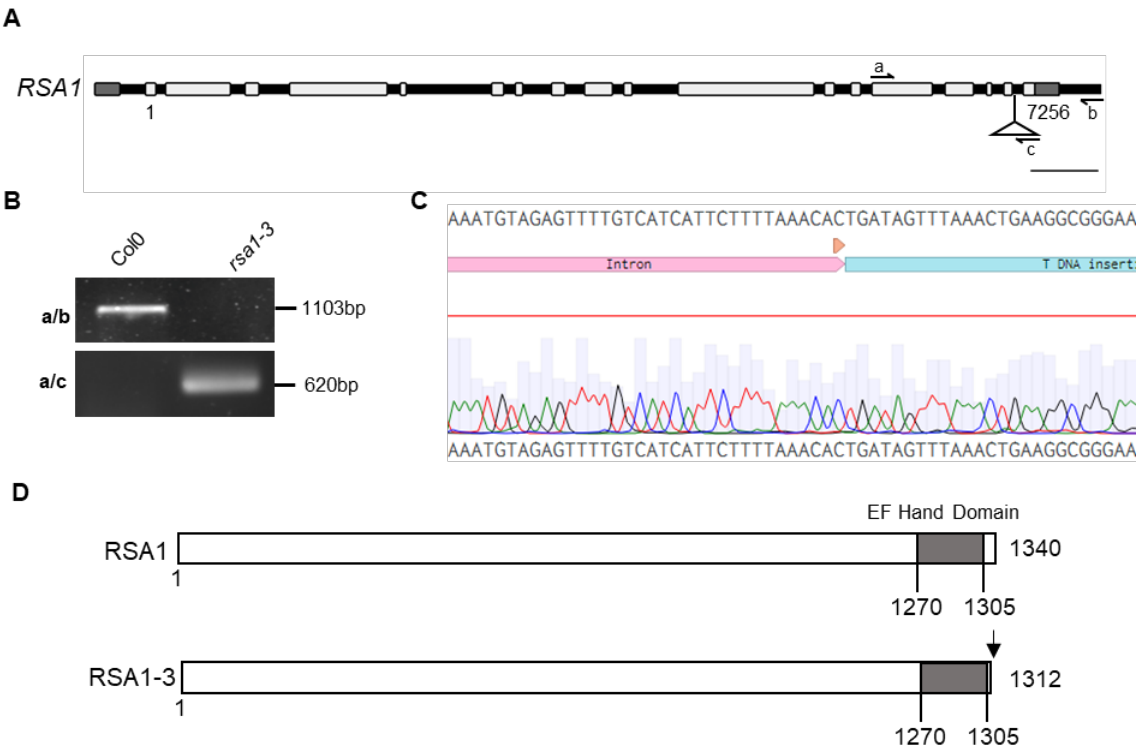


Figure 5.3 Characterisation of *rsa1-3*.

(A) Schematic showing the gene structure of *RSA1* and the position of the *rsa1-3* T DNA insertion site. Dark grey boxes represent the 5' and 3' UTR, light grey boxes represent exons, and black lines represent introns. The white triangle represents the location of the T DNA insertion. Primers used for genotyping and their positions are labelled as a, b and c. **(B)** Genotyping of *rsa1-3* via PCR, using the primers labelled in **(A)**. Primer sequences can be found in Table 2.1. **(C)** The exact location of the T DNA insertion site was determined via sequencing of the band in **(B)**. The intron is labelled in pink, the T DNA insertion sequence in blue, and the insertion site in orange. **(D)** Schematic of the amino acid sequence of RSA1 and RSA1-3, showing the location of the EF hand domain in grey. RSA1-3 is truncated, as highlighted by the arrow.

5.2.3 *rsa1-3* and *dmi1-2 rsa1-3* have shorter primary root lengths and increased lateral root densities.

rsa1-3 has been shown to have significantly shorter primary root lengths compared to wild type (Zhang et al., 2020), as does *cngc15*^{D408N} (Tipper et al., 2023). To assess how the primary root length of *rsa1-3* compares to *cngc15*^{D408N}, I measured the root lengths at 6 and 12 days post germination (dpg). Whilst both *rsa1-3* and *cngc15*^{D408N} had significantly shorter root lengths when compared to their respective wild types, *rsa1-3* was significantly shorter than *cngc15*^{D408N} (Figure 5.4 A and B). This is consistent with the hypothesis that

RSA1 could be decoding the nuclear calcium signature generated by CNGC15 and DMI1; the D408N mutation in CNGC15 reduces the frequency, but does not abolish the nuclear calcium spiking, so you would expect removing a decoder to have a more severe phenotypic effect.

To try to ascertain whether RSA1 is acting as a nuclear calcium decoder, *dmi1-2 rsa1-3* double mutants were generated. The aim of generating this double mutant was to conduct an epistatic analysis, to assess if RSA1 is acting in the same pathway, or in a different one. If RSA1 is acting downstream of the nuclear calcium signal, I would expect the *dmi1-2 rsa1-3* double mutant to have a similar phenotype to *rsa1-3*. If, however, DMI1 and RSA1 are acting in different pathways to inhibit primary root growth, I would expect a synergistic effect, where the double mutant has a more severe growth phenotype than each of the mutations individually. Primary root length analysis revealed that the *dmi1-2 rsa1-3* mutant had the same primary root length phenotype as *rsa1-3*, and both had more severe growth phenotypes than *dmi1-2* (Figure 5.4 A and B). Although this is not proof that RSA1 is the decoder, it may be consistent with that hypothesis. However, one issue with this approach is that the root length phenotype of *rsa1-3* is already considerably reduced, and it possible that the detrimental effect of this mutation would mask any additional effect of the *dmi1-2* mutation.

Whilst measuring the primary root lengths, I observed that *rsa1*-3 appeared to develop increased numbers of lateral roots, and developed them at an earlier timepoint than wild type seedlings. To document this, I measured the lateral root densities. This revealed that at both 6 and 12 dpg, *rsa1-3* and *dmi1-2 rsa1-3* lines had increased lateral root densities than wild type, *dmi1-2* and *cngc15*^{D408N} (Figure 5.4 C and D). At 6 dpg, *dmi1-2 rsa1-3* had an increased lateral root density than *rsa1-3*, but this difference was not sustained at 12dpg. At 12dpg, *dmi1-2* also had an increased lateral root density when compared to wild type, but not as much as *rsa1-3* or *dmi1-2 rsa1-3* (Figure 5.4D). Given that *dmi1-2 rsa1-3* has an increased lateral root density at an earlier timepoint than either *rsa1-3* or *dmi1-2*, this could suggest a synergistic effect in the double mutant. In addition, the increased lateral root density of *dmi1-2* is of interest as it suggests a role for nuclear calcium signalling in lateral root development. Given that

DMI1 is a non-selective cation channel, and *cngc15*^{D408N} did not have a lateral root phenotype, it is possible DMI1 is interfacing with another calcium ion channel in the context of lateral root development.

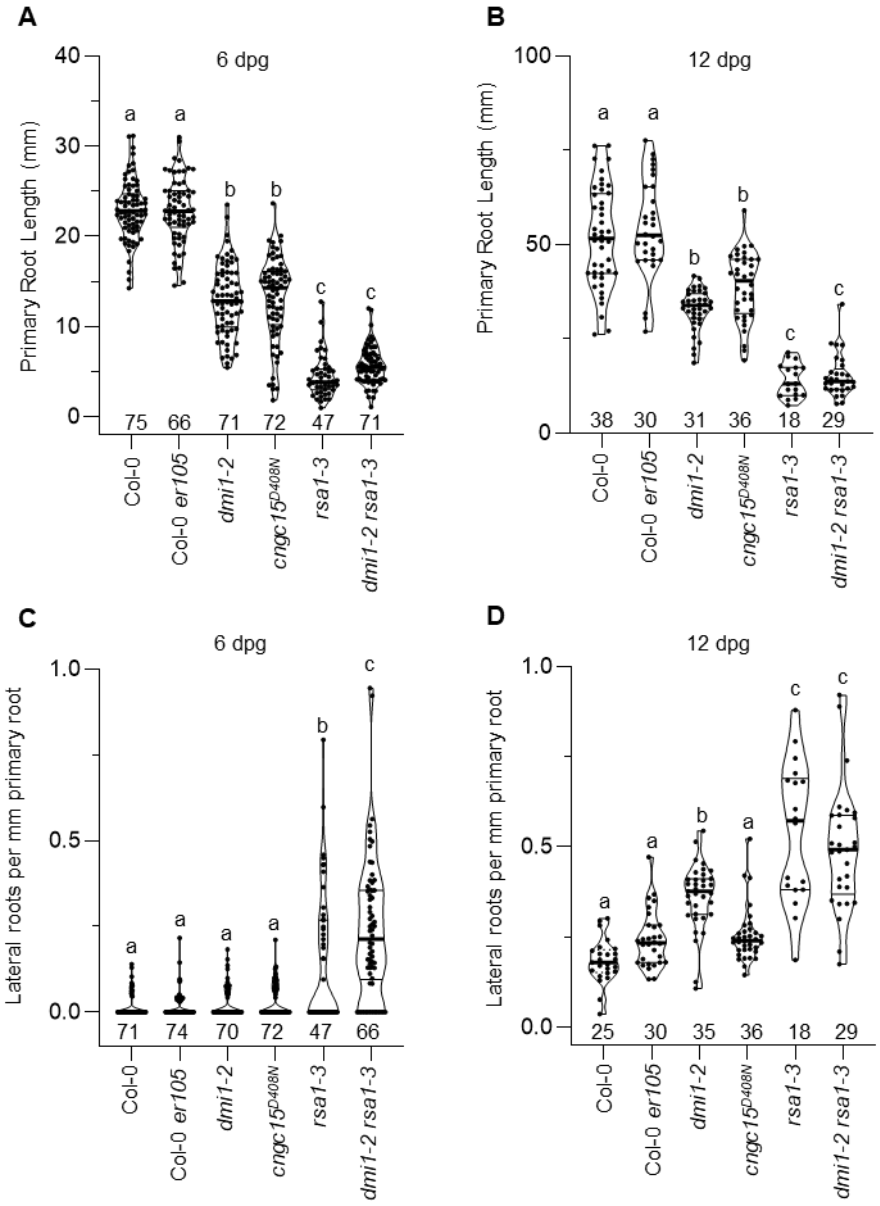


Figure 5.4 *rsa1-3* and *dmi1-2 rsa1-3* have significantly shorter primary root lengths, and an increased lateral root density.

(A), (B) Violin plots of primary root length measurements at 6 and 12 days post germination (dpg). **(C), (D)** Violin plots of lateral root density at 6 and 12 dpg. Lateral root density was calculated by normalising the number of lateral roots to the primary root length. Data represents at least 2 independent sowings, and n numbers are denoted underneath the plots. Statistical significance was calculated using one-way ANOVA with Tukey's multiple comparison post-test, with letters denoting statistical significance.

5.2.4 *rsa1-3* and *dmi1-2 rsa1-3* have reduced primary root meristem sizes.

dmi1-2 causes a reduced primary root length due to a reduction in the size of the meristem, caused by a reduced number of meristematic cells (Leitão et al., 2019). The same is true for *rsa1-3*, which has been previously published to have a reduced meristem size (Zhang et al., 2020). To see if this is the same for *dmi1-2 rsa1-3*, I used propidium iodide staining to visualise the primary root meristem and measure the length from the quiescent centre to the first elongating cell (Figure 5.5). This revealed that *rsa1-3* has a more severe effect on meristem length than *dmi1-2*, which was also observed in the double mutant *dmi1-2 rsa1-3* (Figure 5.5). Taken together, these results are consistent with the hypothesis that RSA1 is the decoder responsible for responding to the nuclear calcium spikes generated by DMI1 and CNGC15. However, it is also possible that the primary root meristem has reached a minimum viable size in *rsa1-3*, and that this would mask any additional effects of the *dmi1-2* mutation.

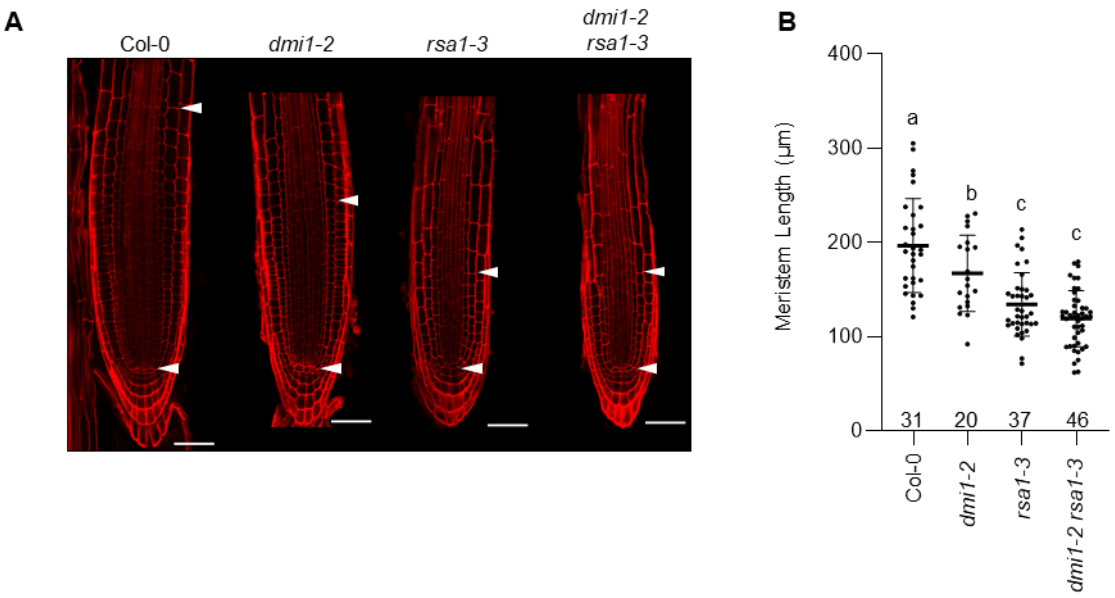


Figure 5.5 *rsa1-3* and *dmi1-2 rsa1-3* have significantly shorter root apical meristems.

(A) Representative images of Col-0, *dmi1-2, rsa1-3 and dmi1-2 rsa1-3* root apical meristems 6 days post germination. Meristems were stained with propidium iodide. The quiescent centre and start of the transition zone are marked with arrowheads. Scale bar represents 50µm. **(B)** Root apical meristem lengths of Col-0, *dmi1-2, rsa1-3 and dmi1-2 rsa1-3* 6 days post germination. Data represents 3 independent sowings, and n numbers are denoted underneath the plots. Statistical significance was calculated using one-way ANOVA with Tukey's multiple comparison post-test, with letters denoting statistical significance.

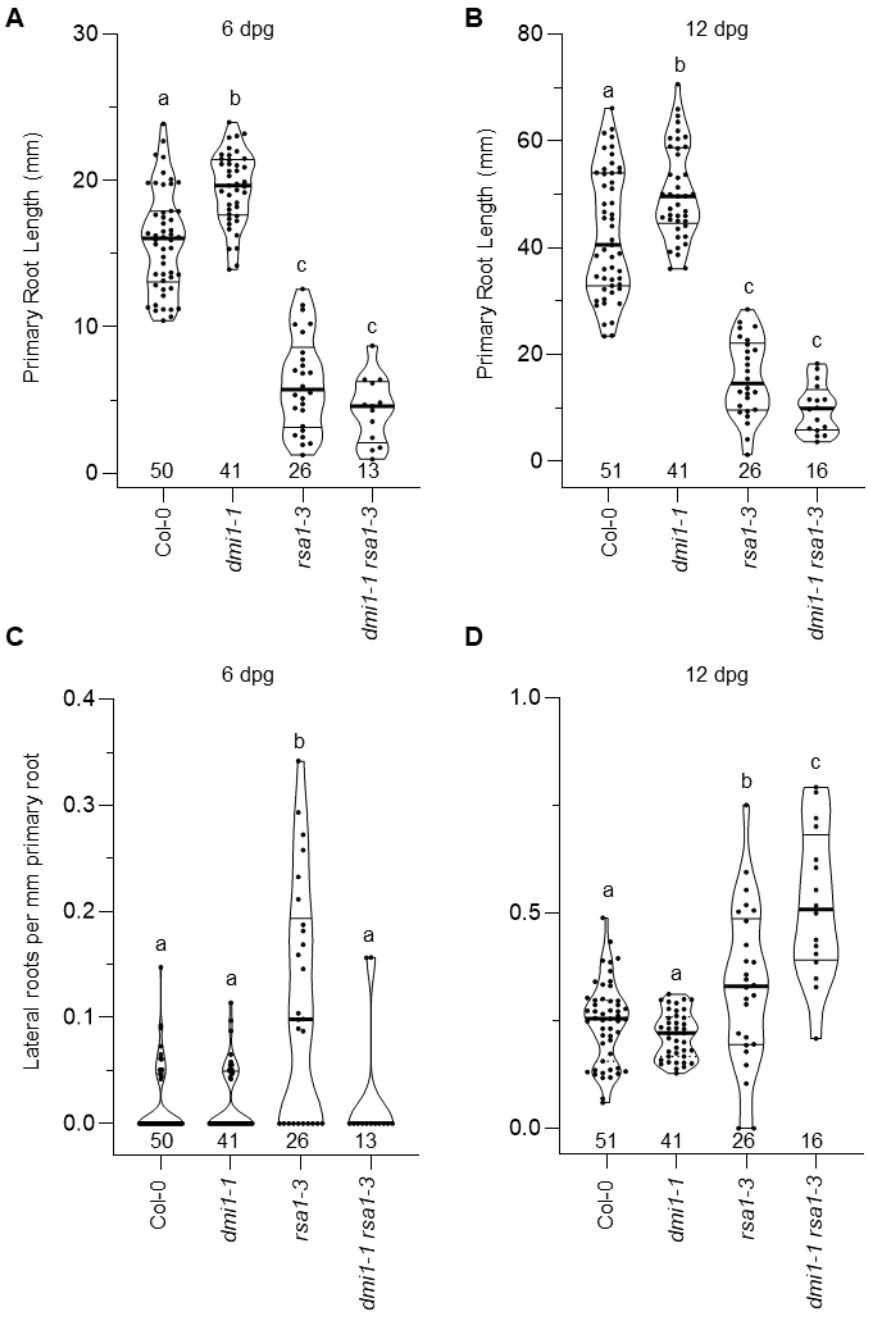


Figure 5.6 *dmi1-1 rsa1-3* has a significantly shorter primary root length, and an increased lateral root density.

(A), (B) Violin plots of primary root length measurements at 6 and 12 days post germination (dpg). **(C), (D)** Violin plots of lateral root density at 6 and 12 dpg. Lateral root density was calculated by normalising the number of lateral roots to the primary root length. Data represents one sowing, and n numbers are denoted underneath the plots. Statistical significance was calculated using one-way ANOVA with Tukey's multiple comparison post-test, with letters denoting statistical significance. Sowing and photography was carried out with the assistance of Nico Rossner and Sunny Lau (JIC).

5.2.5 *dmi1-1 rsa1-3* also displays a short primary root phenotype and increased lateral root density.

dmi1-1, a DMI1 knockout line, has an increased primary root length, caused by an increased rise time and fall time of the nuclear calcium release (Leitão et al., 2019). Therefore, if RSA1 is acting as a nuclear calcium decoder, one would expect the *dmi1-1 rsa1-3* double mutant to have the same phenotype as *rsa1-3*. The double mutant was generated via crossing and phenotyped, and indeed, displayed the same primary root phenotype as *rsa1-3* at 6 and 12dpg (Figure 5.6 A and B). Whilst this does not prove RSA1 is the decoder, it is consistent with that hypothesis, as if RSA1 and DMI1 were controlling primary root length in separate pathways, I would expect *dmi1-1 rsa1-3* to have an intermediate primary root length. In addition, *dmi1-1 rsa1-3* displayed increased lateral root density at 12dpg, which appears to be more severe than *rsa1-3*, again implying a synergistic role of DMI1 and RSA1 in lateral root development. This will need to be validated with further sowings to increase the sample size.

5.3 Discussion

In this chapter, I have utilised two different methods to try to identify calcium regulators or decoders that may be responding to the nuclear calcium influx mediated by DMI1 and CNGC15 in the RAM. The EMS suppressor screen and subsequent whole genome sequence analysis did not reveal any candidate calcium regulators. This is most likely due to the fact that the mutations in each of the five lines were in independent genes.

RSA1 was identified as a candidate calcium decoder from a literature search, due to the remarkable phenotypic similarities between *rsa1* knockout lines and *cngc15*^{D408N}, as well as its ability to bind calcium, expression in the root apical meristem, and localisation to the nucleus (Guan et al. (2013b); Zhang et al. (2020)). The null mutant *rsa1-3* has a more severe root length phenotype than *cngc15*^{D408N}, consistent with its role as a potential decoder, and also has an increased lateral root density (Figure 5.3). The reduced primary root length is due to a reduced meristem size (Figure 5.4). The *dmi1-2 rsa1-3* double mutant also has a reduced primary root length and meristem size, and an increased

lateral root density (Figures 5.3 and 5.4). Given the phenotype of this double mutant is similar in severity to *rsa1-3*, there is no synergistic effect, in support of the hypothesis that RSA1 is acting as a calcium decoder. If RSA1 was acting in a different pathway, independent of the nuclear calcium signal generated by DMI1 and CNGC15, I might expect the double mutant to have a more severe phenotype than either of the single mutations. However, it could also be possible that the *rsa1-3* mutation causes such a severe primary root phenotype that any additional effect of the *dmi1-2* mutation in the double mutant is masked. In addition, the double mutant *dmi1-1 rsa1-3* displayed the same short primary root length phenotype as *rsa1-3*, consistent with RSA1 acting as a decoder. Given *dmi1-1* has an increased primary root length compared to wild-type (Leitão et al., 2019), if RSA1 was acting in an alternate pathway, I might expect *dmi1-1 rsa1-3* to have an intermediate primary root length. This will need to be validated with further replicates, and I am also in the process of generating *cngc15*^{D408N} *rsa1-3* double mutant lines, which may further support this hypothesis in the future.

The lateral root density phenotype of *dmi1-2 rsa1-3* is interesting, as it appears to be more severe than both *dmi1-2* and *rsa1-3* at 6dpg (Figure 5.3C) and more severe than *dmi1-2* at 12dpg (Figure 5.3D). This could indicate a synergistic effect of these two mutations on lateral root development, where perhaps RSA1 has an additional role. Moreover, the increased lateral root density of *dmi1-2* at 12dpg (Figure 5.3D) suggests a potential role of nuclear calcium influx in lateral root development. Given that *dmi1-2* is associated with perturbations in auxin homeostasis (Leitão et al., 2019), the increased lateral root density could be due to increased levels of auxin, which is known to promote lateral root initiation. The same could be true for *rsa1-3*; knocking out RSA1 could also perturb auxin homeostasis leading to increased lateral root densities.

Whilst comparison of root phenotypes provides an indication as to whether DMI1 and RSA1 are acting in the same pathway, it does not prove that RSA1 is acting as a nuclear calcium decoder. One method to validate this would be to generate RSA1 constructs with either the EF hand removed, or the EF hand modified so it could bind calcium with a higher affinity, creating a higher order

RSA1 mutant. These constructs could then be transformed into *dmi1-2 rsa1-3* and *cngc15*^{D408N} *rsa1-3* double mutants, to see if the increased calcium binding affinity of RSA1 mutant could rescue the short root length phenotype of *dmi1-2* and *cngc15*^{D408N}. I investigated modifying the EF hand structure of RSA1 to increase its binding affinity for calcium by examining the amino acid composition of the 12 amino acids that make up the calcium binding pocket, especially those in the x, y, z, -x, -y and -z positions that directly provide oxygen for calcium chelation. RSA1 has an aspartate residue in position 12, whereas most EF hand domains contain a glutamate (Day et al., 2002). However, the structural difference between aspartate and glutamate is simply that glutamate has an extra carbon in its backbone, so whilst changing the amino acid sequence of RSA1 in this position might confer a tighter calcium binding pocket, it is unlikely to significantly impact the calcium binding affinity. Another potential site for modification is the valine in position 7, as many EF hand domains contain an isoleucine in this position (Guan et al., 2013b). However, again the difference between valine and isoleucine is simply the length of the amino acid chain, and is unlikely to significantly alter the binding properties of the channel.

An alternative method to test whether RSA1 is decoding the CNGC15 and DMI1 generated calcium signature would be to screen published databases of genes misregulated in *rsa1* null mutants, and see if these genes are misregulated in the same way in *dmi1-2*. For example, Guan et al. (2013b) published a whole-genome microarray analysis of *rsa1-1* which identified 41 genes that were upregulated and 54 genes that were downregulated at least two-fold compared to wild type under control conditions. The material used was 7 day old seedlings that had been grown on MS medium, so these genes would need to be screened to identify those expressed in the RAM. Additionally, the expression of genes known to be differentially regulated in *dmi1-2*, such as genes involved in auxin homeostasis (Leitão et al., 2019), could be tested in *rsa1-3*, to see if they have a similar pattern of regulation.

It has already been demonstrated that RSA1 can bind to the bHLH transcription factor RITF1. Once we have established if there is a set of genes that may be regulated by RSA1 upon nuclear calcium influx, their expression can

be tested in the *ritf1* null mutant to see if they follow the same pattern of regulation. If so, this would indicate that it is RITF1 that is regulating their transcription. Alternatively, other transcription factors could be involved, which could be identified using protein-protein interaction screening methodologies, such as TurboID, which allows for the detection of even transient interactions in the cell type and subcellular compartment of interest (Mair et al., 2019).

Chapter VI – General Discussion

The aim of this thesis was to investigate the regulation and decoding of nuclear calcium release in root apical meristem development, as well as to investigate the regulation of the G protein β subunit in root legume endosymbioses. In Chapter III, an interactor of the Medicago G protein β subunit, which is a positive regulator of root nodule symbioses, was found to have a role in the regulation of AM symbiosis, but not nodulation, and was found to be regulated by phosphate availability. In Chapter IV, the C-linker region of AtCNGC15 was found to be important for regulating the opening and closing of the channel in *X. laevis* oocytes, with the application of cAMP potentially assisting the opening of AtCNGC15^{D408N}. In addition, AtCNGC15 was found to have a dual role in both nitrate signalling and primary root development, and was shown to relocalise in a cell type and nutrient status specific manner. Chapter IV also revealed a role of nuclear calcium signalling in regulating the transcription of the primary nitrate response gene *LBD39*. Finally, Chapter V aimed to identify candidate decoders and regulators of the nuclear calcium release mediated by CNGC15 and DMI1 in Arabidopsis. This revealed RSA1 as a candidate decoder.

6.1 The common symbiosis pathway and the regulation of endosymbiosis

Whilst the initial perception of either rhizobia or AM fungi requires different combinations of LysM receptors at the plasma membrane, many of the downstream signalling components, including the generation of nuclear calcium oscillations, are conserved between the two pathways. In both AM and rhizobial symbioses these nuclear calcium oscillations activate MtDMI3 through the presumed binding of holo-CaM, which then activates MtIPD3 and facilitates the activation of symbiosis specific transcription factors (Gleason et al., 2006, Miller et al., 2013, Messinese et al., 2007). Therefore, the question remains as to where the specificity is encoded in the system that ensures that the correct repertoire of genes is activated depending on the endosymbiont.

Various mechanisms have been proposed to explain how specificity is determined. Starting with initial perception, rhizobia trigger calcium oscillations in root hair cells, as that is where the bacteria are entrapped and where infection threads form. In contrast, AM fungi preferentially infect atrichoblast cells (Chabaud et al., 2011), and differential expression of LysM receptors or downstream components in each cell type could help confer specificity. The activation of LjCCaMK (homolog of MtDMI3) appears to be dependent on CaM binding during rhizobia infection, but not in AM fungi infection, indicating another stage in the pathway that can confer specificity (Shimoda et al., 2012).

The way in which nodulation and AM colonisation are regulated by nutrient availability is also different. Nodulation is negatively regulated by high nitrogen availability, as the establishment of endosymbiosis is energetically expensive, and only carried out to the degree that it is necessary (Streeter and Wong, 1988). In addition to nitrogen availability, nodulation is also regulated by light and carbohydrate status (Wang et al., 2021b). Whilst nodulation is negatively regulated by low Pi in *Phaseolus vulgaris* (common bean) (Isidra-Arellano et al., 2020) via mechanisms that have not been fully characterised yet, AM colonization is positively regulated by low Pi (Thomson et al., 1986), via the pathways described in Chapter III.

With regard to nuclear calcium, it has been suggested that the nuclear calcium oscillations induced by rhizobia and AM have slightly different properties which could convey specificity (Kosuta et al., 2008, Russo et al., 2013), however another report found the calcium signatures triggered by both endosymbionts to be very similar (Sieberer et al., 2012). Such differences could be attributed to the use of different elicitors, with Kosuta et al. (2008) comparing oscillations induced by *Rhizophagus irregularis* versus 1nM Nod factor, Russo et al. (2013) using *Gigaspora margarita* spore exudates, CO4 and Nod factor, and Sieberer et al. (2012) using live imaging of the fungi and the bacteria.

As well as the endosymbiont potentially impacting the nuclear calcium signature, it has been proposed that the nutrient status of the plant could also

affect nuclear calcium oscillations. As described in Chapter III, two studies investigating the role of phosphate on nuclear calcium oscillations revealed different results, even when the same nuclear calcium reporter (*p35S:NupYC2.1*) and the same concentrations of KH_2PO_4 were used (Balzergue et al., 2013, Russo et al., 2013). The inconsistencies could be due to the use of different species of fungi, as well as the different ways in which the calcium imaging data is analysed, and the different parameters that were measured and compared. In addition, Li et al. (2022a) showed that in Medicago, nuclear calcium oscillations in response to LCOs were enhanced under nitrate starvation conditions, and combined nitrate and phosphate starvation conditions, suggesting the presence of a mechanism to regulate nuclear calcium oscillations, and subsequently colonisation levels in response to nutrient availability.

A screen for interactors of the Medicago G protein β subunit revealed APSR1, which was confirmed as an interactor via Yeast 2 Hybrid in one direction. In this thesis, I explored the function of APSR1 using a combination of phylogenetics, expression analyses, and nodulation and AM phenotyping. This revealed that MtAPSR1, like its homolog in Arabidopsis, is induced by phosphate treatment and that removal of APSR1 impairs AM colonisation, but not nodulation. APSR1 could, therefore, play a role in the regulation of nuclear calcium under different phosphate conditions, and the 'priming' of cells under low phosphate conditions to perceive AM fungi. Understanding more about the function of APSR1 could reveal new insights into how various nutrient conditions influence root legume endosymbioses. Further work needs to be done to identify the precise role of APSR1 in the regulation of AM colonization upon phosphate treatment. First, AM colonization should be measured in WT and NF4464 and NF12622 lines under high and low phosphate conditions. If APSR1 is involved in the negative regulation of AM colonisation under high phosphate treatment, you would expect this regulation to be perturbed in the knockout mutant lines. This means NF4464 and NF12622 would not display the phosphate-induced reduction in AM colonisation. The interaction between APSR1 and the G protein β subunit could also be confirmed by Biolayer Interferometry and *in planta* by BiFC. Finally, calcium imaging in NF4464 or

NF12622 plants crossed with a Yellow Cameleon YC3.6 calcium reporter could reveal whether APSR1 plays a role in altering calcium signalling in high phosphate conditions.

6.2 A dual role of CNGC15 in root apical meristem development and nitrate signalling

As well as their role in producing nuclear calcium oscillations in Medicago, CNGC15 and DMI1 have roles in generating single nuclear calcium releases in Arabidopsis root apical meristems (Leitão et al., 2019, Tipper et al., 2023). Given Arabidopsis does not form symbioses with rhizobia bacteria or AM fungi, these nuclear calcium releases must have different roles, and they were found to be responsible for the precise fine tuning of primary root growth and development (Leitão et al., 2019, Tipper et al., 2023). The novel allele *cngc15*^{D408N} was found to cause a reduced primary root length, due to a reduced number of meristematic cells (Tipper et al., 2023). In Chapter IV, homology modelling was used to predict what affect the D408N point mutation would have on CNGC15 structure and function. This revealed that the D408N point mutation is positioned in the C-linker region of the ion channel. CNGCs form homo- and heterotetramers, and subunits have a highly conserved protein structure, with six transmembrane segments (S1-S6), a pore region containing the pore loop determining pore selectivity and diameter between S5 and S6, a cyclic nucleotide binding domain (CNBD), a CaM binding domain, and a C-linker region (Matulef and Zagotta, 2003). In plants, the positioning and functionality of the CaM binding domain varies between CNGCs, with some CaM binding domains overlapping the CNBD at the C terminus (Köhler and Neuhaus, 2000), others at a downstream isoleucine glutamine (IQ) domain (Fischer et al., 2013), and others at the N terminus (DeFalco et al., 2016). The C-linker region connects the CNBD to the S6 transmembrane domain segment. In animals it is known to contribute to the opening and closing of the channel (channel gating), as well as the tetramerization of the channel, as it facilitates contact between the subunits (Matulef and Zagotta, 2003, Rosenbaum and Gordon, 2002). In accordance with this, in our homology model the D408N

mutation was predicted to interfere with a salt bridge that usually forms between the D408 of one subunit and the R398 of the neighbouring subunit (Figure 4.1). The positioning of the D408N mutation in the C-linker region raised the question as to whether this was interfering with the ability of the ion channel to open and close, which was investigated using two electrode voltage clamp experiments in *X. laevis* oocytes. This revealed that indeed the gating is affected in CNGC15^{D408N}, as there was a reduction in the proportion of the oocytes that displayed inward current, but the permeability to calcium was unaffected (Figure 4.2). This highlights an important role of the C-linker region in the gating and potentially channel tetramerization of plant CNGCs, which has not been previously shown.

In animals, the role of cyclic nucleotides, such as cAMP and cGMP, in the gating of CNG channels has been well described (Matulef and Zagotta, 2003). In plants, the degree to which cyclic nucleotides play a role in CNGC gating is a subject of debate. There are several examples of CNGCs where cNMPs are required to stimulate the channels, for example, CNGCs 1, 2, 4, 7, 8, 9, 10 and 16 (Gao et al., 2016, Leng et al., 2002b, Hua et al., 2003, Balagué et al., 2003). At the same time, CNGCs 11 and 12 do not require cNMPs for their activation (Zhang et al., 2019). All of these studies used heterologous systems; the CNGC channels were either expressed in *X. laevis* oocytes or in HEK293 cells, making it difficult to draw conclusions about what is happening *in planta*. When whole cells are used, it is impossible to determine whether the cNMPs are having a direct effect on the CNGCs by binding, or if they are acting independently, by activating other cyclic nucleotide binding proteins. In addition, cNMPs will be naturally present in the cell system, so it is the effect of elevated cNMP levels that is being tested, rather than cNMP requirement *per se*. In the case of CNGCs 2 and 4, membrane patch clamp experiments were performed where part of the oocyte membrane was excised, and the voltage measured across it (Hua et al., 2003, Balagué et al., 2003). This has the benefit of being carried out in a cytoplasm-free environment, so tests for the direct role of cNMPs on the channel activity. However, in these early studies, CNGC2 and CNGC4 were studied as putative K^+ channels, where the addition of cNMPs was

required for inward flow of K^+ (Leng et al., 2002b, Balagué et al., 2003). Later work revealed that in oocytes CNGC2 and 4 only display calcium channel activity when co-expressed, and this does not require elevated cNMP levels (Tian et al., 2019). In this thesis, I show that in two instances application of cAMP allowed for calcium flow through $CNGC15^{D408N}$ in oocytes that has previously not shown calcium flow (Figure 4.3). This suggests that the gating inflexibility conferred by the D408N mutation can be improved with binding of cAMP. This work needs to be expanded to increase the sample size, and also to test the affect of cAMP in oocytes expressing $CNGC15^{D408N}$ that display inward current.

In Arabidopsis roots, the subcellular localisation of CNGC15 is dependent on the developmental stage of the seedling. At 6 days post germination (dpg), CNGC15 was found to be nuclear localised (Leitão et al., 2019, Wang et al., 2021c), and at 12 dpg, when a constitutive promoter is used, it is localised at the plasma membrane (Wang et al., 2021c). At later stages of root development, CNGC15 was implicated in the cytoplasmic calcium influx upon nitrate treatment, due to a proposed conformational change and uncoupling with the nitrate transceptor NRT1.1 (Wang et al., 2021c). This suggests that at 6 dpg, when CNGC15 is nuclear localised, its function is in regulation of primary root development only, and that nitrate responsive genes are not induced by the NRT1.1-CNGC15 pathway at this time point.

In Chapter IV, this hypothesis was tested, and it was found that not only are primary nitrate response genes induced by nitrate at 6dpg, but that there is a requirement for different inputs of cytoplasmic and nuclear calcium. Induction of *LBD39* was found to be enhanced in both in both *Atdmi1-2* and $Atcngc15^{D408N}$, suggesting that *LBD39* expression is negatively regulated by nuclear calcium release (Figure 4.4C). This suggests a role of the nuclear calcium release mediated by CNGC15 and DMI1 in nitrate signalling, which has not been previously described. Calcium is known to regulate primary nitrate responses, with the cytoplasmic calcium influx upon nitrate treatment being responsible for activating calcium binding CPKs 10, 30 and 32. This triggers their translocation to the nucleus, where they phosphorylate NLP7 and facilitate

its nuclear retention (Liu et al., 2017). As well as being a transcription activator, NLP7 has also been found to be a nitrate sensor, able to bind nitrate directly (Liu et al., 2022). In addition, it was found that in the NLP septuple mutant *nlp2,4,5,6,7,8,9* the primary nitrate response was abolished, where it is only partially reduced in the NRT1.1 null mutant *chl1-5* (Liu et al., 2022). This suggests that NLPs are vital in the transcriptional response to nitrate, and implies the existence of other nitrate sensors independent of NRT1.1. The binding of nitrate to NLP7 triggers a conformational change in the protein, which is predicted to activate it (Liu et al., 2022). This is in conjunction with the phosphorylation by CPK10/30/32 which enables its nuclear retention. It is possible that nuclear calcium release is induced by nitrate, activated by an as yet unknown mechanism, and this nuclear calcium is also required for the activation of CPK10/30/32, or other unknown calcium binding proteins, facilitating normal primary nitrate responses.

Unexpectedly, induction of *LBD38* was significantly reduced in *Atcngc15*^{D408N} but not in *Atdmi1-2* root tips (Figure 4.4B). The normal induction in *Atdmi1-2* root tips, which have a reduced frequency of nuclear calcium release (Leitão et al., 2019), suggests that impaired nuclear calcium release does not interfere with *LBD38* expression. However, the reduced induction in *Atcngc15*^{D408N} suggests that potentially it is the cytoplasmic calcium influx upon nitrate treatment that is impacted and affecting *LBD38* induction. This implies a dual role of CNGC15 at 6dpg in the presence of high nitrate. Therefore, the localisation of CNGC15 was reassessed at 6dpg using its own promoter, in both the presence and absence of nitrate. This revealed a relocalisation of CNGC15 to the plasma membrane specifically in the columella cell layer upon nitrate treatment (Figure 4.5). The dual localisation of CNGC15 in both the nucleus and the cytoplasm in this cell layer is consistent with a dual role in both root meristem development and nitrate signalling. Whilst relocalisation of CNGCs has not been previously described in plants, in animals has been documented that CNG channels are trafficked to specific compartments, dependent on cell type, and that this localisation is dependent on the subunit composition of the tetramer (Wojtyniak et al., 2013). Therefore,

this cell type and nutrient status specific relocalisation is a novel contribution to the study of plant CNGCs.

Currently, the vast majority of Arabidopsis CNGCs have been described as plasma membrane localised, but these experiments have largely been carried out in leaf mesophyll protoplasts or by transient expression in *N. benthamiana* leaves or yeast cells (Brost et al., 2019, Gobert et al., 2006, Urquhart et al., 2007). One exception to this is the localisation of CNGC19 and CNGC20 to the tonoplast when expressed transiently in leaf protoplasts (Yuen and Christopher, 2013). Another exception is the localisation of CNGC7, 8 and 18 in the pollen tube, which has been studied *in planta*, although a pollen tube specific promoter was used rather than the own promoters. Even so, two independent studies assessing the localisation of CNGC7 and 8 using transient expression and the pollen tube specific promoter *LAT52* showed completely different localisation patterns (Chang et al., 2007, Pan et al., 2019). Extensive localisation experiments using the own promoters in a range of cell types have not been carried out for most CNGCs, so whether this relocalisation is common amongst the family remains to be determined.

6.3 RSA1 as a putative nuclear calcium signalling in Arabidopsis primary root development

In Chapter V, an EMS suppressor screen and whole genome sequencing was used to try to identify candidate regulators of the DMI1/CNGC15 nuclear calcium release in Arabidopsis. Seedlings from independent EMS lines were selected that recovered wild-type root length in the *cngc15*^{D408N} background. Unfortunately, the whole genome sequencing analysis did not reveal a candidate regulator. The most likely explanation for this is that each line contains point mutations in independent genes, so they could not be identified. However, a literature search of nuclear localised calcium binding proteins revealed RSA1 as a putative nuclear calcium decoder. RSA1 is an intriguing candidate, as its knockout phenotype is remarkably similar to that of *cngc15*^{D408N} (Guan et al., 2013b, Zhang et al., 2020). Root architecture phenotyping supports the hypothesis that RSA1 is a decoder. It has been shown

in Chapter 5 that *rsa1-3* phenocopies the short root phenotype and reduced RAM size of *cngc15*^{D408N}, but that its phenotype is more severe, consistent with the hypothesis that it is acting as a decoder. The double mutants *dmi1-1 rsa1-3* and *dmi1-2 rsa1-3* also display this severe short root phenotype, suggesting that RSA1 may be acting downstream of the nuclear calcium release. However, this is not proof that RSA1 is the decoder in this scenario. Further investigation should aim to see if *rsa1-3* phenocopies *cngc15*^{D408N} at the transcriptional level, i.e., are genes that are misregulated in *rsa1-3* also misregulated in *cngc15*^{D408N} and vice versa. This can be done using genes known to be misregulated in either line, as published in Guan et al. (2013b) and Leitão et al. (2019).

Proving that a calcium binding protein is acting as a decoder in a particular system, and pinning down the precise mechanism of activation can be difficult, and there are only a few examples in plants where this has been done. One such example is MtDMI3/LjCCaMK. DMI3 contains a kinase domain, a CaM binding domain, and three EF hand domains (Mitra et al., 2004, Lévy et al., 2004), and knockout mutants do not form nodules and are not colonised by AM, although they do display nuclear calcium oscillations (Catoira et al., 2000, Sieberer et al., 2009). In addition to these domains, DMI3 was found to have an autoinhibition domain, which negatively regulates its kinase activity, and a autophosphorylation site which is phosphorylated in the presence of calcium (Gleason et al., 2006).

The site of autophosphorylation was identified as the threonine 265 in Lotus CCaMK (Tirichine et al., 2006) and threonine 271 in Medicago DMI3 (Gleason et al., 2006). Complementation studies using truncated proteins revealed that expression of just the kinase domain in Medicago (Gleason et al., 2006), as well as mutating the autophosphorylation site in *Lotus* (Tirichine et al., 2006), caused spontaneous nodulation without rhizobia, indicating that the EF hands and autophosphorylation are essential in the deactivation of DMI3. Consistent with this, removal of EF hand 2, EF hands 2 and 3, or the calcium binding properties of the EF hands gave rise to spontaneous nodulation (Miller et al., 2013). Calcium binding to the EF hands was shown to promote the phosphorylation of DMI3 at threonine 271, which deactivates the protein (Miller

et al., 2013). Miller et al., (2013) proposed that at basal concentrations of calcium, at least one EF hand is calcium bound, facilitating the phosphorylation at Thr-271 and keeping DMI3 inactive. However, during calcium oscillations, the higher concentrations of calcium enable holo-CaM to bind to DMI3, blocking the phosphorylation at Thr-271 and shifting the balance of DMI3 to the active form. In this way, dual regulation by calcium maintains the specificity of DMI3 activation during nuclear calcium oscillations. The binding of CaM to DMI3 has not yet been demonstrated *in planta*, but has been demonstrated for the *Lotus* homolog LjCCaMK (Shimoda et al., 2012).

One issue in the study of decoders is that one decoder can be used in several contexts, making it hard to pin down how it is being regulated in response to different stimuli. For example, CPK32, which is implicated in the primary nitrate signalling pathway and responsible for the phosphorylation of NLP7 (Liu et al., 2017), also has roles in the regulation of flowering time (Li et al., 2022b), ammonium transport (Qin et al., 2020), cellulose biosynthesis (Xin et al., 2023) and aluminium stress (Sadhukhan et al., 2021). CIPK23, responsible for phosphorylating NRT1.1 and switching it from a low to a high affinity nitrate transporter, is also known as a master regulator of nutrient homeostasis and acquisition (Ródenas and Vert, 2020). This raises the question as to how one decoder can respond to a range of different signals and activate the correct downstream components. In some cases, the specificity could be conferred by the use of different organs or cell types. However, in the case of CIPK23, much of the nutrient regulation is occurring in the root, and in several cases, the root epidermis specifically (Ródenas and Vert, 2020). Specificity is believed to be conferred by interactions with different CBLs, different subcellular localisation, target protein discrimination, different calcium signatures, and membrane nanodomains (Ródenas and Vert, 2020). Similarly, RSA1 has been implicated in a wide range of contexts: it is involved in primary and lateral root development, root apical meristem development, salt stress response, and the regulation of flowering time by controlling *FLC* expression (Guan et al., 2013b, Zhang et al., 2020). Therefore, in order to fully understand the mechanisms behind these

different roles, we must understand its subcellular localisation and interacting partners in different organs and cell types.

6.4 Final Thoughts

The research conducted in this thesis falls broadly into two main research areas: the regulation of nuclear calcium signalling upon the perception of endosymbionts in Medicago, and the regulation and decoding of nuclear calcium release during primary root development in Arabidopsis. Both of these nuclear calcium signalling events are generated by the calcium permeable channel CNGC15, and the counter cation channel DMI1. However, the function of the nuclear calcium signal is different in both contexts. In Medicago, the nuclear calcium signalling is required to kickstart the developmental programming required for endosymbiosis, by inducing specific gene expression patterns (Ehrhardt et al., 1996; Wais et al., 2000; Kosuta et al., 2008; Charpentier et al., 2016). In Arabidopsis, which does not form endosymbiosis, the nuclear calcium signalling is required for normal primary root development, as perturbations in the signalling result in longer or shorter primary root lengths, and smaller root meristems containing fewer cells (Leitão et al., 2019; Tipper et al., 2023). This likely also involves the regulation of gene expression, potentially by RSA1.

The study of endosymbiosis in legumes is an important and topical area of research. Their association with both rhizobia bacteria and AM fungi mean that legumes obtain fixed nitrogen and phosphates from these endosymbionts, and so require reduced fertiliser application (Stagnari et al., 2017). It is well known that overuse of artificial fertilisers is damaging to the environment, as their production relies on fossil fuels and releases carbon dioxide into the atmosphere, and surface runoff into nearby waterways can cause eutrophication. In addition, phosphorus reserves are depleting globally, whilst demands for phosphorus fertilisers are only increasing (Bindraban et al., 2020). One method of reducing our reliance on chemical fertilisers is to increase our understanding of the formation and regulation of endosymbiosis in legumes, in

order to improve the efficiency of endosymbiosis in other food crops. It may even allow engineering of cereal crops to form associations with nitrogen-fixing microbes, or to even be able to fix nitrogen themselves, a complex and challenging area of current research (Huisman & Geurts, 2019).

In particular, the regulation of the nuclear calcium oscillations in legumes is particularly exciting, as acceleration of these nuclear calcium oscillations has been shown to increase nodulation in Medicago (del Cerro et al., 2022). G protein signalling has been implicated in the signal transduction from the plasma membrane to the nucleus in soybean and in the activation of nuclear calcium oscillations. Nodulation gene expression can be induced by the G protein agonist mastoparan independently of DMI1 and DMI2 (Charron et al., 2004) and nuclear calcium oscillations can be induced by the synthetic analogue of mastoparan Mas7, and this activation does not require DMI1, DMI2 or NFP, implicating a role of G protein signalling in activating the nuclear calcium oscillations without DMI1 or Nod/Myc factor perception (Sun et al., 2007).

In this thesis, a putative interactor of the Medicago G protein β subunit, APSR1, was found to be required for normal AM colonisation and be regulated by phosphate. Since AM colonisation is positively regulated by low phosphate conditions, APSR1 could be involved in the 'priming' of cells under low phosphate conditions to perceive AM fungi. As mentioned in section 6.1, further work will need to be carried out to test this, and understanding the regulation of endosymbiosis under different nutrient conditions could enable engineering of legumes, or other crop species, for enhanced AM colonisation under low phosphate conditions, reducing the need to apply artificial fertilisers.

Interestingly, although Arabidopsis does not form endosymbiosis with either rhizobia bacteria or AM fungi, it does still have CNGC15 and DMI1 localised to the nuclear envelope in root apical meristem cells, where they generate single nuclear calcium releases (Leitão et al., 2019; Tipper et al., 2023). I have identified that the D408N point mutation in the C-linker region of $CNGC15^{D408N}$ impairs the ability of the channel to open and close. Future work could manipulate the C-linker region in other CNGCs, to assess whether the C-

linker region has a universal role in channel gating or not. In the case of *cngc15*^{D408N}, there is reduced calcium input that results in a shorter root apical meristem and therefore reduced primary root length. In addition, the frequency of nuclear calcium release is positively correlated with primary root length (Leitão et al., 2019). Future work could translate this research into crop plants, to potentially engineer different primary root lengths optimal for different environmental conditions. In addition, CNGCs have diverse roles in both biotic and abiotic stress responses (Dong et al., 2022), so the manipulation of the C-linker region in other CNGCs could alter these responses. If this manipulation in other CNGCs also reduces calcium input, this could allow for evaluation of the effects of reduced (but not eliminated) calcium input on downstream signalling processes.

List of Abbreviations

A: arbuscule
AD: activation domain of GAL4
AF2: AlphaFold2
AHK: Arabidopsis Histidine Kinase
AM: Arbuscular Mycorrhizal
ANOVA: Analysis of Variance
Arabidopsis: *Arabidopsis thaliana*
ARF: Auxin Response Factor
ARR: Arabidopsis Response Regulator
ATP: adenosine triphosphate
BAM: Binary Alignment Map
BD: binding domain of GAL4
bHLH: basic helix-loop-helix
BiFC: Bimolecular Fluorescence Complementation
BLAST: Basic Local Alignment Search Tool
BNF: Biological Nitrogen Fixation
BNM: Buffered Nodulation Medium
BWA-MEM: Burrows-Wheeler Aligner Maximal Exact Match
Ca^{2+}: calcium ion
CaM: calmodulin
cAMP: cyclic adenosine monophosphate
CBL: calcineurin B-like
CCaMK: calcium calmodulin dependent protein kinase
cDNA: complementary DNA
CDS: coding sequence
cGMP: cyclic guanosine monophosphate
CIPK: CBL-interacting protein kinase
CML: calmodulin like
CNBD: cyclic nucleotide binding domain
CNG: cyclic nucleotide-gated
CNGC: cyclic nucleotide gated channel
cNMP: cyclic nucleotide
CO: chitooligosaccharide
Co-IP: co-immunioprecipitation
Col-0: Columbia 0
CDPK: Ca^{2+}-dependent protein kinase
CPK: Ca^{2+}-dependent protein kinases
dH_2O: distilled water
DIC: differential interference contrast
DSLR: Digital Single Lens Reflex
DMSO: dimethyl sulfoxide
DNA: deoxyribonucleic acid
dpg: days post germination
E: primer amplification efficiency
EMS: ethyl methanesulfonate
ERF-VII: group VII ethylene responsive factors
EZ: elongation zone
FRET-FLIM: Förster resonance energy transfer by fluorescence lifetime imaging
Fwd: forward
GA: gibberellic acid
GAPs: GTPase activity accelerating proteins
GDP: guanosine diphosphate
GFP: green fluorescent protein
GSE: germinated spore exudates
GTP: guanosine triphosphate
HCN: hyperpolarization-activated cyclic nucleotide-gated
HEK: Human Embryonic Kidney
IAA: indole-3-acetic acid
IGV: Integrative Genomics Viewer
IRH: intraradical hyphae
IQ: isoleucine glutamine

JIC: John Innes Centre
LB: lysogeny broth
LCO: lipochitooligosaccharide
LL-PS liquid-liquid phase separation
LRR: leucine rich repeat
LUC: luciferase
LysM: lysin motif
MAFFT: Multiple Alignment using Fast Fourier Transform
Mas7: synthetic analogue of mastoparan
MBS: modified Barth's solution
Medicago: *Medicago truncatula*
Mg^{2+}: magnesium ion
MLD: malectin-like domain
ModFP: Modified Fahraeus Plant
MS: Murashige and Skoog
MVA: mevalonate
Myc: mycorrhizal
n.s.: non-significant
N: nitrogen
N_2: atmospheric nitrogen gas
NCBI: National Centre for Biotechnology Information
Nod: nodulation
OD_{600}: Optical Density at 600nm
P: Promoter
P35S: Cauliflower mosaic virus 35S promoter
PAM: peri arbuscular membrane
PAMP: pathogen-associated molecular patterns
PCR: polymerase chain reaction
Pi: inorganic phosphate
PLC: phospholipase C
PM: proximal meristem
PO_4^{3-}: phosphate ion
PSR: phosphate starvation response
PT: phosphate transporter
PTI: PAMP triggered immunity
QC: quiescent centre
qRT-PCR: quantitative reverse transcription PCR
RAM: root apical meristem
Rev: reverse
RLK: receptor like kinase
RNA: ribonucleic acid
RNAi: RNA interference
rpm: revolutions per minute
SAM: Sequence Alignment Map
SD: synthetic dextrose
SM: SWISS-MODEL
SNP: single nucleotide polymorphism
SOC: Super Optimal broth with Catabolite repression
TEVC: two electrode voltage clamp
TY: tryptone yeast extract
TZ: Transition zone
V: vesicle
WT: wild type
YC3.6: yellow cameleon 3.6
YFP: yellow fluorescent protein

List of References

ADAVI, B. S., PANDESHA, P. H., B, J., JHA, S. K., CHINNUSAMY, V. & SATHEE, L. 2023. Nitrate supply regulates tissue calcium abundance and transcript level of Calcineurin B-like (CBL) gene family in wheat. *Plant Physiol Biochem,* 199**,** 107724.

AKIYAMA, K., MATSUZAKI, K. & HAYASHI, H. 2005. Plant sesquiterpenes induce hyphal branching in arbuscular mycorrhizal fungi. *Nature,* 435**,** 824-7.

ALBERTI S, GLADFELTER A, MITTAG T. Considerations and Challenges in Studying Liquid-Liquid Phase Separation and Biomolecular Condensates. Cell. 2019 Jan 24;176(3):419-434.

ALDON, D., MBENGUE, M., MAZARS, C. & GALAUD, J. P. 2018. Calcium Signalling in Plant Biotic Interactions. *Int J Mol Sci,* 19.

ALI, R., MA, W., LEMTIRI-CHLIEH, F., TSALTAS, D., LENG, Q., VON BODMAN, S. & BERKOWITZ, G. A. 2007. Death Don't Have No Mercy and Neither Does Calcium: Arabidopsis CYCLIC NUCLEOTIDE GATED CHANNEL2 and Innate Immunity. *The Plant Cell,* 19**,** 1081-1095.

ALLEN, G. J., CHU, S. P., HARRINGTON, C. L., SCHUMACHER, K., HOFFMANN, T., TANG, Y. Y., GRILL, E. & SCHROEDER, J. I. 2001. A defined range of guard cell calcium oscillation parameters encodes stomatal movements. *Nature,* 411**,** 1053-1057.

ALVAREZ, J. M., SCHINKE, A.-L., BROOKS, M. D., PASQUINO, A., LEONELLI, L., VARALA, K., SAFI, A., KROUK, G., KRAPP, A. & CORUZZI, G. M. 2020. Transient genome-wide interactions of the master transcription factor NLP7 initiate a rapid nitrogen-response cascade. *Nature Communications,* 11**,** 1157.

ANÉ, J.-M., KISS, G. B., RIELY, B. K., PENMETSA, R. V., OLDROYD, G. E. D., AYAX, C., LÉVY, J., DEBELLÉ, F., BAEK, J.-M., KALO, P., ROSENBERG, C., ROE, B. A., LONG, S. R., DÉNARIÉ, J. & COOK, D. R. 2004. Medicago truncatula DMI1; Required for Bacterial and Fungal Symbioses in Legumes. *Science,* 303**,** 1364.

ANÉ, J.-M., LÉVY, J., THOQUET, P., KULIKOVA, O., DE BILLY, F., PENMETSA, V., KIM, D.-J., DEBELLÉ, F., ROSENBERG, C., COOK, D. R., BISSELING, T., HUGUET, T. & DÉNARIÉ, J. 2002. Genetic and Cytogenetic Mapping of DMI1, DMI2, and DMI3 Genes of Medicago truncatula Involved in Nod Factor Transduction, Nodulation, and Mycorrhization. *Molecular Plant-Microbe Interactions®,* 15**,** 1108-1118.

ANTOLÍN-LLOVERA, M., RIED, MARTINA K. & PARNISKE, M. 2014. Cleavage of the SYMBIOSIS RECEPTOR-LIKE KINASE Ectodomain Promotes Complex Formation with Nod Factor Receptor 5. *Current Biology,* 24**,** 422-427.

ARRIGHI, J. F., BARRE, A., BEN AMOR, B., BERSOULT, A., SORIANO, L. C., MIRABELLA, R., DE CARVALHO-NIEBEL, F., JOURNET, E. P., GHÉRARDI, M., HUGUET, T., GEURTS, R., DÉNARIÉ, J., ROUGÉ, P. & GOUGH, C. 2006. The Medicago truncatula lysin [corrected] motif-receptor-like kinase gene family includes NFP and new nodule-expressed genes. *Plant Physiol,* 142**,** 265-79.

AZCÓN, R., GOMEZ-ORTEGA, M. & BAREA, J. M. 1982. COMPARATIVE EFFECTS OF FOLIAR- OR SOIL-APPLIED NITRATE ON VESICULAR-ARBUSCULAR MYCORRHIZAL INFECTION IN MAIZE. *New Phytologist,* 92**,** 553-559.

BACH EM, NARVAEZ-RIVERA G, MURRAY K, BAUER JT, HOFMOCKEL KS. The dynamic life of arbuscular mycorrhizal fungal symbionts. Ecology. 2018 Apr;99(4):978-980.

BAGO, B., PFEFFER, P. E., ABUBAKER, J., JUN, J., ALLEN, J. W., BROUILLETTE, J., DOUDS, D. D., LAMMERS, P. J. & SHACHAR-HILL, Y. 2003. Carbon export from arbuscular mycorrhizal roots involves the translocation of carbohydrate as well as lipid. *Plant Physiol,* 131**,** 1496-507.

BAI, L., ZHANG, G., ZHOU, Y., ZHANG, Z., WANG, W., DU, Y., WU, Z. & SONG, C.-P. 2009. Plasma membrane-associated proline-rich extensin-like receptor kinase 4, a novel regulator of Ca2+ signalling, is required for abscisic acid responses in Arabidopsis thaliana. *The Plant Journal,* 60**,** 314-327.

BALAGUÉ, C., LIN, B., ALCON, C., FLOTTES, G., MALMSTRÖM, S., KÖHLER, C., NEUHAUS, G., PELLETIER, G., GAYMARD, F. & ROBY, D. 2003. HLM1, an essential signaling component in the hypersensitive response, is a member of the cyclic nucleotide-gated channel ion channel family. *Plant Cell,* 15**,** 365-79.

BALZERGUE, C., CHABAUD, M., BARKER, D., BÉCARD, G. & ROCHANGE, S. 2013. High phosphate reduces host ability to develop arbuscular mycorrhizal symbiosis without affecting root calcium spiking responses to the fungus. *Frontiers in Plant Science,* 4.

BALZERGUE, C., PUECH-PAGÈS, V., BÉCARD, G. & ROCHANGE, S. F. 2010. The regulation of arbuscular mycorrhizal symbiosis by phosphate in pea involves early and systemic signalling events. *Journal of Experimental Botany,* 62**,** 1049-1060.

BEYHL D, HÖRTENSTEINER S, MARTINOIA E, FARMER EE, FROMM J, MARTEN I, HEDRICH R. The fou2 mutation in the major vacuolar cation channel TPC1 confers tolerance to inhibitory luminal calcium. Plant J. 2009 Jun;58(5):715-23.

BI G, SU M, LI N, LIANG Y, DANG S, XU J, HU M, WANG J, ZOU M, DENG Y, LI Q, HUANG S, LI J, CHAI J, HE K, CHEN YH, ZHOU JM. The ZAR1 resistosome is a calcium-permeable channel triggering plant immune signaling. Cell. 2021 Jun 24;184(13):3528-3541.e12.

BIBIKOVA TN, ZHIGILEI A, GILROY S. Root hair growth in Arabidopsis thaliana is directed by calcium and an endogenous polarity. Planta. 1997 Dec;203(4):495-505. doi: 10.1007/s004250050219. PMID: 9421933.

BIDARTONDO, M. I., READ, D. J., TRAPPE, J. M., MERCKX, V., LIGRONE, R. & DUCKETT, J. G. 2011. The dawn of symbiosis between plants and fungi. *Biol Lett,* 7**,** 574-7.

BLOWERS, D. P. & TREWAVAS, A. J. 1989. Rapid Cycling of Autophosphorylation of a Ca2+-Calmodulin Regulated Plasma Membrane Located Protein Kinase from Pea. *Plant Physiology,* 90**,** 1279-1285.

BOER, D. R., FREIRE-RIOS, A., VAN DEN BERG, W. A., SAAKI, T., MANFIELD, I. W., KEPINSKI, S., LÓPEZ-VIDRIEO, I., FRANCO-ZORRILLA, J. M., DE VRIES, S. C., SOLANO, R., WEIJERS, D. & COLL, M. 2014. Structural basis for DNA binding specificity by the auxin-dependent ARF transcription factors. *Cell,* 156**,** 577-89.

BONAVENTURE G, GFELLER A, PROEBSTING WM, HÖRTENSTEINER S, CHÉTELAT A, MARTINOIA E, FARMER EE. A gain-of-function allele of TPC1 activates oxylipin biogenesis after leaf wounding in Arabidopsis. Plant J. 2007 Mar;49(5):889-98.

BONFANTE, P. & GENRE, A. 2010. Mechanisms underlying beneficial plant–fungus interactions in mycorrhizal symbiosis. *Nature Communications,* 1**,** 48.

BOVIN, A. D., PAVLOVA, O. A., DOLGIKH, A. V., LEPPYANEN, I. V. & DOLGIKH, E. A. 2021. The Role of Heterotrimeric G-Protein Beta Subunits During Nodulation in Medicago truncatula Gaertn and Pisum sativum L. *Front Plant Sci,* 12**,** 808573.

BREUILLIN, F., SCHRAMM, J., HAJIREZAEI, M., AHKAMI, A., FAVRE, P., DRUEGE, U., HAUSE, B., BUCHER, M., KRETZSCHMAR, T., BOSSOLINI, E., KUHLEMEIER, C., MARTINOIA, E., FRANKEN, P., SCHOLZ, U. & REINHARDT, D. 2010. Phosphate systemically inhibits

development of arbuscular mycorrhiza in Petunia hybrida and represses genes involved in mycorrhizal functioning. *The Plant Journal,* 64**,** 1002-1017.

BROGHAMMER, A., KRUSELL, L., BLAISE, M., SAUER, J., SULLIVAN, J. T., MAOLANON, N., VINTHER, M., LORENTZEN, A., MADSEN, E. B., JENSEN, K. J., ROEPSTORFF, P., THIRUP, S., RONSON, C. W., THYGESEN, M. B. & STOUGAARD, J. 2012. Legume receptors perceive the rhizobial lipochitin oligosaccharide signal molecules by direct binding. *Proceedings of the National Academy of Sciences,* 109**,** 13859-13864.

BROST, C., STUDTRUCKER, T., REIMANN, R., DENNINGER, P., CZEKALLA, J., KREBS, M., FABRY, B., SCHUMACHER, K., GROSSMANN, G. & DIETRICH, P. 2019. Multiple cyclic nucleotide-gated channels coordinate calcium oscillations and polar growth of root hairs. *Plant J,* 99**,** 910-923.

BURLEIGH, S. M. & HARRISON, M. J. 1998. Characterization of the Mt4 gene from Medicago truncatula. *Gene,* 216**,** 47-53.

BUSTOS, R., CASTRILLO, G., LINHARES, F., PUGA, M. I., RUBIO, V., PÉREZ-PÉREZ, J., SOLANO, R., LEYVA, A. & PAZ-ARES, J. 2010. A Central Regulatory System Largely Controls Transcriptional Activation and Repression Responses to Phosphate Starvation in Arabidopsis. *PLOS Genetics,* 6**,** e1001102.

CAPOEN, W., SUN, J., WYSHAM, D., OTEGUI, M. S., VENKATESHWARAN, M., HIRSCH, S., MIWA, H., DOWNIE, J. A., MORRIS, R. J., ANÉ, J.-M. & OLDROYD, G. E. D. 2011. Nuclear membranes control symbiotic calcium signaling of legumes. *Proceedings of the National Academy of Sciences,* 108**,** 14348-14353.

CARAFOLI, E. & KREBS, J. 2016. Why Calcium? How Calcium Became the Best Communicator*. *Journal of Biological Chemistry,* 291**,** 20849-20857.

CARRERE, S., VERDIER, J. & GAMAS, P. 2021. MtExpress, a Comprehensive and Curated RNAseq-based Gene Expression Atlas for the Model Legume Medicago truncatula. *Plant Cell Physiol,* 62**,** 1494-1500.

CATOIRA, R., GALERA, C., DE BILLY, F., PENMETSA, R. V., JOURNET, E.-P., MAILLET, F., ROSENBERG, C., COOK, D., GOUGH, C. & DÉNARIÉ, J. 2000. Four Genes of Medicago truncatula Controlling Components of a Nod Factor Transduction Pathway. *The Plant Cell,* 12**,** 1647-1665.

CHABAUD, M., GENRE, A., SIEBERER, B. J., FACCIO, A., FOURNIER, J., NOVERO, M., BARKER, D. G. & BONFANTE, P. 2011. Arbuscular mycorrhizal hyphopodia and germinated spore exudates trigger Ca2+ spiking in the legume and nonlegume root epidermis. *New Phytol,* 189**,** 347-55.

CHAKRABORTY, S., TOYOTA, M., MOEDER, W., CHIN, K., FORTUNA, A., CHAMPIGNY, M., VANNESTE, S., GILROY, S., BEECKMAN, T., NAMBARA, E. & YOSHIOKA, K. 2021. CYCLIC NUCLEOTIDE-GATED ION CHANNEL 2 modulates auxin homeostasis and signaling. *Plant Physiology,* 187**,** 1690-1703.

CHANG, F., YAN, A., ZHAO, L.-N., WU, W.-H. & YANG, Z. 2007. A Putative Calcium-Permeable Cyclic Nucleotide-Gated Channel, CNGC18, Regulates Polarized Pollen Tube Growth. *Journal of Integrative Plant Biology,* 49**,** 1261-1270.

CHANG, L., RAMIREDDY, E. & SCHMÜLLING, T. 2015. Cytokinin as a positional cue regulating lateral root spacing in Arabidopsis. *J Exp Bot,* 66**,** 4759-68.

CHAPMAN EJ, ESTELLE M. Mechanism of auxin-regulated gene expression in plants. Annu Rev Genet. 2009;43:265-85. doi: 10.1146/annurev-genet-102108-134148. PMID: 19686081.

CHARPENTIER, M., BREDEMEIER, R., WANNER, G., TAKEDA, N., SCHLEIFF, E. & PARNISKE, M. 2008. Lotus japonicus CASTOR and POLLUX are ion channels essential for perinuclear calcium spiking in legume root endosymbiosis. *Plant Cell,* 20**,** 3467-79.

CHARPENTIER, M., SUN, J., VAZ MARTINS, T., RADHAKRISHNAN, G. V., FINDLAY, K., SOUMPOUROU, E., THOUIN, J., VERY, A. A., SANDERS, D., MORRIS, R. J. & OLDROYD,

G. E. 2016. Nuclear-localized cyclic nucleotide-gated channels mediate symbiotic calcium oscillations. *Science,* 352**,** 1102-5.

CHARRON, D., PINGRET, J. L., CHABAUD, M., JOURNET, E. P. & BARKER, D. G. 2004. Pharmacological evidence that multiple phospholipid signaling pathways link Rhizobium nodulation factor perception in Medicago truncatula root hairs to intracellular responses, including Ca2+ spiking and specific ENOD gene expression. *Plant Physiol,* 136**,** 3582-93.

CHEN CW, YANG YW, LUR HS, TSAI YG, CHANG MC. A novel function of abscisic acid in the regulation of rice (Oryza sativa L.) root growth and development. Plant Cell Physiol. 2006 Jan;47(1):1-13.

CHEN, L.-Q., HOU, B.-H., LALONDE, S., TAKANAGA, H., HARTUNG, M. L., QU, X.-Q., GUO, W.-J., KIM, J.-G., UNDERWOOD, W., CHAUDHURI, B., CHERMAK, D., ANTONY, G., WHITE, F. F., SOMERVILLE, S. C., MUDGETT, M. B. & FROMMER, W. B. 2010. Sugar transporters for intercellular exchange and nutrition of pathogens. *Nature,* 468**,** 527-532.

CHENG YAO, QIUYING TIAN, WEN-HAO ZHANG, Glutamate receptors are involved in mitigating effects of amino acids on seed germination of Arabidopsis thaliana under salt stress, Environmental and Experimental Botany, Volume 130, 2016, Pages 68-78,

CHEONG, Y. H., PANDEY, G. K., GRANT, J. J., BATISTIC, O., LI, L., KIM, B. G., LEE, S. C., KUDLA, J. & LUAN, S. 2007. Two calcineurin B-like calcium sensors, interacting with protein kinase CIPK23, regulate leaf transpiration and root potassium uptake in Arabidopsis. *Plant J,* 52**,** 223-39.

CHOUDHURY, S. R. & PANDEY, S. 2013. Specific Subunits of Heterotrimeric G Proteins Play Important Roles during Nodulation in Soybean *Plant Physiology,* 162**,** 522-533.

CHOUDHURY, S. R. & PANDEY, S. 2015. Phosphorylation-Dependent Regulation of G-Protein Cycle during Nodule Formation in Soybean. *The Plant Cell,* 27**,** 3260-3276.

CLIQUET, J. B., MURRAY, P. J. & BOUCAUD, J. 1997. Effect of the arbuscular mycorrhizal fungus Glomus fasciculatum on the uptake of amino nitrogen by Lolium perenne. *New Phytol,* 137**,** 345-349.

CLOUGH, S. J., FENGLER, K. A., YU, I. C., LIPPOK, B., SMITH, R. K., JR. & BENT, A. F. 2000. The Arabidopsis dnd1 "defense, no death" gene encodes a mutated cyclic nucleotide-gated ion channel. *Proc Natl Acad Sci U S A,* 97**,** 9323-8.

COLE, K. S. 1950. *Dynamic electrical characteristics of the squid axon membrane,* Bethesda, Maryland, Naval Medical Research Institute, National Naval Medical Center Bethesda, Maryland.

COSTA, A., CANDEO, A., FIERAMONTI, L., VALENTINI, G. & BASSI, A. 2013. Calcium Dynamics in Root Cells of Arabidopsis thaliana Visualized with Selective Plane Illumination Microscopy. *PLOS ONE,* 8**,** e75646.

COSTA, A., NAVAZIO, L. & SZABO, I. 2018. The contribution of organelles to plant intracellular calcium signalling. *Journal of Experimental Botany,* 69**,** 4175-4193.

DADACZ-NARLOCH B, BEYHL D, LARISCH C, LÓPEZ-SANJURJO EJ, RESKI R, KUCHITSU K, MÜLLER TD, BECKER D, SCHÖNKNECHT G, HEDRICH R. A novel calcium binding site in the slow vacuolar cation channel TPC1 senses luminal calcium levels. Plant Cell. 2011 Jul;23(7):2696-707.

DAS, D., PARIES, M., HOBECKER, K., GIGL, M., DAWID, C., LAM, H.-M., ZHANG, J., CHEN, M. & GUTJAHR, C. 2022. PHOSPHATE STARVATION RESPONSE transcription factors enable arbuscular mycorrhiza symbiosis. *Nature Communications,* 13**,** 477.

DAVIÈRE, J.-M. & ACHARD, P. 2013. Gibberellin signaling in plants. *Development,* 140**,** 1147-1151.

DAVIES JM. Annexin-Mediated Calcium Signalling in Plants. Plants (Basel). 2014 Feb 26;3(1):128-40.

DAVIS, M. W. & JORGENSEN, E. M. 2022. ApE, A Plasmid Editor: A Freely Available DNA Manipulation and Visualization Program. *Frontiers in Bioinformatics,* 2.

DAY, I. S., REDDY, V. S., SHAD ALI, G. & REDDY, A. S. N. 2002. Analysis of EF-hand-containing proteins in Arabidopsis. *Genome Biology,* 3**,** research0056.1.

DEFALCO, T. A., MARSHALL, C. B., MUNRO, K., KANG, H.-G., MOEDER, W., IKURA, M., SNEDDEN, W. A. & YOSHIOKA, K. 2016. Multiple Calmodulin-Binding Sites Positively and Negatively Regulate Arabidopsis CYCLIC NUCLEOTIDE-GATED CHANNEL12. *The Plant Cell,* 28**,** 1738-1751.

Dekomah SD, Bi Z, Dormatey R, Wang Y, Haider FU, Sun C, Yao P, Bai J. The role of CDPKs in plant development, nutrient and stress signaling. Front Genet. 2022 Sep 30;13:996203. doi: 10.3389/fgene.2022.996203. PMID: 36246614; PMCID: PMC9561101.

DEL CERRO, P., COOK, N. M., HUISMAN, R., DANGEVILLE, P., GRUBB, L. E., MARCHAL, C., HO CHING LAM, A. & CHARPENTIER, M. 2022. Engineered CaM2 modulates nuclear calcium oscillation and enhances legume root nodule symbiosis. *Proc Natl Acad Sci U S A,* 119**,** e2200099119.

DELAUX, P. M., BÉCARD, G. & COMBIER, J. P. 2013. NSP1 is a component of the Myc signaling pathway. *New Phytol,* 199**,** 59-65.

DELLO IOIO, R., LINHARES, F. S., SCACCHI, E., CASAMITJANA-MARTINEZ, E., HEIDSTRA, R., COSTANTINO, P. & SABATINI, S. 2007. Cytokinins Determine Arabidopsis Root-Meristem Size by Controlling Cell Differentiation. *Current Biology,* 17**,** 678-682.

DEMIDCHIK, V., SHABALA, S., ISAYENKOV, S., CUIN, T. A. & POTTOSIN, I. 2018. Calcium transport across plant membranes: mechanisms and functions. *New Phytologist,* 220**,** 49-69.

DESVOYES B, ECHEVARRÍA C, GUTIERREZ C. A perspective on cell proliferation kinetics in the root apical meristem. J Exp Bot. 2021 Oct 13;72(19):6708-6715.

DHALLAN, R. S., YAU, K.-W., SCHRADER, K. A. & REED, R. R. 1990. Primary structure and functional expression of a cyclic nucleotide-activated channel from olfactory neurons. *Nature,* 347**,** 184-187.

DIETRICH, P., MOEDER, W. & YOSHIOKA, K. 2020. Plant Cyclic Nucleotide-Gated Channels: New Insights on Their Functions and Regulation. *Plant Physiology,* 184**,** 27-38.

DINDAS, J., SCHERZER, S., ROELFSEMA, M. R. G., VON MEYER, K., MÜLLER, H. M., AL-RASHEID, K. A. S., PALME, K., DIETRICH, P., BECKER, D., BENNETT, M. J. & HEDRICH, R. 2018. AUX1-mediated root hair auxin influx governs SCFTIR1/AFB-type Ca2+ signaling. *Nature Communications,* 9**,** 1174.

DING, Y., YANG, H., WU, S., FU, D., LI, M., GONG, Z. & YANG, S. 2022. CPK28-NLP7 module integrates cold-induced Ca²⁺ signal and transcriptional reprogramming in Arabidopsis. *Science Advances,* 8**,** eabn7901.

DODD AN, KUDLA J, SANDERS D. The language of calcium signaling. Annu Rev Plant Biol. 2010;61:593-620. doi: 10.1146/annurev-arplant-070109-104628. PMID: 20192754.

DONG Q, BAI B, ALMUTAIRI BO, KUDLA J. Emerging roles of the CBL-CIPK calcium signaling network as key regulatory hub in plant nutrition. J Plant Physiol. 2021 Feb;257:153335. doi: 10.1016/j.jplph.2020.153335. Epub 2020 Dec 16. PMID: 33388664.

DONG Q, WALLRAD L, ALMUTAIRI BO, KUDLA J. Ca^{2+} signaling in plant responses to abiotic stresses. J Integr Plant Biol. 2022 Feb;64(2):287-300. doi: 10.1111/jipb.13228. PMID: 35048537.

DOS SANTOS MARASCHIN, F., MEMELINK, J. & OFFRINGA, R. 2009. Auxin-induced, SCFTIR1-mediated poly-ubiquitination marks AUX/IAA proteins for degradation. *The Plant Journal,* 59**,** 100-109.

ECHEVARRÍA C, GUTIERREZ C, DESVOYES B. Tools for Assessing Cell-Cycle Progression in Plants. Plant Cell Physiol. 2021 Nov 10;62(8):1231-1238. doi: 10.1093/pcp/pcab066. PMID: 34021583; PMCID: PMC8579159.

EHRHARDT, D. W., WAIS, R. & LONG, S. R. Calcium spiking in plant root hairs responding to *Rhizobium* nodulation signals. *Cell* **85**, 673–681 (1996).

ENDRE, G., KERESZT, A., KEVEI, Z., MIHACEA, S., KALÓ, P. & KISS, G. B. 2002. A receptor kinase gene regulating symbiotic nodule development. *Nature,* 417**,** 962-6.

FAN, B., LIAO, K., WANG, L.-N., SHI, L.-L., ZHANG, Y., XU, L.-J., ZHOU, Y., LI, J.-F., CHEN, Y.-Q., CHEN, Q.-F. & XIAO, S. 2023. Calcium-dependent activation of CPK12 facilitates its cytoplasm-to-nucleus translocation to potentiate plant hypoxia sensing by phosphorylating ERF-VII transcription factors. *Molecular Plant,* 16**,** 979-998.

FENDRYCH, M., LEUNG, J. & FRIML, J. 2016. TIR1/AFB-Aux/IAA auxin perception mediates rapid cell wall acidification and growth of Arabidopsis hypocotyls. *Elife,* 5.

FENG, F., SUN, J., RADHAKRISHNAN, G. V., LEE, T., BOZSÓKI, Z., FORT, S., GAVRIN, A., GYSEL, K., THYGESEN, M. B., ANDERSEN, K. R., RADUTOIU, S., STOUGAARD, J. & OLDROYD, G. E. D. 2019. A combination of chitooligosaccharide and lipochitooligosaccharide recognition promotes arbuscular mycorrhizal associations in Medicago truncatula. *Nature Communications,* 10**,** 5047.

FESENKO, E. E., KOLESNIKOV, S. S. & LYUBARSKY, A. L. 1985. Induction by cyclic GMP of cationic conductance in plasma membrane of retinal rod outer segment. *Nature,* 313**,** 310-3.

FIELDS, S. & SONG, O.-K. 1989. A novel genetic system to detect protein–protein interactions. *Nature,* 340**,** 245-246.

FISCHER, C., KUGLER, A., HOTH, S. & DIETRICH, P. 2013. An IQ Domain Mediates the Interaction with Calmodulin in a Plant Cyclic Nucleotide-Gated Channel. *Plant and Cell Physiology,* 54**,** 573-584.

FLOSS, D. S., LEVY, J. G., LÉVESQUE-TREMBLAY, V., PUMPLIN, N. & HARRISON, M. J. 2013. DELLA proteins regulate arbuscule formation in arbuscular mycorrhizal symbiosis. *Proceedings of the National Academy of Sciences,* 110**,** E5025.

FRIETSCH, S., WANG, Y.-F., SLADEK, C., POULSEN, L. R., ROMANOWSKY, S. M., SCHROEDER, J. I. & HARPER, J. F. 2007. A cyclic nucleotide-gated channel is essential for polarized tip growth of pollen. *Proceedings of the National Academy of Sciences,* 104**,** 14531-14536.

FUKAKI, H., TAMEDA, S., MASUDA, H. & TASAKA, M. 2002. Lateral root formation is blocked by a gain-of-function mutation in the SOLITARY-ROOT/IAA14 gene of Arabidopsis. *The Plant Journal,* 29**,** 153-168.

GAO, Q.-F., GU, L.-L., WANG, H.-Q., FEI, C.-F., FANG, X., HUSSAIN, J., SUN, S.-J., DONG, J.-Y., LIU, H. & WANG, Y.-F. 2016. Cyclic nucleotide-gated channel 18 is an essential Ca²⁺ channel in pollen tube tips for pollen tube guidance to ovules in Arabidopsis. *Proceedings of the National Academy of Sciences,* 113**,** 3096-3101.

GENRE, A., CHABAUD, M., BALZERGUE, C., PUECH-PAGÈS, V., NOVERO, M., REY, T., FOURNIER, J., ROCHANGE, S., BÉCARD, G., BONFANTE, P. & BARKER, D. G. 2013. Short-chain chitin oligomers from arbuscular mycorrhizal fungi trigger nuclear Ca2+ spiking in Medicago truncatula roots and their production is enhanced by strigolactone. *New Phytol,* 198**,** 190-202.

GENRE, A., CHABAUD, M., FACCIO, A., BARKER, D. G. & BONFANTE, P. 2008. Prepenetration apparatus assembly precedes and predicts the colonization patterns of arbuscular

mycorrhizal fungi within the root cortex of both Medicago truncatula and Daucus carota. *Plant Cell,* 20**,** 1407-20.

GENRE, A., CHABAUD, M., TIMMERS, T., BONFANTE, P. & BARKER, D. G. 2005. Arbuscular Mycorrhizal Fungi Elicit a Novel Intracellular Apparatus in Medicago truncatula Root Epidermal Cells before Infection[W]. *The Plant Cell,* 17**,** 3489-3499.

GIETZ, R. D. & SCHIESTL, R. H. 2007. High-efficiency yeast transformation using the LiAc/SS carrier DNA/PEG method. *Nature Protocols,* 2**,** 31-34.

GIOVANNETTI, M. & MOSSE, B. 1980. AN EVALUATION OF TECHNIQUES FOR MEASURING VESICULAR ARBUSCULAR MYCORRHIZAL INFECTION IN ROOTS. *New Phytologist,* 84**,** 489-500.

GLEASON, C., CHAUDHURI, S., YANG, T., MUÑOZ, A., POOVAIAH, B. W. & OLDROYD, G. E. D. 2006. Nodulation independent of rhizobia induced by a calcium-activated kinase lacking autoinhibition. *Nature,* 441**,** 1149-1152.

GOBBATO, E., MARSH, J. F., VERNIÉ, T., WANG, E., MAILLET, F., KIM, J., MILLER, J. B., SUN, J., BANO, S. A., RATET, P., MYSORE, K. S., DÉNARIÉ, J., SCHULTZE, M. & OLDROYD, G. E. 2012. A GRAS-type transcription factor with a specific function in mycorrhizal signaling. *Curr Biol,* 22**,** 2236-41.

GOBERT, A., PARK, G., AMTMANN, A., SANDERS, D. & MAATHUIS, F. J. M. 2006. Arabidopsis thaliana Cyclic Nucleotide Gated Channel 3 forms a non-selective ion transporter involved in germination and cation transport. *Journal of Experimental Botany,* 57**,** 791-800.

GONZÁLEZ-MENDOZA, V., ZURITA-SILVA, A., SÁNCHEZ-CALDERÓN, L., SÁNCHEZ-SANDOVAL, M. E., OROPEZA-ABURTO, A., GUTIÉRREZ-ALANÍS, D., ALATORRE-COBOS, F. & HERRERA-ESTRELLA, L. 2013. APSR1, a novel gene required for meristem maintenance, is negatively regulated by low phosphate availability. *Plant Science,* 205-206**,** 2-12.

GONZÁLEZ, E., SOLANO, R., RUBIO, V., LEYVA, A. & PAZ-ARES, J. 2005. PHOSPHATE TRANSPORTER TRAFFIC FACILITATOR1 Is a Plant-Specific SEC12-Related Protein That Enables the Endoplasmic Reticulum Exit of a High-Affinity Phosphate Transporter in Arabidopsis [W]. *The Plant Cell,* 17**,** 3500-3512.

GOODSTEIN, D. M., SHU, S., HOWSON, R., NEUPANE, R., HAYES, R. D., FAZO, J., MITROS, T., DIRKS, W., HELLSTEN, U., PUTNAM, N. & ROKHSAR, D. S. 2012. Phytozome: a comparative platform for green plant genomics. *Nucleic Acids Res,* 40**,** D1178-86.

GROTH, M., TAKEDA, N., PERRY, J., UCHIDA, H., DRÄXL, S., BRACHMANN, A., SATO, S., TABATA, S., KAWAGUCHI, M., WANG, T. L. & PARNISKE, M. 2010. NENA, a Lotus japonicus homolog of Sec13, is required for rhizodermal infection by arbuscular mycorrhiza fungi and rhizobia but dispensable for cortical endosymbiotic development. *Plant Cell,* 22**,** 2509-26.

GUAN, B., CHEN, X. & ZHANG, H. 2013a. Two-Electrode Voltage Clamp. *In:* GAMPER, N. (ed.) *Ion Channels: Methods and Protocols.* Totowa, NJ: Humana Press.

GUAN, Q., WU, J., YUE, X., ZHANG, Y. & ZHU, J. 2013b. A nuclear calcium-sensing pathway is critical for gene regulation and salt stress tolerance in Arabidopsis. *PLoS Genet,* 9**,** e1003755.

HANEY, C. H., RIELY, B. K., TRICOLI, D. M., COOK, D. R., EHRHARDT, D. W. & LONG, S. R. 2011. Symbiotic Rhizobia Bacteria Trigger a Change in Localization and Dynamics of the Medicago truncatula Receptor Kinase LYK3. *The Plant Cell,* 23**,** 2774-2787.

HARRISON, M. J., DEWBRE, G. R. & LIU, J. 2002. A phosphate transporter from Medicago truncatula involved in the acquisition of phosphate released by arbuscular mycorrhizal fungi. *Plant Cell,* 14**,** 2413-29.

HAZAK, O., MAMON, E., LAVY, M., STERNBERG, H., BEHERA, S., SCHMITZ-THOM, I., BLOCH, D., DEMENTIEV, O., GUTMAN, I., DANZIGER, T., SCHWARZ, N., ABUZEINEH, A.,

MOCKAITIS, K., ESTELLE, M., HIRSCH, J. A., KUDLA, J. & YALOVSKY, S. 2019. A novel Ca2+-binding protein that can rapidly transduce auxin responses during root growth. *PLOS Biology,* 17**,** e3000085.

HE, J., ZHANG, C., DAI, H., LIU, H., ZHANG, X., YANG, J., CHEN, X., ZHU, Y., WANG, D., QI, X., LI, W., WANG, Z., AN, G., YU, N., HE, Z., WANG, Y.-F., XIAO, Y., ZHANG, P. & WANG, E. 2019. A LysM Receptor Heteromer Mediates Perception of Arbuscular Mycorrhizal Symbiotic Signal in Rice. *Molecular Plant,* 12**,** 1561-1576.

HELLEMANS, J., MORTIER, G., DE PAEPE, A., SPELEMAN, F. & VANDESOMPELE, J. 2007. qBase relative quantification framework and software for management and automated analysis of real-time quantitative PCR data. *Genome Biol,* 8**,** R19.

HEPPER, C. M. 1983. THE EFFECT OF NITRATE AND PHOSPHATE ON THE VESICULAR-ARBUSCULAR MYCORRHIZAL INFECTION OF LETTUCE. *New Phytologist,* 93**,** 389-399.

HERNÁNDEZ, G., VALDÉS-LÓPEZ, O., RAMÍREZ, M., GOFFARD, N., WEILLER, G., APARICIO-FABRE, R., FUENTES, S. I., ERBAN, A., KOPKA, J., UDVARDI, M. K. & VANCE, C. P. 2009. Global Changes in the Transcript and Metabolic Profiles during Symbiotic Nitrogen Fixation in Phosphorus-Stressed Common Bean Plants *Plant Physiology,* 151**,** 1221-1238.

HIRSCH, S., KIM, J., MUÑOZ, A., HECKMANN, A. B., DOWNIE, J. A. & OLDROYD, G. E. 2009. GRAS proteins form a DNA binding complex to induce gene expression during nodulation signaling in Medicago truncatula. *Plant Cell,* 21**,** 545-57.

HIRUMA, K., GERLACH, N., SACRISTÁN, S., NAKANO, R. T., HACQUARD, S., KRACHER, B., NEUMANN, U., RAMÍREZ, D., BUCHER, M., O'CONNELL, R. J. & SCHULZE-LEFERT, P. 2016. Root Endophyte Colletotrichum tofieldiae Confers Plant Fitness Benefits that Are Phosphate Status Dependent. *Cell,* 165**,** 464-74.

HO, C.-H., LIN, S.-H., HU, H.-C. & TSAY, Y.-F. 2009. CHL1 Functions as a Nitrate Sensor in Plants. *Cell,* 138**,** 1184-1194.

HOK, S., DANCHIN, E. G. J., ALLASIA, V., PANABIÈRES, F., ATTARD, A. & KELLER, H. 2011. An Arabidopsis (malectin-like) leucine-rich repeat receptor-like kinase contributes to downy mildew disease. *Plant, Cell & Environment,* 34**,** 1944-1957.

HORTON, P., PARK, K. J., OBAYASHI, T., FUJITA, N., HARADA, H., ADAMS-COLLIER, C. J. & NAKAI, K. 2007. WoLF PSORT: protein localization predictor. *Nucleic Acids Res,* 35**,** W585-7.

HOU C, TIAN W, KLEIST T, HE K, GARCIA V, BAI F, HAO Y, LUAN S, LI L. DUF221 proteins are a family of osmosensitive calcium-permeable cation channels conserved across eukaryotes. Cell Res. 2014 May;24(5):632-5.

HU, B., JIANG, Z., WANG, W., QIU, Y., ZHANG, Z., LIU, Y., LI, A., GAO, X., LIU, L., QIAN, Y., HUANG, X., YU, F., KANG, S., WANG, Y., XIE, J., CAO, S., ZHANG, L., WANG, Y., XIE, Q., KOPRIVA, S. & CHU, C. 2019. Nitrate-NRT1.1B-SPX4 cascade integrates nitrogen and phosphorus signalling networks in plants. *Nat Plants,* 5**,** 401-413.

HU, H. C., WANG, Y. Y. & TSAY, Y. F. 2009. AtCIPK8, a CBL-interacting protein kinase, regulates the low-affinity phase of the primary nitrate response. *Plant J,* 57**,** 264-78.

HU M, QI J, BI G, ZHOU JM. Bacterial Effectors Induce Oligomerization of Immune Receptor ZAR1 In Vivo. Mol Plant. 2020 May 4;13(5):793-801.

HUA, B.-G., MERCIER, R. W., LENG, Q. & BERKOWITZ, G. A. 2003. Plants Do It Differently. A New Basis for Potassium/Sodium Selectivity in the Pore of an Ion Channel. *Plant Physiology,* 132**,** 1353-1361.

HUANG, F., LUO, J., NING, T., CAO, W., JIN, X., ZHAO, H., WANG, Y. & HAN, S. 2017. Cytosolic and Nucleosolic Calcium Signaling in Response to Osmotic and Salt Stresses Are Independent of Each Other in Roots of Arabidopsis Seedlings. *Frontiers in Plant Science,* 8.

HUISMAN R, GEURTS R. A Roadmap toward Engineered Nitrogen-Fixing Nodule Symbiosis. Plant Commun. 2019 Dec 28;1(1):100019. doi: 10.1016/j.xplc.2019.100019.

HUMPHREYS, C. P., FRANKS, P. J., REES, M., BIDARTONDO, M. I., LEAKE, J. R. & BEERLING, D. J. 2010. Mutualistic mycorrhiza-like symbiosis in the most ancient group of land plants. *Nature Communications,* 1**,** 103.

HWANG, I. & SHEEN, J. 2001. Two-component circuitry in Arabidopsis cytokinin signal transduction. *Nature,* 413**,** 383-9.

IMAIZUMI-ANRAKU, H., TAKEDA, N., CHARPENTIER, M., PERRY, J., MIWA, H., UMEHARA, Y., KOUCHI, H., MURAKAMI, Y., MULDER, L., VICKERS, K., PIKE, J., DOWNIE, J. A., WANG, T., SATO, S., ASAMIZU, E., TABATA, S., YOSHIKAWA, M., MUROOKA, Y., WU, G. J., KAWAGUCHI, M., KAWASAKI, S., PARNISKE, M. & HAYASHI, M. 2005. Plastid proteins crucial for symbiotic fungal and bacterial entry into plant roots. *Nature,* 433**,** 527-31.

IOIO, R. D., NAKAMURA, K., MOUBAYIDIN, L., PERILLI, S., TANIGUCHI, M., MORITA, M. T., AOYAMA, T., COSTANTINO, P. & SABATINI, S. 2008. A Genetic Framework for the Control of Cell Division and Differentiation in the Root Meristem. *Science,* 322**,** 1380-1384.

ISIDRA-ARELLANO, M. C., POZAS-RODRÍGUEZ, E. A., DEL ROCÍO REYERO-SAAVEDRA, M., ARROYO-CANALES, J., FERRER-ORGAZ, S., DEL SOCORRO SÁNCHEZ-CORREA, M., CARDENAS, L., COVARRUBIAS, A. A. & VALDÉS-LÓPEZ, O. 2020. Inhibition of legume nodulation by Pi deficiency is dependent on the autoregulation of nodulation (AON) pathway. *Plant J,* 103**,** 1125-1139.

JACOB P, KIM NH, WU F, EL-KASMI F, CHI Y, WALTON WG, FURZER OJ, LIETZAN AD, SUNIL S, KEMPTHORN K, REDINBO MR, PEI ZM, WAN L, DANGL JL. Plant "helper" immune receptors are Ca^{2+}-permeable nonselective cation channels. Science. 2021 Jul 23;373(6553):420-425.

JAKOBSEN, I. 1985. The role of phosphorus in nitrogen fixation by young pea plants (Pisum sativum). *Physiologia Plantarum,* 64**,** 190-196.

JARRATT-BARNHAM, E., WANG, L., NING, Y. & DAVIES, J. M. 2021. The Complex Story of Plant Cyclic Nucleotide-Gated Channels. *Int J Mol Sci,* 22.

JAVOT, H., PENMETSA, R. V., TERZAGHI, N., COOK, D. R. & HARRISON, M. J. 2007. A Medicago truncatula phosphate transporter indispensable for the arbuscular mycorrhizal symbiosis. *Proceedings of the National Academy of Sciences,* 104**,** 1720-1725.

JIN, Y., CHEN, Z., YANG, J., MYSORE, K. S., WEN, J., HUANG, J., YU, N. & WANG, E. 2018. IPD3 and IPD3L Function Redundantly in Rhizobial and Mycorrhizal Symbioses. *Front Plant Sci,* 9**,** 267.

JING, Z., LIU, C., QI, R. & REN, P. 2018. Many-body effect determines the selectivity for Ca²⁺ and Mg²⁺ in proteins. *Proceedings of the National Academy of Sciences,* 115**,** E7495-E7501.

JUMPER, J., EVANS, R., PRITZEL, A., GREEN, T., FIGURNOV, M., RONNEBERGER, O., TUNYASUVUNAKOOL, K., BATES, R., ŽÍDEK, A., POTAPENKO, A., BRIDGLAND, A., MEYER, C., KOHL, S. A. A., BALLARD, A. J., COWIE, A., ROMERA-PAREDES, B., NIKOLOV, S., JAIN, R., ADLER, J., BACK, T., PETERSEN, S., REIMAN, D., CLANCY, E., ZIELINSKI, M., STEINEGGER, M., PACHOLSKA, M., BERGHAMMER, T., BODENSTEIN, S., SILVER, D., VINYALS, O., SENIOR, A. W., KAVUKCUOGLU, K., KOHLI, P. & HASSABIS, D. 2021. Highly accurate protein structure prediction with AlphaFold. *Nature,* 596**,** 583-589.

JUNG, J.-Y., RIED, M. K., HOTHORN, M. & POIRIER, Y. 2018. Control of plant phosphate homeostasis by inositol pyrophosphates and the SPX domain. *Current Opinion in Biotechnology,* 49**,** 156-162.

JURKOWSKI, G. I., SMITH, R. K., JR., YU, I. C., HAM, J. H., SHARMA, S. B., KLESSIG, D. F., FENGLER, K. A. & BENT, A. F. 2004. Arabidopsis DND2, a second cyclic nucleotide-gated ion channel gene for which mutation causes the "defense, no death" phenotype. *Mol Plant Microbe Interact,* 17**,** 511-20.

KALYAANAMOORTHY, S., MINH, B. Q., WONG, T. K. F., VON HAESELER, A. & JERMIIN, L. S. 2017. ModelFinder: fast model selection for accurate phylogenetic estimates. *Nature Methods,* 14**,** 587-589.

KANAMORI, N., MADSEN, L. H., RADUTOIU, S., FRANTESCU, M., QUISTGAARD, E. M., MIWA, H., DOWNIE, J. A., JAMES, E. K., FELLE, H. H., HAANING, L. L., JENSEN, T. H., SATO, S., NAKAMURA, Y., TABATA, S., SANDAL, N. & STOUGAARD, J. 2006. A nucleoporin is required for induction of Ca2+ spiking in legume nodule development and essential for rhizobial and fungal symbiosis. *Proc Natl Acad Sci U S A,* 103**,** 359-64.

KAPLAN, B., DAVYDOV, O., KNIGHT, H., GALON, Y., KNIGHT, M. R., FLUHR, R. & FROMM, H. 2006. Rapid transcriptome changes induced by cytosolic Ca2+ transients reveal ABRE-related sequences as Ca2+-responsive cis elements in Arabidopsis. *Plant Cell,* 18**,** 2733-48.

KATOH, K. & STANDLEY, D. M. 2013. MAFFT multiple sequence alignment software version 7: improvements in performance and usability. *Mol Biol Evol,* 30**,** 772-80.

KATZEN, F. 2007. Gateway(®) recombinational cloning: a biological operating system. *Expert Opin Drug Discov,* 2**,** 571-89.

KAUPP, U. B., NIIDOME, T., TANABE, T., TERADA, S., BÖNIGK, W., STÜHMER, W., COOK, N. J., KANGAWA, K., MATSUO, H., HIROSE, T., MIYATA, T. & NUMA, S. 1989. Primary structure and functional expression from complementary DNA of the rod photoreceptor cyclic GMP-gated channel. *Nature,* 342**,** 762-766.

KAWAHARADA, Y., KELLY, S., NIELSEN, M. W., HJULER, C. T., GYSEL, K., MUSZYŃSKI, A., CARLSON, R. W., THYGESEN, M. B., SANDAL, N., ASMUSSEN, M. H., VINTHER, M., ANDERSEN, S. U., KRUSELL, L., THIRUP, S., JENSEN, K. J., RONSON, C. W., BLAISE, M., RADUTOIU, S. & STOUGAARD, J. 2015. Receptor-mediated exopolysaccharide perception controls bacterial infection. *Nature,* 523**,** 308-12.

KAWAHARADA, Y., NIELSEN, M. W., KELLY, S., JAMES, E. K., ANDERSEN, K. R., RASMUSSEN, S. R., FÜCHTBAUER, W., MADSEN, L. H., HECKMANN, A. B., RADUTOIU, S. & STOUGAARD, J. 2017. Differential regulation of the Epr3 receptor coordinates membrane-restricted rhizobial colonization of root nodule primordia. *Nature Communications,* 8**,** 14534.

KAZMIERCZAK, J., KEMPE, S. & KREMER, B. 2013. Calcium in the Early Evolution of Living Systems: A Biohistorical Approach. *Current Organic Chemistry,* 17**,** 1738-1750.

KEINATH, N. F., WAADT, R., BRUGMAN, R., SCHROEDER, J. I., GROSSMANN, G., SCHUMACHER, K. & KREBS, M. 2015. Live Cell Imaging with R-GECO1 Sheds Light on flg22- and Chitin-Induced Transient [Ca(2+)]cyt Patterns in Arabidopsis. *Mol Plant,* 8**,** 1188-200.

KELNER, A., LEITÃO, N., CHABAUD, M., CHARPENTIER, M. & DE CARVALHO-NIEBEL, F. 2018. Dual Color Sensors for Simultaneous Analysis of Calcium Signal Dynamics in the Nuclear and Cytoplasmic Compartments of Plant Cells. *Frontiers in Plant Science,* 9.

KEPINSKI, S. & LEYSER, O. 2005. The Arabidopsis F-box protein TIR1 is an auxin receptor. *Nature,* 435**,** 446-51.

KHALVATI, M. A., HU, Y., MOZAFAR, A. & SCHMIDHALTER, U. 2005. Quantification of water uptake by arbuscular mycorrhizal hyphae and its significance for leaf growth, water relations, and gas exchange of barley subjected to drought stress. *Plant Biol (Stuttg),* 7**,** 706-12.

KIBA T, KRAPP A. Plant Nitrogen Acquisition Under Low Availability: Regulation of Uptake and Root Architecture. Plant Cell Physiol. 2016 Apr;57(4):707-14. doi:

10.1093/pcp/pcw052. Epub 2016 Mar 29. PMID: 27025887; PMCID: PMC4836452.

KIM NH, JACOB P, DANGL JL. Con-Ca^{2+} -tenating plant immune responses via calcium-permeable cation channels. New Phytol. 2022 May;234(3):813-818. doi: 10.1111/nph.18044. Epub 2022 Mar 17. PMID: 35181918; PMCID: PMC9994437.

KIRCHHELLE C, MOORE I. A Simple Chamber for Long-term Confocal Imaging of Root and Hypocotyl Development. J Vis Exp. 2017 May 17;(123):55331

KLECZKOWSKI, L. A. & IGAMBERDIEV, A. U. 2021. Magnesium Signaling in Plants. *Int J Mol Sci,* 22.

KÖHLER, C. & NEUHAUS, G. 2000. Characterisation of calmodulin binding to cyclic nucleotide-gated ion channels from Arabidopsis thaliana. *FEBS Lett,* 471**,** 133-6.

KOSUTA, S., HAZLEDINE, S., SUN, J., MIWA, H., MORRIS, R. J., DOWNIE, J. A. & OLDROYD, G. E. D. 2008. Differential and chaotic calcium signatures in the symbiosis signaling pathway of legumes. *Proceedings of the National Academy of Sciences,* 105**,** 9823-9828.

KOWDLEY GC, ACKERMAN SJ, JOHN JE 3RD, JONES LR, MOORMAN JR. Hyperpolarization-activated chloride currents in Xenopus oocytes. J Gen Physiol. 1994 Feb;103(2):217-30.

KRETSINGER, R. H. 1997. EF-hands embrace. *Nat Struct Biol,* 4**,** 514-6.

KROUK, G., LACOMBE, B., BIELACH, A., PERRINE-WALKER, F., MALINSKA, K., MOUNIER, E., HOYEROVA, K., TILLARD, P., LEON, S., LJUNG, K., ZAZIMALOVA, E., BENKOVA, E., NACRY, P. & GOJON, A. 2010. Nitrate-regulated auxin transport by NRT1.1 defines a mechanism for nutrient sensing in plants. *Dev Cell,* 18**,** 927-37.

KUDLA, J., XU, Q., HARTER, K., GRUISSEM, W. & LUAN, S. 1999. Genes for calcineurin B-like proteins in Arabidopsis are differentially regulated by stress signals. *Proc Natl Acad Sci U S A,* 96**,** 4718-23.

KUDLA J, BECKER D, GRILL E, HEDRICH R, HIPPLER M, KUMMER U, PARNISKE M, ROMEIS T, SCHUMACHER K. Advances and current challenges in calcium signaling. New Phytol. 2018 Apr;218(2):414-431. doi: 10.1111/nph.14966. Epub 2018 Jan 14. PMID: 29332310.

KUMAR MEENA, M., KUMAR VISHWAKARMA, N., TRIPATHI, V. & CHATTOPADHYAY, D. 2018. CBL-interacting protein kinase 25 contributes to root meristem development. *Journal of Experimental Botany,* 70**,** 133-147.

KURUSU T, YAGALA T, MIYAO A, HIROCHIKA H, KUCHITSU K. Identification of a putative voltage-gated Ca2+ channel as a key regulator of elicitor-induced hypersensitive cell death and mitogen-activated protein kinase activation in rice. Plant J. 2005 Jun;42(6):798-809.

LACOMBE, B., BECKER, D., HEDRICH, R., DESALLE, R., HOLLMANN, M., KWAK, J. M., SCHROEDER, J. I., LE NOVÈRE, N., NAM, H. G., SPALDING, E. P., TESTER, M., TURANO, F. J., CHIU, J. & CORUZZI, G. 2001. The identity of plant glutamate receptors. *Science,* 292**,** 1486-7.

LAOHAVISIT A, SHANG Z, RUBIO L, CUIN TA, VÉRY AA, WANG A, MORTIMER JC, MACPHERSON N, COXON KM, BATTEY NH, BROWNLEE C, PARK OK, SENTENAC H, SHABALA S, WEBB AA, DAVIES JM. Arabidopsis annexin1 mediates the radical-activated plasma membrane Ca^{2}+- and K+-permeable conductance in root cells. Plant Cell. 2012 Apr;24(4):1522-33.

LAURESSERGUES, D., DELAUX, P. M., FORMEY, D., LELANDAIS-BRIÈRE, C., FORT, S., COTTAZ, S., BÉCARD, G., NIEBEL, A., ROUX, C. & COMBIER, J. P. 2012. The microRNA miR171h modulates arbuscular mycorrhizal colonization of Medicago truncatula by targeting NSP2. *Plant J,* 72**,** 512-22.

LECOURIEUX, D., LAMOTTE, O., BOURQUE, S., WENDEHENNE, D., MAZARS, C., RANJEVA, R. & PUGIN, A. 2005. Proteinaceous and oligosaccharidic elicitors induce different calcium signatures in the nucleus of tobacco cells. *Cell Calcium,* 38**,** 527-538.

LEITÃO, N., DANGEVILLE, P., CARTER, R. & CHARPENTIER, M. 2019. Nuclear calcium signatures are associated with root development. *Nature Communications,* 10**,** 4865.

LENG, Q., MERCIER, R. W., HUA, B.-G., FROMM, H. & BERKOWITZ, G. A. 2002a. Electrophysiological Analysis of Cloned Cyclic Nucleotide-Gated Ion Channels. *Plant Physiology,* 128**,** 400-410.

LENG, Q., MERCIER, R. W., HUA, B. G., FROMM, H. & BERKOWITZ, G. A. 2002b. Electrophysiological analysis of cloned cyclic nucleotide-gated ion channels. *Plant Physiol,* 128**,** 400-10.

LÉRAN, S., EDEL, K. H., PERVENT, M., HASHIMOTO, K., CORRATGÉ-FAILLIE, C., OFFENBORN, J. N., TILLARD, P., GOJON, A., KUDLA, J. & LACOMBE, B. 2015. Nitrate sensing and uptake in Arabidopsis are enhanced by ABI2, a phosphatase inactivated by the stress hormone abscisic acid. *Science Signaling,* 8**,** ra43-ra43.

LEROUGE, P., ROCHE, P., FAUCHER, C., MAILLET, F., TRUCHET, G., PROMÉ, J. C. & DÉNARIÉ, J. 1990. Symbiotic host-specificity of Rhizobium meliloti is determined by a sulphated and acylated glucosamine oligosaccharide signal. *Nature,* 344**,** 781-4.

LETUNIC, I. & BORK, P. 2019. Interactive Tree Of Life (iTOL) v4: recent updates and new developments. *Nucleic Acids Res,* 47**,** W256-w259.

LÉVY, J., BRES, C., GEURTS, R., CHALHOUB, B., KULIKOVA, O., DUC, G., JOURNET, E. P., ANÉ, J. M., LAUBER, E., BISSELING, T., DÉNARIÉ, J., ROSENBERG, C. & DEBELLÉ, F. 2004. A putative Ca2+ and calmodulin-dependent protein kinase required for bacterial and fungal symbioses. *Science,* 303**,** 1361-4.

LI, H. & DURBIN, R. 2009. Fast and accurate short read alignment with Burrows–Wheeler transform. *Bioinformatics,* 25**,** 1754-1760.

LI, H., HANDSAKER, B., WYSOKER, A., FENNELL, T., RUAN, J., HOMER, N., MARTH, G., ABECASIS, G., DURBIN, R. & SUBGROUP, G. P. D. P. 2009. The Sequence Alignment/Map format and SAMtools. *Bioinformatics,* 25**,** 2078-2079.

LI, X.-R., SUN, J., ALBINSKY, D., ZARRABIAN, D., HULL, R., LEE, T., JARRATT-BARNHAM, E., CHIU, C. H., JACOBSEN, A., SOUMPOUROU, E., ALBANESE, A., KOHLEN, W., LUGINBUEHL, L. H., GUILLOTIN, B., LAWRENSEN, T., LIN, H., MURRAY, J., WALLINGTON, E., HARWOOD, W., CHOI, J., PASZKOWSKI, U. & OLDROYD, G. E. D. 2022a. Nutrient regulation of lipochitooligosaccharide recognition in plants via NSP1 and NSP2. *Nature Communications,* 13**,** 6421.

LI, X., CHEN, L., YAO, L., ZOU, J., HAO, J. & WU, W. 2022b. Calcium-dependent protein kinase CPK32 mediates calcium signaling in regulating Arabidopsis flowering time. *Natl Sci Rev,* 9**,** nwab180.

LI, Y., YUAN, F., WEN, Z. *et al.* Genome-wide survey and expression analysis of the OSCA gene family in rice. *BMC Plant Biol* **15**, 261 (2015)

LIMPENS, E., FRANKEN, C., SMIT, P., WILLEMSE, J., BISSELING, T. & GEURTS, R. 2003. LysM domain receptor kinases regulating rhizobial Nod factor-induced infection. *Science,* 302**,** 630-3.

LIU, H. & NAISMITH, J. H. 2008. An efficient one-step site-directed deletion, insertion, single and multiple-site plasmid mutagenesis protocol. *BMC Biotechnology,* 8**,** 91.

LIU, K.-H., LIU, M., LIN, Z., WANG, Z.-F., CHEN, B., LIU, C., GUO, A., KONISHI, M., YANAGISAWA, S., WAGNER, G. & SHEEN, J. 2022. NIN-like protein 7 transcription factor is a plant nitrate sensor. *Science,* 377**,** 1419-1425.

LIU, K. H., NIU, Y., KONISHI, M., WU, Y., DU, H., SUN CHUNG, H., LI, L., BOUDSOCQ, M., MCCORMACK, M., MAEKAWA, S., ISHIDA, T., ZHANG, C., SHOKAT, K., YANAGISAWA,

S. & SHEEN, J. 2017. Discovery of nitrate-CPK-NLP signalling in central nutrient-growth networks. *Nature,* 545**,** 311-316.

LIU, K. H. & TSAY, Y. F. 2003. Switching between the two action modes of the dual-affinity nitrate transporter CHL1 by phosphorylation. *Embo j,* 22**,** 1005-13.

LIU, W., KOHLEN, W., LILLO, A., OP DEN CAMP, R., IVANOV, S., HARTOG, M., LIMPENS, E., JAMIL, M., SMACZNIAK, C., KAUFMANN, K., YANG, W.-C., HOOIVELD, G. J. E. J., CHARNIKHOVA, T., BOUWMEESTER, H. J., BISSELING, T. & GEURTS, R. 2011. Strigolactone Biosynthesis in Medicago truncatula and Rice Requires the Symbiotic GRAS-Type Transcription Factors NSP1 and NSP2 *The Plant Cell,* 23**,** 3853-3865.

LIU X, WANG J, SUN L. Structure of the hyperosmolality-gated calcium-permeable channel OSCA1.2. Nat Commun. 2018 Nov 29;9(1):5060.

LU, M., CHENG, Z., ZHANG, X. M., HUANG, P., FAN, C., YU, G., CHEN, F., XU, K., CHEN, Q., MIAO, Y., HAN, Y., FENG, X., LIU, L. & FU, Y. F. 2020. Spatial Divergence of PHR-PHT1 Modules Maintains Phosphorus Homeostasis in Soybean Nodules. *Plant Physiol,* 184**,** 236-250.

LV, B., TIAN, H., ZHANG, F., LIU, J., LU, S., BAI, M., LI, C. & DING, Z. 2018. Brassinosteroids regulate root growth by controlling reactive oxygen species homeostasis and dual effect on ethylene synthesis in Arabidopsis. *PLOS Genetics,* 14**,** e1007144.

LV, Q., ZHONG, Y., WANG, Y., WANG, Z., ZHANG, L., SHI, J., WU, Z., LIU, Y., MAO, C., YI, K. & WU, P. 2014. SPX4 Negatively Regulates Phosphate Signaling and Homeostasis through Its Interaction with PHR2 in Rice *The Plant Cell,* 26**,** 1586-1597.

MADSEN, E. B., MADSEN, L. H., RADUTOIU, S., OLBRYT, M., RAKWALSKA, M., SZCZYGLOWSKI, K., SATO, S., KANEKO, T., TABATA, S., SANDAL, N. & STOUGAARD, J. 2003. A receptor kinase gene of the LysM type is involved in legume perception of rhizobial signals. *Nature,* 425**,** 637-40.

MAEDA, D., ASHIDA, K., IGUCHI, K., CHECHETKA, S. A., HIJIKATA, A., OKUSAKO, Y., DEGUCHI, Y., IZUI, K. & HATA, S. 2006. Knockdown of an Arbuscular Mycorrhiza-inducible Phosphate Transporter Gene of Lotus japonicus Suppresses Mutualistic Symbiosis. *Plant and Cell Physiology,* 47**,** 807-817.

MAFFEI, M., BOSSI, S., SPITELLER, D., MITHÖFER, A. & BOLAND, W. 2004. Effects of feeding Spodoptera littoralis on lima bean leaves. I. Membrane potentials, intracellular calcium variations, oral secretions, and regurgitate components. *Plant Physiol,* 134**,** 1752-62.

MAILLET, F., POINSOT, V., ANDRÉ, O., PUECH-PAGÈS, V., HAOUY, A., GUEUNIER, M., CROMER, L., GIRAUDET, D., FORMEY, D., NIEBEL, A., MARTINEZ, E. A., DRIGUEZ, H., BÉCARD, G. & DÉNARIÉ, J. 2011. Fungal lipochitooligosaccharide symbiotic signals in arbuscular mycorrhiza. *Nature,* 469**,** 58-63.

MAIR, A., XU, S.-L., BRANON, T. C., TING, A. Y. & BERGMANN, D. C. 2019. Proximity labeling of protein complexes and cell-type-specific organellar proteomes in Arabidopsis enabled by TurboID. *eLife,* 8**,** e47864.

MALABARBA J, MEENTS AK, REICHELT M, SCHOLZ SS, PEITER E, RACHOWKA J, KONOPKA-POSTUPOLSKA D, WILKINS KA, DAVIES JM, OELMÜLLER R, MITHÖFER A. ANNEXIN1 mediates calcium-dependent systemic defense in Arabidopsis plants upon herbivory and wounding. New Phytol. 2021 Jul;231(1):243-254.

MALAMY, J. E. & BENFEY, P. N. 1997. Organization and cell differentiation in lateral roots of Arabidopsis thaliana. *Development,* 124**,** 33-44.

MARASCHIN FDOS, S., MEMELINK, J. & OFFRINGA, R. 2009. Auxin-induced, SCF(TIR1)-mediated poly-ubiquitination marks AUX/IAA proteins for degradation. *Plant J,* 59**,** 100-9.

MARKMANN, K. & PARNISKE, M. 2009. Evolution of root endosymbiosis with bacteria: how novel are nodules? *Trends in Plant Science,* 14**,** 77-86.

MARMONT, G. 1949. Studies on the axon membrane. I. A new method. *Journal of Cellular and Comparative Physiology,* 34**,** 351-382.
MARUTA N, BURDETT H, LIM BYJ, HU X, DESA S, MANIK MK, KOBE B. Structural basis of NLR activation and innate immune signalling in plants. Immunogenetics. 2022 Feb;74(1):5-26.
MÄSER, P., THOMINE, S., SCHROEDER, J. I., WARD, J. M., HIRSCHI, K., SZE, H., TALKE, I. N., AMTMANN, A., MAATHUIS, F. J., SANDERS, D., HARPER, J. F., TCHIEU, J., GRIBSKOV, M., PERSANS, M. W., SALT, D. E., KIM, S. A. & GUERINOT, M. L. 2001. Phylogenetic relationships within cation transporter families of Arabidopsis. *Plant Physiol,* 126**,** 1646-67.
MATULEF, K. & ZAGOTTA, W. N. 2003. Cyclic Nucleotide-Gated Ion Channels. *Annual Review of Cell and Developmental Biology,* 19**,** 23-44.
MAZZOLINI, M., ARCANGELETTI, M., MARCHESI, A., NAPOLITANO, L. M. R., GROSA, D., MAITY, S., ANSELMI, C. & TORRE, V. 2018. The gating mechanism in cyclic nucleotide-gated ion channels. *Sci Rep,* 8**,** 45.
MESSINESE, E., MUN, J. H., YEUN, L. H., JAYARAMAN, D., ROUGÉ, P., BARRE, A., LOUGNON, G., SCHORNACK, S., BONO, J. J., COOK, D. R. & ANÉ, J. M. 2007. A novel nuclear protein interacts with the symbiotic DMI3 calcium- and calmodulin-dependent protein kinase of Medicago truncatula. *Mol Plant Microbe Interact,* 20**,** 912-21.
MILLER, J. B., PRATAP, A., MIYAHARA, A., ZHOU, L., BORNEMANN, S., MORRIS, R. J. & OLDROYD, G. E. 2013. Calcium/Calmodulin-dependent protein kinase is negatively and positively regulated by calcium, providing a mechanism for decoding calcium responses during symbiosis signaling. *Plant Cell,* 25**,** 5053-66.
MIRDITA, M., SCHÜTZE, K., MORIWAKI, Y., HEO, L., OVCHINNIKOV, S. & STEINEGGER, M. 2022. ColabFold: making protein folding accessible to all. *Nat Methods,* 19**,** 679-682.
MITRA, R. M., GLEASON, C. A., EDWARDS, A., HADFIELD, J., DOWNIE, J. A., OLDROYD, G. E. D. & LONG, S. R. 2004. A Ca²⁺/calmodulin-dependent protein kinase required for symbiotic nodule development: Gene identification by transcript-based cloning. *Proceedings of the National Academy of Sciences,* 101**,** 4701-4705.
MOHANASUNDARAM, B. & PANDEY, S. 2022. Moving beyond the arabidopsis-centric view of G-protein signaling in plants. *Trends in Plant Science*.
MOLING, S., PIETRASZEWSKA-BOGIEL, A., POSTMA, M., FEDOROVA, E., HINK, M. A., LIMPENS, E., GADELLA, T. W. J. & BISSELING, T. 2014. Nod Factor Receptors Form Heteromeric Complexes and Are Essential for Intracellular Infection in Medicago Nodules. *The Plant Cell,* 26**,** 4188-4199.
MONSHAUSEN, G. B., MILLER, N. D., MURPHY, A. S. & GILROY, S. 2011. Dynamics of auxin-dependent Ca2+ and pH signaling in root growth revealed by integrating high-resolution imaging with automated computer vision-based analysis. *The Plant Journal,* 65**,** 309-318.
MORRIS, J. L., PUTTICK, M. N., CLARK, J. W., EDWARDS, D., KENRICK, P., PRESSEL, S., WELLMAN, C. H., YANG, Z., SCHNEIDER, H. & DONOGHUE, P. C. J. 2018. The timescale of early land plant evolution. *Proceedings of the National Academy of Sciences,* 115**,** E2274-E2283.
MOUBAYIDIN, L., DI MAMBRO, R. & SABATINI, S. 2009. Cytokinin-auxin crosstalk. *Trends Plant Sci,* 14**,** 557-62.
MOUBAYIDIN, L., SALVI, E., GIUSTINI, L., TERPSTRA, I., HEIDSTRA, R., COSTANTINO, P. & SABATINI, S. 2016. A SCARECROW-based regulatory circuit controls Arabidopsis thaliana meristem size from the root endodermis. *Planta,* 243**,** 1159-1168.
MULDER, L., LEFEBVRE, B., CULLIMORE, J. & IMBERTY, A. 2006. LysM domains of Medicago truncatula NFP protein involved in Nod factor perception. Glycosylation state,

molecular modeling and docking of chitooligosaccharides and Nod factors. *Glycobiology,* 16**,** 801-9.

MÜLLER, B. & SHEEN, J. 2008. Cytokinin and auxin interaction in root stem-cell specification during early embryogenesis. *Nature,* 453**,** 1094-1097.

MÜLLER, R., BLECKMANN, A. & SIMON, R. D. 2008. The Receptor Kinase CORYNE of Arabidopsis Transmits the Stem Cell–Limiting Signal CLAVATA3 Independently of CLAVATA1. *The Plant Cell,* 20**,** 934-946.

NAKAYAMA, S., KAWASAKI, H. & KRETSINGER, R. 2000. Evolution of EF-Hand Proteins. *In:* CARAFOLI, E. & KREBS, J. (eds.) *Calcium Homeostasis.* Berlin, Heidelberg: Springer Berlin Heidelberg.

NGUYEN, L.-T., SCHMIDT, H. A., VON HAESELER, A. & MINH, B. Q. 2014. IQ-TREE: A Fast and Effective Stochastic Algorithm for Estimating Maximum-Likelihood Phylogenies. *Molecular Biology and Evolution,* 32**,** 268-274.

NGUYEN, N. N. T., CLUA, J., VETAL, P. V., VUARAMBON, D. J., DE BELLIS, D., PERVENT, M., LEPETIT, M., UDVARDI, M., VALENTINE, A. J. & POIRIER, Y. 2020. PHO1 family members transport phosphate from infected nodule cells to bacteroids in Medicago truncatula. *Plant Physiology,* 185**,** 196-209.

NINH, T. T., GAO, W., TRUSOV, Y., ZHAO, J. R., LONG, L., SONG, C. P. & BOTELLA, J. R. 2021. Tomato and cotton G protein beta subunit mutants display constitutive autoimmune responses. *Plant Direct,* 5**,** e359.

NOURI, E., SURVE, R., BAPAUME, L., STUMPE, M., CHEN, M., ZHANG, Y., RUYTER-SPIRA, C., BOUWMEESTER, H., GLAUSER, G., BRUISSON, S. & REINHARDT, D. 2021. Phosphate Suppression of Arbuscular Mycorrhizal Symbiosis Involves Gibberellic Acid Signaling. *Plant and Cell Physiology,* 62**,** 959-970.

OKUSHIMA, Y., FUKAKI, H., ONODA, M., THEOLOGIS, A. & TASAKA, M. 2007. ARF7 and ARF19 Regulate Lateral Root Formation via Direct Activation of LBD/ASL Genes in Arabidopsis. *The Plant Cell,* 19**,** 118-130.

OKUSHIMA, Y., OVERVOORDE, P. J., ARIMA, K., ALONSO, J. M., CHAN, A., CHANG, C., ECKER, J. R., HUGHES, B., LUI, A., NGUYEN, D., ONODERA, C., QUACH, H., SMITH, A., YU, G. & THEOLOGIS, A. 2005. Functional Genomic Analysis of the AUXIN RESPONSE FACTOR Gene Family Members in Arabidopsis thaliana: Unique and Overlapping Functions of ARF7 and ARF19 *The Plant Cell,* 17**,** 444-463.

OLDROYD, G. E. & DOWNIE, J. A. 2006. Nuclear calcium changes at the core of symbiosis signalling. *Curr Opin Plant Biol,* 9**,** 351-7.

OLDROYD, G. E. D. & DOWNIE, J. A. 2008. Coordinating Nodule Morphogenesis with Rhizobial Infection in Legumes. *Annual Review of Plant Biology,* 59**,** 519-546.

OLDROYD GED, LEYSER O. A plant's diet, surviving in a variable nutrient environment. Science. 2020 Apr 3;368(6486):eaba0196. doi: 10.1126/science.aba0196. PMID: 32241923.

OWCZARZY, R., TATAUROV, A. V., WU, Y., MANTHEY, J. A., MCQUISTEN, K. A., ALMABRAZI, H. G., PEDERSEN, K. F., LIN, Y., GARRETSON, J., MCENTAGGART, N. O., SAILOR, C. A., DAWSON, R. B. & PEEK, A. S. 2008. IDT SciTools: a suite for analysis and design of nucleic acid oligomers. *Nucleic Acids Res,* 36**,** W163-9.

PAN, Y., CHAI, X., GAO, Q., ZHOU, L., ZHANG, S., LI, L. & LUAN, S. 2019. Dynamic Interactions of Plant CNGC Subunits and Calmodulins Drive Oscillatory Ca2+ Channel Activities. *Developmental Cell,* 48**,** 710-725.e5.

PARK CJ, SHIN R. Calcium channels and transporters: Roles in response to biotic and abiotic stresses. Front Plant Sci. 2022 Sep 8;13:964059. doi: 10.3389/fpls.2022.964059. PMID: 36161014; PMCID: PMC9493244.

PARNISKE, M. 2008. Arbuscular mycorrhiza: the mother of plant root endosymbioses. *Nature Reviews Microbiology,* 6**,** 763-775.

PEARSON, J. N. & JAKOBSEN, I. 1993. The relative contribution of hyphae and roots to phosphorus uptake by arbuscular mycorrhizal plants, measured by dual labelling with 32P and 33P. *New Phytologist,* 124**,** 489-494.

PETTERSEN, E. F., GODDARD, T. D., HUANG, C. C., MENG, E. C., COUCH, G. S., CROLL, T. I., MORRIS, J. H. & FERRIN, T. E. 2021. UCSF ChimeraX: Structure visualization for researchers, educators, and developers. *Protein Sci,* 30**,** 70-82.

PFAFFL, M. W. 2001. A new mathematical model for relative quantification in real-time RT-PCR. *Nucleic Acids Res,* 29**,** e45.

PHYSIOLOGYWEB. 2014. *Resting Membrane Potential - Membrane Ionic Current Equations* [Online]. Available: https://www.physiologyweb.com/lecture_notes/resting_membrane_potential/resting_membrane_potential_membrane_ionic_current_equations.html [Accessed 18th August 2023].

PIMPRIKAR, P., CARBONNEL, S., PARIES, M., KATZER, K., KLINGL, V., BOHMER, MONICA J., KARL, L., FLOSS, DANIELA S., HARRISON, MARIA J., PARNISKE, M. & GUTJAHR, C. 2016. A CCaMK-CYCLOPS-DELLA Complex Activates Transcription of RAM1 to Regulate Arbuscule Branching. *Current Biology,* 26**,** 987-998.

PIROZYNSKI, K. A. & MALLOCH, D. W. 1975. The origin of land plants: a matter of mycotrophism. *Biosystems,* 6**,** 153-64.

QIN, D. B., LIU, M. Y., YUAN, L., ZHU, Y., LI, X. D., CHEN, L. M., WANG, Y., CHEN, Y. F., WU, W. H. & WANG, Y. 2020. CALCIUM-DEPENDENT PROTEIN KINASE 32-mediated phosphorylation is essential for the ammonium transport activity of AMT1;1 in Arabidopsis roots. *J Exp Bot,* 71**,** 5087-5097.

RADUTOIU, S., MADSEN, L. H., MADSEN, E. B., JURKIEWICZ, A., FUKAI, E., QUISTGAARD, E. M., ALBREKTSEN, A. S., JAMES, E. K., THIRUP, S. & STOUGAARD, J. 2007. LysM domains mediate lipochitin-oligosaccharide recognition and Nfr genes extend the symbiotic host range. *Embo j,* 26**,** 3923-35.

RAHNI, R., BIRNBAUM, K.D. Week-long imaging of cell divisions in the Arabidopsis root meristem. *Plant Methods* 15, 30 (2019).

REMANS, T., NACRY, P., PERVENT, M., FILLEUR, S., DIATLOFF, E., MOUNIER, E., TILLARD, P., FORDE, B. G. & GOJON, A. 2006. The Arabidopsis NRT1.1 transporter participates in the signaling pathway triggering root colonization of nitrate-rich patches. *Proc Natl Acad Sci U S A,* 103**,** 19206-11.

RICH, M. K., VIGNERON, N., LIBOUREL, C., KELLER, J., XUE, L., HAJHEIDARI, M., RADHAKRISHNAN, G. V., LE RU, A., DIOP, S. I., POTENTE, G., CONTI, E., DUIJSINGS, D., BATUT, A., LE FAOUDER, P., KODAMA, K., KYOZUKA, J., SALLET, E., BÉCARD, G., RODRIGUEZ-FRANCO, M., OTT, T., BERTRAND-MICHEL, J., OLDROYD, G. E. D., SZÖVÉNYI, P., BUCHER, M. & DELAUX, P.-M. 2021. Lipid exchanges drove the evolution of mutualism during plant terrestrialization. *Science,* 372**,** 864-868.

RICHARDS SL, LAOHAVISIT A, MORTIMER JC, SHABALA L, SWARBRECK SM, SHABALA S, DAVIES JM. Annexin 1 regulates the H2O2-induced calcium signature in Arabidopsis thaliana roots. Plant J. 2014 Jan;77(1):136-45.

RIED, M. K., ANTOLÍN-LLOVERA, M. & PARNISKE, M. 2014. Spontaneous symbiotic reprogramming of plant roots triggered by receptor-like kinases. *eLife,* 3**,** e03891.

RIVERAS, E., ALVAREZ, J. M., VIDAL, E. A., OSES, C., VEGA, A. & GUTIÉRREZ, R. A. 2015. The Calcium Ion Is a Second Messenger in the Nitrate Signaling Pathway of Arabidopsis. *Plant Physiol,* 169**,** 1397-404.

ROBINSON, J. T., THORVALDSDÓTTIR, H., WINCKLER, W., GUTTMAN, M., LANDER, E. S., GETZ, G. & MESIROV, J. P. 2011. Integrative genomics viewer. *Nat Biotechnol,* 29**,** 24-6.

RÓDENAS, R. & VERT, G. 2020. Regulation of Root Nutrient Transporters by CIPK23: 'One Kinase to Rule Them All'. *Plant and Cell Physiology,* 62**,** 553-563.
ROSENBAUM, T. & GORDON, S. E. 2002. Dissecting Intersubunit Contacts in Cyclic Nucleotide-Gated Ion Channels. *Neuron,* 33**,** 703-713.
ROSENBLUETH, M., ORMEÑO-ORRILLO, E., LÓPEZ-LÓPEZ, A., ROGEL, M. A., REYES-HERNÁNDEZ, B. J., MARTÍNEZ-ROMERO, J. C., REDDY, P. M. & MARTÍNEZ-ROMERO, E. 2018. Nitrogen Fixation in Cereals. *Frontiers in Microbiology,* 9.
ROY CHOUDHURY, S. & PANDEY, S. 2022. SymRK-dependent phosphorylation of Gα protein and its role in signaling during soybean (Glycine max) nodulation. *The Plant Journal,* 110**,** 277-291.
ROY S, LIU W, NANDETY RS, CROOK A, MYSORE KS, PISLARIU CI, FRUGOLI J, DICKSTEIN R, UDVARDI MK. Celebrating 20 Years of Genetic Discoveries in Legume Nodulation and Symbiotic Nitrogen Fixation. Plant Cell. 2020 Jan;32(1):15-41. doi: 10.1105/tpc.19.00279. Epub 2019 Oct 24. PMID: 31649123; PMCID: PMC6961631.
RUBIO, V., LINHARES, F., SOLANO, R., MARTÍN, A. C., IGLESIAS, J., LEYVA, A. & PAZ-ARES, J. 2001. A conserved MYB transcription factor involved in phosphate starvation signaling both in vascular plants and in unicellular algae. *Genes Dev,* 15**,** 2122-33.
RUSSO, G., SPINELLA, S., SCIACCA, E., BONFANTE, P. & GENRE, A. 2013. Automated analysis of calcium spiking profiles with CaSA software: two case studies from root-microbe symbioses. *BMC plant biology,* 13**,** 224-224.
SADHUKHAN, A., AGRAHARI, R. K., WU, L., WATANABE, T., NAKANO, Y., PANDA, S. K., KOYAMA, H. & KOBAYASHI, Y. 2021. Expression genome-wide association study identifies that phosphatidylinositol-derived signalling regulates ALUMINIUM SENSITIVE3 expression under aluminium stress in the shoots of Arabidopsis thaliana. *Plant Science,* 302**,** 110711.
SAHA, S., DUTTA, A., BHATTACHARYA, A. & DASGUPTA, M. 2014. Intracellular catalytic domain of symbiosis receptor kinase hyperactivates spontaneous nodulation in absence of rhizobia. *Plant Physiol,* 166**,** 1699-708.
SAITO, K., YOSHIKAWA, M., YANO, K., MIWA, H., UCHIDA, H., ASAMIZU, E., SATO, S., TABATA, S., IMAIZUMI-ANRAKU, H., UMEHARA, Y., KOUCHI, H., MUROOKA, Y., SZCZYGLOWSKI, K., DOWNIE, J. A., PARNISKE, M., HAYASHI, M. & KAWAGUCHI, M. 2007. NUCLEOPORIN85 Is Required for Calcium Spiking, Fungal and Bacterial Symbioses, and Seed Production in Lotus japonicus. *The Plant Cell,* 19**,** 610-624.
SAKAKIBARA, H., KOBAYASHI, K., DEJI, A. & SUGIYAMA, T. 1997. Partial Characterization of the Signaling Pathway for the Nitrate-Dependent Expression of Genes for Nitrogen-Assimilatory Enzymes Using Detached Maize Leaves. *Plant and Cell Physiology,* 38**,** 837-843.
SÁNCHEZ-MARTÍN, J., STEUERNAGEL, B., GHOSH, S., HERREN, G., HURNI, S., ADAMSKI, N., VRÁNA, J., KUBALÁKOVÁ, M., KRATTINGER, S. G., WICKER, T., DOLEŽEL, J., KELLER, B. & WULFF, B. B. H. 2016. Rapid gene isolation in barley and wheat by mutant chromosome sequencing. *Genome Biology,* 17**,** 221.
SCHIEFELBEIN JW, SHIPLEY A, ROWSE P. Calcium influx at the tip of growing root-hair cells of Arabidopsis thaliana. Planta. 1992 Jul;187(4):455-9.
SCHULZE, C., STICHT, H., MEYERHOFF, P., AND DIETRICH, P. (2011). Differential contribution of EF-hands to the Ca^{2+}-dependent activation in the plant two-pore channel TPC1. *Plant J.* 68, 424–432. doi: 10.1111/j.1365-313X.2011.04697.x
SCHUURINK, R. C., SHARTZER, S. F., FATH, A. & JONES, R. L. 1998. Characterization of a Calmodulin-Binding Transporter from the Plasma Membrane of Barley Aleurone. *Proceedings of the National Academy of Sciences of the United States of America,* 95**,** 1944-1949.

SERRE, N. B. C., WERNEROVÁ, D., VITTAL, P., DUBEY, S. M., MEDVECKÁ, E., JELÍNKOVÁ, A., PETRÁŠEK, J., GROSSMANN, G. & FENDRYCH, M. 2023. The AUX1-AFB1-CNGC14 module establishes a longitudinal root surface pH profile. *eLife,* 12**,** e85193.

SHI, J., KIM, K.-N., RITZ, O., ALBRECHT, V., GUPTA, R., HARTER, K., LUAN, S. & KUDLA, J. 1999. Novel Protein Kinases Associated with Calcineurin B–like Calcium Sensors in Arabidopsis. *The Plant Cell,* 11**,** 2393-2405.

SHI, J., ZHAO, B., ZHENG, S., ZHANG, X., WANG, X., DONG, W., XIE, Q., WANG, G., XIAO, Y., CHEN, F., YU, N. & WANG, E. 2021. A phosphate starvation response-centered network regulates mycorrhizal symbiosis. *Cell,* 184**,** 5527-5540.e18.

SHIH, H.-W., DEPEW, CODY L., MILLER, NATHAN D. & MONSHAUSEN, GABRIELE B. 2015. The Cyclic Nucleotide-Gated Channel CNGC14 Regulates Root Gravitropism in Arabidopsis thaliana. *Current Biology,* 25**,** 3119-3125.

SHIMODA, Y., HAN, L., YAMAZAKI, T., SUZUKI, R., HAYASHI, M. & IMAIZUMI-ANRAKU, H. 2012. Rhizobial and Fungal Symbioses Show Different Requirements for Calmodulin Binding to Calcium Calmodulin–Dependent Protein Kinase in Lotus japonicus</em&gt. *The Plant Cell,* 24**,** 304.

SIEBERER, B. J., CHABAUD, M., FOURNIER, J., TIMMERS, A. C. & BARKER, D. G. 2012. A switch in Ca2+ spiking signature is concomitant with endosymbiotic microbe entry into cortical root cells of Medicago truncatula. *Plant J,* 69**,** 822-30.

SIEBERER, B. J., CHABAUD, M., TIMMERS, A. C., MONIN, A., FOURNIER, J. & BARKER, D. G. 2009. A nuclear-targeted cameleon demonstrates intranuclear Ca2+ spiking in Medicago truncatula root hairs in response to rhizobial nodulation factors. *Plant Physiol,* 151**,** 1197-206.

SIMON AA, NAVARRO-RETAMAL C, FEIJÓ JA. Merging Signaling with Structure: Functions and Mechanisms of Plant Glutamate Receptor Ion Channels. Annu Rev Plant Biol. 2023 May 22;74:415-452

SINGH, S., KATZER, K., LAMBERT, J., CERRI, M. & PARNISKE, M. 2014. CYCLOPS, a DNA-binding transcriptional activator, orchestrates symbiotic root nodule development. *Cell Host Microbe,* 15**,** 139-52.

SINGH SK, CHIEN CT, CHANG IF. The Arabidopsis glutamate receptor-like gene GLR3.6 controls root development by repressing the Kip-related protein gene KRP4. J Exp Bot. 2016 Mar;67(6):1853-69.

SINGH A, KANWAR P, YADAV AK, MISHRA M, JHA SK, BARANWAL V, PANDEY A, KAPOOR S, TYAGI AK, PANDEY GK. Genome-wide expressional and functional analysis of calcium transport elements during abiotic stress and development in rice. FEBS J. 2014 Feb;281(3):894-915.

SMIT, P., LIMPENS, E., GEURTS, R., FEDOROVA, E., DOLGIKH, E., GOUGH, C. & BISSELING, T. 2007. Medicago LYK3, an entry receptor in rhizobial nodulation factor signaling. *Plant Physiol,* 145**,** 183-91.

SOLAIMANAND, M. Z. & SAITO, M. 1997. Use of sugars by intraradical hyphae of arbuscular mycorrhizal fungi revealed by radiorespirometry. *New Phytol,* 136**,** 533-538.

STAGNARI, F., MAGGIO, A., GALIENI, A. *et al.* Multiple benefits of legumes for agriculture sustainability: an overview. *Chem. Biol. Technol. Agric.* **4**, 2 (2017).

STEINHORST, L., HE, G., MOORE, L. K., SCHÜLTKE, S., SCHMITZ-THOM, I., CAO, Y., HASHIMOTO, K., ANDRÉS, Z., PIEPENBURG, K., RAGEL, P., BEHERA, S., ALMUTAIRI, B. O., BATISTIČ, O., WYGANOWSKI, T., KÖSTER, P., EDEL, K. H., ZHANG, C., KREBS, M., JIANG, C., GUO, Y., QUINTERO, F. J., BOCK, R. & KUDLA, J. 2022. A Ca(2+)-sensor switch for tolerance to elevated salt stress in Arabidopsis. *Dev Cell,* 57**,** 2081-2094.e7.

STEPHENS NR, QI Z, SPALDING EP. Glutamate receptor subtypes evidenced by differences in desensitization and dependence on the GLR3.3 and GLR3.4 genes. Plant Physiol. 2008 Feb;146(2):529-38.

STEUERNAGEL, B., WITEK, K., JONES, J. D. G. & WULFF, B. B. H. 2017. MutRenSeq: A Method for Rapid Cloning of Plant Disease Resistance Genes. *Methods Mol Biol,* 1659**,** 215-229.

STRACKE, S., KISTNER, C., YOSHIDA, S., MULDER, L., SATO, S., KANEKO, T., TABATA, S., SANDAL, N., STOUGAARD, J., SZCZYGLOWSKI, K. & PARNISKE, M. 2002. A plant receptor-like kinase required for both bacterial and fungal symbiosis. *Nature,* 417**,** 959-62.

STREET, I. H., AMAN, S., ZUBO, Y., RAMZAN, A., WANG, X., SHAKEEL, S. N., KIEBER, J. J. & SCHALLER, G. E. 2015. Ethylene Inhibits Cell Proliferation of the Arabidopsis Root Meristem. *Plant Physiol,* 169**,** 338-50.

STREETER, J. & WONG, P. P. 1988. Inhibition of legume nodule formation and N2 fixation by nitrate. *Critical Reviews in Plant Sciences,* 7**,** 1-23.

STRULLU-DERRIEN, C., KENRICK, P., PRESSEL, S., DUCKETT, J. G., RIOULT, J.-P. & STRULLU, D.-G. 2014. Fungal associations in Horneophyton ligneri from the Rhynie Chert (c. 407 million year old) closely resemble those in extant lower land plants: novel insights into ancestral plant–fungus symbioses. *New Phytologist,* 203**,** 964-979.

SUDA, H., MANO, H., TOYOTA, M., FUKUSHIMA, K., MIMURA, T., TSUTSUI, I., HEDRICH, R., TAMADA, Y. & HASEBE, M. 2020. Calcium dynamics during trap closure visualized in transgenic Venus flytrap. *Nature Plants,* 6**,** 1219-1224.

SUEYOSHI, K., MITSUYAMA, T., SUGIMOTO, T., KLEINHOFS, A., WARNER, R. L. & OJI, Y. 1999. Effects of inhibitors for signaling components on the expression of the genes for nitrate reductase and nitrite reductase in excised barley leaves. *Soil Science and Plant Nutrition,* 45**,** 1015-1019.

SUN, J., MIWA, H., DOWNIE, J. A. & OLDROYD, G. E. D. 2007. Mastoparan Activates Calcium Spiking Analogous to Nod Factor-Induced Responses in Medicago truncatula Root Hair Cells. *Plant Physiology,* 144**,** 695-702.

SUN, L. R., WANG, Y. B., HE, S. B. & HAO, F. S. 2018. Mechanisms for Abscisic Acid Inhibition of Primary Root Growth. *Plant Signal Behav,* 13**,** e1500069.

SVOLACCHIA, N., SALVI, E. & SABATINI, S. 2020. Arabidopsis primary root growth: let it grow, can't hold it back anymore! *Current Opinion in Plant Biology,* 57**,** 133-141.

SYROVATKINA V, ALEGRE KO, DEY R, HUANG XY. Regulation, Signaling, and Physiological Functions of G-Proteins. J Mol Biol. 2016 Sep 25;428(19):3850-68. doi: 10.1016/j.jmb.2016.08.002. Epub 2016 Aug 8. PMID: 27515397; PMCID: PMC5023507.

TAKEDA, N., HANDA, Y., TSUZUKI, S., KOJIMA, M., SAKAKIBARA, H. & KAWAGUCHI, M. 2014. Gibberellins Interfere with Symbiosis Signaling and Gene Expression and Alter Colonization by Arbuscular Mycorrhizal Fungi in Lotus japonicus *Plant Physiology,* 167**,** 545-557.

TAN, Y. Q., YANG, Y., ZHANG, A., FEI, C. F., GU, L. L., SUN, S. J., XU, W., WANG, L., LIU, H. & WANG, Y. F. 2020. Three CNGC Family Members, CNGC5, CNGC6, and CNGC9, Are Required for Constitutive Growth of Arabidopsis Root Hairs as Ca(2+)-Permeable Channels. *Plant Commun,* 1**,** 100001.

TANG RJ, WANG C, LI K, LUAN S. The CBL-CIPK Calcium Signaling Network: Unified Paradigm from 20 Years of Discoveries. Trends Plant Sci. 2020 Jun;25(6):604-617. doi: 10.1016/j.tplants.2020.01.009. Epub 2020 Mar 19. PMID: 32407699.

TAPKEN D, ANSCHÜTZ U, LIU LH, HUELSKEN T, SEEBOHM G, BECKER D, HOLLMANN M. A plant homolog of animal glutamate receptors is an ion channel gated by multiple hydrophobic amino acids. Sci Signal. 2013 Jun 11;6(279):ra47.

THOMSON, B. D., ROBSON, A. D. & ABBOTT, L. K. 1986. EFFECTS OF PHOSPHORUS ON THE FORMATION OF MYCORRHIZAS BY GIGASPORA CALOSPORA AND GLOMUS FASCICULATUM IN RELATION TO ROOT CARBOHYDRATES. *New Phytologist,* 103**,** 751-765.

THOR K, JIANG S, MICHARD E, GEORGE J, SCHERZER S, HUANG S, DINDAS J, DERBYSHIRE P, LEITÃO N, DEFALCO TA, KÖSTER P, HUNTER K, KIMURA S, GRONNIER J, STRANSFELD L, KADOTA Y, BÜCHERL CA, CHARPENTIER M, WRZACZEK M, MACLEAN D, OLDROYD GED, MENKE FLH, ROELFSEMA MRG, HEDRICH R, FEIJÓ J, ZIPFEL C. The calcium-permeable channel OSCA1.3 regulates plant stomatal immunity. Nature. 2020 Sep;585(7826):569-573.

TIAN, W., HOU, C., REN, Z., WANG, C., ZHAO, F., DAHLBECK, D., HU, S., ZHANG, L., NIU, Q., LI, L., STASKAWICZ, B. J. & LUAN, S. 2019. A calmodulin-gated calcium channel links pathogen patterns to plant immunity. *Nature,* 572**,** 131-135.

TIAN, W., WANG, C., GAO, Q. *ET AL.* Calcium spikes, waves and oscillations in plant development and biotic interactions. *Nat. Plants* **6**, 750–759 (2020).

TIPPER, E., LEITÃO, N., DANGEVILLE, P., LAWSON, D. M. & CHARPENTIER, M. 2023. A novel mutant allele of AtCNGC15 reveals a dual function of nuclear calcium release in the root meristem. *J Exp Bot,* 74**,** 2572-2584.

TIRICHINE, L., IMAIZUMI-ANRAKU, H., YOSHIDA, S., MURAKAMI, Y., MADSEN, L. H., MIWA, H., NAKAGAWA, T., SANDAL, N., ALBREKTSEN, A. S., KAWAGUCHI, M., DOWNIE, A., SATO, S., TABATA, S., KOUCHI, H., PARNISKE, M., KAWASAKI, S. & STOUGAARD, J. 2006. Deregulation of a Ca2+/calmodulin-dependent kinase leads to spontaneous nodule development. *Nature,* 441**,** 1153-1156.

TO, J. P., HABERER, G., FERREIRA, F. J., DERUÈRE, J., MASON, M. G., SCHALLER, G. E., ALONSO, J. M., ECKER, J. R. & KIEBER, J. J. 2004. Type-A Arabidopsis response regulators are partially redundant negative regulators of cytokinin signaling. *Plant Cell,* 16**,** 658-71.

TRINICK, M. J. 1973. Symbiosis between Rhizobium and the Non-legume, Trema aspera. *Nature,* 244**,** 459-460.

TRINICK, M. J. 1977. VESICULAR-ARBUSCULAR INFECTION AND SOIL PHOSPHORUS UTILIZATION IN LUPINUS SPP. *New Phytologist,* 78**,** 297-304.

TSAY, Y.-F., SCHROEDER, J. I., FELDMANN, K. A. & CRAWFORD, N. M. 1993. The herbicide sensitivity gene CHL1 of arabidopsis encodes a nitrate-inducible nitrate transporter. *Cell,* 72**,** 705-713.

TUNC-OZDEMIR, M., RATO, C., BROWN, E., ROGERS, S., MOONEYHAM, A., FRIETSCH, S., MYERS, C. T., POULSEN, L. R., MALHÓ, R. & HARPER, J. F. 2013. Cyclic Nucleotide Gated Channels 7 and 8 Are Essential for Male Reproductive Fertility. *PLOS ONE,* 8**,** e55277.

UBEDA-TOMÁS, S., FEDERICI, F., CASIMIRO, I., BEEMSTER, G. T. S., BHALERAO, R., SWARUP, R., DOERNER, P., HASELOFF, J. & BENNETT, M. J. 2009. Gibberellin Signaling in the Endodermis Controls Arabidopsis Root Meristem Size. *Current Biology,* 19**,** 1194-1199.

URQUHART, W., GUNAWARDENA, A. H. L. A. N., MOEDER, W., ALI, R., BERKOWITZ, G. A. & YOSHIOKA, K. 2007. The chimeric cyclic nucleotide-gated ion channel ATCNGC11/12 constitutively induces programmed cell death in a Ca2+ dependent manner. *Plant Molecular Biology,* 65**,** 747-761.

VANDESOMPELE, J., DE PRETER, K., PATTYN, F., POPPE, B., VAN ROY, N., DE PAEPE, A. & SPELEMAN, F. 2002. Accurate normalization of real-time quantitative RT-PCR data by geometric averaging of multiple internal control genes. *Genome Biology,* 3**,** research0034.1.

VASCONCELOS, M. W., GRUSAK, M. A., PINTO, E., GOMES, A., FERREIRA, H., BALÁZS, B., CENTOFANTI, T., NTATSI, G., SAVVAS, D., KARKANIS, A., WILLIAMS, M., VANDENBERG, A., TOMA, L., SHRESTHA, S., AKAICHI, F., BARRIOS, C. O., GRUBER, S., JAMES, E. K., MALUK, M., KARLEY, A. & IANNETTA, P. 2020. The Biology of Legumes and Their Agronomic, Economic, and Social Impact. *In:* HASANUZZAMAN, M., ARAÚJO, S. & GILL, S. S. (eds.) *The Plant Family Fabaceae: Biology and Physiological Responses to Environmental Stresses.* Singapore: Springer Singapore.

VENKATESHWARAN, M., JAYARAMAN, D., CHABAUD, M., GENRE, A., BALLOON, A. J., MAEDA, J., FORSHEY, K., DEN OS, D., KWIECIEN, N. W., COON, J. J., BARKER, D. G. & ANÉ, J.-M. 2015. A role for the mevalonate pathway in early plant symbiotic signaling. *Proceedings of the National Academy of Sciences,* 112**,** 9781-9786.

VINCILL ED, CLARIN AE, MOLENDA JN, SPALDING EP. Interacting glutamate receptor-like proteins in Phloem regulate lateral root initiation in Arabidopsis. Plant Cell. 2013 Apr;25(4):1304-13.

WAIS R.J., GALERA C., OLDROYD G., CATOIRA R., PENMETSA R.V., COOK D., GOUGH C., DENARIÉ J., LONG S.R. Genetic analysis of calcium spiking responses in nodulation mutants of Medicago truncatula. *Proc. Natl. Acad. Sci. USA.* 2000; **97**: 13407-13412

WANG, B. & QIU, Y. L. 2006. Phylogenetic distribution and evolution of mycorrhizas in land plants. *Mycorrhiza,* 16**,** 299-363.

WANG C, TANG RJ, KOU S, XU X, LU Y, RAUSCHER K, VOELKER A, LUAN S. Mechanisms of calcium homeostasis orchestrate plant growth and immunity. Nature. 2024 Mar;627(8003):382-388.

WANG, H.-Y., LI, Y., XUE, T., CHENG, N. & DU, H.-N. 2016. Construction of a series of pCS2+ backbone-based Gateway vectors for overexpressing various tagged proteins in vertebrates. *Acta Biochimica et Biophysica Sinica,* 48**,** 1128-1134.

WANG J, HU M, WANG J, QI J, HAN Z, WANG G, QI Y, WANG HW, ZHOU JM, CHAI J. Reconstitution and structure of a plant NLR resistosome conferring immunity. Science. 2019 Apr 5;364(6435):eaav5870.

WANG, P., SNIJDERS, R., KOHLEN, W., LIU, J., BISSELING, T. & LIMPENS, E. 2021a. Medicago SPX1 and SPX3 regulate phosphate homeostasis, mycorrhizal colonization, and arbuscule degradation. *The Plant Cell,* 33**,** 3470-3486.

WANG, R., XING, X., WANG, Y., TRAN, A. & CRAWFORD, N. M. 2009. A genetic screen for nitrate regulatory mutants captures the nitrate transporter gene NRT1.1. *Plant Physiol,* 151**,** 472-8.

WANG, T., GUO, J., PENG, Y., LYU, X., LIU, B., SUN, S. & WANG, X. 2021b. Light-induced mobile factors from shoots regulate rhizobium-triggered soybean root nodulation. *Science,* 374**,** 65-71.

WANG, X., FENG, C., TIAN, L., HOU, C., TIAN, W., HU, B., ZHANG, Q., REN, Z., NIU, Q., SONG, J., KONG, D., LIU, L., HE, Y., MA, L., CHU, C., LUAN, S. & LI, L. 2021c. A transceptor-channel complex couples nitrate sensing to calcium signaling in Arabidopsis. *Mol Plant,* 14**,** 774-786.

WANG, Y.-Y., CHENG, Y.-H., CHEN, K.-E. & TSAY, Y.-F. 2018. Nitrate Transport, Signaling, and Use Efficiency. *Annual Review of Plant Biology,* 69**,** 85-122.

WANG, Y. & BOUWMEESTER, H. J. 2018. Structural diversity in the strigolactones. *Journal of Experimental Botany,* 69**,** 2219-2230.

WANG, Z., RUAN, W., SHI, J., ZHANG, L., XIANG, D., YANG, C., LI, C., WU, Z., LIU, Y., YU, Y., SHOU, H., MO, X., MAO, C. & WU, P. 2014. Rice SPX1 and SPX2 inhibit phosphate starvation responses through interacting with PHR2 in a phosphate-dependent manner. *Proc Natl Acad Sci U S A,* 111**,** 14953-8.

WATERHOUSE, A., BERTONI, M., BIENERT, S., STUDER, G., TAURIELLO, G., GUMIENNY, R., HEER, F. T., DE BEER, T. A P., REMPFER, C., BORDOLI, L., LEPORE, R. & SCHWEDE, T.

2018. SWISS-MODEL: homology modelling of protein structures and complexes. *Nucleic Acids Research,* 46**,** W296-W303.
WEBER W. Ion currents of Xenopus laevis oocytes: state of the art. Biochim Biophys Acta. 1999 Oct 15;1421(2):213-33.
WETTSCHURECK, N. & OFFERMANNS, S. 2005. Mammalian G proteins and their cell type specific functions. *Physiol Rev,* 85**,** 1159-204.
WHICHER, J. R. & MACKINNON, R. 2016. Structure of the voltage-gated K^+ channel Eag1 reveals an alternative voltage sensing mechanism. *Science,* 353**,** 664-9.
WOJTYNIAK, M., BREAR, A. G., O'HALLORAN, D. M. & SENGUPTA, P. 2013. Cell- and subunit-specific mechanisms of CNG channel ciliary trafficking and localization in C. elegans. *J Cell Sci,* 126**,** 4381-95.
WU, Q., XU, F., LIU, L., CHAR, S. N., DING, Y., JE, B. I., SCHMELZ, E., YANG, B. & JACKSON, D. 2020. The maize heterotrimeric G protein β subunit controls shoot meristem development and immune responses. *Proceedings of the National Academy of Sciences,* 117**,** 1799-1805.
WYMER CL, BIBIKOVA TN, GILROY S. Cytoplasmic free calcium distributions during the development of root hairs of Arabidopsis thaliana. Plant J. 1997 Aug;12(2):427-39.
XIN, X., WEI, D., LEI, L., ZHENG, H., WALLACE, I. S., LI, S. & GU, Y. 2023. CALCIUM-DEPENDENT PROTEIN KINASE32 regulates cellulose biosynthesis through post-translational modification of cellulose synthase. *New Phytologist,* 239**,** 2212-2224.
YANG, J., DENG, X., WANG, X., WANG, J., DU, S. & LI, Y. 2019. The calcium sensor OsCBL1 modulates nitrate signaling to regulate seedling growth in rice. *PLOS ONE,* 14**,** e0224962.
YANG, T. & POOVAIAH, B. W. 2003. Calcium/calmodulin-mediated signal network in plants. *Trends Plant Sci,* 8**,** 505-12.
YANO, K., YOSHIDA, S., MÜLLER, J., SINGH, S., BANBA, M., VICKERS, K., MARKMANN, K., WHITE, C., SCHULLER, B., SATO, S., ASAMIZU, E., TABATA, S., MUROOKA, Y., PERRY, J., WANG, T. L., KAWAGUCHI, M., IMAIZUMI-ANRAKU, H., HAYASHI, M. & PARNISKE, M. 2008. CYCLOPS, a mediator of symbiotic intracellular accommodation. *Proceedings of the National Academy of Sciences,* 105**,** 20540-20545.
YE, F., XU, L., LI, X., ZENG, W., GAN, N., ZHAO, C., YANG, W., JIANG, Y. & GUO, J. 2021. Voltage-gating and cytosolic Ca²⁺ activation mechanisms of Arabidopsis two-pore channel AtTPC1. *Proceedings of the National Academy of Sciences,* 118**,** e2113946118.
YE, J., COULOURIS, G., ZARETSKAYA, I., CUTCUTACHE, I., ROZEN, S. & MADDEN, T. L. 2012. Primer-BLAST: A tool to design target-specific primers for polymerase chain reaction. *BMC Bioinformatics,* 13**,** 134.
YOSHIOKA, K., MOEDER, W., KANG, H.-G., KACHROO, P., MASMOUDI, K., BERKOWITZ, G. & KLESSIG, D. F. 2006. The Chimeric Arabidopsis CYCLIC NUCLEOTIDE-GATED ION CHANNEL11/12 Activates Multiple Pathogen Resistance Responses. *The Plant Cell,* 18**,** 747-763.
YU B, WU Q, LI X, ZENG R, MIN Q, HUANG J. GLUTAMATE RECEPTOR-like gene OsGLR3.4 is required for plant growth and systemic wound signaling in rice (Oryza sativa). New Phytol. 2022 Feb;233(3):1238-1256.
YU B, LIU N, TANG S, QIN T, HUANG J. Roles of Glutamate Receptor-Like Channels (GLRs) in Plant Growth and Response to Environmental Stimuli. Plants (Basel). 2022 Dec 9;11(24):3450.
YU, J., HU, S., WANG, J., WONG, G. K., LI, S., LIU, B., DENG, Y., DAI, L., ZHOU, Y., ZHANG, X., CAO, M., LIU, J., SUN, J., TANG, J., CHEN, Y., HUANG, X., LIN, W., YE, C., TONG, W., CONG, L., GENG, J., HAN, Y., LI, L., LI, W., HU, G., HUANG, X., LI, W., LI, J., LIU, Z., LI, L., LIU, J., QI, Q., LIU, J., LI, L., LI, T., WANG, X., LU, H., WU, T., ZHU, M., NI, P., HAN,

H., DONG, W., REN, X., FENG, X., CUI, P., LI, X., WANG, H., XU, X., ZHAI, W., XU, Z., ZHANG, J., HE, S., ZHANG, J., XU, J., ZHANG, K., ZHENG, X., DONG, J., ZENG, W., TAO, L., YE, J., TAN, J., REN, X., CHEN, X., HE, J., LIU, D., TIAN, W., TIAN, C., XIA, H., BAO, Q., LI, G., GAO, H., CAO, T., WANG, J., ZHAO, W., LI, P., CHEN, W., WANG, X., ZHANG, Y., HU, J., WANG, J., LIU, S., YANG, J., ZHANG, G., XIONG, Y., LI, Z., MAO, L., ZHOU, C., ZHU, Z., CHEN, R., HAO, B., ZHENG, W., CHEN, S., GUO, W., LI, G., LIU, S., TAO, M., WANG, J., ZHU, L., YUAN, L. & YANG, H. 2002. A draft sequence of the rice genome (Oryza sativa L. ssp. indica). *Science,* 296**,** 79-92.

YU, X., XU, G., LI, B., DE SOUZA VESPOLI, L., LIU, H., MOEDER, W., CHEN, S., DE OLIVEIRA, M. V. V., ARIÁDINA DE SOUZA, S., SHAO, W., RODRIGUES, B., MA, Y., CHHAJED, S., XUE, S., BERKOWITZ, G. A., YOSHIOKA, K., HE, P. & SHAN, L. 2019. The Receptor Kinases BAK1/SERK4 Regulate Ca2+ Channel-Mediated Cellular Homeostasis for Cell Death Containment. *Current Biology,* 29**,** 3778-3790.e8.

YUAN, F., YANG, H., XUE, Y., KONG, D., YE, R., LI, C., ZHANG, J., THEPRUNGSIRIKUL, L., SHRIFT, T., KRICHILSKY, B., JOHNSON, D. M., SWIFT, G. B., HE, Y., SIEDOW, J. N. & PEI, Z.-M. 2014. OSCA1 mediates osmotic-stress-evoked Ca2+ increases vital for osmosensing in Arabidopsis. *Nature,* 514**,** 367-371.

YUEN, C. C. Y. & CHRISTOPHER, D. A. 2013. The group IV-A cyclic nucleotide-gated channels, CNGC19 and CNGC20, localize to the vacuole membrane in Arabidopsis thaliana. LID - plt012.

ZHANG B, LIU M, WANG Y, YUAN W, ZHANG H. Plant NLRs: Evolving with pathogen effectors and engineerable to improve resistance. Front Microbiol. 2022 Sep 28;13:1018504.

ZHANG, C., HE, J., DAI, H., WANG, G., ZHANG, X., WANG, C., SHI, J., CHEN, X., WANG, D. & WANG, E. 2021. Discriminating symbiosis and immunity signals by receptor competition in rice. *Proceedings of the National Academy of Sciences,* 118**,** e2023738118.

ZHANG, S., PAN, Y., TIAN, W., DONG, M., ZHU, H., LUAN, S. & LI, L. 2017. Arabidopsis CNGC14 Mediates Calcium Influx Required for Tip Growth in Root Hairs. *Mol Plant,* 10**,** 1004-1006.

ZHANG, Y., LI, Z., CHEN, N., HUANG, Y. & HUANG, S. 2020. Phase separation of Arabidopsis EMB1579 controls transcription, mRNA splicing, and development. *PLoS Biol,* 18**,** e3000782.

ZHANG, Z., HOU, C., TIAN, W., LI, L. & ZHU, H. 2019. Electrophysiological Studies Revealed CaM1-Mediated Regulation of the Arabidopsis Calcium Channel CNGC12. *Front Plant Sci,* 10**,** 1090.

ZHOU, X., LI, Q., CHEN, X., LIU, J., ZHANG, Q., LIU, Y., LIU, K. & XU, J. 2011. The Arabidopsis RETARDED ROOT GROWTH Gene Encodes a Mitochondria-Localized Protein That Is Required for Cell Division in the Root Meristem *Plant Physiology,* 157**,** 1793-1804.

ZOU, J.-J., LI, X.-D., RATNASEKERA, D., WANG, C., LIU, W.-X., SONG, L.-F., ZHANG, W.-Z. & WU, W.-H. 2015. Arabidopsis CALCIUM-DEPENDENT PROTEIN KINASE8 and CATALASE3 Function in Abscisic Acid-Mediated Signaling and H2O2 Homeostasis in Stomatal Guard Cells under Drought Stress. *The Plant Cell,* 27**,** 1445-1460.